Theses at NTNU, 2007:215

Alex Klein-Paste

Runway Operability under Cold Weather Conditions

Tire-pavement friction creation by sand particles on iced pavements, and non-contacting detection of sand particles on pavements

Doctoral Thesis

NTNU
Norwegian University of Science and Technology
Thesis for the degree of philosophiae doctor
Faculty of Engineering Science and Technology
Department of Civil and Transport Engineering

NTNU
Innovation and Creativity

Alex Klein-Paste

Runway Operability under Cold Weather Conditions

Tire-pavement friction creation by sand particles on iced pavements, and non-contacting detection of sand particles on pavements

Thesis for the degree of philosophiae doctor

Trondheim, November 2007

Norwegian University of
Science and Technology
Faculty of Engineering Science and Technology
Department of Civil and Transport Engineering

NTNU
Innovation and Creativity

NTNU
Norwegian University of Science and Technology

Thesis for the degree of philosophiae doctor

Faculty of Engineering Science and Technology
Department of Civil and Transport Engineering

ISBN 978-82-471-4736-8 (printed ver.)
ISBN 978-82-471-4753-5 (electronic ver.)
ISSN 1503-8181

Theses at NTNU, 2007:215

Printed by Tapir Uttrykk

ABSTRACT

Airports that operate under cold weather conditions face major challenges in ensuring that runways, taxiways and aprons provide sufficient tire-pavement friction to the operating aircraft. This thesis is motivated by two practical problems: (1) maintaining or improving the pavement surface conditions in an, for airline companies, acceptable state and (2) accurately reporting the actual surface conditions to the relevant actors (pilots, air traffic control, winter maintenance services). The primary objective of this thesis is to broaden the general knowledge base of these problems. The work can be divided into a practical, a fundamental, and an applied part of the thesis.

The practical part includes a field study on how runway surface conditions change in time and the consequences for runway operability. Different situations were documented where the runway surface conditions changed due to snow fall, sand displacement by aircraft, ice deposition, snow compaction, and melting of the contamination layer. These cases highlighted two weaknesses in the current reporting system: (1) the constrained inspection frequency of the runway surface and (2) the limited possibilities to monitor the surface conditions while the runway is open for air traffic. The practical part also included field studies on a new sanding method, based on pre-wetting the sand with hot water. Practical experiences from maintenance personnel were collected, runway surface conditions were documented, and comments from pilots on the reported conditions were investigated. The method provides a solution for the problem that loose sand can be displaced or blown off the runway by the engine thrust of operating aircraft. In addition, the study highlighted some potential negative effects related to the sanding method. The high friction values that are typically measured on surfaces treated with warm pre-wetted sand can create a too optimistic picture of the prevailing conditions for aircrafts. Cases are documented where pilots faced worse conditions than they expected from the provided friction numbers. In 66 % of the cases there were clear indications available that the situation was not as good as suggested by the friction measurements. Another aspect is the risk of Foreign Object Damage (FOD). Maintenance personnel pointed out the importance of proper pavement cleaning prior to the sand application.

The fundamental part of the thesis focuses on the role of sand in the creation of tire-pavement friction on iced surfaces. The presence of sand particles changes the interaction between the tire, the pavement, the contamination layer, and the atmosphere in which the interaction takes place. Hence, it changes the way friction is created. The interactions were studied on a macroscopic scale by observing tire tracks on sanded, iced runways and by aircraft braking experiments on ice treated with loose and warm, pre-wetted sand. These observations showed that loose sand particles, ones trapped between the tire and the ice, can slide together with the rubber tread and plough into the ice layer. Loose sand particles can pile-up in front of, and under, locked tires (full skid). Such tire lock-ups can occur, even though when aircraft are equipped with anti-skid braking systems because these systems become disabled below a certain threshold speed (ranging between 30 and 45 km/h, depending on the aircraft type). On freeze bonded sand (produced by the warm, pre-wetted sanding method), friction can be provided by both loose particles that plough into the ice and by particles that stay fixed to the ice and force the tire tread to deform.
The sand-ice and rubber-ice interactions were also studied on a microscopic scale by etching and replicating the ice surface. These observations revealed that the sliding friction process involved ice deformation in both cases. During rubber-ice sliding friction,

the original crystal structure of the ice remained intact during the interaction. However, small scale ice deformation was evident by the formation of dislocations, aligned in rows along the sliding direction, and by the formation of small scale ploughing tracks. In the case of sand-ice interaction, the ploughing of sand particles was accompanied with the formation of cells within the original crystal structure of the ice. This re-crystallization was observed both in the laboratory and in the field. The rubber-ice and sand-ice sliding friction mechanisms were studied quantitatively by using a British Pendulum Tester in a cold laboratory experiment. It was found that the observed variability in friction measurements was significantly larger than the uncertainties introduced by the instrument itself. The variability may be caused by poorly controllable/reproducible, microscopic or nanoscopic surface properties of the ice and rubber. Rubber-ice interaction resulted in appreciable friction coefficients ($0.5 \geq \mu \geq 0.2$) at ice temperatures below -5°C. However, it dropped significantly (down to $\mu = 0.05$) over the whole tested temperature range to by the presence of little snow on the ice (less than 1 mm). It demonstrated that friction provided by rubber-ice interaction is very vulnerable to snow contamination. In contrast, sand-ice friction measurements did not show the dramatic drop in friction by the same amount of snow. Hence, the ploughing of relatively large sand particles provided a more robust mechanism of friction, compared to rubber-ice friction.

The applied part of the thesis comprises an exploratory study on a non-contacting measurement principle to quantify the amount and distribution of sand particles on a pavement. A static laboratory arrangement was build where sanded pavements were illuminated by a visible laser light source (wavelength: 635 nm) at different angles of incidence. The radiance from the illuminated area was recorded with a digital camera at different angles. The test matrix included dry and iced pavements and different sand application rates. A correlation between the total radiance and sand application rate was only found when there was negligible radiance from the pavement in the scene. The sand detection therefore required a distinction between radiance originating from the sand and the radiance originating from the pavement. However, due to the similarities in optical properties of the sand and the aggregates in the pavement (both originate from crushed rock) and the transparency of ice in the visible range, it seemed unlikely that the distinction can be made on the basis of radiance intensity. An alternative approach was investigated, based on triangulation. Image analysis techniques were used to define a region of interest where the radiance only originates from the sand. Within this region, individual sand particles can be identified and counted. The principle was developed theoretically for flat surfaces and adapted for application on rough surfaces of unknown topography. It was tested on a selected group of images, taken under favourable incidence and camera angles. The algorithm placed the region of interest reasonably well in all analyzed images, resulting in a rather conservative input in the subsequent analyses. The sand detection algorithm had a success rate between 63 and 100 %, depending on the surface contamination. The errors were mainly caused by not detecting particles that were located in the lower parts of the surface topography. Only few mistakes were made by incorrectly identifying particles. Hence, the number of detected particles was a conservative estimate of the actual number of particles located in the region.

ACKNOWLEDGEMENTS

The genesis of this thesis started for me on the sea ice of Van Mijenfjorden, Svalbard in the spring of 2002. While I conducted field work for my master thesis, I expressed my wish to continue in the field of Arctic Technology to Prof. Sveinung Løset. Sveinung offered me a place in his group and he became my supervisor. I have never felt unsupported during my stay in his group, at the department of Civil and Transport Engineering. I am very grateful for his active efforts to create and maintain an enthusiastic group of people that are interested in snow and ice related engineering problems.

What I did not knew at that particular moment on the sea ice was that two persons had worked for years to raise money for a project on snow and ice contaminated runways. Armann Norheim was working at Luftfartsverket, now called Avinor, which operates the majority of airports in Norway. He knew from practice how difficult it is to provide pilots accurate information on the runway surface conditions. During the years, I noticed that his devotion to the problem has no boundaries. Armann, thank you for all the financial, material, and immaterial support you have arranged for me. You have been a big inspiration during my study.

The second person was Dr. Nirmal Sinha. Nirmal worked for many years on ice related engineering problems at the National Research Council Canada and had become close friends with Armann through the Joint Winter Runway Friction Measurement Program. I still don't know exactly how this person from India managed to teach me something about ice. But when he in told me (while standing on an iced runway at -27°C in North Bay, Canada): "Alex, never forget that ice is a very hot material", I knew that I was convicted to ice research for at least the next four years, and probably even longer. Words cannot describe how much I learned from Nirmal. He did not only try to fill my mental backpack with knowledge on the structure and mechanics of ice, he also showed me how to be flexible in the field. To be critical to everything you read and hear, to observe and enjoy the beauty and complexity of Mother Nature, and what it means to be your own worst critic. I may never approach the standards you apply to yourself Nirmal, but you have caused permanent changes in my brain and for that I am very grateful.

During this project I received a large amount of financial support. I like to acknowledge Erik Gill, Oslo Airport OSL, Norway, for the financial support within The Safe Winter Operations Project. Secondly, I also like to thank Angelo Boccanfuso, Transportation Development Centre, Transport Canada and Øystein Larsen, Norwegian Public Road Administration, Norway, for their contributions.

Special thanks go to technical staff at NTNU, in particular Gustav Jakobsen, Tore Menne, Stein Hoseth, and Lisbeth Johansen, for their support during the experimental work.

I like to thank all my colleagues in "the basement" for the help and the wonderful working environment: Ronny Winther, Basile Bonnemaire, Morten Bjerkås, Jens Laugesen, Svetlana Shaftrova, Shokrollah Zare, Simon-Philip Breton, Fredrik Sandquist, Arne Gurtner, Kenneth Eik, Raed Lubbad, Haiyan Long, Nicolas Serre, and Ada Rapetto. I also thank Kai-Rune Lysbakken and Bård Nonstad for their useful comments on the manuscript.

Extensive field studies were undertaken at different Norwegian airports. I would like to acknowledge Vidar Snerten, Oslo Airport Gardermoen, Svein Pedersen, Hammerfest Airport, Bjørn Stiberg, Tromsø Airport Langnes, Knut Kristoffersen, Kirkenes Airport Høybuktmoen, Ole Martinus Rambech, Svalbard Airport Longyear, and Odd Helge Wang, Bardufoss Air force Base for the hospitality at these airports. Without any exception I always felt welcome and supported.

I like to thank all the airport employees I have been in contact with during the field studies. Unfortunately the list is too long to name each person individually. Some I just had a little talk with, some I worked together with for months. I have asked people countless of favours: allowance to let me inspect the runway area closely in between scheduled flights, a front loader to lift my laboratory container, the calibration of a friction measurement device, a place to drink coffee, the installation of sensors, and assistance during experiments. People have worked overtime for me, people have worked in their own time for me, coffee has been flushed through the drain to help me, and additional work load was accepted to help me. The efforts of these people lie invisibly behind the work presented in this thesis. Nobody, not even I, can fully appreciate the magnitude of those efforts.

Finally, I like to thank my friends and family. Judith, you have been a big mental support to me throughout this work. Thanks alot. Dialing 93641 was all it took when I needed a coffee break with a good friend. Bjarte, thanks! And from a distance, but very close indeed, there was this caring, humble mother. Always standby on the sideline, in case I needed some love or understanding. Thanks mom!

TABLE OF CONTENTS

NOMENCLATURE

Terms

Aircraft ground operations	take-off, aborted take-off, landing, and taxiing.
Braking action	the aircraft's ability to obtain tire-pavement friction.
Cold weather conditions	situations where the air, pavement, or precipitation temperature is below 0°C.
Movement areas	runways, taxiways and aprons.
S-2 ice	columnar-grained, transversely isotropic ice
SNOWTAM	special type of a Notice to Airmen (NOTAM), concerning snow, slush, ice, and standing water.
Tribosystem	Set of two interacting (contacting) surfaces, an interfacial medium, and the environment in which the interaction takes place.
Winter contaminants	snow, ice and slush, in all its appearances, on movement areas.
Winter maintenance	all efforts to control the surface conditions of movement areas.

Abbreviations

ATC	Air Traffic Control
ATIS	Automatic Terminal Information System
BPN	British Pendulum Number
BV-11	Bromsvagn-11 (friction measurement device)
CAA	Civil Aviation Authority
CCD	Charge Coupled Device
CRFI	Canadian Runway Friction Index
ERD	Electronic Recording Decellerometer (friction measurement device)
FAA	Federal Aviation Administration
FOD	Foreign Object Damage
GMT	Greenwich Mean Time
GPS	Global Positioning System
ICAO	International Civil Aviation Organization
IRFI	International Runway Friction Index
IRHD	International Rubber Hardness Degrees
IRV	International Reference Vehicle
JPEG	Joint Photographic Experts Group
JWRFMP	Joint Winter Runway Friction Measurement Program
METAR	METeorological Aerodrome Report
NOTAM	NOtice To AirMan
RGB	Red Green Blue
ROI	Region Of Interest
SEM	Scanning Electron Microscopy
SFT	Saab Friction Tester (friction measurement device)
TRRL	Transport and Road Research Laboratory

Roman symbols

A, A_a,	area, apparent contact area
A_l, A_p	projected area that carries the load, projected area of the groove
a	ROI width
a'	ROI width margin
a_T	shift factor
B_1, B_2, B_3 ,B_4	boundaries
C	convolution mask
c_p	specific thermal capacity
c_1, c_2	effective refractive indices
D	thermal diffusivity of ice
d_1, d_2, d_i	asperity contact length material 1, asperity contact length material 2, ice asperity contact length
D_a, D_i, D_f	aerodynamic drag, impingement drag, friction drag
E^*, E', E''	complex elastic modulus, storage modulus (real part), loss modulus (imaginary part)
e	phase shift
F	F-number
f	focal length
F_a, F_d	friction force due to adhesion, friction force due to deformation
F_e, F_r	engine thrust, rolling resistance force
F_t, F_n	resultant frictional force, normal force
F_b, F_s	braking friction force, side friction force
G	path length difference
$g(x,y)$	surface topography
$h(x,y)$	height
h_0, h_1	initial height, height at highest point after the swing
H_i	hardness of ice
I, I_n , I_{th}	pixel intensity, noise level, threshold level
I_s, $I_{s,\perp}$, $I_{s,\theta}$	intensity of the scattered light, intensity normal to the surface, intensity at angle θ from the surface normal
k	constant
k_1, k_2	lines
k_s, k_i	thermal conductivity of the slider, thermal conductivity ice
L	radiance
l, l_c	sliding length, contact length
l_1, l_2,, l_2', l_3	object to lens distance, laser to object distance, projected laser to object distance, line
L_a	aerodynamic lift
M	magnification
m	convolution mask size
n	number
n_a, n_{cd},	number of actual sand particles, number of correctly detected particles,
n_e, n_m, n_{nd}	number of total errors, number of mistakes, number of not-detected particles
n_{seg}	number of segments

P	perimeter
p, p_y, p_i	pressure, yield pressure, ploughing strength of ice
$P_{\min 1}$, P_{min2}	minimum perimeter criterion 1 and 2
Q	wind direction
q_h	latent heat of fusion of ice
R	diameter of the slider
RH	relative humidity
r, r_1, r_2	radii
S, S_i	interfacial shear strength, shear strength of ice
s	average speckle size
sr	skid resistance
t, t_e	time, exposure time
T. T_h. T_m. T_r	temperature, homologous temperature, melting temperature, reference temperature
T_a, T_d	air temperature, dew point temperature,
T_i, T_s, T_w	ice temperature, snow temperature, water temperature
$T_{i,0}$	Ice temperature at infinite distance from the interface
T_p, T_{ps},	pavement surface temperature, pavement sub-surface temperature
U	crystal thickness
u	pavement footprint width
V	aircraft ground velocity
v	sliding velocity
$\bar{v}$	average sliding velocity
v_w	wind velocity
W	aircraft weight /effective weight of the swinging arm
w, w_c, w_s	width, contact width, scratch width

Greek symbols

α	constant
β	constant
γ, γ_1, γ_2, $\gamma_{1,2}$	surface energy, surface energy material 1, surface energy material 2, surface energy of the interface between 1 and 2.
ΔE	energy loss
ΔT	temperature difference between the interface and the bulk,
ΔT_m. ΔV, ΔS	equilibrium melting point depression, change in volume, change in entropy
$\Delta\mu_r$	maximum observed variability within a run
$\Delta\mu_b$	maximum observed variability within a batch
δsr	error in skid resistance
$\delta\mu$	error in friction coefficient
$\delta\mu_1$, $\delta\mu_2$, $\delta\mu_{12}$	reading error, height adjustment error, combined error
ε	runway slope
ζ	scaling factor in *xy*-plane
ζ^H	scaling factor in *z*-direction
Θ	static contact angle of a sessile drop of liquid on a solid
θ, θ_c, θ_l, θ_d	angle, camera angle, laser angle, divergence angle
θ_k	projected divergence angle
κ	thermal conductivity
λ	wavelength
μ, μ_A, μ_{BP}	friction coefficient, aircraft braking friction coefficient, British Pendulum friction coefficient
μ_i	friction coefficient during measurement i (i=1,2,3,4,5) taken with a British Pendulum
μ_p, μ_m	friction coefficient due to ploughing, friction coefficient due to required energy to melt the ice surface layer
$\overline{\mu}_b$	average friction coefficient within a batch
$\overline{\mu}_r$	average friction coefficient within a run
ρ_i, ρ_s, ρ_w	ice density, snow density, water density
σ, σ_r, σ_b	standard deviation, standard deviation within a run, standard deviation within a batch
Φ	slip ratio
ϕ	light power
Ω	solid angle
η	viscosity of water

1 INTRODUCTION

1.1 Motivations and objective

Modern societies have become dependent on a reliable, efficient, and all-year round air transportation system. The different elements in the system (e.g. airports, air traffic control, airline companies, and aircraft) are usually able to function normally. However, it occurs that the whole system is hampered because one or a few elements face difficulties to stay operational. This thesis concentrates on the operability of one element, the airport, under one particular type conditions; cold weather conditions. Cold weather conditions can be defined as situations where the air, pavement, or precipitation temperature is below the melting point of water.

Airports require considerable efforts to stay operational under cold weather conditions. Frost protection of infrastructure, aircraft de-icing facilities, and snow and ice removal services are just a few examples of the required precautions. The motivations for this thesis are two particular aspects of airport operability under cold weather conditions: (1) maintaining or improving the runway surface conditions in an, for airline companies, acceptable state and (2) accurately reporting the actual runway surface conditions. Hence, only runway operability is considered, forming a part of the operability of the whole airport.

A central element in runway operability under cold weather conditions is the level of tire-pavement friction that the runway can provide to the operating aircraft. During the last 50 years, significant efforts have been made to measure the level of tire-pavement friction that pavements can provide. A large number of different measuring devices are currently in operational use. But different devices give different readings on a given surface. This led to the desire for a common, device independent, standard and the establishment of correlations between device readings and aircraft performance on snow, ice, or slush contaminated pavements. A large international program, the Joint Winter Runway Friction Measurement Program (JWRFMP), addressed this problem. However, after extensive testing it was found that correlating and harmonizing these devices is not an easy task (Boccanfuso, 2004). The need arose for a more holistic insight into the problem.

The primary objective of this thesis is to broaden the general knowledge base for runway operability under cold weather conditions. Given the history and complexity of the problem it was not aimed at any kind of operational solution within the thesis work. However, the need for workable, operational solutions was not neglected.

1.2 Thesis structure

The work contained in this thesis may be divided into a practical, a fundamental, and an applied part. The practical part starts with a brief introduction on runway operability under cold weather conditions in Chapter 2. It describes the current practice of Norwegian airports and current international regulations that largely dictate these practices. It also explains the methodology and outcome of the JWRFMP. It is followed by a study on runway operability in Chapter 3. It investigates how runway surface conditions change in time and what the consequences are for the operability of the runway.

The fundamental part of the thesis concentrates on the question how sand particles create friction on ice contaminated pavements. It requires first an overview of existing

knowledge on tire-pavement interaction, which is given in Chapter 4. Following, Chapter 5 is an experimental study on sand-ice and rubber-ice frictional interaction by investigating the ice surface, using the etching and replicating method. Chapter 6 compares rubber-ice and sand-ice interaction quantitatively in a laboratory experiment. It investigates variability in friction measurements with one type of friction measurement device.

The applied part of the thesis was motivated by the desire to measure the amount and distribution of sand particles, while they are located on pavements. Laboratory experiments were performed to investigate a non-contacting optical detection technique. The experiments are described in Chapter 7. Chapter 8 continues on the topic by establishing a measurement principle, using triangulation and digital image processing and analysing techniques.

Chapter 9 describes a collection of smaller studies on a new sanding method that recently has been developed in Norway and has been implemented at different Norwegian airports. The chapter is mainly of practical relevance, but also addresses the fundamental question how friction is provided by this sanding method.

The thesis is finalized in Chapter 10 by a short summary, the main conclusions, and recommendations for further work. A microstructural study of snow compacted by an aircraft tire is given in Appendix A.

2 RUNWAY OPERABILITY UNDER COLD WEATHER CONDITIONS

2.1 Introduction

The main function of a runway is to allow safe and efficient take-offs and landings. In addition it has to allow a safe aborted take-off, in case the aircraft experiences a critical malfunction. Take-off, aborted take-off, landing, and taxiing is summarized by the term "aircraft ground operations". Aircraft need sufficient acceleration, retardation and directional control during the ground operations. This implies requires that acceleration is not hampered by excessive rolling resistance or other forms of drag and it demands a certain amount of tire-pavement friction (FAA, 1991).

Cold weather conditions can lead to the deposition of snow, ice and slush on the movement areas (runways, taxiways and aprons). The presence of these materials reduces the attainable tire-pavement friction, can increase free-rolling resistance and can cause impingement drag (drag forces due to collision with the fuselage). Hence, it affects the operability of aircraft, commonly referred to as "aircraft ground operation performance", or shortly "aircraft performance".

Snow, ice, and slush in all its appearances on movement areas are called "winter contaminants". The activities of controlling these pavement contaminants are called "snow and ice control", "winter runway maintenance", or shortly "winter maintenance". It embraces mechanical and chemical removal of snow and ice, chemical prevention of ice deposition, and surface enhancement (e.g. sand application, scarifying). These countermeasures are performed to maintain the surface conditions within the requirements for aircraft ground operations. Winter maintenance is essential for runway operability and involves significant economical costs in form of labor, equipment and runway closure time. Hence, airport operators are stimulated to optimize their winter maintenance activities. Despite all efforts, it is practically impossible to avoid the presence of winter contaminants at all times. Aircraft can continue to operate with reduced tire-pavement friction, but it requires sufficient margins such as sufficient runway length and little cross-wind (the wind speed component perpendicular to the runway direction). The pilot has to determine whether the conditions are within the legal envelope to operate the aircraft. Hence, accurate and valid information on the prevailing runway surface conditions is crucial.

A central issue in safe winter operation is the description of the surface conditions, specifically in terms of its ability to provide friction. This information is not only used to by pilots, but also by other actors, such as Air Traffic Control (ATC) and winter maintenance personnel. By regulation, airport operators are obliged to collect, report, and disseminate this information in an agreed format. It is not only used to determine if it is still safe to operate, but also to plan and initiate winter maintenance operations. Both airport operators and users have different guidelines, procedures, and regulations that are based on the reported information.

2.2 Current reporting system

Information regarding the surface conditions is collected during inspections that are performed on the movement areas. The inspected area is closed for air traffic while the officer in charge collects visual information and performs friction measurements. Different types of friction measurement devices are in use in Norway. Two of them are

illustrated in Fig. 2-1. The inspections and reporting format are governed by international standards (ICAO) and are embedded in national regulations. In Norway, these regulations are contained in BSL E 4-2 (CAA, 2004a).

The collected information is documented in a status report. It's content and format is specified in the SNOWTAM format (ICAO, 2003). National regulations can further detail this format; in Norway this performed in Appendix 1 of BSL E 4-2 (CAA, 2004a). The status report is transmitted to Air Traffic Control (ATC), which in turn generates a SNOWTAM[1] report. The SNOWTAM is a condensed version of the status report, transmitted in coded form. In Norway, the SNOWTAM is disseminated either by the Internet[2], by the Automatic Terminal Information Service (ATIS) system or directly by radio communication. The latter method is faster and is typically used to inform the pilots shortly before take-off or landing.

(a) (b)

Figure 2-1. Two friction measurement devices used in Norway: (a) the Skiddometer BV-11 and (b) the Saab Friction Tester.

The status report (and SNOWTAM) covers all movement areas, but the runways are most detailed. Each runway is divided into three equally sized sections (section A, B, and C) and the conditions are reported for each section. The visually collected information includes the type of contamination, as specified in Table 2-1, the percentage of coverage, and the contamination depth (for dry snow, wet snow, and slush). Combinations of different deposition types are allowed, for example code 47 stands for dry snow on ice.

Friction measurements give an index number, the average friction coefficient μ for each runway section. The friction coefficient typically ranges between 0 and 1 and reported in two decimals. For convenience it is multiplied by a factor 100, before it is communicated to pilots. This multiplied number is referred to as "measured braking action", or shortly "braking action". In absence of friction measurements, the officer in charge can judge the surface conditions in terms of good, medium, or poor, as shown in Table 2-2. Also these terms are transmitted in code form. It is referred to as the "estimated surface friction". In practice, Table 2-2 is used as a correlation table; it is used to interpret the outcome of the friction measurement devices in terms of good, medium, or poor. However, the use of the table for such interpretation has been an issue of discussion (Castellano, 2005).

[1] The term SNOWTAM is derived from NOTAM (Notice to Airmen). It is a special type of NOTAM with information concerning snow, slush, ice, and standing water.
[2] www.ippc.no

Table 2-1. Deposit type specification used in status reports (ICAO, 2003).

Code	Deposit type
NIL	Clear and dry
1	Damp
2	Wet or water patches
3	Rime or frost covered (depth normally less than 1 mm)
4	Dry snow
5	Wet snow
6	Slush
7	Ice
8	Compacted or rolled snow
9	Frozen ruts or ridges

Table 2-2. Friction measurement or estimated surface friction specification (ICAO, 2003).

Measured or calculated friction coefficient	or	Estimated surface friction	Code
0.40 and above		Good	- 5
0.39 to 0.36		medium to good	- 4
0.30 to 0.35		Medium	- 3
0.26 to 0.29		poor to medium	- 2
0.25 and below		Poor	- 1
9 – unreliable		Unreliable	- 9

2.3 Status report update

After the information is collected, it represents the surface conditions for a certain period of time; until the report is updated. The maximum validity of a status report is 24 hours. However, a new report is to be issued whenever there is a significant change in the conditions. The following changes are considered significant (ICAO, 2003):

- A change in the coefficient of friction of about 0.05
- Changes in depth of deposit greater than the following: 20 mm for dry snow, 10 mm for wet snow, 3 mm for slush
- A change in the available length or width of a runway of 10 percent or more
- Any change in the type of deposit or the extent of coverage which requires reclassification of the deposit or other, explained in clear language, with remarks
- When critical snow banks exist on one or both sides of the runway, any change in height or distance from centerline
- Any change in the conspicuity of runway lighting caused by obstruction of the lights
- Any other conditions known to be significant based on experience or local circumstances.

With respect to the second item above, the Norwegian regulation specifies reporting intervals for contamination depths as 8 mm for dry snow, 6 mm for wet snow, and 3 mm for slush (CAA, 2004b).

2.4 Ground friction measurement devices

The use of friction measurement devices started in the late 1940s and today, many different types of devices are in operational use throughout the world (Norheim, 2004). The historical development of these devices is illustrated in Fig. 2-2.

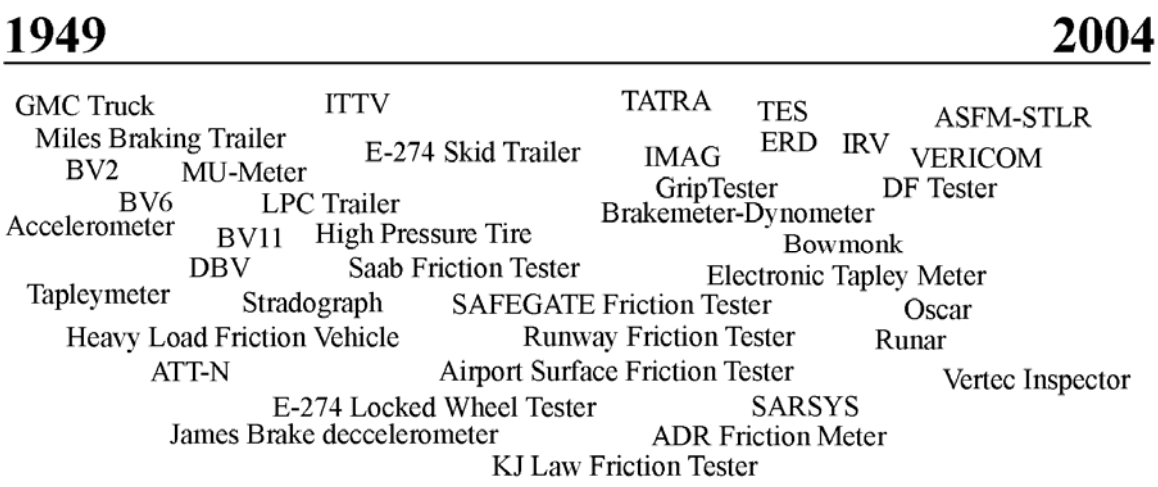

Figure 2-2. Historical development of friction measurement devices between 1949 and 2004 (Norheim, 2004). Reprint permission requested.

The measurement principle of these devices can be divided into deceleration measurements and force/torque measurements. Deceleration measurements use the deceleration of a braking vehicle, from which the friction coefficient is derived. The vehicle is accelerated to a certain speed after which the brakes are applied. Examples of deceleration devices are the Tapleymeter and Electronic Recording Decelerometer (ERD). Deceleration measurements only give spot measurements, due to the required deceleration and acceleration. Force/torque measurements measure the (horizontal) resistance force or torque on a braking test wheel. These measurements can be performed in a continuous manner. Examples of force/torque devices are the Skiddometer BV-11, Saab Friction Tester (SFT), and the Griptester. In practice, friction measurement devices fulfill a central role in the reporting system, probably because measurements interpreted with Table 2-2 provides a simple “objective” answer “how good” the surface conditions are.

2.5 Deficiencies

The current reporting system does have deficiencies. Incidents and accidents have shown that the reported conditions not always represent the conditions experienced by operating aircraft (HSL, 2000a; HSL, 2000b; Dutch Transport Safety Board, 2001; HSL, 2001a; HSL, 2001b; Wismar and Elinder, 2003). Pilots also reported this discrepancy (Klein-Paste and Sinha, in press) and indicate that the supplied information requires improvement (Biggs and Hamilton, 2002).

A fatal aircraft crash in Dryden, Ontario, in 1989, brought the subject into sharp focus. Among its many recommendations, the Dryden Commission of Inquiry that investigated the disaster stressed the need “to expedite the search for a technically accurate means of defining runway surface conditions and their effects on aircraft performance” (Moshansky, 1992). In a response to this recommendation, an international effort, the Joint Winter Runway Friction Measurement Program (JWRFMP), addressed the issue. It was recognized that while most countries have guidelines, no universal measures or

practices have been established (Andrássy, 1999). The main goal of the program was to harmonize different friction measurement devices to a device independent, International Runway Friction Index (IRFI) and establish correlations between IRFI and aircraft performance.

2.6 The methodology of the JWRFMP

The methodology used in the JWRFMP was to compare the readings of different devices on snow and ice contaminated test surfaces with the reading of one particular device, the International Reference Vehicle (IRV) (Deffieux, 1999). The readings from the other devices were correlated with this designated reference by means of linear regression (Andresen and Wambold, 1999).

A selected group of friction devices (the IRV, ERD and SFT) were used in direct comparison with aircraft braking performance of different aircraft. This was derived using the general equation for aircraft acceleration along the runway (Croll et al., 2002):

$$\frac{W}{g}\frac{dV}{dt} = F_e - D_a - D_i - W\sin\varepsilon - D_F, \quad D_F = \mu_a(W\cos\varepsilon - L_a) \tag{2.1}$$

where, W is the aircraft weight, $\frac{dV}{dt}$ the acceleration, F_e the engine thrust, D_a the aerodynamic drag, D_i the impingement drag, ε the runway slope, D_f the friction drag, μ_A the aircraft braking friction coefficient and L_a the aerodynamic lift.

2.7 Outcome of the JWRFMP

The JWRFMP came to an official end in 2004. It had lasted for nine years and included over 300.000 test runs. More than twelve different friction measuring devices and eight different aircraft types were involved. The JWRFMP has played an important role in the whole problem of reporting surface conditions. Improvement and awareness with respect to friction equipment deficiencies over the years has been a direct result of the JWRFMP international testing effort (Boccanfuso, 2004). The program has established correlations between particular devices and particular aircraft, which form the basis of the Canadian Runway Friction Index (CRFI) that uses the ERD (Croll, 2004). However, the main goal, the International Runway Friction Index, has not yet been accomplished. A lesson that were learned within the JWRFMP was that the problem is not so easy to solve (Boccanfuso, 2004). It was found very difficult to maintain the test conditions constant during data collection. A few tests could be performed where the test conditions were similar for all participating vehicles because the devices measured at the same time, parallel to each other, uniformly contaminated surfaces. The data from these tests showed a large variability in readings. On a uniform, undisturbed snow cover the different devices described the surface between “Poor” and “Good”, depending on the friction measurement device (Sinha, 2004). This shows that there is a large difference in response of the different devices.

2.8 Implications

The most evident implication of the deficiencies in the current reporting system is that there still exist situations where pilots do not face the surface conditions they expected, based on the supplied information. With respect to safety, these situations are of main concern. But also winter maintenance personnel experience difficulties. They lack a

consistent, objective reference to judge if countermeasures are required and how successful their efforts are. Finally, the effectiveness of regulations, procedures and guidelines is affected because they are often based on friction measurement criteria. There is therefore still need for improvements in the reporting system.

2.9 Choices for further research directions

Considering the numerous friction measurement devices that have been developed in the last 50 years, and the large efforts undertaken by the JWRFMP, it was judged that developing another friction measurement device would not lead to the desired improvements in the reporting system. The JWRFMP also showed that correlating existing friction measurement devices to aircraft performance is not an easy task.

The size and complexity of the problem made in unrealistic to attempt developing any kind of workable operational solution within the scope of this thesis. It was realized during and after the JWRFMP that there was a strong need for a larger physical understanding of the problem (Sinha, 2004). Therefore it was intended to broaden the general knowledge base of runway operability under cold weather conditions and tire-pavement interaction on snow, ice and slush contaminated pavements. This objective, however, does not imply that the need for operational solutions was forgotten. The work does not differ from the recommendation of Moshansky in 1992. It is still an effort to search for a technically accurate means of defining runway surface conditions and their effects on aircraft performance. The first step was to study *how* runway surface conditions change in time, and what the consequences are for runway operability.

3 OBSERVATIONS FROM OPERATIONAL RUNWAYS – A CASE STUDY

3.1 Introduction

The technological shortcomings in accurately defining and measuring runway surface conditions (Chapter 2) hamper runway operability. Maintenance personnel have to maintain the runway surface conditions without objective and accurate means of determining the quality of their efforts. Pilots may not get the appropriate awareness of situation and can experience worse or better runway surface conditions than expected.

The JWRFMP focused on the correlation and harmonization issue. But there may also be other causes of the problem. Canadian pilots indicated that the update frequency of the information needs improvement (Biggs and Hamilton, 2002) and the validity of friction measurements after a few minutes have been questioned (Horrigan, 2004). Hence, even with the correlation and harmonization issues solved, there may still be measurement difficulties. The primary reason for the measurements is that runway surface conditions change in time (measurements would be redundant if the surface conditions stayed constant). Hence, to improve the understanding of runway operability it is of interest to address the question *how* surface conditions change and what the consequences for the operability of the airport.

Studying runway surface conditions on operative runways is not straightforward. It requires that a ground vehicle enters the area. As part of the safety regulations, Air Traffic Control (ATC) has to temporarily close the runway and give clearance for the inspection. These inspections have to be scheduled with departing and arriving aircraft. Such study thus adds significantly to the workload of ATC. Nevertheless, two Norwegian airports were willing to give full support. The documentation could therefore be performed and was based on opportunities, determined and controlled by ATC.

To utilize the available resources as efficiently as possible it was decided to document the runway surface conditions only during selected periods of time. All other relevant data, such as aircraft ground operations, winter maintenance operations, regular runway inspections (as a part of the reporting system), SNOWTAM reports and weather data, were collected. The data was structured in time series, combining all the information in a chronological order. Each observation period with its supplementing data formed an individual case. The complete documentation is presented elsewhere (Klein-Paste and Sinha, 2006). This chapter summarizes the study.

3.2 Airports

Tromsø Airport, Norway is located at 69° 40’ 53’’ N and 18° 55’ 04’’ E. Its location is shown in Fig. 3-1. With about 100 aircraft movements per day, Tromsø Airport is Norway’s largest civil airport above the Arctic Circle. On a national scale, Tromsø Airport was in 2005 the sixths largest civil airport (Avinor, 2005). It is a regional hub and fulfils thereby a key role in the aviation network of Northern Norway. For the airport this implies that many connecting flights are scheduled to arrive and depart within short time windows. Tromsø Airport is situated on an island between the Norwegian mainland and the island Kvaløya. It is surrounded by two sounds: Tromsøysundet and Sandnessundet. The high latitude and coastal climate of the location result in long winter seasons with heavy snowfalls and frequently shifting weather, often around 0°C. During winter time, the daily air temperature typically ranges between +5°C and -15°C. At Tromsø Airport,

all measured meteorological and runway pavement data is stored in a database. The climate and traffic characteristics, the available meteorological and runway pavement data, and the full corporation of the airport management and employees made it an ideal location to perform the planned study.

Kirkenes Airport is located at 69° 43' 30'' N and 029° 53' 16'' E in the north east of Norway, close to the Russian border. Its location is shown in Fig. 3-1. On a national scale, Kirkenes Airport is a middle-sized airport and served over 6300 aircraft movements in 2005 (Avinor, 2005) It is part of the regional network of airports in Northern Norway. Although there are no scheduled flights during the night, the airport is kept open 24 hours per day for ambulance traffic. Kirkenes Airport has an inland type of climate. The average winter temperature lower, compared to Tromsø Airport. The daily air temperature during the winter months ranges between 0 and -25°C. There is open water in the vicinity of the airport and fog sometimes occurs.

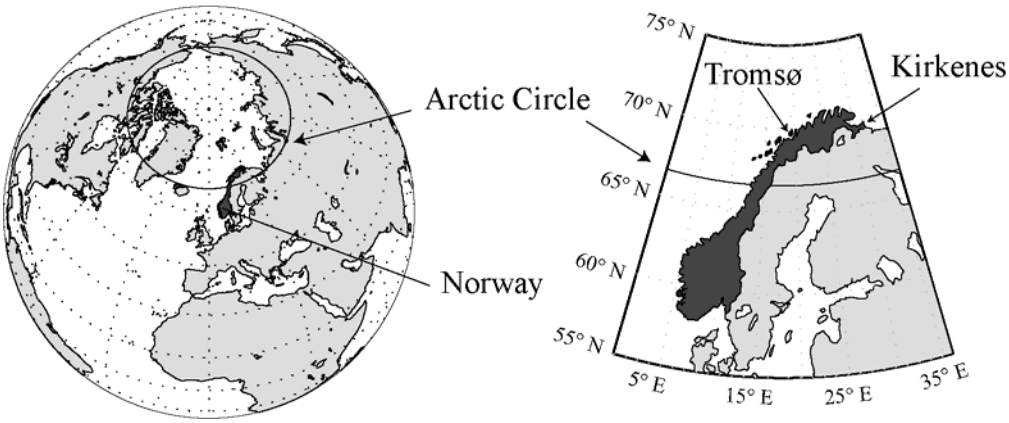

Figure 3-1. The location of Tromsø Airport and Kirkenes Airport.

3.3 Method

During the observation periods, all activities on the runway were followed from a ground vehicle that was positioned close to the runway area. From this position the departure and arrival time of aircraft were recorded, as well as the time, type, and duration of all maintenance activities and the regular runway inspections (as a part of the reporting system). The communication between the officer in charge and ATC was followed by radio.

After receiving clearance from ATC, the runway was entered and the surface conditions could be inspected. It was decided to perform detailed visual inspections. Friction measurements would require too much time on the runway and were therefore not performed. ATC determined the available time to collect data. It was attempted to inspect the runway after each aircraft movement, but in practice this was not always feasible. The conditions were documented by taking photographs. Focus was directed to the tire tracks that were left by the operating aircraft. The time, date, and location of the photographs were recorded with a handheld GPS receiver. All times in this chapter are reported as Greenwich Mean Time (GMT).

The observations were complemented with all relevant records kept at the airports. This included: (1) confirmed departure and arrival times (which included aircraft type), (2)

runway status reports (3) relevant pilot comments received at ATC, and (4) meteorological and runway pavement data.

The meteorological and runway pavement data included: air temperature T_a, dew points temperature $T_{d,}$, wind speed v_w and direction Q, precipitation type and rate, and pavement sub-surface temperature $T_{ps,}$ (about 10 mm depth). At Tromsø Airport, these data were continuously recorded. The precipitation and pavement sub-surface temperature at Kirkenes Airport were manually recorded on the METeorological Aerodrome Reports (METAR) and runway status reports, respectively. The METAR had a measurement frequency of 0.5 hours. Runway status reports were produced at variable intervals, depending on the local conditions at the airport.

Each observation period with all complementary information was structured in a chronological order and formed a separate case. For each case, the 24-hour meteorological and runway data of that day is summarized in a meteogram. An example of a meteogram is shown in Fig. 3-2. The observation period is marked by the grey background. The air temperature, dew points temperature, and sub-surface temperature, are presented as continuous lines. The precipitation rate is presented as vertical bars, where each bar represents the 2.5 minutes average (in mm water equivalent/hour). For Kirkenes, the precipitation rate is given in light, moderate, heavy. The wind speed and direction are given as the 1-hour average and are presented by an integer (m/s) and arrow, respectively.

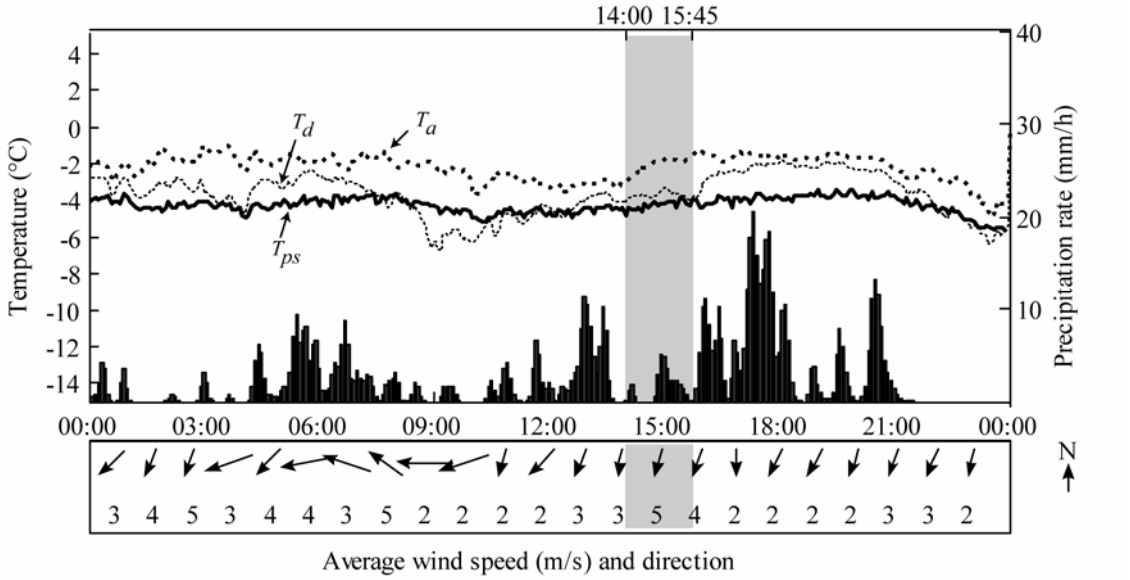

Figure 3-2. Example of a 24-hour meteogram.

All runway status reports that were generated at Tromsø Airport between November 1, 2004 and March 31, 2005 were made available by the airport. These reports were used to investigate the update frequency during a whole winter season.

3.4 Results

3.4.1 Case: heavy snowfall

Tromsø Airport, January 14, 2005, 16:30-19:00 GMT

Weather and runway conditions

During the day it snowed heavily in separate showers. There was little wind and the sun stayed below the horizon throughout the day (polar night). The air temperature, T_a, dew point temperature, T_d and pavement sub-surface temperature, T_{ps}, were -2°C, -2.5°C, and -4°C, respectively. The days prior to the observations had been relatively cold. At the beginning of the observations, there was little or no ice present on the runway.

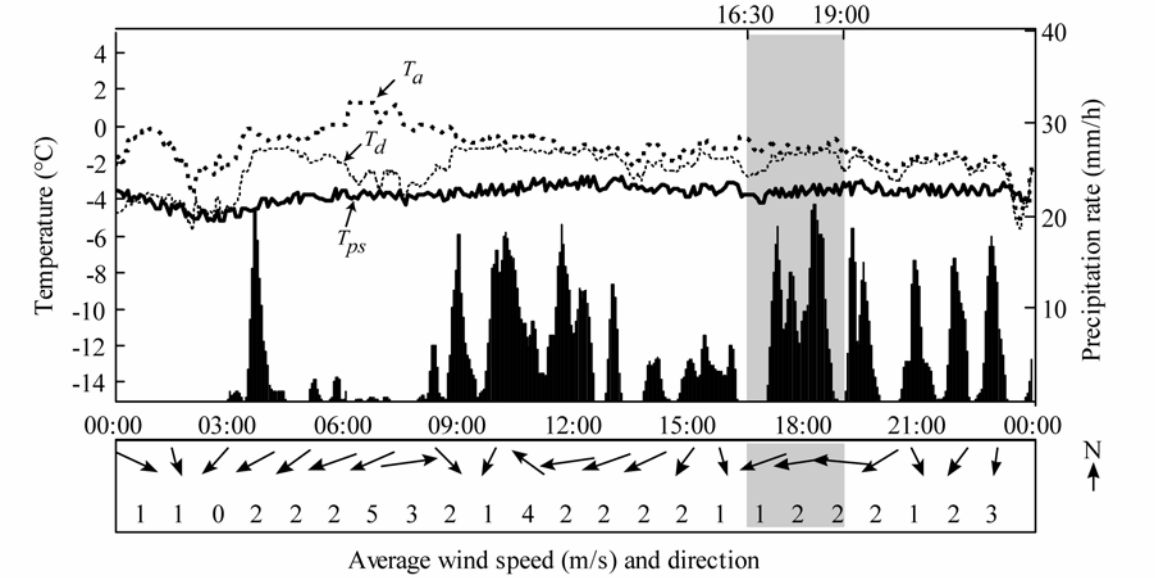

Figure 3-3. Meteorological data Tromsø Airport January 14, 2005.

Observations

During the observation period of 2.5 hours, from 16:30 to 19:00 GMT (Fig. 3-3), the runway pavement was cleaned three times using runway sweepers (combined plowing, sweeping, and blowing), followed by sand application (30 g/m^2, 2-4 mm crushed rock). Between the cleanings, there were two periods where the runway was open for air traffic. The first period started at 16:50 and lasted 43 minutes. The surface conditions were described as: "up to 8 mm dry snow on sanded ice, 100 % coverage, braking action 20 / 23 / 29 (poor / poor / poor-medium)". Six aircraft movements took place, before the second snow cleaning operation was initiated. This required about 20 minutes of runway closure time. The second period (starting approximately at 17:55) lasted 39 minutes and the surface conditions were described as "up to 8 mm dry snow on ice, 100% coverage, braking action 30 / 33 / 30 (medium / medium / medium)". Also in this period, six aircraft movements took place.

The friction measurements were taken at the end of each cleaning operation, just before the runway reopened for air traffic. During these measurements there was virtually no loose snow on the runway. While the runway was open for air traffic, it became progressively contaminated with freshly fallen snow. The snow deposited initially uniformly, but it became displaced by the engine thrust of the operating aircraft. This

changed the consistency into lumps with a typical diameter of a few centimetres. Aircraft operated on a runway that was considerably more contaminated, compared to the surface conditions during the friction measurements. This is illustrated in Fig. 3-4 where the surface conditions are shown during the friction measurements at 17:53 and 27 minutes later, after the landing of a Boeing 737.

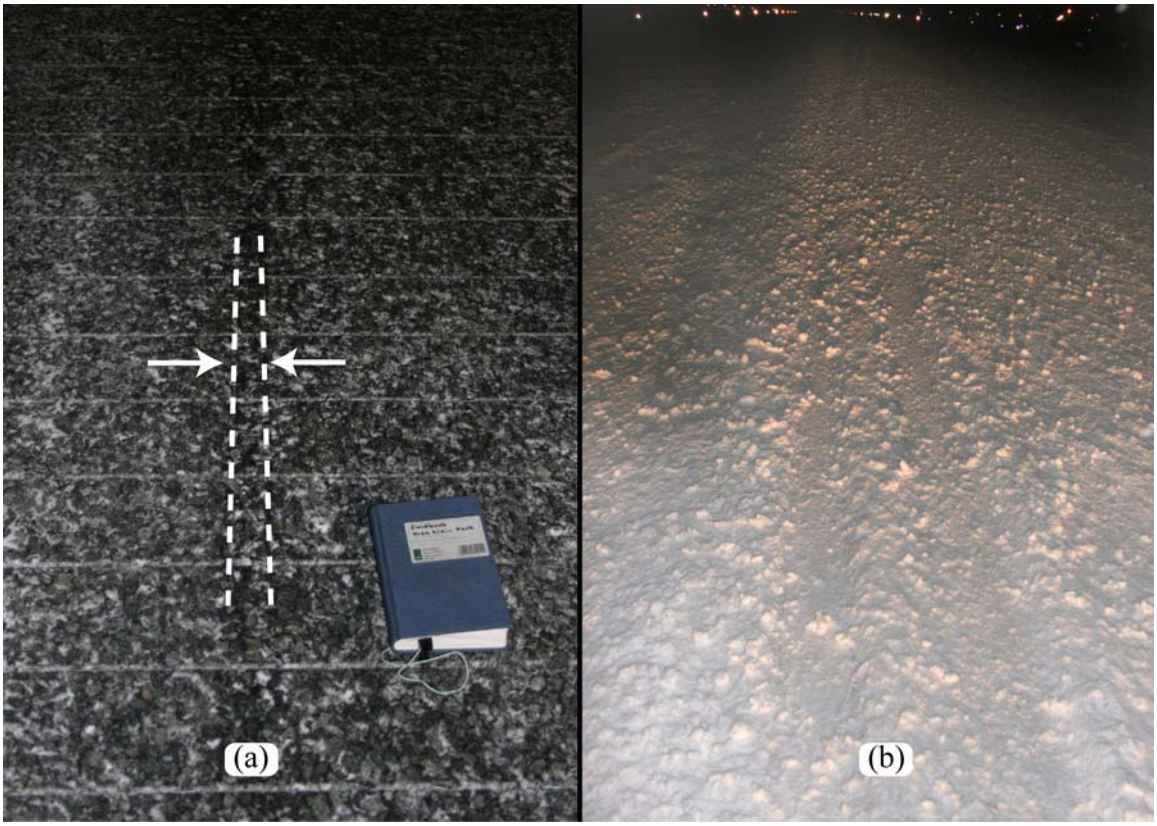

Figure 3-4. The tire tracks and runway surface conditions (a) during friction measurements and (b) 27 minutes later, after landing of a Boeing 737. The dashed lines in (a) marks the location of the test tire track.

3.4.2 Case: sand displacement

Tromsø Airport, January 26, 2005, 07:00-10:00 GMT

Weather and runway conditions

The observation day was the second mild day ($T_a \approx 0$°C) after a colder period. The temperatures at the beginning of the observations (T_a = -2°C, $T_d = T_{ps}$ = -4°C) decreased about 1°C during the three-hour observation period. It had been snowing for about 36 hours in several showers and the runway was cleaned seven times. The mild weather, the colder runway, and the frequent snow showers contributed to the build up of compacted snow and ice on the runway.

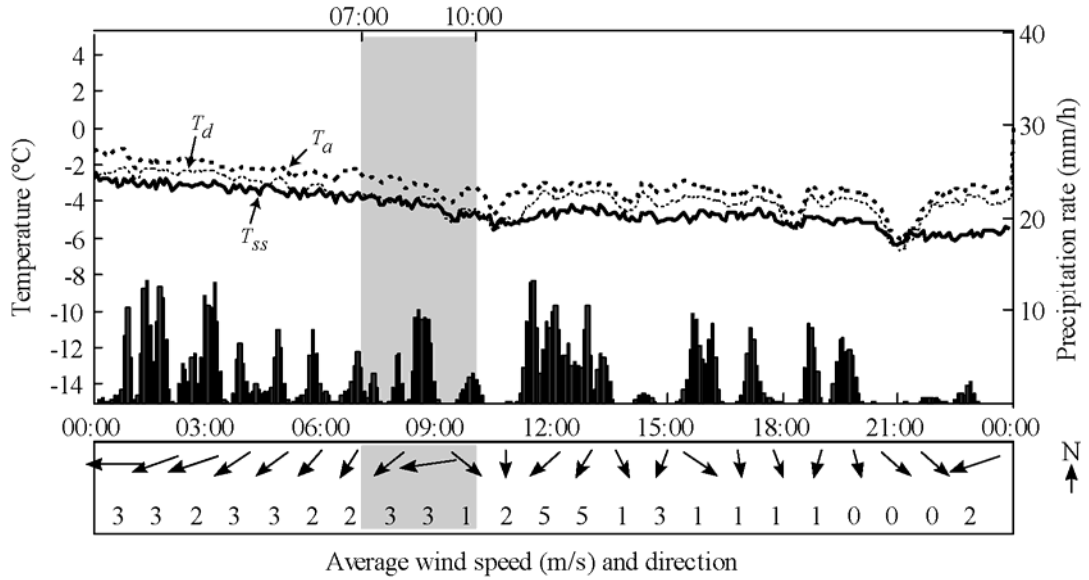

Figure 3-5. Meteorological data Tromsø Airport January 26, 2005.

Observations

The preparation of the runway at 7:15 (using sweepers and sand application at 30 g/m^2) was not sufficient to obtain acceptable braking action. The measurements (NA[3] / 13 / 16) were aborted before completion and a second preparation run was initiated, again using sweepers and sand application. This time, 33% more sand was applied (40 g/m^2). The measured braking action (31 / 31 / 31) doubled by the second treatment. These measurements indicated a medium braking action. The runway opened for air traffic at 8:00.

Two take-offs and one landing took place within 10 minutes. Examination of the runway conditions at 8:11 revealed that the sand was blown to the sides by the operating aircraft (Fig. 3-6). Hence, the efforts to improve the surface conditions by sanding only had short-term effect. Air traffic continued (two landings and one take-off) and at 8:55 the runway status report was updated: "8 mm dry snow on sanded ice, braking action 23 / 19 / 24" (poor / poor / poor). At 9:10 a new runway cleaning was initiated.

[3] NA: Not Available due to aborted measurements.

Figure 3-6. The runway surface conditions on January 26 (a) during friction measurements at 08:00 and (b) 11 minutes later, after three aircraft movements. The sand, initially uniformly distributed has been blown to the sides and towards the centreline. The regions with sand are indicated by dashed lines.

3.4.3 Case: snow compaction

Tromsø Airport, January 15, 2005 14:00 – 15:45 GMT

Weather and runway conditions

During the day it snowed in separate showers and the air temperature fluctuated around -2°C (T_d = T_{ps} = -4°C). The runway had been swept and sanded several times in the 24 hours before the observations. The asphalt pores were filled with compacted snow but the top of the aggregates was still visible.

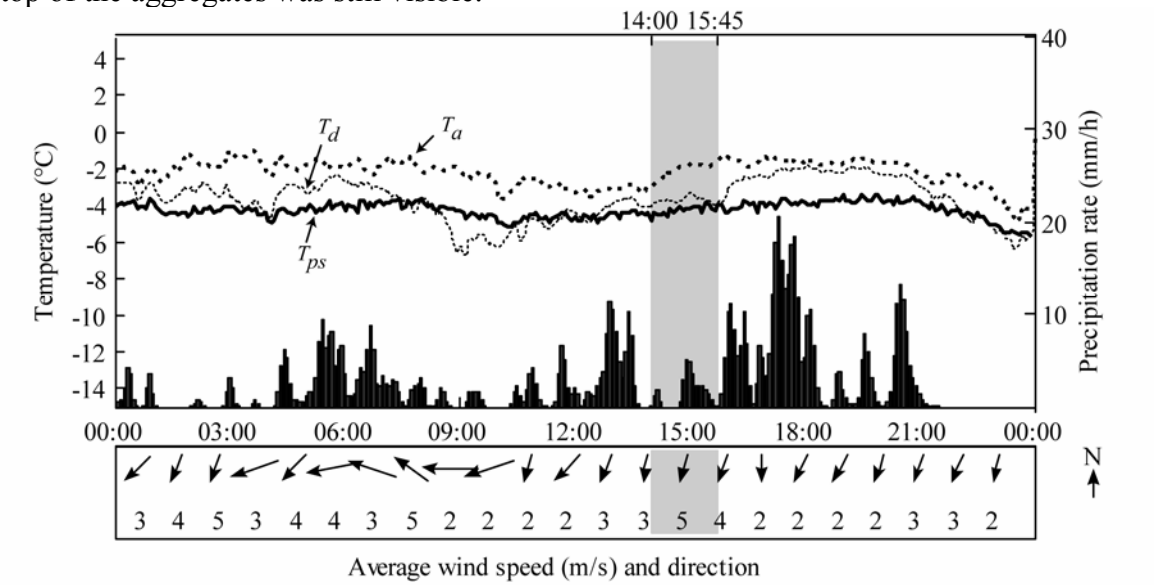

Figure 3-7. Meteorological data Tromsø Airport January 15, 2005.

Observations

At around 14:25 the runway opened for air traffic after a cleaning operation. During the cleaning it had stopped snowing and 10 minutes prior to the first landing, a Boeing 737-500, it started snowing again. The wind was calm and snow deposited uniformly on the runway. The aircraft landed at 14:57 on an undisturbed snow layer, about 10 mm thick (T_s = -2.6°C, T_a = -2.8°C, T_p = -3.1°C, ρ_s = 120 kg/m^3). After landing, the tire track of the right landing gear was photographed at different locations, indicated in Fig. 3-8.

The track exhibited differences in snow compaction and snow displacement, depending on the landing phase. Close to touchdown (Fig. 3-9a) there was little snow present in the track. Outside the track, the snow appeared almost undisturbed. In the main retardation phase some compaction occurred but most snow was displaced a few meters aside the track. The aircraft used reversed thrust at this stage of the landing. The compacted snow can be seen as white stripes in (Fig. 3-9b). The track became covered with blowing snow after the aircraft had past. During taxiing (Fig. 3-9c and 3-9d) snow was compacted to a continuous layer with embedded sand particles. The loose snow, seen in Fig. 9c, was blown on the track after the aircraft had past.

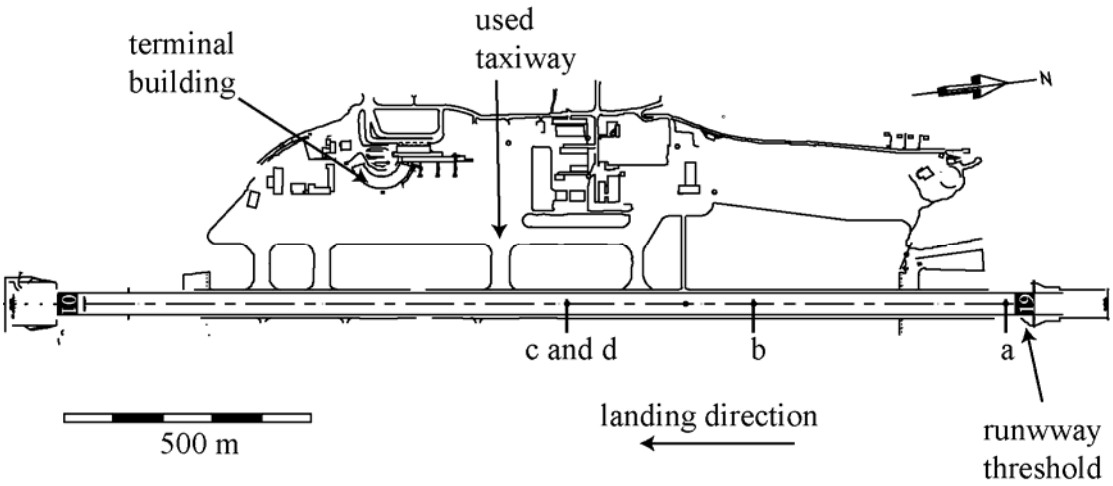

Figure 3-8. Map of Tromsø Airport with the locations of the photographs in Fig. 3-9.

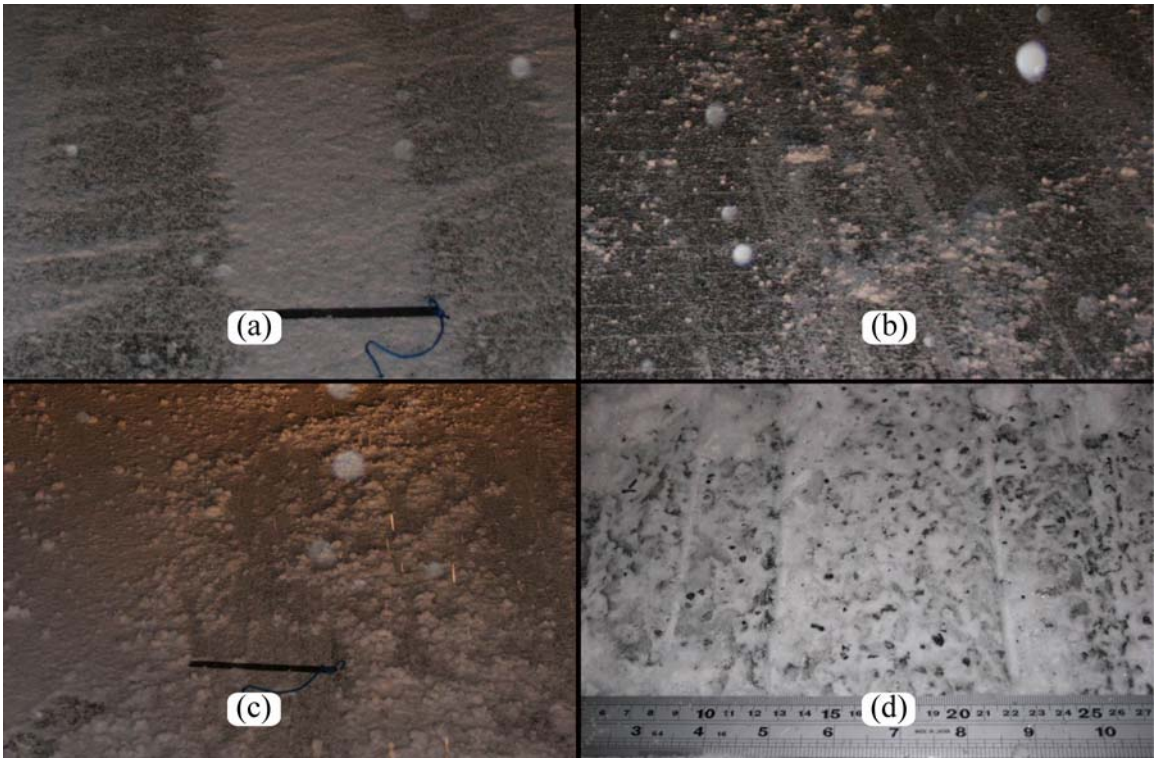

Figure 3-9. The snow compaction at different stages of the landing: (a) Close to the point of touchdown. A ruler (30 cm long) indicates the scale. (b) The main retardation phase, where the aircraft used reversed thrust. (c) During taxiing. (d) Detail at the same location as (c). Here, the snow mainly compacted during taxiing into a continuous layer with embedded sand particles.

3.4.4 Case: decaying ice

Tromsø Airport, February 6, 2005 11:25 – 14:50 GMT

Weather and runway conditions

The day started with several wet snowfalls. The snow was difficult to remove and a persistent layer of compacted (wet) snow and ice covered most of the asphalt texture. This layer was filled with sand particles that had been applied after the several cleaning operations. The air temperature rose above 0°C and the contamination layer started to decay.

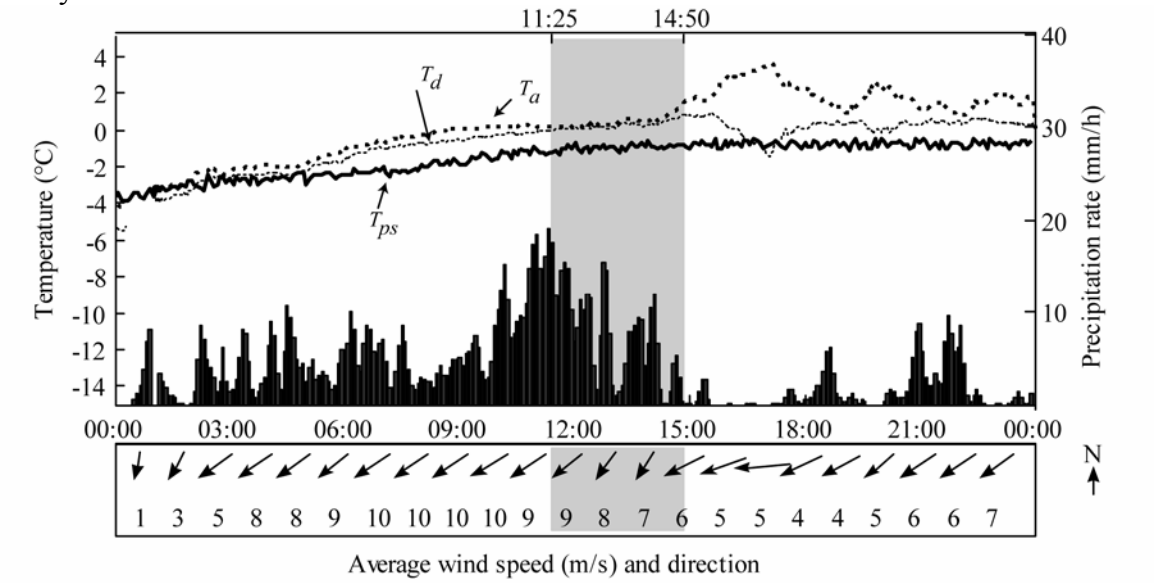

Figure 3-10. Meteorological data Tromsø Airport February 6, 2005.

Observations

At the beginning of the observation period, the runway was covered with wet, compacted snow. During friction measurements at 11:42 (braking action: 37 / 32 / 32), the sand particles that became trapped under the test tire were found embedded in the compacted snow (Fig. 3-11a). The first signs of changes in the behaviour of the contamination layer were observed at 12:27, in a track of a landing Boeing 737. Sand particles had broken loose, together with fragments compacted snow. Meanwhile, the runway contamination had started to change colour from white to grey, which became more pronounced after the sweeping at 12:53. During friction measurements at 13:13 (braking action: 36 / 34 / 33), a similar fragmentation of the contamination layer was observed in the track of the braking test tire (Fig. 3-11b). The fragments were larger (about 10-20 mm) than the sand particles (2-4 mm). At 13:21 a Dash-8 landed and the track showed an even more clear fragmentation. At some locations, the asphalt texture reappeared (Fig. 3-11c and 3-11d).

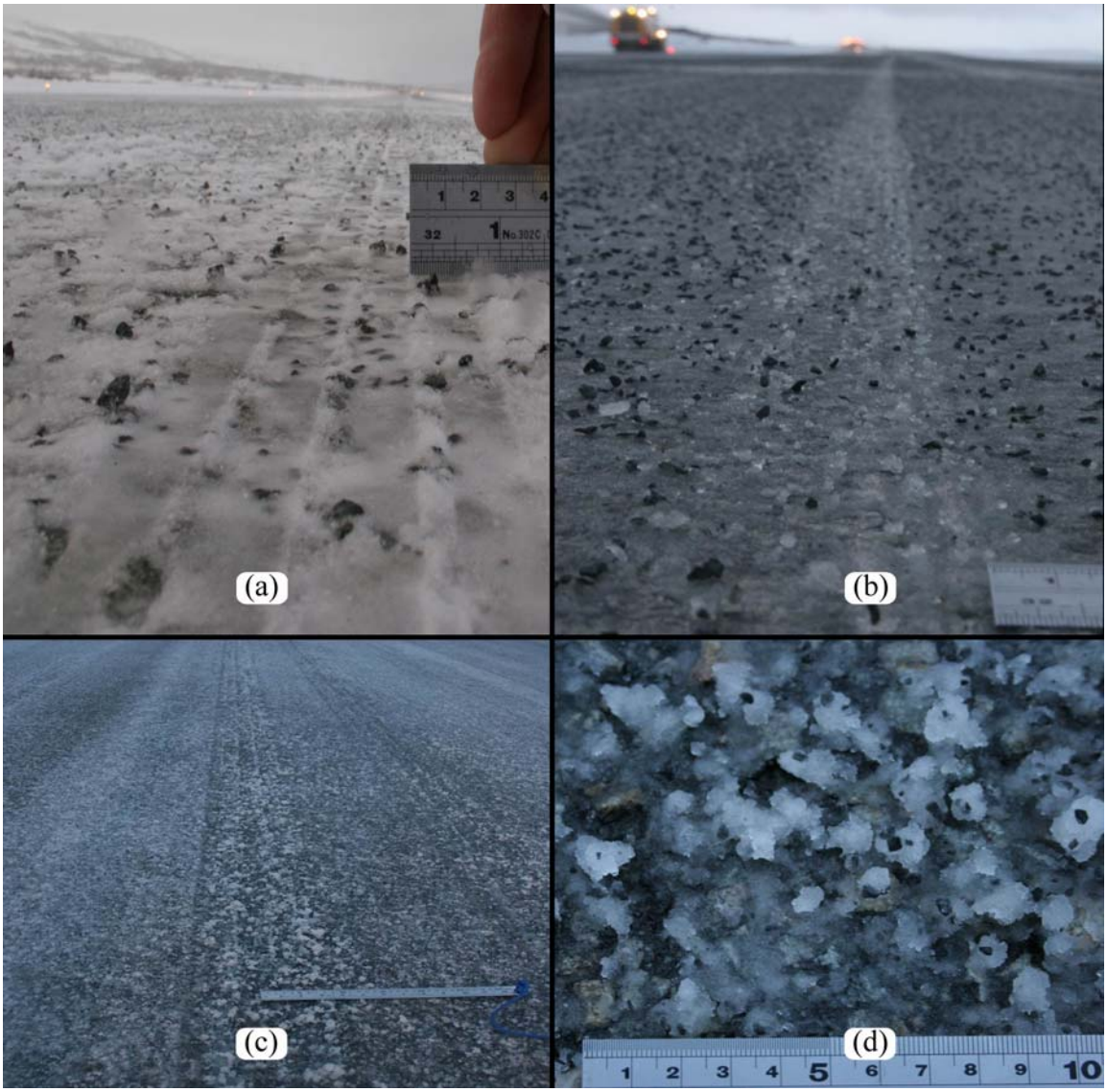

Figure 3-11. Tire tracks on the decaying contamination layer. (a) During the friction measurements at 11:42. The sand particles remained embedded in the track. (b) Friction measurement at 13:13. At this time, most particles broke loose together with ice fragments. (c) Fragmentation of the contamination layer by a landing Dash-8 at 13:21. (d) Detail of the fragmentation. Asphalt aggregates have become visible. Note that most fragmented pieces contain one or a few sand particles.

3.4.5 Case: ice deposition

Kirkenes Airport, February 24, 2005 08:23-20:00 GMT

Weather and runway conditions

The day was windy and the air temperature gradually decreased from 0°C at 0:00 to -7°C at 22:00.The runway was iced and treated with warm, pre-wetted sand. The braking action was reported as good, which was confirmed by two pilots that landed at 10:05 and 10:26, respectively. In the afternoon the weather changed: the humidity increased while the temperature decreased. It started snowing at around 16:00.

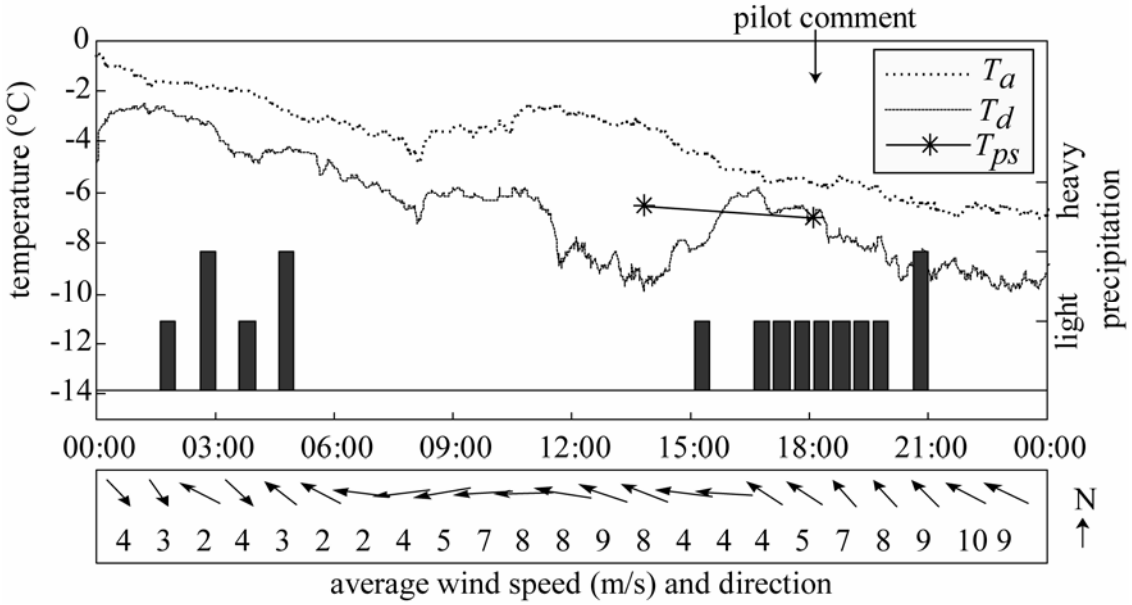

Figure 3-12. Meteorological data Kirkenes Airport February 24, 2005.

Observations

The runway was swept at 17:30 without additional sand application. The friction measurements taken at ±18:14 indicated good braking action (42 / 39 / 45). However, it was noticed that the surface felt slippery while walking on the runway. The test tire track is shown in Fig. 3-13a. It was noticed that a thin layer of ice had covered the pavement, which can be seen in the reflected light from the car head lights. A Dash-8 landed three minutes later and the pilot informed ATC that it was slippery. This pilot report was forwarded to the next incoming aircraft. The second Dash-8 landed at 18:27, without further commenting the conditions. At 18:27 the runway could be inspected. A Dash-8 track was found (determined from its dimensions), but it was not clear whether it originated was from the first or the second landing. The tire track is shown in Fig. 3-13b, where the ice layer can be seen. Note that there are no large sand particles in the vicinity of the track. Five minutes later, a third aircraft (a Saab 340) landed at 18:33.

When all three aircraft were parked, ATC asked the pilots from the second Dash-8 and the Saab how they perceived the braking action. Both replied: “It was OK.” Control friction measurements were performed at 18:34, with a new test tire. The measurements (39 / 40 / 43) consistently described the conditions as good. Maintenance personnel could not find any malfunction in the measurement equipment and it remained in-service where it functioned “normally”.

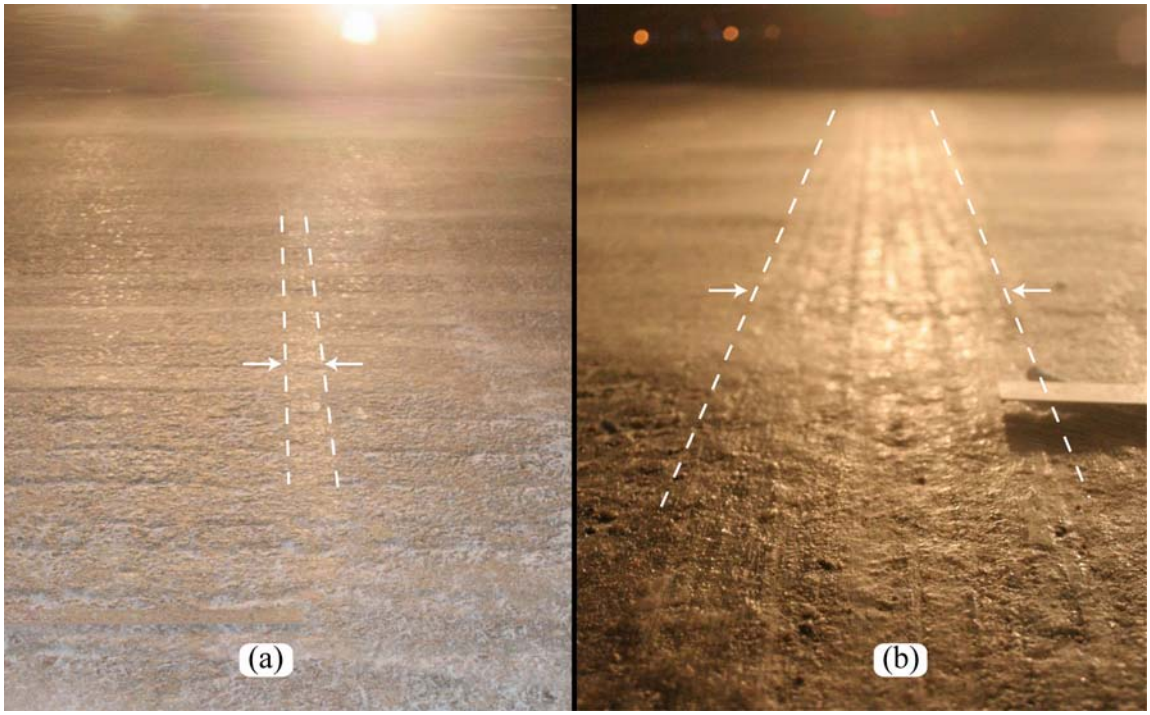

Figure 3-13. Tire tracks from (a) the friction measurements at 18:14 and (b) after the landing of a Dash-8, taken at 18:28. The dashed lines indicate where the tracks are located. The ice layer can be seen in both images. Note the blowing snow above the pavement, suggesting a high relative humidity, and the lack of large sand particles on the pavement.

3.4.6 Case: thin ice cover

Tromsø Airport, March 3, 2005 07:50-10:05 GMT

Weather and runway conditions

The day had several periods of snowfall and sunshine. At 8:19, the air temperature measured 150 mm above the runway surface was -6°C, and was increasing due to the heating by the sun. Throughout the day, the runway was swept 12 times and the runway status report was updated 14 times. The runway was contaminated with thin ice and compacted snow. Meteorological data were not available for this day.

Observations

The friction measurements taken at 07:58 and 08:57 indicated poor conditions: 23 / 24 / 25 and 25 / 25 / 24, respectively. Variability in runway contamination was evident while inspecting the runway (Fig. 3-14a). The contamination consisted of sections where snow was only located in the deeper parts of the asphalt texture, giving it a gray appearance, and sections where the aggregates were fully covered with compacted snow (wheel tracks). A large part of the runway area was covered with a very thin, transparent layer of ice was present. The layer could be removed by scratching the surface and was less than 1 mm in thickness. The ice layer was clearly visible in the reflected sunlight (Fig. 3-14b). A detail of the layer, giving a smooth finish to the top aggregates is shown in Fig. 3-14c.

The measured surface temperature varied from -3.4°C to -1.1°C. A black surface area was about 1.2°C warmer than a white surface area. The thin ice cover was noticed while walking on the pavement. Throughout the observation period, air traffic continued as normal and ATC did not receive comments from pilots regarding the braking action.

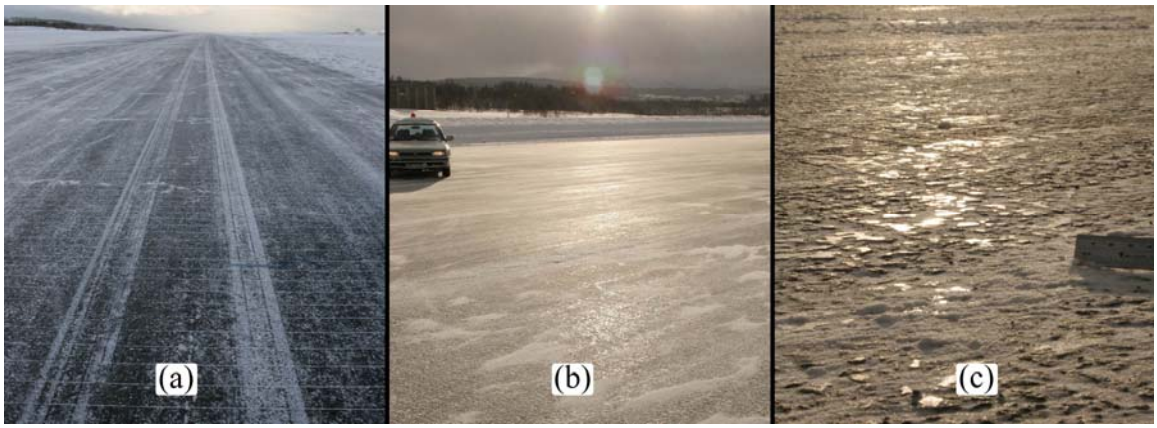

Figure 3-14. (a) Tracks of compacted snow resulted in spatial variability of the contamination. (b) The thin ice cover is visible by the reflected sunlight. (c) The asphalt texture is still visible and the top of the aggregates is covered with a thin layer of ice.

3.4.7 Update frequency of status reports

During the period between November 1, 2004 and March 31, 2005, Tromsø Airport generated 817 runway status reports. The average update frequency was 5.5 reports per day, which corresponds to an average report lifetime of 4.4 hours. The distribution of the report lifetime is shown in Fig. 3-15.

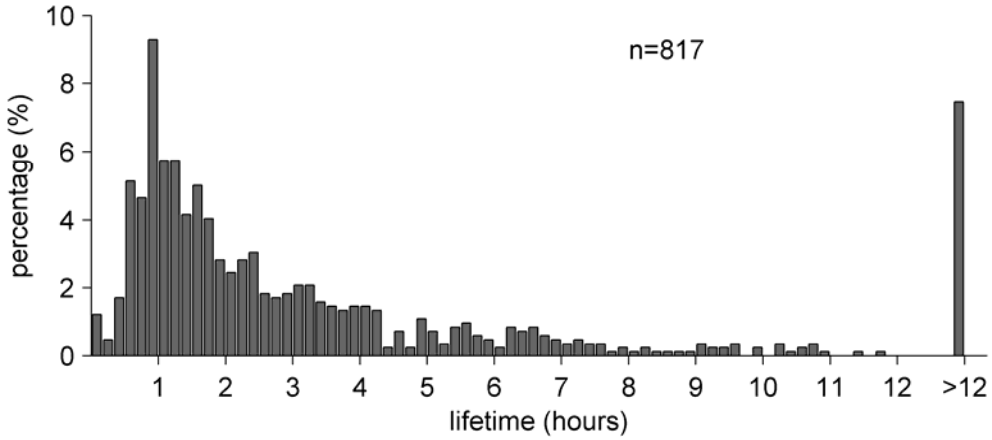

Figure 3-15. Distribution of report lifetime for all runway status reports generated at Tromsø Airport between November 1, 2004 and March 31, 2005.

In 97 reports (12 %) the runway surface conditions were described as "poor" or "unreliable" in at least one of the three runway sections. The average update frequency of these reports was 11 day $^{-1}$ which corresponds to an average lifetime 2.2 hours. The lifetime distribution of these reports is shown in Fig. 3-16.

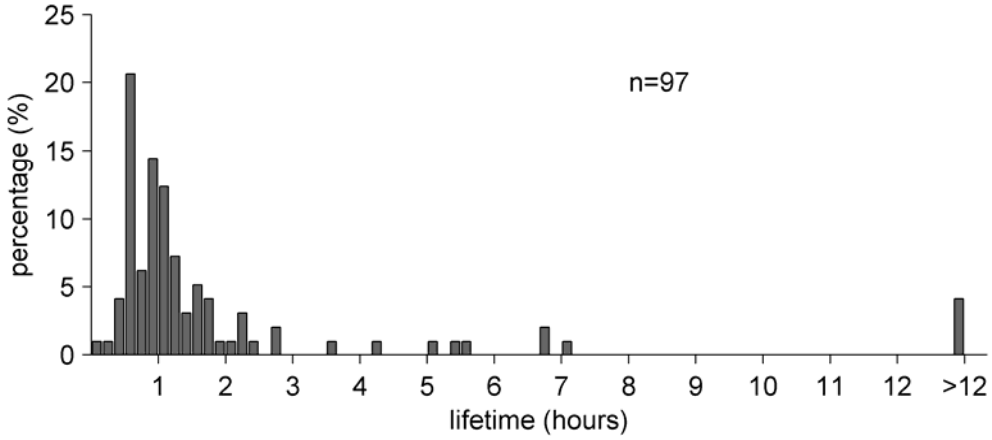

Figure 3-16. Distribution of report lifetime for runway status reports generated at Tromsø Airport between November 1, 2004 and March 31, 2005, when at least one runway section is described as "poor" or "unreliable".

3.5 Discussion

The cases illustrated different ways how runway surface conditions changed: by snow fall, the displacement of sand by operating aircraft, by the deposition of ice for the air above the pavement, by the compaction of snow, and by melting. There are of course other processes that can change runway surface conditions (for example freezing of a wet runway) but they were not observed during the study. First, the consequences for runway operability will be discussed for the individual cases, followed by discussion on general aspects that can be derived from the study.

The cases “heavy snowfall” and “sand displacement” are two examples where the runway surface conditions rapidly changed in time. The pilots clearly experienced different (worse) conditions than reported in the status report. From the photographs (Fig. 3-4 and 3-6) it is evident that the measured friction numbers had no relation to the actual conditions at the time the photographs were taken. Hence, the friction numbers were found not valid after 27 and 11 minutes, respectively. The result was that the reported information gave a too optimistic picture of the actual situation.

The case “snow compaction” showed how the landing of one aircraft created compacted snow. Snow compaction results in persistent runway contaminations that cannot be removed by runway sweepers. It thereby hampers the objective to maintain the runway surface conditions in an acceptable state. The interesting aspect of the observation was that it was mainly during taxiing that most snow was compacted. This observation can be rationalized by the longer loading time of the snow, the higher load on the snow (little aerodynamic lift) and no reversed engine trust that can blow loose snow away before it gets compacted. Taxiing on the runway is significantly reduced when the airport has taxiways connecting the aprons to the runway thresholds.

When the weather becomes mild, the contamination changes more rapidly, specifically when the melting point of ice is reached. This involves a rather rapid change in the mechanical properties of the layer. Such transition is illustrated in the case “decaying ice”. The compacted snow and ice that had formed days, maybe even weeks earlier started to melt. The friction measurement described the conditions as “medium” and “medium to good” throughout the time of observation. Since no pilot comments were received, it appears that the conditions indeed have been acceptable throughout the observed transition. The case therefore does not show direct problems for runway operability. But it did show a clear change in the properties of the ice. So despite the “medium” or “medium to good” measurements, it was not a stable situation. The changing conditions justifies (even requires) a higher level of alertness, compared to more stable situations where the conditions are also described as “medium” or “medium to good”.

The case “ice deposition” was probably the clearest example of a situation where the airport operator failed to accurately report the actual surface conditions. The runway was prepared; the friction measurements described the surface as “good”; and yet a pilot reports that it is slippery. The noticed slipperiness of the surface (by walking on it), and the photographs of the ice layer (Fig. 3-13) leave little doubt that the conditions were indeed significantly worse than reported. But why did the measurement fail to describe the surface correctly? Control measurements with a new test tire consistently described the surface as “good”, no malfunctions in the equipment were detected, and the device

remained in-service afterwards where it functioned normally. It appears therefore that the known correlation issue was the most probable cause for the discrepancy between reported and experienced conditions. Earlier that day the conditions were also reported as "good" and pilots did not complain. Hence the question arises why did the runway surface conditions change?

It was noticed that the weather changed in the afternoon and that it started to snow around 16:00, about 2 hours prior to the pilot comment. From Fig. 3-12 it can be seen that the humidity increased significantly during this period and exceeded the sub-surface temperature of the pavement. Although the real surface temperature was not recorded, it suggests that the air above the pavement became oversaturated, relative to the surface temperature. This creates the conditions for water vapour deposit (as ice) onto the runway.

The case "thin ice cover" shows a surface that was reported as "poor" throughout the observation period of 2 hours. But despite these reported conditions, air traffic continued as normal and the pilots did not comment the braking action. Apparently, other factors were favourable (for example cross wind, visibility, landing weight, etc.) that allowed the pilots to accept the poor surface conditions and continued to operate. ATC did not receice any pilot comments. This makes it difficult to get any reference how good, or poor the conditions were for aircraft. But the case showed a situation where the air traffic continued "normally", even though the conditions were reported as "poor".

The cases presented in this study are not more than a few snapshots of the whole winter season on an airport. But general aspects of runway operability under cold weather conditions can be derived from the study as a whole.

The surface conditions reporting system is first of all intended to give pilots, air traffic controllers, and maintenance personnel a correct mental picture of the situation. This is an important element in safe and efficient airport operation and is called "situation awareness". The reporting system is based on describing the status at a given point in time in a compact package of information. How long this information stays valid, depend on how quickly the surface conditions change. ICAO specifies that the information is to be updated when the surface conditions have changed significantly (outlined in Chapter 2). It specifies different "significant changes" that require an update.

Identification of significant changes requires monitoring. The surface conditions and the weather are to be monitored while the runway is open for air traffic. But while performing this study it was clearly noticed monitoring the conditions is not easy when the runway is open for air traffic. In order to inspect the runway, ATC has to temporary close the runway for air traffic and give clearance to enter the area with a ground vehicle. Inspecting a runway takes time. To inspect a 2000 m runway at 65 km/h on both sides of the centreline takes about four to five minutes. Hence the runway cannot always be inspected before each landing or take-off because it would cause significant delays in the scheduled air traffic. This means that the inspection frequency of the runway surface is constrained. The analysis of the update frequency of status reports shows that very few reports (6%) are updated within 30 minutes, even though the conditions were reported as "poor". But the case "heavy snowfall" and particularly the case "sand displacement" showed how quickly surface conditions can have changed.

How successful the airport operator is in accurately reporting the actual conditions thus depends mainly on the alertness of the person in charge of monitoring the surface conditions. The same monitoring task was performed during this study. It was attempted to document as detailed as possible how runway surface conditions change. The arrangements at the airport were such that the observer and a ground vehicle were fully dedicated to the monitoring task. Air Traffic Control was cooperating by allowing as much runway inspections as possible between the operating aircraft, accepting thereby a significant additional workload. It was an ideal setting to perform the monitoring. Yet, it was felt very difficult to have a full overview of the surface conditions on the 2000 m long runway. The means for monitoring the runway surface conditions while it is operative are very limited. It is therefore not possible to immediately identify significant changes. Efforts to improve runway operability under winter conditions, and particularly the reporting system should address this issue.

The rapidly changing surface conditions and the limited update frequency of status reports that were documented in this study are not unknown issues: "It is a known problem that sand can be blown of the runway by wind or engine thrust" (FAA, 1991; Comfort and Gong, 1999). "Canadian pilots indicate that the update frequency of status reports need improvement" (Biggs and Hamilton, 2002). "At issue: no research to support CRFI validity[4] beyond a few minutes" (Horrigan, 2004). The contribution of this study is therefore not the identification these issues itself, but the documentation of the issues and the consequences for runway operability.

When a reporting system is envisioned that performs well within the practical constrains of the airport, it should have the following features:

- An indication for the required alertness (ie. measure for probability for significant changes to occur).
- Better means of continuously monitoring the surface conditions.
- A prediction for the nearby future, rather than a status report.

3.6 Conclusion

Situations were documented where the runway surface conditions changed due to snow fall, sand displacement by aircraft, ice deposition, snow compaction and melting.

Clear significant changes in runway surface conditions were documented shortly (11 and 27 minutes) after the conditions were reported. These changes made the reported information invalid.

Practical constrains such as the time required for performing friction measurements and required clearance procedures to enter the runway area restricts the inspection frequency of the runway.

The current possibilities to monitor runway surface conditions are limited while the runway is open for air traffic. Significant changes can therefore not always be immediately detected and reported.

[4] The validity of the Canadian Runway Friction Index (CRFI). This index is based on the readings from the Electronic Recording Decellerometer (ERD).

4 FRICTION MECHANISMS DURING TIRE-PAVEMENT INTERACTION

Ice was slippery when I was born, I never knew otherwise, and to put it shortly, it was slippery because it was ice. Osborne Reynolds, 1901

4.1 Introduction

The complexity of the runway surface conditions can be overwhelming. The observations presented in Chapter 3 give not more than a glimpse of the diversity of runway contaminations. The contamination layer can consist of water, snow, ice, and rubber deposits, occurring in various combinations and consistencies. Additionally there can be chemicals and sand present that have been applied as winter maintenance measures. The properties of the layer vary both in space and time. Despite this complexity, somebody or some instrument has to assess how much tire-pavement friction can be obtained by the aircraft. Hence, an understanding of the tribological interaction processes has to be developed (Sinha, 1999; Sinha, 2004), in order to interpret that instrument, assist and educate that person, and improve decision supporting systems. The objective of this chapter is to contribute to this understanding by giving an overview of theories on tribological processes that are applicable to tire-pavement interaction on contaminated pavement.

Tire-pavement interaction is a complex phenomenon, in the sense that many different physical processes act simultaneously. Tire deflections, heat generation in the tire, deformations in the pavement, and the friction between the rubber tread and pavement are just a few of the processes that constitute the whole interaction. The presence of snow, ice, water, sand, and chemicals makes the interaction even more complex. A common approach to developing an understanding of complex systems as a whole is to study the elements of the system and their interactions individually (reductionism). This approach is also adopted here, but it is first attempted to give a holistic description of the whole system, before concentrating to some of its elements and some of the interactions between the elements.

The chapter therefore starts by describing the relevant forces on an aircraft landing gear that gives an aircraft retardation and directional control. It is followed by describing the tire in contact with the contaminated pavement as a mechanical system, called the tribosystem. Relevant triboelements are identified and different scales of view are explained. It then solely concentrates on the frictional interaction that occurs within the contact area. It briefly describes friction theories on dry and wet pavements, as an introduction, but concentrates on iced pavements. Iced runways are usually improved by applying sand. The role of sand particles in creating friction is therefore considered. The focus on iced pavements was motivated by its common occurrence on Norwegian movement areas. “Ice” and “dry snow on ice” were the two most frequently reported runway surface conditions at Tromsø Airport during the winter 2004-2005, together occurring 41 % of the total winter season (Klein-Paste and Sinha, 2006).

The description of friction theories is categorized under the headers “rubber friction”, “ice friction”, and “sand friction”. Each section starts with a brief description of the respective material. It is followed by an overview of experimental work on rubber-ice friction. Finally, a few observations from the field are included to illustrate some of the friction mechanisms.

4.2 Forces on a landing gear

Consider an aircraft landing gear that travels in contact with the pavement along the pavement length axis (see Fig. 4-1). The *x*-direction of the Cartesian coordinate system is placed along the travel direction of the aircraft. The *y*-direction is perpendicular to the travel direction, within the pavement surface plane. Two interaction modes can be distinguished: (1) free-rolling tires, and (2) a braking tires.

A pneumatic tire consists of a structural part, called the tire carcass, and a profiled layer of rubber, called the tire tread. The tire tread is the part of the tire that becomes in contact with the pavement. The region where close contact is made between the tire tread and the pavement is called the apparent contact area, or shortly contact area.

During free rolling (Fig. 4-1a), the tires experience a resistance force F_r, known as the rolling resistance force. The rolling resistance originate from deformations in the tire and acts on the wheel axis in the negative *x*-direction. Rolling resistance therefore contributes to the retardation and hampers the acceleration of the aircraft.

On a free-rolling tire, shear forces between tire and pavement can only be transferred in the *y*-direction (for simplicity it is assumed that the wheel bearings have negligible friction). An external force on the aircraft in the *y*-direction (for example cross-wind drag) can therefore by transferred to the pavement. In other words, the external force can be counterbalanced by a friction force in opposite *y*-direction. This friction force is denoted as the side friction force F_s. It is a force that gives the aircraft directional control. The normal force F_n on the landing gear originate from the gravitational force, reduced by the aerodynamic lift of the aircraft (Croll et al., 2002).

When the brakes are applied, the circumferential motion of the tires is resisted by the braking system. Now it is possible to transfer shear force the *x*-direction and the braking friction force F_b is generated in the contact area (Fig. 4-1b). This force is utilized to retard the aircraft. During braΦking, the total (resultant) friction force F_t is composed of F_b and F_s.

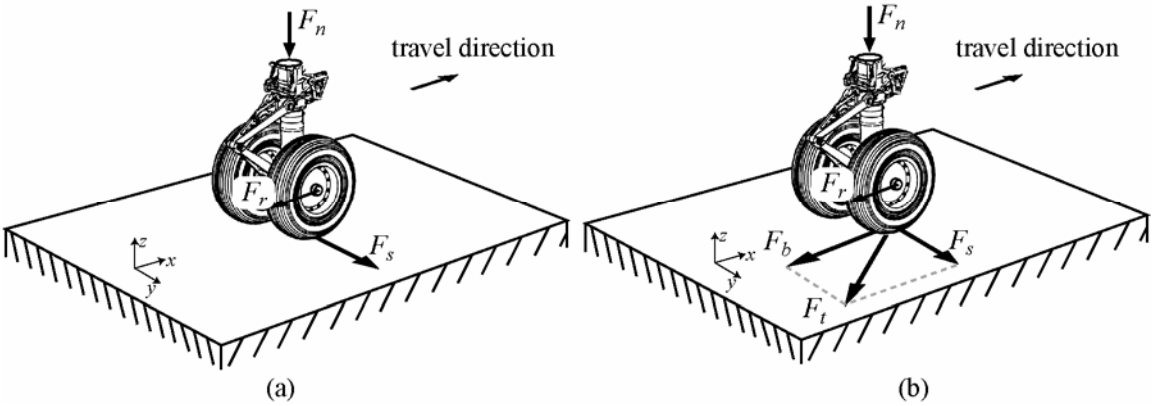

Figure 4-1 The main resistance forces acting on an aircraft tire: (a) during free-rolling, and (b) during braking.

Resisting the circumferential motion of the tire causes the tire to slip, relative to the pavement. The severity of the slip is commonly expressed by the slip ratio Φ (Pacejka, 2002):

$$\Phi = \frac{v_v - v_t}{v_v}, \tag{4.1}$$

where v_v is the vehicle velocity and v_t the velocity of the tire tread, both in the x-direction. Eq. 4.1 shows that $\Phi = 0$ corresponds to a free rolling tire and $\Phi = 1$ to a fully skidding (locked) tire. Hence, during braking, the tire is both rolling and sliding.

A slip ratio of $\Phi = 0$, however, does not imply that there is no slip in the contact area. The initially circular shaped tire tread has to comply with the nominally flat pavement. This can only be achieved when the tire tread slightly slips relative to the pavement. This type of slip is known as micro slip (Moore, 1975). The slip ratio described in Eq. 4.1 only refers to gross slip.

The magnitude of F_b is primarily determined by the severity of the braking. The pilot (or the auto-brake[5] system of the aircraft) therefore determines how much braking friction force is generated to retard the aircraft. There are, however, physical limits on the magnitude of friction forces (both F_b and F_s) that can be generated. These limits are denoted "attainable friction forces". It describes the maximum friction force that the aircraft can utilize for retardation and directional control. Pilots refer to these limits as the "braking action".

Tire-pavement friction is not the only source to obtain retardation and directional control. Retardation is also obtained by aerodynamic drag and engine thrust reversing and directional control is obtained from the tail and rudder. These sources are very effective at high travel speeds. At lower ground speeds, however, the effectiveness reduces. Aircraft therefore have most need for tire-pavement friction at low ground speeds, both for retardation and directional control.

4.3 Description of the tribosystem

So far, tire-pavement friction was considered as a force. A force that is necessary to give the aircraft retardation and directional control. It is common to consider friction as a force, as illustrated by the following definition of friction:*"* friction is the resistance to motion during sliding or rolling, that is experienced when one body moves tangentially over another with which it is in contact" (Bhushan, 1999).

But resistance to motion (the force) does not just simply exist. There occur physical processes in the contact area that cause the resistance. Friction can therefore also be considered as the interaction phenomenon that produce the resistance force, rather than a force itself (Zhang, 2004). In the case of the aircraft, friction forces result from the interaction between tire, pavement, contamination, and the environment in which the interaction takes place (Sinha and Norheim, 2000; Norheim et al., 2001). The collection of these four elements are known as a tribosystem, and the elements are referred to as triboelements (Czichos, 1978). The triboelements of a tire - pavement tribosystem are illustrated in Fig. 4-2.

[5] Auto-brake systems are systems where the pilot sets a desired level of retardation. The system controls the brake pressure to obtain this retardation.

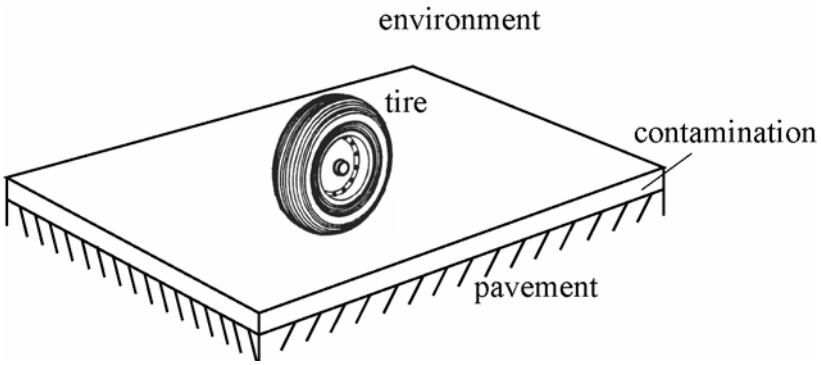

Figure 4-2. Schematic representation of the aircraft tire - pavement tribosystem and its triboelements.

The complexity of tire-pavement interaction can be overwhelming. Multiple physical processes occur simultaneously on different length scales. Therefore it is useful to have a general framework because it gives a reference where in the system a particular process occurs. It was outlined that the focus of this chapter was limited to ice contaminated pavements and how sand particles to create friction. This problem will be outlined with the tribosystem approach as framework.

4.4 General analysis of friction creation by sand particles

Consider the situation where a pavement is contaminated with a continuous ice layer. A tribosystem is formed when the tires of an aircraft come in contact with this pavement. Probably, the response of this system (the friction forces F_b and F_s) is insufficient to safely operate aircraft. Maintenance personnel now try to improve the pavement surface conditions by applying sand particles. The introduction of sand particles changes the interactions of the tribosystem. These interactions can be viewed on different length scales.

The macroscopic scale is the scale that shows the whole tire, rolling and/or sliding on the pavement. Here, the interaction starts with how particles enter the contact area. This process may be influenced by for example: (1) the slip ratio of the tire, and (2) the use of reversed engine thrust. Once inside the contact area, the interaction takes place on a smaller scale. This scale shows individual sand particles and will be denoted as the "sub-macroscopic scale". It is called sub-macroscopic because it is smaller than the whole tire, and yet large enough to be viewed without magnification aids. This view shows the particles that are trapped between the rubber tire tread and the ice, schematically represented in Fig. 4-3.

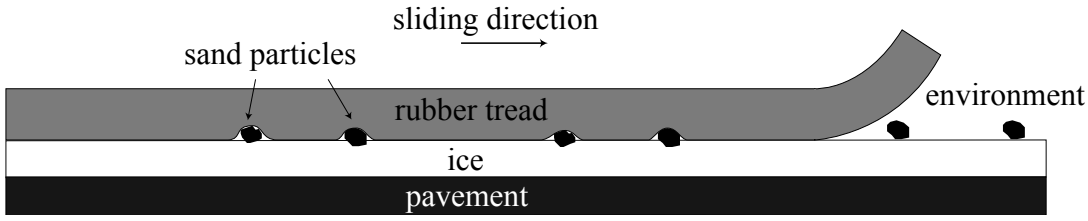

Figure 4-3. Schematic representation of the tribosystem on a sub-macroscopic scale.

Locally, the particles separate the rubber tread from the ice. Here, rubber-ice friction mechanisms are prevented and replaced by rubber-sand and sand-ice friction mechanisms. On this scale, the rubber tread rather than the whole tire is considered as an element. The sand particles are also considered as a separate element. The interaction is at this scale characterized by the following possible particle motions: (1) a rolling particle, (2) a particle fixed to the ice, (3) a particle fixed to the rubber tread, or (4) a particle that slides relative to both the rubber tread and the ice.

At a higher level of magnification, the microscopic scale, the interaction takes place between the surface asperities of the different triboelements. Here, the interaction is characterized by the (soft) rubber draping around sand or ice asperities, and by the indentation of sand asperities into the ice.

On again a higher level of magnification, the nanoscopic scale, the interaction takes place between the rubber (macro) molecules, the ice molecules and the molecules of the mineral from which the sand originates. On the microscopic and nanoscopic scale, other types of surface contaminations will also become visible, such as grease, oil, dust, and adsorbed gasses.

The response of the tribosystem, the friction forces F_b and F_s, will be different in the un-sanded and sanded situation. How effective the sanding is, depends on the friction mechanisms that were replaced and the total set of interactions in the two cases.

4.5 Friction theories

4.5.1 General concepts

Nearly all solid surfaces have a surface roughness that exceeds molecular dimensions. Intimate contact is made between the asperities of both surfaces when two solids are pressed against each other. Intimate contact is understood as the situation where asperities are in the range of attractive and repulsive contact forces. The real area of contact is therefore significantly smaller than the apparent contact area.

As outlined earlier, friction is the resistance to motion during sliding or rolling that is experienced when one body moves tangentially over another with which it is in contact. Static friction is the resistance against motion while there is no relative motion between the two surfaces. Kinetic friction, (also called dynamic friction or sliding friction) is the resistance against motion while there is relative motion between the two surfaces. It is customary to express the friction not as a force but as a friction coefficient μ, defined by Amonton's friction law (Amontons, 1699):

$$\mu = \frac{F_t}{F_n}, \tag{4.2}$$

This empirical law states that the friction force is directly proportional to the normal load, and that the friction coefficient is a constant. However, "It should be emphasized that μ is strictly constant only for a given pair of sliding materials under a given set of operating conditions (temperature, humidity, normal pressure and sliding velocity). Many materials show dependence of normal load, sliding velocity, and apparent area on the coefficient of static and kinetic friction in dry and lubricated contacts" (Bhushan, 1999).

Friction, lubrication, and wear are closely related to each other. As with friction, wear can be seen as the result of interaction mechanisms. It involves the structural damage to one or both surfaces, resulting in material loss or material transfer from one surface to the other. A high wear rate is usually accompanied with a high level of friction.

Lubrication is a process where friction and wear are reduced by an additional medium in the tribosystem. This interfacial medium can be a gas, liquid, or solid. In absence of a lubricating medium, the interaction of the two solids is also called “dry friction”. Full fluid-film lubrication is the situation where the solid surfaces are fully separated from each other by the lubricating medium.

There are different regimes of lubrication. Fluid-film lubrication is also called hydrodynamic lubrication. The surfaces are fully separated from each other and the friction arises from viscous deformation in the lubricating film. Elastohydrodynamic lubrication is a regime where the surfaces are still separated, but the pressures in the fluid film cause deformation of asperities in one or both surfaces. Mixed lubrication is a regime where most of the load is still carried by the fluid film but contact between the asperities frequently occurs. Boundary lubrication is the regime where the solids are separated only by a monomolecular layer, or a layer of only a few molecules thick.

4.5.2 Rubber friction

Rubber characteristics

The word “rubber” is often used to refer to a rubber compound, or in a broad sense as synonym for elastomer (Zhang, 2004). The term “elastomer” generally refers to a group of polymers with some common characteristics such as a low elastic modulus, viscoelasticity and glass transition temperature far below room temperature. Raw rubbers have limited applicability as engineering materials. To develop the required level of chemical and physical properties, they have to be mixed with various ingredients, shaped, and cured (Johnson, 2001). The result is a manufactured material, called rubber compound or vulcanizate. Rubber compounds are applied to form the carcass matrix and the tire tread of pneumatic tires. They typically consist of the following ingredients: (Gehman, 1971)

- The rubber, which may be a single polymer or a blend of polymers, and may include extending oil.
- Fillers, such as carbon-blacks.
- Softeners and plasticizers.
- The chemical vulcanization system.
- Chemically protective agents.

During curing, a chemical process called vulcanization introduces chemical cross-links, or bonds, between the long chain polymer molecules. The physical properties of the rubber compound depend upon the state of cure, that is, upon how far the chemical vulcanization reactions have been carried.

Rubber sliding friction on dry rough surfaces

Grosch (1963) conducted friction measurements with different rubber compounds on dry surfaces. It was shown that the friction coefficient, obtained at different sliding velocities and temperatures, could be described by a single master curve when the data was shifted

along the velocity axis by a factor $\log_{10} a_T$. This is known as the Williams, Landel, Ferry (WLF) transformation (1955) and the required shift factor is predicted by:

$$\log_{10} a_T = \frac{-8.86(T - T_r)}{101.5 + T - T_r}, \tag{4.3}$$

Where T is the temperature at which the data was obtained and T_r is a common reference temperature. The reference temperature was chosen 50°C below the glass transition temperature of the rubber. The viscoelastic properties of the rubber, measured as the complex modulus E^*, could also be described by a similar master curve. By using these master curves it was found that the ratio between the velocity of maximum friction and the frequency of maximum loss modulus E'' was a constant, irrespective of the rubber compound. Master curves were obtained on rough surfaces (silicon carbide paper) and on smoother surfaces (wavy glass). Measurements were included where the surfaces were dusted with fine magnesia powder to prevent direct contact.

It was concluded that the friction of rubber on dry surfaces is governed by the viscoelastic properties of the rubber and that two mechanisms contribute to the friction: the adhesion between the rubber and substrate and energy losses arising from the deformation of the rubber by surface asperities. Grosch pointed out that besides the normal hysteresis losses, energy could be lost when the stresses around tip of the asperity caused some rubber to detach from the bulk (rubber wear).

A review of adhesion theories for elastomers is given by Moore (1972). At a molecular scale, the adhesive resistance forces have been addressed to a cycle of bonding and detachment of rubber molecules with the substrate (Schallamach, 1963; Bartenev and El'kin, 1965). This bonding and breaking is a thermally activated process. The sliding is viewed as a molecularly stick-slip motion where a rubber macromolecule is stretched until the bond breaks. The molecule relaxes and jumps a certain distance before a new bond is formed. It is difficult, however, to predict the contribution of adhesive forces to during tire-pavement interaction due to contamination of the rubber with for example dust, grease or adsorbed gasses (Persson, 2000; Zhang, 2004).

Schallamach (1971) showed that sliding of rubber under the condition of high adhesion is accompanied with macroscopic waves of detachment. These waves are now known as Schallamach waves. They travel through the contact area from front to rear. No relative motion could be observed in between the waves, hence most gross displacement was provided by them. These observations are an example of the interaction between interface adhesion and bulk deformation. It shows that adhesion and deformation mechanisms are not necessarily independent of each other, as assumed by the general friction model of Bowden and Tabor (1954; 1964):

$$F_t = F_a + F_d, \tag{4.4}$$

where F_a is the friction force due to adhesion and F_d is the friction force due to deformation.

The contribution of hysteresis (bulk deformation) to the total sliding resistance force has been described in detail by Moore (1972; 1975). The low elastic modulus of the rubber

and its near incompressible properties (poissions ratio ≈ 0.5) causes the rubber to drape around surface asperities. The rubber undergoes cyclic compression and relaxation as it slides over the rough surface, dissipating energy inside the rubber tread. Persson (2001) considered these vibrations theoretically when rubber slides over a rigid rough surface that has a self affine fractal surface roughness. The topography (roughness) of self affine fractal surfaces ''looks the same'' when magnified by a scaling factor ζ in the *xy*-plane of the surface and by a factor ζ^H in the *z*-direction.

Rubber friction on wet rough surfaces

The tire-pavement interactions change when water is introduced into the tribosystem. The water acts as a liquid lubricant. Different lubrication regimes can occur, depending mainly on the amount of water entering the contact area. A very thin layer of water (maybe only a few molecules thick) creates the conditions for boundary lubrication, which affect the molecular adhesive interaction characteristics (Persson, 2000). It increases the distance between the two solids in intimate contact, and thereby preventing the adhesive forces which would otherwise take place (Johnson, 1985). With increasing water film thickness, two fluid dynamics phenomena become significant: squeeze films and elastohydrodynamic lubrication. There occurrence depends on the rolling mode of the tire.

In the free-rolling mode ($\Phi = 0$), the rubber tread approaches the pavement approximately vertically. The fluid will be squeezed out of the contact area, under the applied normal load. The water viscously resists this motion, exerting a pressure on the rubber (squeeze films), which partly carries the normal load of the tire (Moore, 1965; Moore, 1972). This process itself requires energy, hence, a new source of energy dissipation is created (Persson, 2000). However, the process also resists that rubber drapes around the surface asperities. The squeezing is time dependent and thus depends on the speed and the geometry (profile) of the tire tread. It takes longer for the rubber to drape around surface asperities, compared to a dry situation. The result is that within the contact areas there are regions where the tread is physically separated from the pavement by the film (Clark, 1971). Hence, despite the presence of a new source of energy dissipation (viscous deformation of the water film), the squeezing of water causes a reduction in hysteresis and lead in total to a reduction in the attainable friction force.

The situation is somewhat different in the braking mode ($\Phi > 0$). Here, the rubber slides relative to the pavement. Also in this case the water has to be squeezed out, but the rubber does not approach the pavement vertically. With the relative motion between the rubber tread and the pavement, a wedge-shaped spacing between the two surfaces can occur, creating the hydrodynamic pressure. The low elasticity of the tire and the rubber allows that the rubber can deform, creating a stable wedge shape, and thereby encouraging full-film lubrication (Persson, 2000). This effect is known as elastohydrodynamic lubrication. Fully developed elastohydrodynamic lubrication separates the whole tire tread from the pavement. This event is popularly referred to as "hydroplaning".

4.5.3 Ice friction

Ice characteristics

In its naturally occurring form (ice Ih), ice is a polycrystalline material with a hexagonal crystal structure. The H_20 molecules in the lattice are arranged such that each O atom is surrounded by four H atoms in a tetrahedral arrangement (Pauling, 1935), two closely

positioned at 1 Å (covalently bonded with the O atom) and two remotely positioned at 1.76 Å from neighbouring molecules (the hydrogen bond) (Bernal and Fowler, 1933). The molecules are all concentrated close to a series of parallel planes, known as basal planes (Hobbs, 1974). The axis normal to the basal plane is called the c-axis. Naturally, a lattice contains defects, which can be point defects (interstitials), line defects (dislocations), or planar defects (sub-grain or tilt boundaries). In polycrystalline state, the boundaries between the crystals (grains) can also be considered as large planar defects. These defects largely determine the mechanical behaviour of the material.

Ice usually exists at temperatures greater than $0.8T_m$, where T_m is the melting point in Kelvin. For solid materials it is convenient to express operating temperatures as the homologous temperature $T_{h,}$ defined by:

$$T_h = \frac{T}{T_m}, \tag{4.5}$$

In most practical cases, ice exists at temperatures above say -40°C. This corresponds to a homologous temperature of 0.85. Polycrystalline materials operating at homologous temperatures above 0.3 can be classified as "high-temperature" materials (Sinha and Norheim, 2000). Hence, from a material point of view, ice usually exists at very high temperatures. For comparison; stainless steel[6] that also exist at T_h = 0.85 would have a temperature of 1240°C. If it is natural to call stainless steel at 1240°C a high-temperature material, then it is equally logic to consider ice at -40°C as a high-temperature material.

At high temperatures, the mechanical responses (deformation) of a material are different from the responses at low temperatures. Many deformation processes are thermally activated and thereby a exhibit time- (rate-sensitivity) and temperature dependency (e.g. Sinha, 1981; Sinha, 1984). The continuous, macroscopic mechanical behaviour of polycrystalline ice to an externally applied load can be divided into an elastic, delayed elastic and viscous response (Sinha, 1978b; Sinha, 1978c). Elastic deformation is due to recoverable changes in intermolecular distances (Hobbs, 1974), delayed elasticity is related to time-dependent, recoverable grain boundary sliding (Sinha, 1979), and viscous, permanent deformation is due to motion of dislocations (Higashi, 1988).

On operational runways, ice can form in different ways: (1) by the freezing of a wet pavement or (supercooled) rain on a cold pavement, (2) by atmospheric water vapour deposition, (3) by the deposition, compaction, and sintering of snow, or (4) by a thaw-refreeze cycle of snow. These mechanisms can produce ice with a wide range of microstructural characteristics and thus with a wide range of mechanical properties.

Theories on ice friction

The sliding friction between ice and other materials are typically in the range of lubricated tribosystems. Hence, the view that the friction between solids on ice is somehow a lubricated phenomenon has dominated for more than a century. Reynolds (1901) suggested that pressure melting could cause a lubricating water film on the ice. The depression ΔT_m of the equilibrium melting point of ice caused by the pressure p is given by the Clausius-Clapeyron equation as (Hobbs, 1974):

[6] Used melting point: T_m = 1780 K

$$\Delta T_m = p\frac{\Delta V}{\Delta S} \approx 0.0074 \quad °C/10^5\ Nm^{-2}, \tag{4.6}$$

where ΔV and ΔS are the change in volume and entropy respectively. This equation predicts that a melting point depression of 10°C requires a pressure of 135 MPa.

The main objection against the pressure melting theory, as given by Bowden and Hughes (1939), is that although local pressures can be significantly higher than the nominal contact pressure (due to the surface roughness of the mating surfaces), the ice asperities will have deformed long before contact pressures are reached a level that significantly depresses the melting point. Hence, pressure melting is expected to be only significant when the ice temperature is close to T_m, say $T \leq$ -1°C.

The frictional heating theory (Bowden and Hughes, 1939) states that the generation of heat (dissipated frictional work) is a more likely explanation for the creation of a lubricating water film. This theory implies that the friction phenomenon is basically thermodynamically controlled and that the friction is directly related to the conductivity of the slider k_s, the ice temperature, and the sliding velocity. They conducted a series of experiments with a turntable tribometer at a maximum sliding velocity v of 4 m/s and found support for their theory.

Evans et al. (1976) developed the theory by considering three routes of energy dissipation: (1) conduction of heat into the slider, (2) conduction of heat into the ice, and (3) heat used to melt the surface layer. Note that this approach does not consider the actual frictional mechanisms; it does not specify *how* the friction is generated, but calculates the kinetic friction coefficient on the basis of the thermodynamics involved and the assumption that the interface is at a constant and known temperature of 0°C. They arrived at the following expression:

$$\mu = \frac{\alpha k_s (T_m - T_{i,0})}{F_n v} + \frac{\beta (T_m - T_{i,0})}{F_n v^{1/2}} + \mu_m, \quad \beta = 1.74 k_i w_c (l_c/\pi D)^{1/2}, \tag{4.7}$$

where α is a constant depending on the size of the apparent contact area, and on the geometry and nature of the slider, $T_{i,0}$ is the ice temperature at infinite distance from the interface, μ_m is the contribution to the friction coefficient due to required energy to melt the surface layer, k_i is the thermal conductivity of ice, l_c and w_c are the maximum length and width of the contact area, respectively, and D is the thermal diffusivity of ice. The upper limit of μ_m was derived from their experimental data and was found to give a minor contribution to the total friction force ($\mu_m \leq 0.005$), the water film thickness would not exceed a few μm, and viscous shearing could not be the mechanism that produces the friction.

Oksanen and Keinonen (1982) and Oksanen (1983) quantified the theory further and arrived at the following expression:

$$\begin{aligned} \mu &= n^{1/4} H_i^{-3/4} F_n^{-1/4} \left\{ \frac{1}{2} \frac{1}{(2v)^{1/2}} K + \left(\frac{1}{8v} K^2 + \eta v q_h \rho_w \right)^{1/2} \right\}, \\ K &= \Delta T_1 (\kappa_1 c_{p1} \rho_1)^{1/2} + \Delta T_2 (\kappa_2 c_{p2} \rho_2)^{1/2} \end{aligned} \tag{4.8}$$

where n is the number of contact points, H_i the indentation hardness of ice, η the viscosity of water, q_h the latent heat of fusion of ice, and ρ_w is the density of water.

Subscripts 1 and 2 refer to the ice and the slider material, respectively. ΔT is the temperature difference between the interface and the bulk, κ is the thermal conductivity, c_p the specific thermal capacity and ρ the density.

The frictional heating theory have been criticized (e.g. Niven, 1959; Niven, 1963; Tusima, 1977) but remains widely supported (e.g. Fowler and Bejan, 1993; Colbeck, 1994; Liang et al., 2003; Dash, 2003; Makkonen, 2003). Calculation of the film thickness, based on a Newtonian fluid gives rather low values (compared to the surface roughness), and this had led to different conclusions (Makkonen, 1994): Evans et al (1976) considered the sliding as a mixed lubrication case, hence a part of the resistance originate from solid-solid interaction of surface asperities. Akkok et al. (1987) suggested that the ice would soften rather than melt, and Derjaguin (1986) concluded that the layer did not behave like a viscous liquid, but like plastic bodies possessing definite slip planes.

Experimental evidence on the existence of the water film appears controversial and is limited to temperatures close to the melting point. Bowden and Hughes (1939) attempted to proof the existence of the water film by means of electrical conductivity measurements. Two electrodes were mounted in a model ebonite ski (15 mm long, 5 mm wide) with a spacing of 2 mm. The ice track was made by rapid freezing of 0.5 % potassium chloride solution in a turntable type tribometer. The normal load and sliding velocity were not reported (maximum F_n and v of the experimental set-up were 10^3 g and 4 m/s, respectively). The cold ice surface was allowed to warm up during the sliding, while the conductivity was measured. The conductivity was less than $5 \cdot 10^{-7}\ \Omega^{-1}$ when the surfaces were cold. The conductivity showed at first little change. It was interpreted as that the melting took place only locally at isolated points of contact. In the neighbourhood of the melting point (actual temperature was not specified) there was a sudden rise in the conductivity to about $5 \cdot 10^{-5}\ \Omega^{-1}$ ($\mu \approx 0.03$). This was interpreted as that the film had become continuous. They made a rough estimate of the layer thickness in the order of 70 μm, assuming that the water film had a similar ionic concentration as the water to make the ice.

Aside from the validity of the assumptions and the estimated film thickness, a more fundamental question has to be raised regarding the validity of the interpretation of the experimental results. When salty water freezes, the ions are not incorporated in the crystal structure, but it will be located in brine pockets (Weeks and Ackley, 1986). At temperatures below the eutectic temperature, the salt precipitates inside the brine pockets (Sinha, 1977b) but at higher temperatures the salt remains in solution. The eutectic temperature of potassium chloride in water is about -11°C; hence the ice that used in the experiment contained liquid, salty water. With this liquid water present it is not possible to attribute a liquid water film exclusively to the process of friction melting.

Kuroiwa (1977) summarized different Japanese studies on the kinetic friction on snow and ice. Direct visual observations were made of the interface between snow and methacrylic acid resin after sliding for 5 min at T_s = -2°C. ($v = 9.7 \cdot 10^{-2}$ m/s F_n = 2.45 N). Abraded ice particles and refrozen melt water was found in the contact area. The observed

refrozen melt water is frequently quoted as the direct experimental evidence for the existence of a lubricating film. However, this particular observation was also accompanied with evidence for insufficient lubrication in the form of ice abrasion. Observations were also made through a glass plate after sliding for 5 min sliding on snow (T_s = -4°C, ρ_s = 340 kg/m^3 $v = 6 \cdot 10^{-2}$ m/s, F_n = 2.74 N, $A_a = 6 \cdot 10^{-4}$ m^2, $\mu \approx 0.36$). The real contact areas of the worn snow crystals were found to be mirror-like flat. Minute air bubbles were entrapped at the interface. Ambach and Mayr (1981) used a capacitor probe to estimate the water film thickness under skies. Based on the changes in the dielectric constant of the ice and water they estimated a thickness ranging from 13 μm at 0°C to 5 μm at -4°C (0< v < 60 km/h). Strausky et al. (1998) attempted to detect liquid water present in the contact area between polymer samples and ice at -2°C using fluorescence spectrometry Liquid water films larger than the detection limit of 50 nm were not observed while the friction coefficient was low; $\mu = 0.03$.

A third theory for the presence of a lubricating water film is the presence of a surface layer that exhibit mobile, quasi-liquid, or liquid-like properties. In contrast to the pressure melting or frictional heating theory, this layer would exist in equilibrium, below the triple point of ice without external pressure or heat supply. The layer was initially suggested by Faraday (1859) and has been extensively debated (for reviews on this topic see Jellinek (1967), Hobbs (1974) and Dash et al (1995)). The effect is also referred to as pre-melting. According to Dash et al. (1995), surface melting typically begins with one or two monolayers' thickness at $T < 0.9T_m$,which thickens gradually with increasing T, and diverges at T_m. There exists, however, a large variation in the thickness measurements of this layer; ranging from a few to 1000 Å (Elbaum et al., 1993). Techniques to measure the thickness and viscosity of the liquid like layer include: wire regelation (Telford and Turner, 1963; Gilpin, 1980), pushing ice cylinders through quartz capillaries (Barer et al., 1980; Churaev et al., 1993), polarized reflectance measurements (Elbaum et al., 1993) and atomic force microscopy (Bluhm et al., 2000).

Other proposed theories on ice friction include the swivelling of ice molecules (Niven, 1959; Niven, 1963), adhesion and deformation (Tusima, 1977) and a theory based on the energy flux required to form surfaces at contact asperities (Makkonen, 1994; Makkonen, 2004). Niven explains qualitatively the low frictional properties of ice to its open tetrahedral structure that can “crush” into a more dense structure that is more like the structure of water. This “swivelling” of the tetrahedral ice structure bear a close resemble to the pressure melting theory of Reynolds. To the author’s knowledge, the theory has not been developed quantitatively. Tusima considered adhesion and deformation during low velocity sliding ($v < 10^{-3}$ m/s) of a steel ball on a single crystal of ice and applies the general friction theory, given in Eq. 4.4, proposed by Bowden and Tabor (1954; 1964). He arrives at the following expression for the kinetic friction coefficient:

$$\mu = \frac{k\pi w_s^2 S_i}{4F_n} + \frac{w_s^3 p_i}{6F_n R}, \tag{4.9}$$

where S_i and p_i are the shear and ploughing strength of the ice, respectively, w_s is the width of the track (scratch) , k is a constant, and R is the diameter of the slider. Makkonen describes the origin of the friction force in terms of the energy required to create a surface behind a contact asperity. The theory considers an asperity of material 1 (for instance ice) sliding on a much larger asperity of material 2 (see Fig. 4-4). At point B the surface 2 is

replaced by the surface 1,2. At point A, the surface 1,2 is replaced by surface 2 again. Energy is released at point B when $\gamma_2 < \gamma_{1,2}$. This energy can only be transformed into heat. Energy is required at point A in order to recreate the surface of material 2. This energy originates from the kinetic energy of the sliding motion and causes the resistance force.

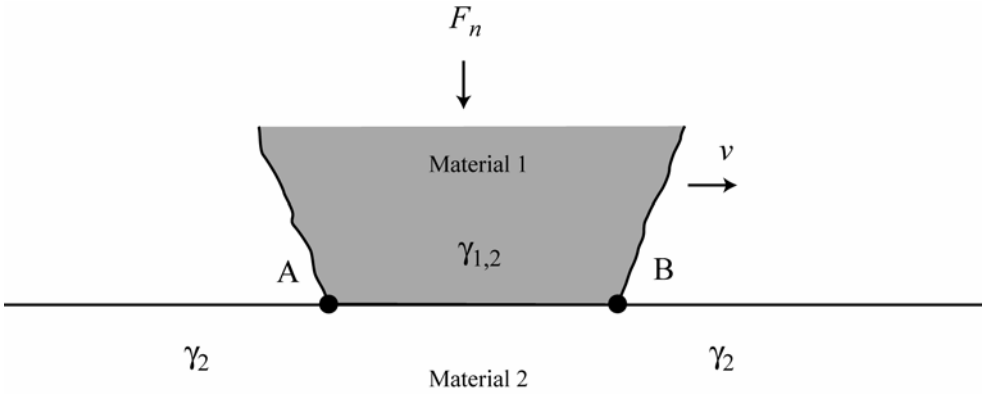

Figure 4-4. Schematic figure of a sliding contact (Makkonen, 1994), reprinted with permission.

By assuming that the asperities of the softer material yield at a pressure that equals the hardness H , assuming that the surface energies of the solid and its melt are approximately the same, and considering ice as the softest material, Makkonen arrives at the following expression for the friction coefficient:

$$\mu = \frac{\gamma_i}{H_i}\left(\frac{1}{d_i}+\frac{1}{d_2}\right)\left(\frac{d_i}{d_2}+\left|\cos\Theta\right|\right), \tag{4.10}$$

where d is the length of the contact and the indexes i and 2 stands for "ice" and "material 2", respectively. The term cos Θ originates from the Young-Dupré equation:

$$\gamma_{1,2}+\gamma_1\cos\Theta=\gamma_2, \tag{4.11}$$

where Θ is the static contact angle of a sessile drop of water on material 2.

For ice slides against ice, Eq. 4.10 reduces to:

$$\mu = \frac{4\gamma_i}{H_i d_i}, \tag{4.12}$$

4.5.4 Sand friction

Sand characteristics

There are considerable differences in the sand properties used at airports. These sand can be divided after origin into natural sand and manufactured sand (also called machined sand). Natural sand is directly harvested from nature, and "machined" sand, which is produced by crushing rock. The sand is sieved to obtain to limit the sand particle size. A review of the sand properties for airport applications is given by Comfort and Gong

(1999). They identified the following relevant properties: (1) angularity, (2) grain size distribution, (3) hardness, (4) mineralogy, and (5) colour.

The grain size distribution is regulated to minimize the damage to aircraft, known as Foreign Object Damage (FOD). The damage may either occur by impact (larger particles) or by abrasion when ingested into turbine engines (smaller particles). The Federal Aviation Administration (FAA) specifies a minimum and maximum size of 0.2 and 4 mm, respectively (FAA, 1991 Change 3, nov 1998).

Theories on sand friction

In winter maintenance, sand is also referred to as abrasives (Keyser, 1981). This term suggests that the friction is provided by the abrasive action of the particles. The presence of harder particles (harder than one or both interacting surfaces) between two sliding surfaces indeed creates the conditions for abrasion to occur.

Abrasion is a type of wear and the mechanisms can be divided into two-body and three-body processes (Burwell, 1957). In two-body abrasion an asperity of a harder surface abrades the softer counter surface. In three-body abrasion, a hard particle is entrapped between the two sliding surface and cause abrasion on one or both surfaces. The particles may either stick to one surface and abrade the mating surface, or remains a free body and rolls between the two surfaces (Bhushan, 1999). The resistance causes by a rolling particles is much less, compared to a sliding particle (Rabinowicz, 1995). In this respect it is illustrative to note that Norwegian maintenance personnel frequently refer to “a ball bearing effect” when they observe a reduced effectiveness of sand, for example at very low temperatures. For now consider the case that the particle becomes trapped in the (soft) rubber and slides over the ice surface.

Three different abrasion modes have been observed when a hard asperities slide over a softer flat surface: ploughing, wedge forming, and cutting. The shape of the abrasive, the hardness, the load and the shear strength at the interface have been identified as four main parameters controlling the wear state (Hokkirigawa and Kato, 1988). In the literature, the term “ploughing” is also used in a broader sense for the sliding action of a hard asperity into a softer surface, irrespective of the abrasion mode. This broad interpretation of the term ploughing has also been adopted in this thesis, unless otherwise mentioned. The main question for the tribosystem of consideration is how much resistance force is generated by a sliding particle.

Early estimates of a ploughing asperity were based on idealized asperity on an ideally plastic, isotropic material. For a cylinder shaped asperity sliding on its side, the friction force as a function of the interfacial shear strength S, scratch width w_s and yield pressure p_y of the softer material is given by (Bowden and Tabor, 1954; Bowden and Tabor, 1964):

$$F_t = Sl_c w_s + \frac{1}{12}\frac{d^3}{r} p_y, \tag{4.13}$$

where l and r are the length and radius of the cylinder, respectively.

For the same assumptions, the friction coefficient can be written as (Rabinowicz, 1995):

$$\mu_p = \frac{F_t}{F_n} = \frac{p_y A_l}{p_y A_p} = \frac{A_l}{A_p}, \tag{4.14}$$

where A_p the projected area of the groove and A_l the projected area carrying the load. The ratio A_l/A_p can be found from the geometry of the asperity (e.g. Bhushan, 1999). More detailed models for rigid asperities ploughing ideally plastic materials have been developed (e.g. Suh and Sin, 1981; Zhang et al., 1991; Azarkhin and Devenpeck, 1997; Liu et al., 2002; Bhushan and Nosonovsky, 2004). However, for a viscoelastic material like ice, which exists at temperatures very close to its melting point, the response of the material on a ploughing sand particle is expected to be more complicated than described by an ideally plastic (time independent) behaviour. This expectation may be supported by considering the complexity of scratch mechanisms on viscoelastic polymers (Briscoe, 1998; Gauthier and Schirrer, 2000) and wear mechanisms at high temperatures (Inman et al., 2005; Liu and Wang, 2007). Here, time and temperature dependency of the material response influences the wear mode and the resulting friction coefficient.

4.6 Rubber on ice friction

Early experimental work on rubber on ice friction (Conant et al., 1949; Pfalzner, 1950; Wilkinson, 1953; Niven, 1955; Niven, 1958) focused on testing different rubber compounds and investigating the dependence of the friction coefficient on temperature, sliding velocity, and normal load. Different laboratory tribometers (so different tribosystems) were used in these experiments; hence the obtained numeric values vary significantly. Nevertheless, general trends in the friction behaviour can be distinguished. All investigators observed a clearly decreasing friction coefficient as ice temperature approached 0°C. A reduction of the friction coefficient with increasing normal load was also generally observed. The experimental set-up used by Wilkinson (1953) allowed measurements over a range of sliding velocities from 10^{-3} to 1 m/s. The maximum friction coefficients were obtained around $2 \cdot 10^{-2}$ m/s and decreased significantly as the sliding velocity was increased further. A number of other factors were mentioned that greatly influenced the friction coefficient, such as: (1) age of the ice, (2) smoothness of the ice, (3) surface impurities, (4) ice adherence on the sample, (5) conditioning time, and (6) occurrence of stick-slip sliding.

A number of laboratory rubber-ice experiments resulted in high friction coefficients ($1 < \mu < 6$) (Southern and Walker, 1972; Southern and Walker, 1974; Gnörich and Grosch, 1974; Roberts and Richardson, 1981). These studies have in common that the sliding velocity did not exceed 50 mm/s and that the ice was conditioned (polished and aged). In this "high friction regime", the friction values are of comparable magnitude as rubber sliding on other "smooth" solids, like glass (Grosch, 1963). The WLF transformation can be applied (Southern and Walker, 1972; Southern and Walker, 1974; Gnörich and Grosch, 1974) and the sliding is accompanied with Schallamach waves (Roberts and Richardson, 1981). These observations are strong evidence that in this regime, the friction mechanisms on ice do not differ from rubber sliding on other solids. It implies that the friction would be governed by the viscoelastic properties of the rubber. The energy dissipation associated with friction appears to be located in the rubber bulk. However, it has to be pointed out that under apparent similar experimental conditions (i.e. temperature, sliding velocity, load) the frictional behaviour can also be significantly different: On freshly prepared ice, the WLF transformation could not be applied (Southern and Walker, 1972; Southern and Walker, 1974) and the slightest sign of snow

crystals on the track, even loose snow debris from the polishing action tended to reduce the friction coefficient drastically (Gnörich and Grosch, 1974).

A transition from the “high friction regime” to a “low friction regime” was also observed as the ice temperature increased, and was accompanied with the disappearance of Schallamach waves (Roberts and Richardson, 1981; Roberts, 1981). The temperature at which the transition took place was found dependent on ionic concentration of the water from which the ice was made (Roberts and Lane, 1983). In the low friction regime, the friction coefficients are of comparable magnitude of well-lubricated tribosystems. Ahagon et al (1988) investigated different rubber compositions with a British Pendulum. It was found that the friction changed over time. No correlation was found between the energy losses in the rubber and the friction force.

The two most common explanations for the “low friction regime” of rubber on ice are the formation of a lubricating water film due to frictional heating and the existence of a mobile, quasi-liquid, or liquid-like surface layer on the ice, which are discussed earlier.

4.7 Field observations

The field activities that were performed on operational runways gave the opportunity to look for signs that could indicate particular interaction characteristics on the macroscopic and sub-macroscopic level. A first macroscopic interaction characteristic was shown earlier in Fig. 3-6. Aircraft engine thrust can displace loose sand and thereby preventing that particles enter the contact area. Another interaction example is illustrated in Fig. 4-5. Iced runways were found to have numerous scratch marks. A high concentration of scratches was typically found close to the runway thresholds, in the retardation zone, and before taxiway turnoffs. The scratches were up to 0.5 m long, approximately 1 mm wide, and aligned along the length axis of the runway (the travel direction of aircraft).

The possibility that these scratches are produced by the rotating steel brush from the runway sweepers was considered, but can be excluded for the following reasons: (1) The brush is aligned at an angle (about 30°) to the direction of travel, which would also cause the scratches to be aligned accordingly; (2) the observed scratch density does not correspond to the brush density. (3) The scratches would have been uniformly distributed over the runway area if they originate from the sweepers. Hence, the most logical explanation for the scratches is that they are formed by sand particles that have been entrained by the rubber tread of aircraft tires during braking or spin-up (the initial phase of the landing where the tires start rotating). In fact, an occasion was found where the sand particle remained stuck in the ice, after it had caused a scratch (Fig. 4-6). An officer in charge indicated that he frequently had noticed these scratches and pointed out that they appear when the weather is mild (Klein-Paste and Sinha, in press). Signs of rolling sand particles (craters on the ice) were not found but they may be difficult to observe.

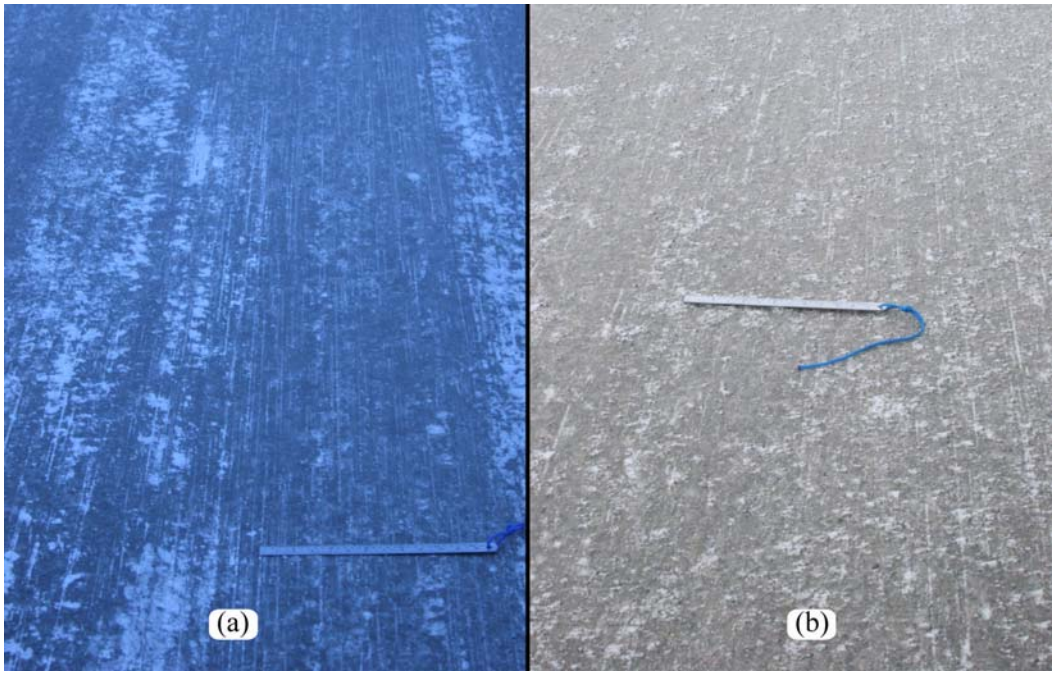

Figure 4-5. Scratch marks on iced runways. (a) The runway at Tromsø Airport, close to the runway threshold. (b) The runway at Kirkenes Airport, approximately one third along the runway length.

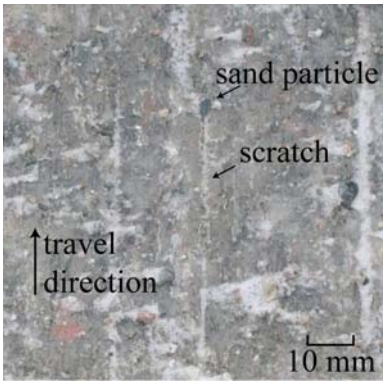

Figure 4-6. A scratch where the sand particle remained in the ice after the interaction.

4.8 Discussion

The description of interaction mechanisms show that tire-pavement friction is not provided by a single friction mechanism. Instead, multiple mechanisms can be operative simultaneously, mechanisms can be lost, or mechanisms replaced by other mechanisms. This can be illustrated analyzing by the following simplified example: A bare and dry pavement becomes wet by a rain shower. Later, the temperature drops below 0°C and the wet pavement freezes. Maintenance personnel notice the ice and apply sand to improve the conditions.

On the bare and dry pavement friction the rubber can easily drape around surface asperities and friction is provided by adhesion and deformations within the rubber tread (hysteresis and rubber wear). The rain changes the conditions because the pavement becomes wet. The presence of water reduces rubber-pavement adhesion. Moreover, the water reduces the ability for the rubber to drape around asperities. Water has to be

squeezed out of the contact area, which takes time. The overall attainable tire-pavement friction is reduced because of the loss in rubber-pavement adhesion and a reduced hysteresis (because it takes longer before the rubber drapes around the asperities). In most situations, there will be sufficient tire-pavement friction left to safely operate aircraft, given that the pavement has the correct texture and hydroplaning is avoided. The conditions change again because the wet pavement freezes. This prevents that water can be squeezed out of the contact area. The ability of the rubber to drape around pavement asperities is strongly reduced or even totally lost. Now the friction is provided by a rubber-ice interaction. This probably results in insufficient tire-pavement friction. Therefore, maintenance personnel apply sand and the surface conditions change again. The sand particles locally replace the rubber-ice interaction by sand-ice interaction (the rubber is locally separated from the ice). Sand-ice interaction is characterised by the motion of the sand particle. When the particle slides together with the rubber tread, it ploughs into the ice surface, creating friction by means of ice deformation. Even with this highly simplified case it becomes clear that it is difficult to find "universal facts" on tire-pavement friction, such as load, speed, and temperature dependency that applies to all types of surface conditions.

An explanation how sand increases the friction has been given as "sanding adds texture to the surface"(FAA, 1991; Comfort and Gong, 1999). Though it does not specifically state the friction mechanism, it makes implicit the association with rubber friction on rough surfaces (Section 4.5.2). In this view, the added texture would force the tire tread to deform more, resulting in a more hysteretic losses and thereby increasing the friction. There are indeed occasions where sand particles become partly embedded in the contamination layer and form surface asperities that remain embedded after the interaction (for example Fig. 3-11a). Here, the sand particles indeed act in a similar fashion as road asperities and the friction increase may be ascribed to the addition of texture. But there are also situations where the particles do not stay attached to the contamination layer. The scratch marks observed in the field show that these particles slide with the (braking) tire on contamination layer. In this case the particle provides friction because it ploughs into the contamination layer. Since the particles slides together with the rubber there will be no significant increase in rubber hysteresis. Hence in this case, "sanding causes ice deformation" appears to be a better explanation for the functionality of the sand, rather than "sanding adds texture to the surface".

Whether sand particles indeed lead to an increased friction force will depend on the friction mechanisms that are replaced by the local separation of rubber tread and (iced) pavement. On smooth, warm, and continuous ice this may very well be the case, since the original rubber-ice mechanisms are expected to give little friction. However, when the original mechanisms gave already a high level of friction (such as on a dry pavement) the sand particles may actually reduce the friction. This appears to be a common observation, at least among Norwegian maintenance personnel. They typically refer to it as a "ball-bearing effect".

The literature on ice friction is clearly dominated by the view that a lubricating film exists, either by frictional heating, by pressure melting (close to the melting point of ice), or as a "stable liquid like" surface layer. Specifically the frictional heating theory still finds wide support. These views may thus be "well established" and the theory has survived for more than 50 years. However, there appears very little direct experimental evidence available for the existence of melt water in the contact area. The evidence that

was found was all collected observed very close to the melting point and appears controversial. Hence, rigid physical evidence that the water film indeed exists under the conditions where the frictional behaviour is ascribed to this film seems still lacking. Moreover, the liquid film itself cannot satisfactory explain the energy dissipation that is related to friction. It thereby does not explain *how* friction is generated, an aspect that was recognized since the theory was developed (Evans et al., 1976). It has also been recognized that solid-solid interaction cannot be neglected in ice friction (Evans et al., 1976; Makkonen, 1994)

Summarizing, the physical nature of rubber-ice friction cannot fully be explained by the formation of a water film. In particular, the question where and how the energy dissipation takes place during the kinetic friction of rubber on ice cannot be satisfactory be answered by this “widely-accepted” theory.

5 ICE SURFACE OBSERVATIONS BY ETCHING AND REPLICATING

5.1 Introduction

Chapter 4 showed that although the dominating view on ice friction is that the friction level is determined by the lubrication with a liquid or liquid-like water phase, solid-solid interaction may not be neglected. A common way to investigate solid-solid interaction mechanisms is to study the surfaces after the frictional interaction. Rubber observations can be made by optical microscopy or by scanning electron microscopy (SEM) (Zhang, 2004). Investigating ice surfaces under a microscope is not that straightforward. The high transparency of ice makes it little suitable for optical microscopy and conventional SEM is performed under very low pressures, which causes the ice to sublimate. There are, however, analytical techniques developed to study the ice surface.

The etching and replicating technique for ice, developed by Sinha (1977a; 1978a), has been used extensively to reveal different microstructrural features such as grain boundaries, sub-grain boundaries, basal and non-basal dislocations, dislocation glide and climb, and dislocation pileups (Sinha, 1977a; Sinha, 1977b; Sinha, 1978a; Sinha, 1987; Barrette and Sinha, 1994). This microstructrural information, combined with the applicability for field studies, makes it an attractive analytical method for tribological investigations. This chapter briefly describes the method and summarizes a study on rubber-ice friction where ice surface observations were performed.

5.2 Etching and replicating method

The etching and replicating method is described in detail in Sinha (1977a). Briefly, the ice surface is coated with a solution of polyvinylformal (formvar) in ethylene dichloride. The fluid is allowed to dry under controlled conditions and leave a plastic film or replica. During the drying process, the ice surface is etched to different degrees, depending on the concentration and drying condition. Hence, the dual process of etching and replicating occurs simultaneously. After drying, the solidified formvar replica can be recovered by peeling it from the surface, or by sublimating the ice. The latter method is time consuming and therefore more suitable in the laboratory than in the field. The replica is transferred to a clean glass plate (replicated surface facing upwards) and can be studied at room temperature for prolonged lengths of time by a transmitted light or scanning electron microscope.

The etching process is driven by the preferential dissolution of ice molecules into the etching fluid and from there into the air above. Imperfections in the ice lattice, such as grain boundaries, tilt boundaries, basal and non-basal dislocations, and dislocation pileups, are at higher energy levels compared to their surrounding lattice. Hence, these regions are etched more, and resulting in topography in the replica. The etching and replicating process is schematically presented in Fig. 5-1.

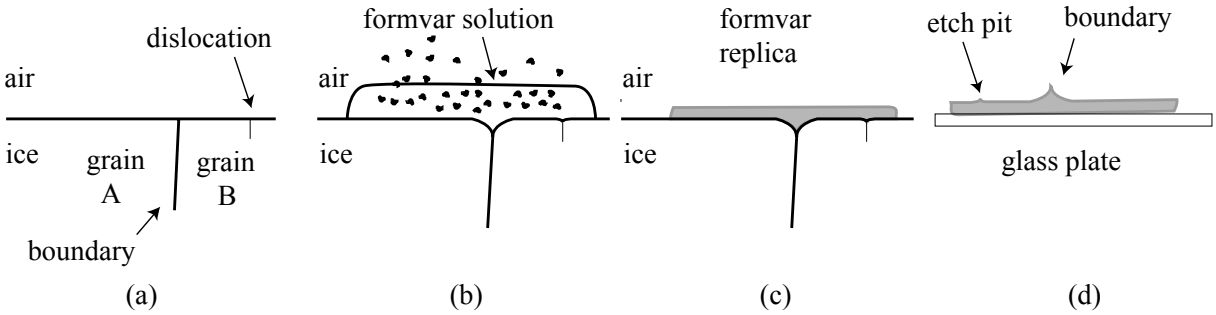

Figure 5-1. The processing steps of the etching and replicating method. (a) The ice surface, (b) the formvar solution is applied and allowed to dry. During the drying the etching and replicating takes place. (c) After drying the solidified formvar forms a replica of the etched surface. (d) The replica is transferred to a glass plate.

5.3 Ice surface observations after rubber – ice friction

A laboratory experiment was carried out to investigate the ice surface after rubber-ice friction by using the etching and replicating technique. The sliding was performed with a British Pendulum Tester (Giles et al., 1964) in a single pass at different ice temperatures. Two different ice surfaces were prepared and the sliding tests were performed in presence and absence of sand particles.

5.3.1 Experimental details

All activities, such as growing ice, specimen preparation, and tests, were conducted inside a large, walk-in cold laboratory. Ice surfaces were prepared following two procedures. In the first procedure, a mist of single distilled water (water temperature, $T_w \approx 0°C$) was sprayed on a flat stone (T_a = -5°C). The water formed a continuous film on the flat surface and was allowed to freeze before subsequent mists were applied. This resulted in smooth but wavy ice. The c-axis of the crystals was randomly oriented and the grain size ranged from 0.1 to 2 mm. This type of ice is designated “sprayed ice”. In the second procedure, columnar grained ice was grown in an insulated tank (500 × 350 × 300 mm) from single distilled water at T_a = -10°C. Rectangular ice specimens (250 × 90 × 10 mm) were cut from the central section, at 30 and 40 mm depth. The surfaces were prepared at T_i = -10°C following the microtoming procedure described by Sinha (1977b). The surfaces were microtomed by 50 passes, removing 10 μm/pass, followed by 50 passes of 5 μm/pass, and finally by 50 passes of 1 μm/pass. The microtoming blade was cleaned before each pass with a soft brush.

The surfaces were allowed to sublimate (self-polish) in a closed chamber containing silica gel for 48 hours ($T_a \approx$ -10°C, relative humidity, $RH \approx$ 80 - 85 %). This procedure minimized the mechanical damage to the surface and resulted in smooth ice with mirror-like finish. The crystals were oriented with their c-axis parallel to the 250 × 90 mm plane and their a-axes randomly oriented. This type of ice is known as S-2 ice (Michel and Ramseier, 1969). Dislocation pits become elongated along the c-axis direction when the c-axis are parallel to the surface plane (Sinha, 1978a; Sinha, 1987). This particular feature was used to identify the c-axis direction of the grains in the S-2 ice.

A British Pendulum (Giles et al., 1964) was used to slide a rubber block on the ice surfaces in a single pass. The rubber specimen (76 × 25 × 7 mm) was made from TRRL rubber, with a hardness of 53 IRHD and resilience of 49 %, at T = 0°C (Munro Stanley London, 2006). The experiments included tests where sand particles were entrained by

the sliding rubber. Here, two sand particles (sieve fraction 2.0 - 3.3 mm) were placed on the ice surface. The sand originated from the sand stockpile at Tromsø Airport, Norway. The whole set-up (pendulum, ice, rubber) was ensured to be at the desired ambient temperature before testing. The rubber block was cleaned with a soft brush before each test.

Etching and replicating was performed at $T_i \approx T_a$ = -11 ± 1°C with 2.5 % Formvar solution. In friction tests at higher temperatures the cold room was cooled down before etching and replicating. During the cooling, the ice was kept in a closed chamber containing snow (saturated humidity) to minimize ice sublimation.

5.3.2 Results

The replicas of a sprayed ice surface before and after passage of rubber at T_i = -10°C are shown in Fig. 5-2. The replicas show grains with different crystallographic orientations. The orientation of grain 2 in Fig. 5-2a is more favourable for etching, creating minute etch pits at the points where dislocations intersect the surface. This causes the differences in texture, compared to the other grains.

The original crystal structure remained intact after exposure to the sliding rubber (Fig. 5-2b), but the ice has deformed. A large number of small ploughing tracks (indicated by no. 5) are visible. These tracks have a width up to about 0.07 mm. However, the ice surface exhibited also much finer scratches that could be revealed (at the same magnification) by the etch pits of the newly produced dislocations (indicated by no. 6).

The scratches terminated at some grain boundaries (for example at the boundary between grain no. 1 and 2), while they continued at other boundaries (for example at the boundary between grain no. 2 and 3). This shows that the morphology of the scratches (and thus how severely the ice deformed) is directly related to crystallographic orientation of the crystal.

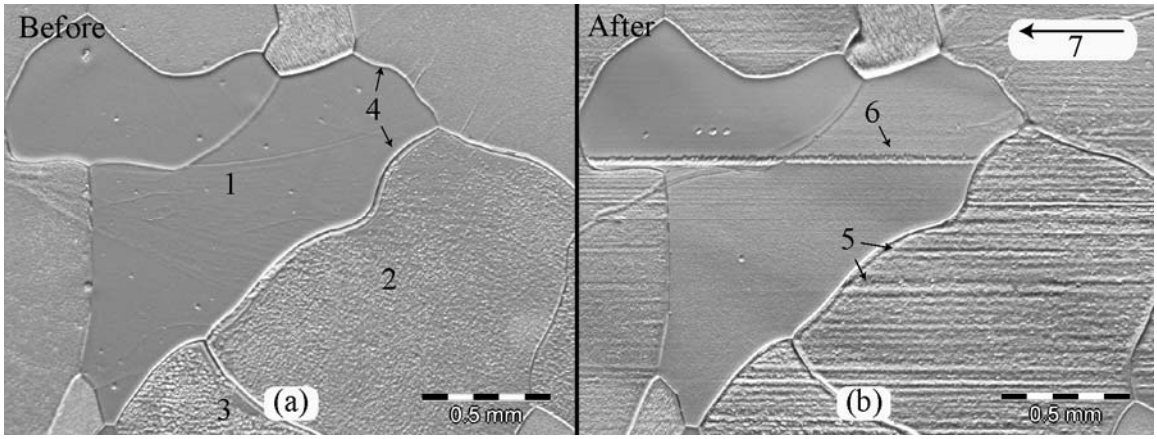

Figure 5-2. Replicas of a sprayed ice surface at T_i = -10°C. (a) The crystal structure before the sliding. Individual grains (no. 1, 2, and 3) and grain boundaries (4) can be distinguished. (b) After sliding the crystal structure remained intact, but the ice has deformed. Small scratches are visible as ploughing tracks (5), and as rows of dislocation etch pits (6). The scratches are aligned along the sliding direction (7).

S-2 ice surfaces were exposed to a single passage of sliding rubber at ice temperatures close to the melting point. Fig. 5-3 shows an example of an S-2 ice surface at T_i = -0.1°C. Outside the track (Fig. 5-3a), the naturally occurring dislocations produced elongated dislocation pits (indicating the c-axis direction). These elongated etch pits were uniformly distributed within the grains. Inside the track (Fig. 5-3b), new dislocations were produced, creating thin rows of elongated dislocation pits. These rows are aligned along the sliding direction. Note that the original crystal structure remained intact, despite the very high ice temperature.

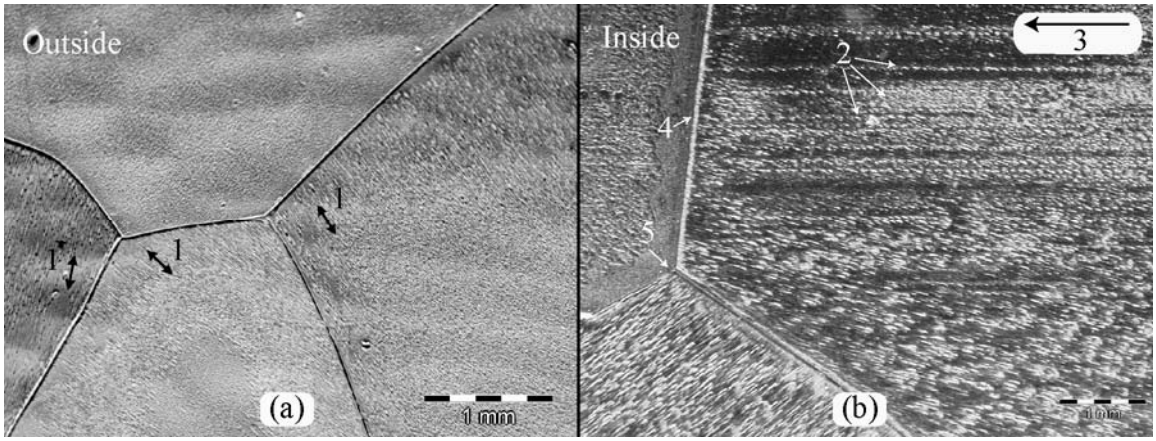

Figure 5-3. Replicas of an S-2 ice surface at T_i = -0.1°C. (a) The crystal structure outside the track. The ice consists of large crystals and the elongated etch pits are uniformly distributed throughout the crystals. The c-axis orientations of the crystals are indicated by the arrows (1). (b) Inside the track, rows of elongated etch pits (2) are aligned along to the sliding direction (3). The original crystal structure (grain boundary (4) and triple point (5)) remained intact.

A sprayed ice surface was exposed to the sliding rubber which entrained sand particles at T_i = -8.4°C. Fig. 5-4 shows a track made by one particle. The total track had a width of about 2 mm, which is comparable to the sand particle size. The single sand particle produced several scratch marks that were deeper (and wider) than the scratch marks that were produced by rubber-ice interaction. Hence, the sand particle caused locally heavily

deformed the ice. The large number of scratch marks show that multiple asperities on the sand particle ploughed into the ice surface. The ploughing action removed chips of ice that deposited aside the track. These chips were found along the whole sliding length and were often spiralled. This helix-shape is easily recognized through the stereo-microscope, but cannot be brought out properly in the micrograph. Inspection of the spiralled chips allowed a rough estimate of the penetration depth, which was in the order of 0.1 mm.

The original crystal structure remained intact, but the ploughing action was accompanied with re-crystallization or cell formation. The produced cells had a typical diameter of about 0.05 mm.

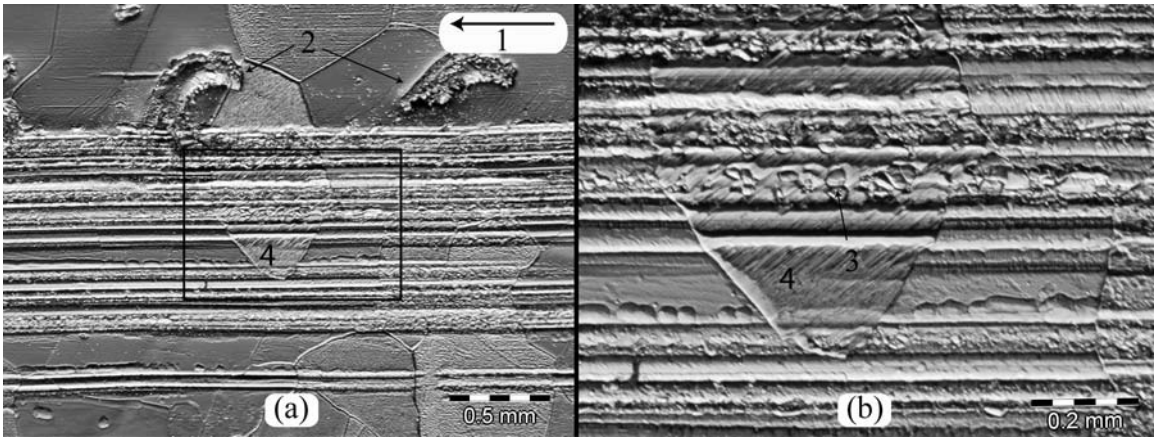

Figure 5-4. Replica of a sprayed ice surface, exposed to sliding sand particle at T_i = -8.4°C. (a) The sand particle caused numerous deep scratches along the sliding direction (1). Chips of ice (2) were removed by the ploughing particle. The black rectangle indicates the magnified view shown in (b). Here, small cells (3) have been created within the original crystal (4).

An S-2 ice surface was exposed to the sliding rubber entraining sand particles at T_i = -0.9°C. The replica (Fig. 5-5) shows that re-crystallization / cell formation occurred along the track. The cells had a typical diameter of about 0.1 mm and were present along the whole scratch length.

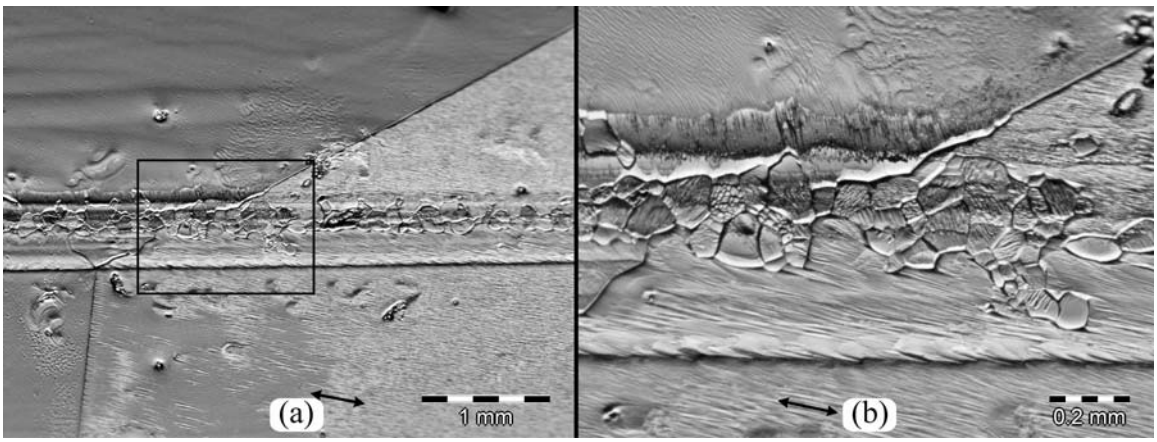

Figure 5-5. Replica of an S-2 ice surface, exposed to a sliding sand particle at T_i = -0.9°C. (a) Inside the track, re-crystallization or cell formation has occurred. (b) A magnified view of the cells. The black arrows indicate the c-axis direction.

5.4 Field observations

The etching and replica method was also applied in various field studies. Ice surface observations after an aircraft braking test on sanded ice will be presented later in Chapter 9. Observations from an apron at Tromsø Airport, Norway are presented here as an illustration. In that particular case the apron was covered with snow that had undergone melting-refreezing metamorphism. The snow had deposited a few days earlier and started to melt in a subsequent mild weather period that included rain. In the night prior to the observations the temperature had dropped again and a solid continuous ice layer had formed. Maintenance personnel applied loose sand on the area to improve the friction. The quality of the surface was assessed with the airport's Skiddometer BV-11 friction measurement device. Measurements were performed at about 30 km/h with a Trelleborg Unitester test tire and an inflation pressure of 700 kPa. The BV-11 and the test tire track are shown in Fig. 5-6a. Replicas were made from a track with a 2.5 % formvar solution and a drying time of about 20 min (T_i = -2.5°C, T_a = +1°C).

The replica in Fig. 5-6b shows the original crystal structure remained intact, but the sand particle has scratched the surface. A deep scratch runs through the original crystal and was accompanied with re-crystallization or cell formation. The cells had a typical diameter of about 0.1 mm. Additionally, small ploughing tracks (without cell formation) can be observed. The width of the scratches was about 0.04-0.1 mm. Finer scratches, that were observed in the laboratory by rows of dislocation etch pits, are not observed in this replica, but this is due to the high temperature at which the etching took place (T_i = -2.5°C). This ice temperature is too high to reveal such fine microstructural details. All scratches are aligned along the sliding direction of the test tire. This shows that the main features that were observed in the laboratory were also found in the track of the friction measurement device on an operational iced surface.

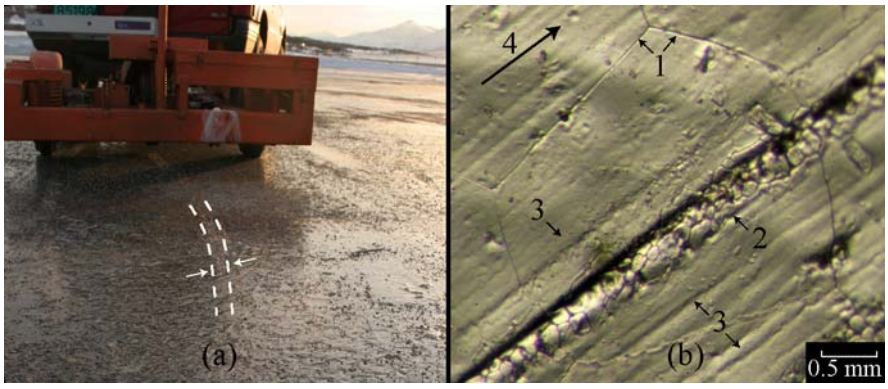

Figure 5-6. Friction measurements with a BV-11 on sanded ice and the replica of the ice surface in the track: (a) the test tire track is indicated by the dashed lines. (b) The original grain boundaries (1) remained intact. A large scratch (2) runs through the grain. Inside this scratch the ice has small cells have been formed. Deformation without cell formation can also be observed by small ploughing tracks (3). All features are aligned along the sliding direction of the track (4).

5.5 Discussion

The ice surface observations, both in the field and in the laboratory study, show clear evidence for deformations in the ice surface. The deformation is observed directly in the form of scratches. The scratches are either large enough to be viewed as ploughing tracks, or they appear (at the same magnification) as rows of dislocation etch pits. The presence

of sand particles causes deeper scratches that were accompanied with re-crystallisation, or cell formation.

Surprisingly, the original crystal structure remained intact, even at ice temperatures as high as -0.1°C. This means that gross melting and refreezing (in case of a continuous melt water film) did not occur during our sliding events. A melting/refreezing cycle would have caused a rapid freezing and a subsequent different grain structure. Note the large difference in crystal structure between the slowly grown S-2 ice (about one week) and the rapidly grown sprayed ice where each water application froze within a few seconds. Hence, whatever lubricating mechanism was operative during our rubber – ice friction process, it was insufficient to prevent direct contact between the rubber and the solid ice. Consequently, ice deformation occurred and was clearly visible afterwards. In this respect, our observations are in line with the view of Evans et al.(1976) that the sliding constitutes (at least partly) of dry friction, which is the interaction of solids without the presence of a lubricating fluid. Also the view of Akkok et al. (1987) that the ice softens, rather than melt, which is in essence a view of ice deformation without a necessarily phase change, is in accordance with our observed deformations. Roberts and Richardson (1981) pointed out that "it would appear that ice governs the friction, either by flow or melting". Again, an ice flow controlled mechanism without a necessary transition to the liquid phase would indeed be in accordance with our observations.

It can be argued that our observations are made from a typical "running-in" stage, involving compliance of surface asperities by permanent deformation (Bhushan, 1999). Indeed, our observations were made only after one pass and the ice surface may progressively comply after multiple exposures on the same track (such as in turn-table experiments). However, this running-in stage is in fact more representative for the aircraft tires tribosystem, than the "conditioned" ice obtained after a period of running-in. The ice present on operational runways is heavily exposed to (repeated) mechanical action from tire interaction and snow cleaning equipment. So also here, there certainly is a level of conditioning. But because the tire-ice-pavement tribosystem is an open system, and the same tire never runs repeatedly on exactly the same track (on an asperity scale), it will not reach a post running-in phase. The ice deformation associated with non-complying surfaces may thus be a part of the total friction force that provides aircraft retardation and directional control.

The presence of sand particles caused deformation to take place deeper into the ice surface. These ploughing tracks can be accompanied with material loss (Fig. 5-4). Both in the field and in the laboratory it was found that the ploughing can also be accompanied with a change in the microstructure. Small crystals were formed inside the original crystal. These crystals can be formed either by re-crystallization (involving large changes in crystallographic orientation) or cell formation (small changes in crystallographic orientation). Sinha (1978a) has shown the offspring of a cell, induced by ice deformation. The deformation caused dislocations to pile-up to low angle tilt boundaries that eventually enclosed a cell. However, at this point it is difficult to exclude the possibility that the cells observed here are the result of local melting and re-freezing mechanism. So, re-crystallization through a phase change may have occurred. Re-crystallization after ice friction have been observed reported earlier (Barnes et al., 1971) but their observations differed from our observations in the following way: (1) They used a single crystal slider and a flat granite substrate. Hence the same area of ice is exposed to frictional action throughout the whole sliding length. In our case the slider was a sand particle in relative

motion to a polycrystalline surface. (2) Our velocity ranged in the order of 1-1.8 m/s whereas their sliding velocity was very low, in the 10^{-8} to 10^{-6} m/s range. The ice temperature comparison could not be made because it was not specified in their observations.

In the experiment we deliberately did not put any effort in cleaning the rubber specimen, other than brushing it clean with a soft brush. Hence the small scale scratches could have been produced by fine foreign particles that contaminated the rubber. In fact, inspection of the rubber surface directly after the run shown in Fig. 5-2 revealed such type of rubber contamination. In practice, foreign particles (e.g. sand, dust, snow) are usually present on the rubber tread of pneumatic tires. So, with or without intentionally applied sand particles, ice deformation can take place, even as the rubber is softer than the ice. This also suggests the importance of rubber contaminations on the rubber-ice interaction mechanism.

5.5.1 Conclusion

The etching and replicating method for ice was found to be a valuable analytical method for tribological studies on ice friction. It provided a wealth of information regarding the interaction processes that took place on a microscopic level. Etching and replicating ice surfaces after exposure to friction revealed that:

1. Both rubber-ice and sand-ice interaction involves ice deformation as a basic friction mechanism.
2. The rubber sliding on ice produced small ploughing tracks (scratches). The observed tracks had a width up to about 0.07 mm.
3. The rubber-ice interaction also generated dislocations, which were revealed by rows of dislocation etch pits.
4. The original crystal structure remained intact after the rubber-ice interaction, even at ice temperatures very close to the melting point (T_i = -0.1°C).
5. The entrainment of sand particles caused deeper and more severe ice deformation. The ploughing track of a single particle (estimated depth about 0.1 mm) involved multiple asperity contact.
6. The ploughing action of sand particles through the ice was accompanied with re-crystallization or cell formation. The produced cells had a diameter in the range 0.05-0.1 mm.

Field observations from the track of a BV-11 friction measuring device on sanded ice revealed similar interaction patterns as observed in the laboratory experiments:

1. The original crystal structure of the ice remained intact.
2. The track contained large ploughing tracks from entrained sand particles, in which small cells were formed (typical diameter about 0.1 mm).
3. The track contained fine scratches without cell formation.

6 VARIABILITY IN FRICTION MEASUREMENTS AND A COMPARISON BETWEEN RUBBER-ICE AND SAND-ICE INTERACTION

6.1 Introduction

The observations shown in Chapter 4 illustrated that when aircraft operate on sanded iced runways, the particles can slide together with the braking tire and scratch the ice surface. Etching and replicating ice surfaces in laboratory experiments (Chapter 5) provided more information on both rubber-ice and sand-ice interaction. Rubber-ice interaction was accompanied with small scale ice deformation. Small scratches (either observed as small ploughing tracks or as rows of dislocations that were revealed by etch pits) had been formed, but the original crystal structure remained intact. During sand-ice interaction, ice deformation also occurred, but the deformation took place deeper in the ice and was accompanied with re-crystallization / cell formation.

The main question is how, in quantitative terms, a given tribosystem respond to these different interaction mechanisms. To interpret the response it is necessary to know all the details of the used tribosystem. Pneumatic tires are mechanically complex structures and combined with advanced anti-skid braking systems it is not an easy task to understand how different friction mechanisms affect the final response of the system. Therefore, it is necessary to simplify the tribosystem and study the response first in this idealized situation, before more complex systems are considered. The purpose of this study is to investigate the response of a mechanically simple tribosystem on in two “extreme” cases: (1) the friction solely created by rubber-ice interaction, and (2) the friction is solely created by sand-ice interaction. An important aspect of such investigation is the experimental procedure to prepare the ice.

Different laboratory studies on rubber-ice friction have been conducted on polished or otherwise conditioned ice (Conant et al., 1949; Wilkinson, 1953; Southern and Walker, 1972; Southern and Walker, 1974; Gnörich and Grosch, 1974; Roberts and Richardson, 1981; Roberts, 1981; Roberts and Lane, 1983). The motivation for polishing / conditioning was that more reproducible results were obtained. The most common ways of polishing are (1) allow the rubber specimen to run repeatedly in the same track and (2) allow the ice to sublimate, also been referred to as self-polishing (Roberts and Richardson, 1981) or ageing (Wilkinson, 1953). Highly variable friction measurements were obtained without these procedures. The question why freshly prepared ice exhibits such high variability has received little attention.

Polishing / conditioning procedures are performed after ice test surfaces are manufactured, typically by freezing water. This results in rough surfaces that have to be smoothened. Two commonly used techniques to smoothen the surface are to iron the surface and wipe off the melted water or to level the surface with a machining tool. These procedures expose the ice to severe thermal and mechanical stresses. Because of its high thermal state, such stresses produces highly deformed and relatively thick (grain-scale) layers of deformed ice with refined structures, such as very high dislocation densities (Sinha, 1977a), fine grains or sub-grains due to cell formations/recrystallization (Sinha, 1978a) and inter- and intra-granular cracks (Sinha, 1984). It is therefore not surprising that polishing/conditioning procedures are required after such severely and poorly controlled surfacing techniques on a material that so close to its melting point. Polishing /conditioning method (1) stresses the surface in a relatively similar way as the friction

measurements because the polishing is performed with the rubber specimen under comparable load and speed conditions as the actual measurements. In this case, a better reproducibility of the results may be obtained after the polishing, but the microstructure of the surface will still be heavily distorted. The method (2) involves the non-mechanical removal of the surface layers, with relatively high and variable dislocation densities, and exposing the interior material with lower dislocation densities (Sinha, 1977a). When these microstructural changes are considered it becomes apparent that the properties of the used ice surfaces are heavily depended on the used experimental procedure.

In an operational situation the iced pavement is also subjected to preparation procedures, such as snow ploughing, sweeping and blowing with cold air. This means that the surface is also heavily exposed to mechanical action and forced sublimation. However, it can never be polished or conditioned in a similar manner as the ice in laboratory experiments. Usually, runways are directly re-opened after a surface preparation operation, in order to allow air traffic to continue. This implies that aircraft operate on rather freshly prepared ice. If it is difficult to obtain reproducible friction measurements on freshly prepared ice under laboratory conditions it may very well be at least as difficult under operational conditions. This will be reflected in the uncertainties of the description how "good" or "poor" the surface is, based on operational friction measurements. Clearly, there a need to investigate the variability in measured friction coefficients (the response of a system) on freshly prepared ice in more detail.

The second issue that is addressed in this study is the role of surface contaminations on the response of the system. The rubber-ice interaction exhibited mainly ice deformation close to the surface, while during sand-ice interaction, the ice deformation extended to greater depths. When the friction is provided by a mechanism that is localised to the surface, it is expected to respond more severely on any surface contamination, compared to a mechanism that takes place deeper in the ice bulk. It has been reported that the presence of snow can have significant effect on the attainable friction for aircraft (SAS, 1972). Also in a laboratory study it was noticed that the presence of snow crystals could cause a drastic drop the friction level (Gnörich and Grosch, 1974). It was therefore decided to investigate effect of snow on rubber-ice interaction, in comparison with sand-ice interaction.

6.2 Description of the British Pendulum Tester

The British Pendulum Tester (Giles et al., 1964) is a fully mechanical tribometer. Its simple design, relatively high sliding velocity and operability made it a suitable device for this study. The British Pendulum measures the total energy losses during the friction process between a rubber block that slides over a test specimen. A drawing of the pendulum is shown in Fig. 6-1.

The pendulum is released from an initial height h_0. The pendulum houses a rectangular rubber block that is attached to a spring-loaded lever. The lever can move to accommodate for the difference between the arc-shaped trajectory of the pendulum and the flat surface of the specimen. The spring is pre-loaded and delivers a load of about 22 N. The rubber block (76 × 25 × 7 mm) slides over the specimen at an angle of approximately 20°. The apparent contact area is about 76 × 2 mm^2, resulting in a nominal contact pressure of about 145 kPa. The block can pivot to ensure that the whole long edge of the rubber is in contact with the test surface. The centre of swing height is adjustable to obtain the desired sliding length of 125 mm. After releasing, the pendulum accelerates by

gravity to a velocity of about 1.8 m/s (6.5 km/h). The friction between the rubber block and the test surface retards the pendulum. The highest point that is reached at the end of the swing is marked with a pointer and the slid resistance can be read manually from the scale.

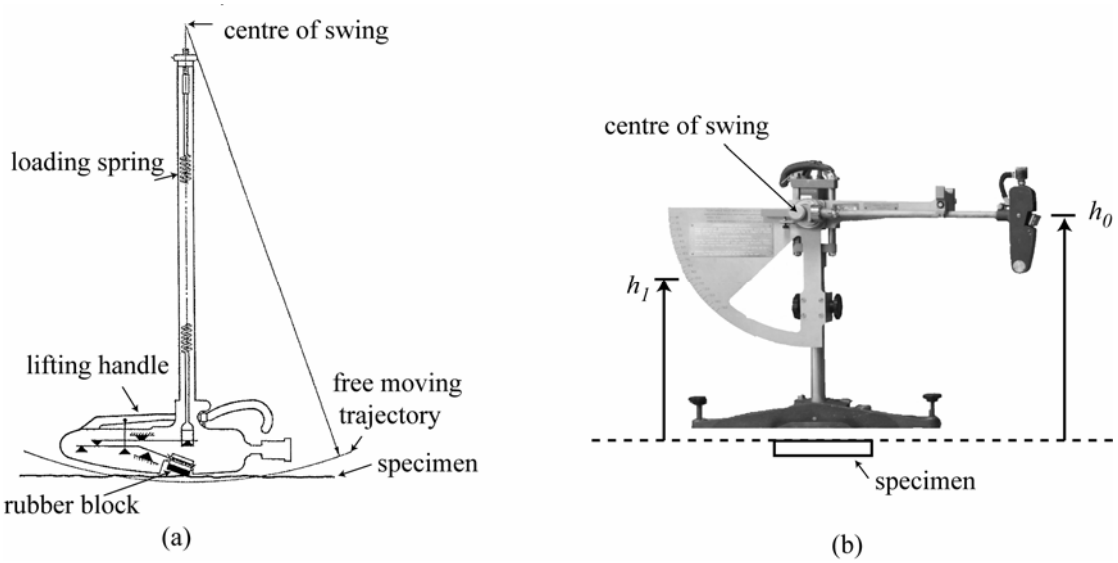

Figure 6-1. (a) Schematic presentation of the British Pendulum construction. After Giles et al. (1964), Crown Copyright 1964, Reproduced by permission of the controller of HMSO. (b) Overview of the experimental setup.

The total energy loss ΔE during the friction process is given by:

$$\Delta E = \int_0^l F_t dl \tag{6.1}$$

where l is the sliding length and F_t the frictional force. For the British Pendulum the energy loss equals (Giles et al., 1964):

$$\Delta E = W(h_0 - h_1), \tag{6.2}$$

where W is the effective weight of the swinging arm, and h_1 the height of the centre of gravity at the highest point reached after the swing. The average friction coefficient of the interaction μ_{BP} is given by:

$$\mu_{BP} = \frac{W(h_0 - h_1)}{lF_n}, \tag{6.3}$$

where F_n the normal load. The scale of the instrument is about 100 times the friction coefficient and referred to as skid resistance sr and has the unit of British Pendulum Number (BPN). It was found, however, that the effective value of F_n is not that set by the calibration procedure of the apparatus. Hence, a correction equation has been developed:

$$sr = \frac{300k\mu_{BP}}{3 + \mu_{BP}}, \tag{6.4}$$

where k is a constant with a value of 1.10 (Giles et al., 1964).

6.3 Experimental details

All activities, such as growing ice, specimen preparation, and friction measurements, were conducted inside a large, walk-in cold laboratory. Ice specimens were grown on a flat rock substrate (gabbro), according to the "sprayed ice" procedure described in Section 5.3.1. This resulted in a smooth but wavy surface. Two types of surface finish were tested: (1) no further finishing treatment after the last spray, and (2) microtoming the surface according the procedure described in Section 5.3.1. The microtoming procedure resulted in a much smoother surface, with a roughness not exceeding a few micrometers. These two surface finishes will be referred to as "sprayed", and "microtomed", respectively. The sprayed and microtomed surfaces were prepared at the desired testing temperature, which ranged between -2 and -22°C. The ice thickness was monitored after the preparation with a dial gauge connected to a fixed stand to ensure that there was no measurable interaction effect from the substrate. The specimens were allowed to sublimate for about 15 minutes prior to the friction measurements.

For reference purposes, a third type of ice was tested at melting conditions. This ice was transversely isotropic, columnar-grained, S-2 ice, grown according to the procedure described in Section 5.3.1. Specimens were cut with the c-axis directed within the plane of the surface. The S-2 ice specimens were first microtomed at $T_i \approx$ -5°C to obtain a flat finish, placed horizontally in the test arrangement, covered by a transparent container, and slowly allowed to warm up. The ice started to melt and the liquid water visibly drained off the surface. Friction measurements were performed on this wetted (by its own melt) ice.

Five sand particles (sieve fraction 2.0 -3.2 mm) were glued with epoxy, equally spaced along one long edge of a new TRRL rubber specimen (Munro Stanley London, 2006). The gluing prevented rolling and ensured that the same particles, in the same position were used in all sand-ice measurements. The load was fully carried by the particles, so rubber-ice contact was prevented. This was verified by placing the pendulum in its lowest position on the ice surface. Fig. 6-2 shows the clearing after a quasi-statically indentation of 30 s on S-2 ice at T_i = -1.5°C. The other long edge of the rubber block could still be used for the direct rubber-ice measurements. Here, the block was placed 180° rotated in the pendulum. In this position the stones did not contact the ice or the pendulum housing.

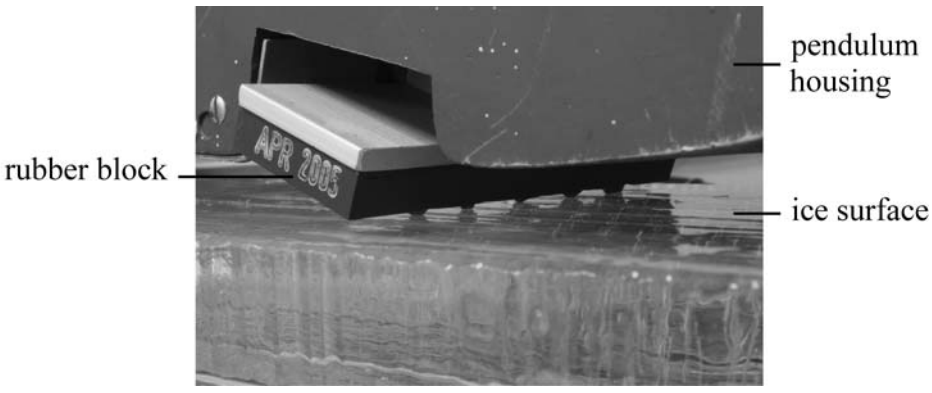

Figure 6-2. The rubber block with five sand particles glued to the long edge of the block, loaded on the ice surface for 30 s (T_i = -1.5°C). The particles prevented direct rubber-ice contact.

Snow was harvested from a naturally deposited, undisturbed snow layer. The snow was sieved (sieve fraction 1-2 mm) and allowed to sinter in the cold laboratory for 72 hours at T_a = -5°C. To apply the snow, a piece of sintered snow was placed in the 1 mm sieve and gently rubbed against the mesh. In this way, fine snow particles broke loose and gently deposited on the ice surface. It was attempted to distribute the snow as uniform as possible, but it remained a rather subjective procedure. Only a very thin layer of snow was applied, typically 1 snow crystal thick, hence not exceeding 1 mm. The result of the snow dusting procedure is illustrated in Fig. 6-3.

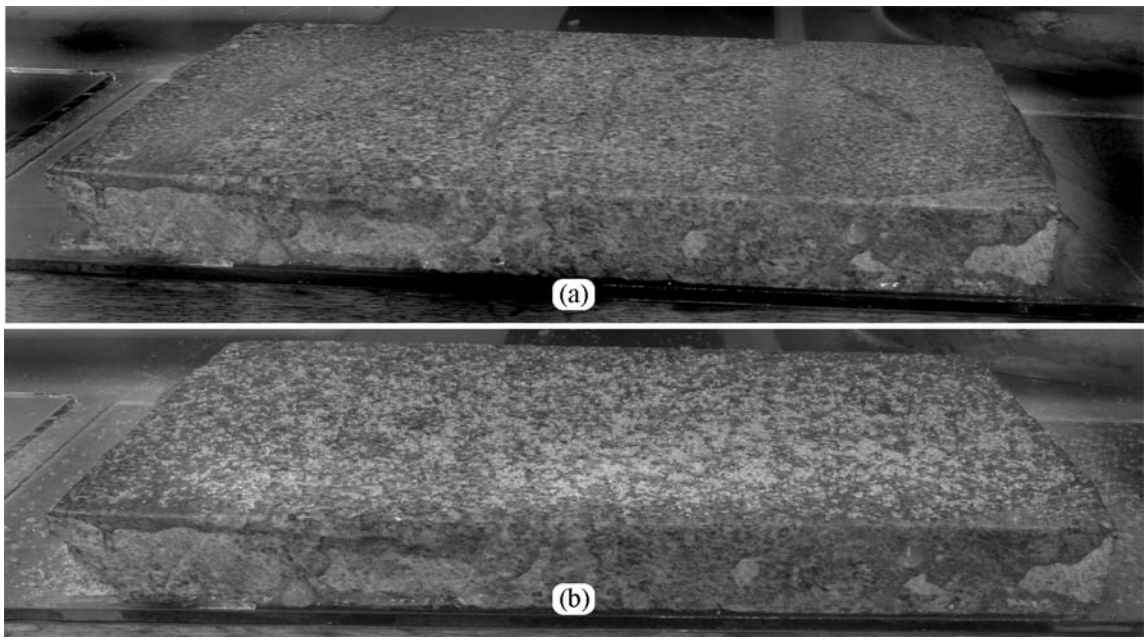

Figure 6-3. Illustration of the snow dusting procedure: (a) the gabbro rock substrate that is covered with ice. (b) The same surface that is dusted with loose snow particles.

The data collection procedure was divided into different batches. Each batch consisted of 5-10 measurement runs on a given surface finish (sprayed, microtomed, or melted) at a given ice temperature. The number of runs was based on the observed variability during the data collection. The specimens and pendulum were clamped to a solid table to ensure a fixed pendulum-specimen position. 5 zero-point measurements of a freely moving pendulum were taken prior to each run and the pendulum height was adjusted to obtain the desired sliding length of 125 mm.

First, five rubber-ice measurements were taken on clean ice. This was typically performed within 30 s. It was followed by five rubber-ice measurements on snow-dusted ice, applying the snow before each measurement. Snow crystals on the rubber block were gently removed with a soft brush after each measurement. It was ensured that the block did not pivot. Finally, one measurement was taken with the sand particles on snow dusted ice. The ice surface became severely damaged after one measurement with the sand particles. Therefore it was not possible to conduct multiple sand-ice measurements within the same run. A whole run including the zero-point measurements and adjustments could be completed within about 120 s. The air and ice temperatures were recorded immediately after each measurement run.

A batch could be completed between 5 and 10 hours, depending on the type of surface finish. After changing the cold room temperature set point (max 5°C increase or decrease), the measurements were postponed for at least 12 hours to allow equipment and specimens to acclimatize. Defrosting the cooling system of the cold room was performed in between the batches. The cooling system ventilation fans were turned off during the spraying and during the measurement runs avoid wind and vibrations. This could be done from inside the cold laboratory, avoiding excessive opening the entrance door and accompanied air temperature disturbances.

6.4 Results

Within-run variability of rubber-clean ice measurements

The average friction coefficient of a run $\overline{\mu}_r$ was calculated from the 5 repetitive rubber-clean ice measurements μ_{1-5}. The variability within the run ($\mu_i - \overline{\mu}_r$) is presented in Fig. 6-4, differentiated for the three types of surface finish. The number of data points *n,* the standard deviation within the runs σ_r, and the maximum observed variability within the runs $\Delta\mu_r$ are given in each figure. $\Delta\mu_r$ is calculated by:

$$\Delta\mu_r = \max(\max(\mu_i) - \min(\mu_i)), \quad i = 1,2,3,4,5 \tag{6.5}$$

Fig. 6-4 shows that the within-run variability is distinctively larger for the microtomed surfaces (σ_r = 0.021, $\Delta\mu_r$ = ± 0.092), compared with the sprayed ice surfaces (σ_r = 0.013, $\Delta\mu_r$ = ± 0.0032). The melting S-2 ice exhibit a low within-run variability (σ_r = 0.003, $\Delta\mu_r$ = ± 0.008) which corresponds to ± 1 BPN. The corresponding normal probability plots are presented in Fig. 6-5. Fig. 6-5 shows that all the distributions deviate from a normal distribution (indicated by the straight dashed line).

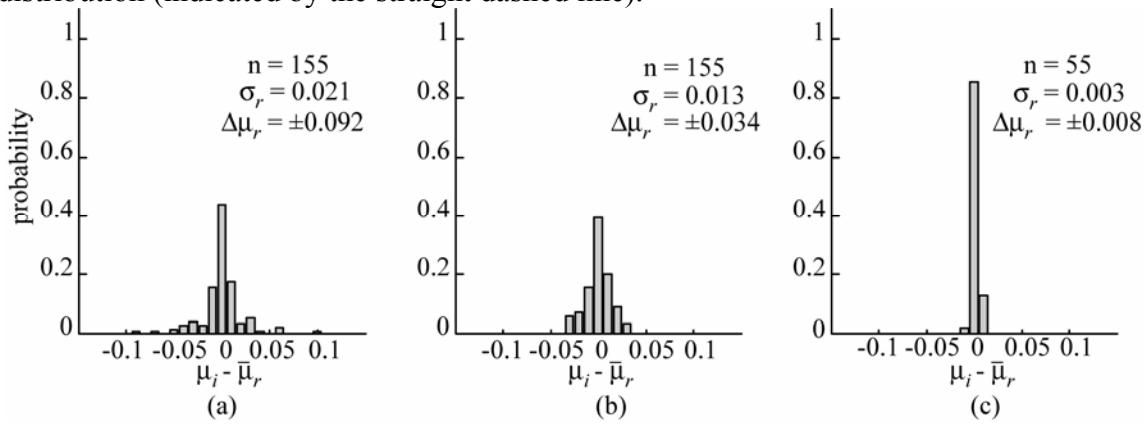

Figure 6-4. Within-run variability of rubber - clean ice measurements: (a) microtomed ice, (b) sprayed ice, and (c) melting S-2 ice.

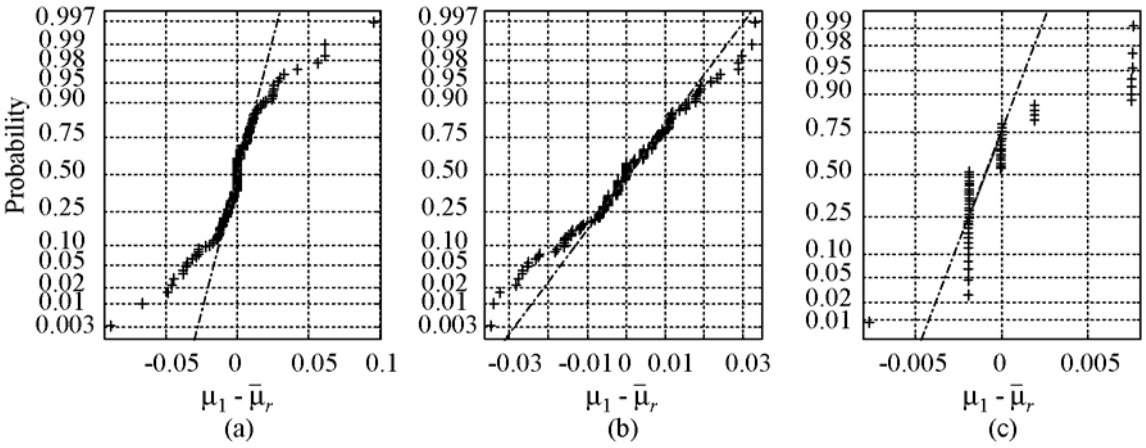

Figure 6-5. Normal probability plot for within-run variability on (a) microtomed ice, (b) sprayed ice, and (c) melting S-2 ice.

The effect of repetitive measurements was investigated by calculating the difference between the last and the first measurement in a run ($\mu_5 - \mu_1$) and was plotted both against $\bar{\mu}_r$ and T_i in Fig. 6-6. The differences are largely scattered and does not exhibit a uniform trend with neither the average friction level nor ice temperature. However, when considering only differences that exceeded the uncertainty due to measurement error ($2\delta\mu_1$, see Section 6.5) it can be seen that in most runs (92 %) the friction level has increased with repetitive measurements.

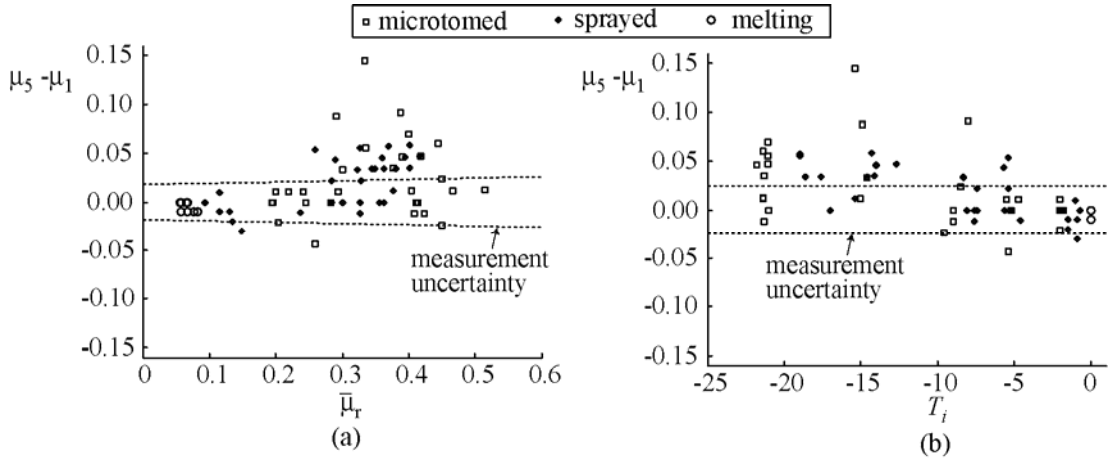

Figure 6-6. The difference between the last and the first measured friction coefficient in a run, plotted against (a) the run average friction coefficient and (b) the ice temperature.

Within-batch variability of rubber-clean ice measurements

The average friction coefficient of a batch $\bar{\mu}_b$ was calculated by averaging all first measurements μ_1 within that batch. The within-batch variability ($\mu_1 - \bar{\mu}_b$) is presented in Fig. 6-7. The maximum observed variability within a batch $\Delta\mu_b$ is calculated by:

$$\Delta\mu_b = \max(\max(\mu_1) - \min(\mu_1)) \tag{6.6}$$

Most variability was present in the microtomed ice batches (σ_b = 0.046, $\Delta\mu_b$ = ±0.105), followed by the sprayed ice batches (σ_b = 0.026, $\Delta\mu_b$ = ±0.049), and finally the melting S-2 ice batches (σ_b = 0.009, $\Delta\mu_b$ = ±0.015).

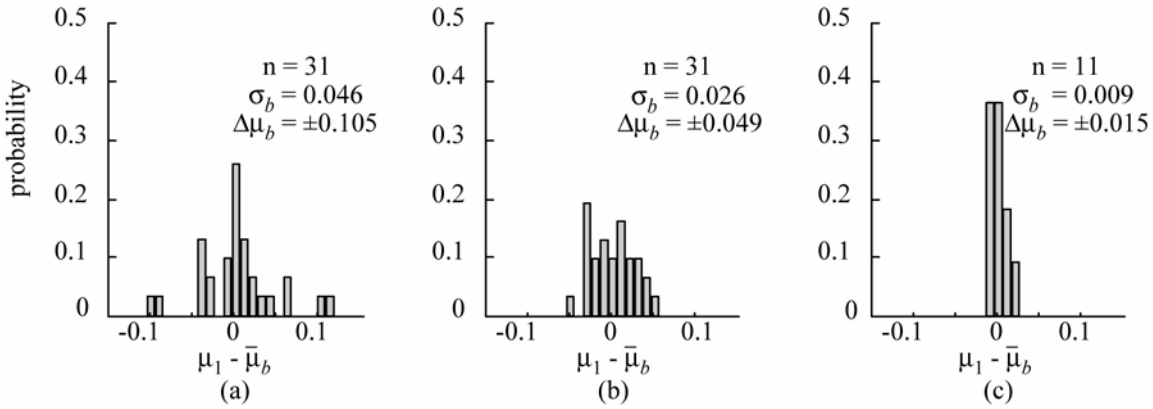

Figure 6-7.Within-batch variability for rubber - clean ice measurements. (a) Microtomed ice, (b) sprayed ice and (c) melting ice.

The effect of ice temperature and surface contamination

The total data set of rubber - clean ice measurements is plotted against the ice temperature in Fig. 6-8. Measurements within the same run are connected by vertical lines. An arbitrary reference at μ_{BP} = 0.2 is added as visual guide. All measurements below -5°C exceeded the arbitrary reference. For temperatures above -10°C the friction level decreased with increasing ice temperature. No clear correlation between temperature and friction coefficient can be distinguished at temperatures below -10°C.

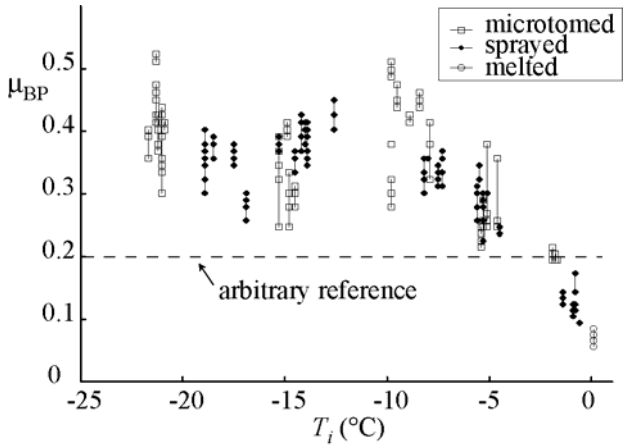

Figure 6-8. The friction coefficient versus ice temperature for rubber sliding on clean ice. Measurements of the same run are connected by vertical lines.

The effect of snow contamination on rubber-ice friction is shown in Fig. 6-9. At all temperatures the snow strongly reduced the friction level. Almost all measurements were lower than the reference μ_{BP} = 0.2. Friction coefficients at T_i = -22°C could be of the same magnitude as rubber on clean melting S-2 ice.

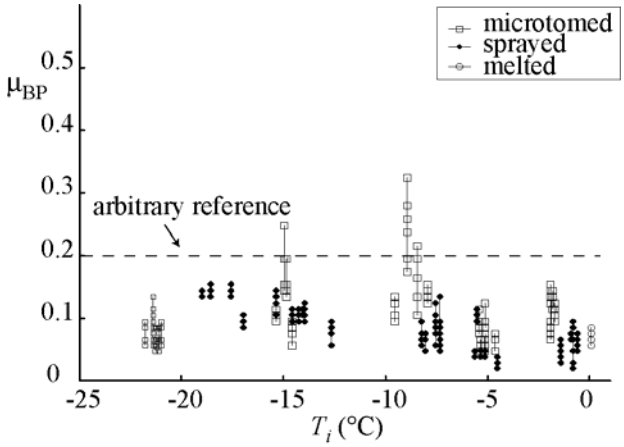

Figure 6-9. The friction coefficient versus ice temperature for rubber sliding on ice dusted with snow. Measurements of the same run are connected with vertical lines.

Fig. 6-10 shows the friction level of the sand particles sliding on snow dusted ice. The friction coefficients vary around μ_{BP} = 0.3 down to T_i = -20°C. Also on melting S-2 ice the friction level stayed above μ_{BP} = 0.3. Below T_i = -20°C a reduction of the friction coefficient was observed, but the friction level was still higher than rubber on snow dusted ice at the same temperature.

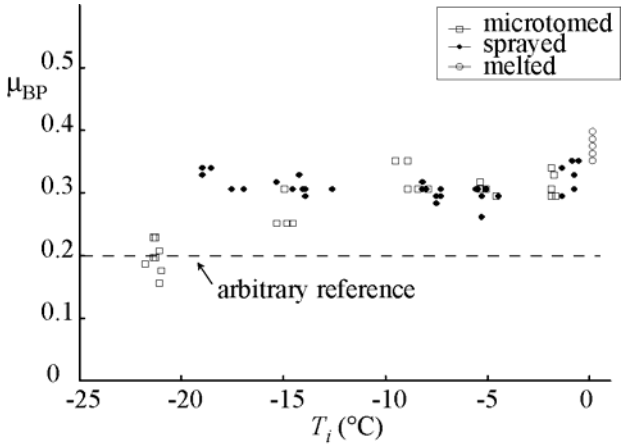

Figure 6-10. The friction coefficient versus ice temperature for sand particles sliding on snow dusted ice.

6.5 Error propagation

An error propagation analysis (Martin, 1971) was carried out to determine how known error sources introduced by operating the British Pendulum propagate into the measured friction coefficient. It is important to note that only random errors are considered here. Any systematic error, for example introduced during the calibration of the instrument, will bias the measured result, but does not introduce variability. Consequently, the result of the analyses does not give an absolute measure for the uncertainty of the friction measurement but it shows how much variability in the results can be explained by the inaccuracies involved in operating the British Pendulum.

There are two known sources of error related to the operation of the British Pendulum. The first source is the inaccuracy of the measurement reading. This error can be

considered as a random error. It is present both in the variability within the runs and in the variability within the batches. The reading inaccuracy of the skid resistance δ_{sr} is estimated to be ± 1 BPN, based on a judgement of the scale and the pointer. The skid resistance converted to a friction coefficient using Eq. 6.4. Eq 6.4 needs to be rearranged to get an explicit expression for the friction coefficient:

$$\mu_{BP} = \frac{3sr}{300k - sr} \tag{6.7}$$

The propagation of the error δ_{sr} into the friction coefficient, $\delta\mu_{1,}$ is given by:

$$\delta\mu_1 = \left|\frac{\partial\mu_{BP}(sr)}{\partial sr}\right|\delta sr \tag{6.8}$$

Differentiation of Eq 6.7 with respect to *sr* results:

$$\frac{\partial\mu_{BP}(sr)}{\partial sr} = \frac{900k}{sr^2 - 600k\,sr + 90000k^2} \tag{6.9}$$

For δ_{sr} = ± 1 BPN, the error in the friction measurement due to the measurement reading is given by:

$$\delta\mu_1 = \left|\frac{900k}{sr^2 - 600k\,sr + 9\cdot 10^4 k^2}\right|\cdot 1\,, \tag{6.10}$$

or alternatively by substituting Eq. 6.4 into Eq 6.10:

$$\delta\mu_1 = \left|\frac{0.01k^{-1}}{\left(\frac{\mu_{BP}{}^2}{(3+\mu_{BP})^2}\right) - \left(\frac{2\mu_{BP}}{3+\mu_{BP}}\right) + 1}\right|\cdot 1 \tag{6.11}$$

The second error source is the height adjustment of the pendulum, necessary to set the required sliding length of 125 mm. The sliding length was measured and could be adjusted within ± 5 mm. This error is not present within the runs (the height and specimen position was kept constant during the runs) but it is present within the batches. The sliding length adjustments were performed before each run and can be considered as a random error. It is shown in Appendix B that the relative error in the sliding length adjustments δl/l directly propagates as relative error in the friction coefficient $\delta\mu_2/\mu$. Hence, the absolute error in the friction coefficient due to the sliding length adjustments, $\delta\mu_{2,}$ is given by:

$$\delta\mu_2 = \mu_{BP}\frac{\delta l}{l} = \mu_{BP}\frac{5}{125} \tag{6.12}$$

The two error sources are independent of each other and the combined error $\delta\mu_{12}$ can be calculated by:

$$\delta\mu_{12} = \sqrt{(\delta\mu_1)^2 + (\delta\mu_2)^2} \tag{6.13}$$

The equations Eq. 6.11 to Eq. 6.13 are plotted Fig. 6-11 for the range of friction coefficients obtained in the experiment.

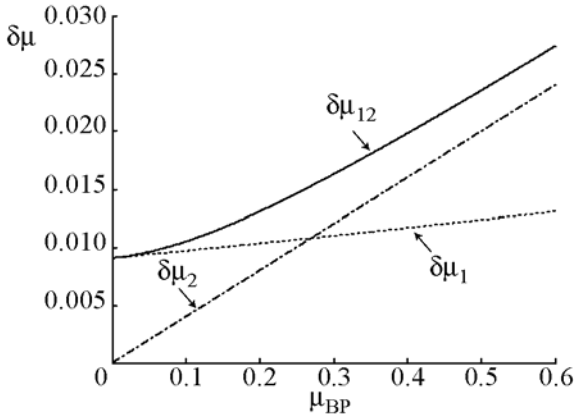

Figure 6-11. Error in the measured friction coefficient due to measurement error $\delta\mu_1$, the sliding length adjustment error $\delta\mu_2$, and the combined error $\delta\mu_{12}$.

6.6 Discussion

Within-run variability

The error propagation analysis (Fig. 6-11) show that a variability of ± 0.01 can be ascribed to, and thus explained by, the measurement reading error $\delta\mu_1$. An evaluation criterion is required to quantify how much of the variability can be explained by the measurement reading error. This can for example be the maximum observed variability in the experiment, or a chosen confidence interval given by $n\sigma$. The maximum observed variability is fully dependent on one (extreme) data value. A given confidence level therefore is more suitable for this purpose.

The within-run variability appears not normally distributed (Fig. 6-5) which indicates that the underlying process that causes the variability is not of pure random nature. The actual distribution remains unclear, due to the rather limited data volume (n = 155 for sprayed and microtomed ice, and n = 55 for melting S-2 ice), and the (still) unknown nature of the underlying processes. A conservative estimate of the 89 % confidence interval of an unknown distribution (Chebyshev's Theorem) is given by 3σ, which is chosen here as evaluation criterion. It can be argued that this confidence level is too low. However, higher confidence levels result in variability that significantly exceeds the maximum variability observed in the experiment. At this stage it would be rather speculative to consider and discuss a variability of a magnitude that is not observed in the experiment.

Using 3σ as the criterion, the within-run variability on melting S-2 ice ($3\sigma_r = \pm 0.009$) is less than ± 0.01. This means that all within-run variability on melting S-2 ice can be explained by the measurement reading error. These measurements show that no other significant error sources were present within the runs. Hence, without readjusting the pendulum it was indeed possible to repeatedly obtain a friction coefficient within an uncertainty of ± 0.01 (± 1 BPN). The observed variability within the runs on melting ice is thus fully explained by the measurement reading error.

The within-run variability on microtomed ice ($3\sigma_r = \pm 0.063$) and on sprayed ice ($3\sigma_r = \pm 0.039$) are significantly larger than the variability on melting ice. Here the measurement reading error explains only 16 % and 26 % of the observed variability, respectively. The remaining (unexplained) within-run variability ($3\sigma - \delta\mu_1$) is ± 0.053 for the microtomed ice and ± 0.029 for the sprayed ice.

Since the five rubber-clean ice measurements were taken in a very short period (< 30 s), it is unlikely that the environmental conditions (air temperature, humidity) had changed sufficiently to cause the within-run variability. A more likely explanation is that the ice surface did not fully recover before the next measurement was taken (about 7.5 s later). The five repetitive measurements were therefore strictly speaking not taken on the same surface. As a result, they cannot be considered as statistically independent measurements. This view is supported by the observed deviation from the normal distribution (Fig. 6-5). Three possible explanations for incomplete recovery were considered: (1) thermal recovery, (2) delayed elastic recovery, and (3) permanent ice deformation.

Heat is dissipated during the friction process. This can warm up the ice and/or the rubber. The time between two successive measurements may have been insufficient to reach the same thermal state in each measurement. Ahagon et al. (1988) also used a British Pendulum on ice and found no correlation between the loss tangent of the rubber and the

friction, showing that the energy dissipation was not located inside the rubber. Assuming that this was also the case in our experiment, residual heat would mainly be located in the ice. It was possible that the surface temperature of the frictional-heated ice did not cool down sufficiently to reach its initial value before the next measurement was undertaken. There is one observation, however, that makes it difficult to ascribe the unexplained within-run variability indeed to residual heat in the ice. With a warmer ice surface, the friction level is expected to be lower (This trend is also observed in Fig. 6-8). However, Fig. 6-6 shows a tendency that the friction level increased with repetitive measurements, at least when the difference between the first and the last measurement exceeded the measurement uncertainty. Therefore, residual heat in the ice appears not a proper explanation for the observed variability.

As outlined in Section 4.5.3 the ice deforms (apart from cracking) in an elastic, delayed elastic, and viscous manner. This means that upon unloading, the ice recovers both from its elastic and delayed elastic deformation. Elastic recovery can for practical purposes be considered as instantaneous, but delayed elastic recovery is time dependent. The total sliding length was 125 mm. Taking an average sliding velocity $\bar{v}$ of 1 m/s (3.6 km/h) (initial velocity is about 1.8 m/s) the total loading time of the specimen is 125 ms. The contact time of a point on the ice is much shorter and given by:

$$t = \frac{l_c}{\bar{v}} \tag{6.14}$$

where l_c is the contact length of the rubber block. With l_c of about 2 mm, the contact time of a point on the ice reduces to 2 ms. Although the time between two successive measurements was short (about 7.5 s), it was still long in comparison with the loading time of the ice. This suggests that the ice specimen had sufficient time to recover from delayed elastic deformation before the next measurement was undertaken.

The third considered explanation is the permanent surface deformation. The surface damages in the form of small localized structural changes in the ice (scratches and dislocations) were shown in Chapter 5. The initial phase of repetitive sliding or rolling contact is known as the "running-in" phase. It generally involves permanent compliance (deformation) of the two mating surfaces (Bhushan, 1999). For lubricated systems, the friction usually reduces during the running-in phase. But as outlined, the experiment showed a tendency that the friction coefficient increased with repetitive measurements. This observation can, however, be rationally interpreted when rubber-ice adhesion[7] is not neglected. A gradual compliance of the two surfaces with repetitive measurements implies an increase in the real contact area, which could increase the total resistance adhesion. This reasoning may also provide a clue why the within-run variability on microtomed ice was distinctively larger than on sprayed ice. The microtomed surface was much smoother than the wavy sprayed ice. The surface roughness of microtomed ice did not exceed a few μm. Hence, less deformation seems required to increase the real contact area, compared to the wavy sprayed ice, causing a larger variability within the same number of exposures (the five measurements).

[7] The term "adhesion" refers in this context in a broad sense to the attractive forces between the molecules of the two interacting surfaces, rather than the mechanism of shearing junctions.

Summarizing, the portion unexplained within-run variability that was observed in the experiment appears best qualitatively explained by the permanent deformation (structural modification) caused by previous measurements.

Within-batch variability

Within-batch variability between ± 0.01 to ± 0.025 (depending on the measured friction coefficient) can be explained by combination of the measurement reading error and the sliding length adjustment error. The same 3σ-criterion (89 % confidence interval) will be used to quantify the explained and unexplained variability.

The measured friction coefficient on melting S-2 ice did not exceed 0.1. Hence a within-batch variability of ± 0.01 can be explained by the measurement and sliding length error $\delta\mu_{12}$ (see Fig. 6-11). The within-batch variability of melting S-2 ice ($3\sigma_b$ = ± 0.027) can for 37 % be explained by the measurement errors. In contrast to within-run variability, the reference melting S-2 ice exhibits a significant amount of unexplained variability (± 0.017). This was not surprising because a batch took considerably longer to complete (5 to 10 hours), compared to a run (30 s). Variations in for example air temperature and humidity can be more prominent in the within-batch variability. The melting S-2 ice was selected as reference because it had the most reproducible microstructure it was thermally more stable, being at its melting point. The within-batch variability of these measurements may be considered as "best possible", with the used equipment and under the prevailing experimental conditions.

On microtomed and sprayed ice the measured friction coefficient did not exceed 0.55 and 0.45, respectively. Hence a maximum within-batch variability of ± 0.025 and ± 0.022, respectively, can be explained by the error $\delta\mu_{12}$. The within-batch variability on microtomed ice ($3\sigma_b$ = ± 0.138) can for 18 % be explained and the remaining portion is ± 0.113. On sprayed ice, the observed within-batch variability ($3\sigma_b$ = ± 0.078) can for 28 % be explained, leaving a remaining portion of ± 0.056. So the unexplained variability on microtomed and sprayed ice is considerably larger than on the reference S-2 ice. This supports the idea that the variability is primarily related to the ice surface properties.

The fact that the microtomed surfaces exhibited the most unexplained variability (both within-run and within-batch) was unexpected. The microtoming procedure was intended to improve the reproducibility of the surface topography of the ice. The surface topography of the sprayed ice is poorly controllable because it is governed by the freezing process, which is only indirect controllable by the amount of water that was applied. The microtoming procedure did produce much smoother surfaces (roughness not exceeding a few micrometers) and visually, specimens appeared much more uniform than the sprayed surfaces. So apparently, the visible variations in topography were less important than variations in the surface on smaller scale (not visible with the naked eye). It also suggests that on this smaller scale, the microtomed surfaces exhibited a larger variation in the surface properties than the sprayed ice (causing within-batch variability) and that the surface is more sensitive to changes (causing within-run variability).

Like any other surface treatment, microtoming disturbs the surface. But the procedure was developed to minimize the mechanical stresses on the ice (Sinha, 1977b). During microtoming the distortion occurs on a small scale (microscopic or smaller). It can produce small scratches and dislocation loops at the surface level. The amount of damage mainly depends on the sharpness of the blade and increments of the shaving.

The sharpness of the blade is not constant and the speed of the microtoming was not accurately controlled. Unfortunately the blade could not be re-sharpened before each run or batch. It was sharpened before the experiment. So, the small scale distortions in the ice surface after the microtoming procedure may very well have been varied significantly within a batch. Hence, the efforts to control the surface roughness in fact introduced more uncertainties than leaving the sprayed surface untreated.

Summarizing, the results suggest that friction provided by rubber-ice interaction on clean, freshly prepared ice is highly dependent on, and maybe even governed by, small scale ice surface properties that can change significantly under the action of the exposed stresses, or due to the environment (experimental conditions) in which the ice is situated. This would imply that the focus should be directed to the microstructural level when ice friction is to be explained and factors like surface roughness should be considered. From a general tribological point of view this may sound too obvious to be mentioned, but Chapter 4 showed that much of the attention for "high sliding velocity[8]" ice friction has been directed to the generation of a lubricating water film and not to general tribological aspects like surface roughness, asperity deformation and interfacial adhesion.

Quantitative comparison between rubber-ice and sand-ice interaction

Before discussing the quantitative friction data it is important to note that the numerical values should not be interpreted blindly in terms of good, medium or poor. As outlined in the introduction, the reported values are the response of one particular tribosystem – in this case the British Pendulum Tester on artificially prepared ice.

Despite the present variability, the rubber - clean ice interaction (Fig. 6-8) show above T_i = -10°C a clear reduction of the friction coefficient with increasing ice temperature. This trend is in accordance to the existing literature. Below T_i = -10°C a clear trend cannot be distinguished, but it is recognised that the data volume is too limited to draw firm conclusions.

The important aspect of the dataset is that, below say T_i = -5°C, the rubber- clean ice interaction provided a friction level that remained at least above a certain level, being about μ = 0.2. In comparison with rubber- wet melting ice interaction, this is an appreciable friction level. However, only little snow (less than 1 mm) was needed to reduce the friction level significantly. Here, the friction level dropped drastically over the whole temperature range (Fig. 6-9) and could be in the range of wet, melting ice conditions even though the ice temperature as low as -20°C. This shows that although a reasonable level of friction was obtained on clean ice, the rubber-ice mechanism providing the friction is very vulnerable to snow contamination. In contrast, friction provided by sand-ice interaction (Fig. 6-10) on snow contaminated ice provided a reasonable friction level over the whole range from -20°C to 0°C. Clearly, this friction mechanism is not as vulnerable as the rubber - ice mechanism to the little amount of applied snow.

Practical relevance

Friction measurements on iced road and runway pavements are performed to inform pilots, to assist winter maintenance personnel decisions, and to define the quality criteria

[8] With high sliding velocities is understood sliding velocities in the m/s range.

for the pavement. So they serve important practical purposes. For maintenance personnel it is often their only "objective" reference available to judge their actions. But their actions take time. After they cleaned and prepared a pavement it will take time before the same area is treated again. This means that a pavement that measures "good" friction coefficients after a cleaning operation is only "good" when it can holds it properties for a certain period of time. Unfortunately, friction measurements do not give any information on how robust or vulnerable the pavement is to changing conditions.

Maintenance personnel usually work to satisfy a "minimum friction" criterion, according the device that is available to them. This leads to the natural perception that with a high measured friction coefficient it takes longer before the minimum friction criterion is reached. The experiments demonstrate that this natural perception is incorrect. A high friction coefficient is in no way a guarantee that the friction coefficient remains high. How quickly and how severely the friction coefficient can drop depends on the vulnerability of the operative friction mechanism to changing conditions.

The magnitude of the variability observed here on freshly prepared ice cannot directly be translated to the variability of operational measurements on freshly prepared pavements. But the fact that the variability was much larger than the uncertainties of the measurement procedure itself provides some food for thought. If the variability on ice exceeds the inaccuracy of the measurement device, the resulting data should be interpreted accordingly. For example, Table 2-2 shows how readings from friction measurement devices are practically interpreted. The resolution between the different classes is 0.05 and the difference between the lowest friction coefficient in the category "good braking action" and the highest friction coefficient in the category "poor braking action" is 0.15. Friction coefficients are typically reported with 2 decimals, suggesting an inaccuracy not exceeding ± 0.01. The laboratory results can of course not blindly be compared with an operational situation. Nevertheless, the variability in the experiment was a factor 4 to 14 larger than the accuracy in which friction coefficients of operational surfaces are reported to pilots (± 0.01). So what is the real uncertainty of the estimate how good or poor the runway is?

6.7 Conclusion

Friction measurements between the rubber and clean, freshly prepared ice exhibited significant variability. Within multiple readings on apparently the "same" surface, the friction coefficient could vary as much as ± 0.063 and ± 0.039 (using 3σ as criterion), depending on the ice preparation procedure. Within the readings on virgin ice samples, the friction coefficient could vary as much as ± 0.138 and ± 0.078, depending on the ice preparation procedure. This variability, obtained in a controlled laboratory environment is a factor 4 to 14 larger than the accuracy in which friction coefficients of operational surfaces are reported to pilots (± 0.01).

The observed variability could only partially (between 16 and 28 %) be explained by known error sources of the used tribometer. The remaining, unexplained, variability appears to be directly related to by poorly controlled/reproduced, microscopic or nanoscopic surface properties of the ice and rubber. Friction between the rubber and clean, freshly prepared ice seems highly dependent on, and is maybe even governed by, small scale ice surface properties that can change significantly by the exposed stresses or due to the environment (experimental conditions) in which the ice is situated.

Below an ice temperature of -5°C, all measured friction coefficients between rubber and clean freshly prepared ice were in range between 0.25 and 0.5. However, the friction coefficient dropped drastically (down to 0.05) by only minor loose snow contamination (less than 1 mm) on the ice surface. These low friction levels are of comparable magnitude as the friction coefficients of rubber sliding wet, melting ice.

When the friction was provided by sand-ice interaction, and possible rolling action of sand particles was prevented, the friction remained at an appreciable level (around 0.3) over the whole temperature range from -20°C to 0°C. Clearly, this interaction mechanism is less vulnerable to little loose snow contaminations on the ice surface.

7 NON-CONTACTING DETECTION OF SAND ON ICED PAVEMENTS

7.1 Introduction

A number of non-contacting measurement principles have been explored in the past to describe and evaluate winter contaminated pavements. Holzwarth and Eichhorn (1993) and Ciamberlini et al. (1995) investigated the absorption and backscatter of infrared and near-infrared radiation on dry, wet and iced pavements. In the microwave frequency range, Finkele (1997) studied the changes in polarization of the scattered radiation, and Sarabandi et al. (1997) theoretically described the scattering from asphalt surfaces. Ogura et al. (2002) used albedo measurements on dry, snow covered, and iced pavements. A common motivation for all these efforts was the desire to identify hazardous surface conditions. This identification can warn maintenance personnel or the users, such as pilots or motorists.

There are many regions in the world where chemicals are used as a preventive measure against ice formation on pavement. For such maintenance strategies, a sensor that can detect the presence of ice on the pavement provides useful information. Maintenance personnel can be warned that new maintenance operations are required or motorists can be encouraged to adjust their driving style. But there are also regions in the world where chemically-based maintenance strategies are less suitable. Here, compacted snow and ice build-up can be reduced (i.e. by ploughing and sweeping) but not totally avoided. In these regions, ice is usually present on the pavement for prolonged periods of time. A common strategy for these surface conditions is to apply sand, intended as a friction enhancing measure. For this maintenance strategy, the detection of the presence of ice does not provide sufficient information to determine hazardous surface conditions. Here it is largely the presence of sand that determines how good or poor the surface conditions are. The application rate and the uniformity of the application are the important quality factors of a sanding operation with a given type of sand (Comfort and Gong, 1999). After the application, the surface conditions can deteriorate, for example when traffic, weather, or other maintenance activities, redistribute or remove the sand particles. So if it is possible to detect the amount and distribution of sand on iced pavement it can provide valuable information to maintenance personnel, motorists or pilots.

In the last decades, the advances in digital photography have created new possibilities to acquire information that is suitable for quantitative image analysis. Image processing and analyzing techniques have matured from ad hoc, empirical approaches to a sound science, based on well-established principles in mathematics and physical sciences (Jähne, 2004). These techniques may be applicable to the detection of sand particles on iced pavements. In photography, the radiance coming from objects in the scene is imaged onto the image plane where it is recorded. The objective of the experiment described in this chapter was to investigate the radiance from a sanded pavement that was illuminated by a visible laser.

When an optically rough surface is illuminated by a light source, a part of the incident light scatters into the hemisphere surrounding the illuminated surface. The intensity of the scattered light I_s is the amount of power ϕ that is scattered from a point within a cone of a given solid angle Ω (Meyer-Arendt, 1995):

$$I_s = \frac{\phi}{\Omega} \tag{7.1}$$

The radiance L is the amount of power emitted per unit projected area $A\cos\theta$ of the illuminated surface, within a cone of a given solid angle:

$$L = \frac{\phi}{A\cos\theta\,\Omega} = \frac{I_s}{A\cos\theta}, \tag{7.2}$$

where θ is the angle between the surface normal and the specific direction.

If a surface is completely non-specular, the intensity is directly proportional to the cosine of the angle θ between the observer's line of sight and the surface normal (Lambert's cosine law):

$$I_{s,\theta} = I_{s,\perp}\cos\theta, \tag{7.3}$$

where $I_{s,\perp}$ is the intensity normal to the surface. Substitution of Eq. 7.3 into Eq. 7.2 shows that on such "Lambertian surface" the radiance is the same in all directions:

$$L = \frac{I_{s,\perp}\cos\theta}{A\cos\theta} = \frac{I_{s,\perp}}{A} \tag{7.4}$$

Dry road surfaces are optically rough and the data presented by Ciamberlini et al. (1995) illustrate its near-Lambertian properties. But when such surface become covered with ice or water, the direction of the scattered light changes towards a more specular reflection (Holzwarth and Eichhorn, 1993). The radiance of the illuminated surface increases in the direction of the specular reflection and decreases in all other directions. This effect is pronounced when the surface is illuminated at a higher angle of incidence.

The total radiance from the illuminated surface can be measured by a single sensor, for example a photodiode. This, however, does not give any information of regions with different radiance within the illuminated area. Such information can be preserved by using the collected radiance to create an image. This requires a lens system and an array of sensors. In this way, regions with different radiance within the illuminated area will have a different intensity (brightness) in the image plane. Note that in digital image analysis, the term intensity refer to the numeric value of a picture element (pixel), rather than the intensity defined in Eq. 7.1. If the illuminated area is observed at an angle sufficiently away from the direction of specular reflection, it will appear brighter when the pavement is dry, compared to a wet or iced pavement. The radiance from the pavement (denoted as "pavement radiance") will decrease as the pavement becomes contaminated. Sand particles that are located on top of the surface form additional scatter sources. The radiance coming from the sand (denoted as "sand radiance") is expected to (locally) increase the brightness. Therefore, it was hypothesized that, for a given pavement contamination, there will be a correlation between sand application rate and the total radiance from the sanded surface.

7.2 Experimental details

The experiments were performed during the field activities at Tromsø Airport, Norway in a large, portable field cold laboratory. The cold laboratory consisted of a main room (4.5 × 2.5 m^2) and an entrance room (1 × 2.5 m^2). The main room was darkened to avoid

unwanted radiation from other light sources. The air temperature was maintained at -5°C ± 1°C. To avoid vibrations, the cooling system was shut down during the measurements.

A piece of asphalt (0.5 × 0.3 m^2), originally belonging to an operational taxiway or apron, was illuminated by a visible laser and photographed at different angles. A photograph and drawing of the set-up is given in Fig. 7-1. A supporting wooden frame allowed the camera to be positioned at camera angles, θ_c between 0 and 85°, while maintaining a constant object to lens distance l_1 of 1.13 m. A semiconductor laser (wavelength λ = 635 nm, ϕ = 0.1 mW), a cylindrical lens, and a slit produced a line-shaped illumination source with divergence angle θ_d = 4.3° and a constant width w = 3 mm. The laser was mounted on a tripod at distance l_2 = 1.18 m from the target, positioned at an angle of incidence θ_l between 45° and 87°. Due to the large slit to target distance, interference around the slit edges was negligible at the target.

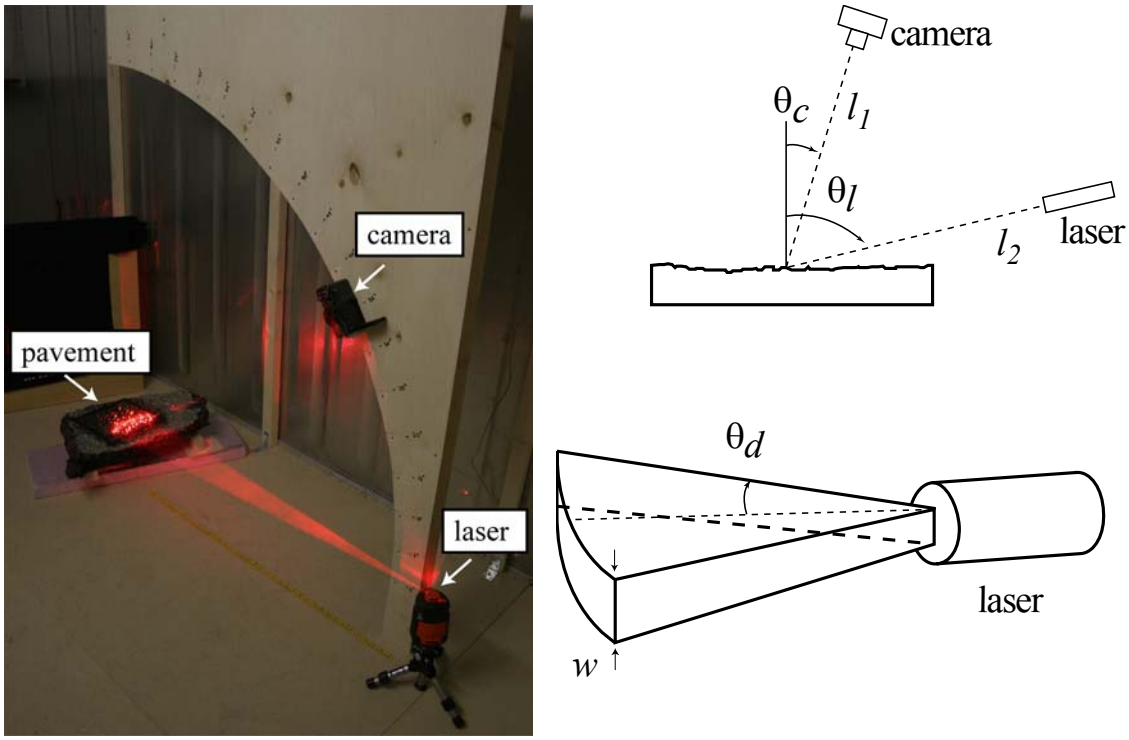

Figure 7-1. Photograph and drawing of the experimental set-up.

A digital camera with a CCD sensor containing 2595 × 1944 effective pixels was used to capture the images. All images were taken at exposure time t_e = 4 s, F-number F = 5.6, ISO 50, and focal length f = 20 mm. These settings resulted in sufficient sensitivity on the smooth ice, without excessive overexposure on the dry pavement. However, local over exposure could not totally be avoided. The images were taken in 8-bits RGB colour space and stored in JPEG format (highest quality).

The used piece of asphalt had incidentally broken off during snow removal. It was cleaned with water and allowed to dry. After drying it was brushed gently to remove loose particles. An area of 0.2 × 0.2 m^2 was marked on the top surface to define the area where sand was to be applied. The light source was aimed such that the illuminated area was located in the centre of the marked area.

Three types of pavement surface conditions were included in the test matrix: (1) a bare and dry pavement, (2) a pavement covered with a thin layer of ice, and (3) a pavement covered with a thick layer of ice. These surface conditions are denoted “dry”, “thin ice”, and “thick ice”, respectively. The iced surfaces were prepared by spraying a fine mist of water above the surface and allow the wetted surface to freeze. A single spray of about 4 ml was used for the thin ice. This was sufficient to obtain a continuous coating. The thickness was calculated to be about 0.1 mm, assuming a uniform distribution of the water. The same procedure was repeated to make the thick ice, allowing the water to freeze after each spray. Ice was deposited until the asphalt texture was covered and a smooth surface finish was obtained.

Sand was obtained from the stockpile at Tromsø Airport. It consisted of 2 - 4 mm crushed rock. Three sand application rates were used: 0, 35 and 70 g/m^2. The 35 g/m^2 application corresponded to the typical application rate used at the airport. Batches of 1.4 g were applied by hand, a few cm above the marked area. This rather subjective way of distributing the sand was adopted after trials where sand was applied at greater heights. The latter method resulted in occasions where no particles were illuminated by the laser.

A laser can produce a sharply defined illumination area, but imaging objects that are illuminated with coherent light causes an interference pattern at the image plane known as speckle. This speckle pattern sets limits to the resolution. Sand particles cannot be detected when their size in the image plane is smaller than the speckle size. The average speckle size s can be estimated by (Dainty, 1975):

$$s \approx 1.2(1+M)\lambda F\,, \tag{7.5}$$

where F is the F-number and M is the magnification given by (Meyer-Arendt, 1995):

$$M = \frac{f}{f - l_1}\,, \tag{7.6}$$

where f is the focal length of the lens system and l_1 the object to lens distance.

The calculated average speckle size in the image plane ($4.19 \cdot 10^{-3}$ mm) was smaller than the calculated minimum sand size at the image plane ($36 \cdot 10^{-3}$ mm), implying that sufficient resolution is obtained with the present experimental set-up.

The test matrix is summarized in Table 7-1. Data were collected according to the hierarchy level, starting with the lowest level (camera angle). This procedure was adopted to ensure that the same illuminated area was recorded at all camera angles and that the number of ice preparations was minimized.

Table 7-1. Overview of the test matrix.

Hierarchy level	Parameter	Settings
1	Laser angle	87°, 75°, 60° and 45°
2	Asphalt contamination	Dry, thin ice layer, thick ice layer
3	Sand application rate	0 g/m^2 , 35 g/m^2 , and 70 g/m^2
4	Camera angle	0° to 85° at 5° intervals

The recorded images were converted to 8-bit greyscale images by discarding the green and blue channel. This gave one intensity signal for each pixel between 0 and 255, where 0 represents a low intensity (black) and 255 a high intensity (white). The images were cropped to a suitable Region Of Interest (ROI). The dimension of the ROI (1200 × 1400 pixels) was determined by fitting the largest recorded footprint fully into the ROI without rotation or scaling operations. The images were cropped such that the centre of the illuminated area was placed in the middle of the ROI. For each ROI an intensity histogram was calculated that shows the number of pixels, n, for each intensity level.

7.3 Results

7.3.1 Radiance reduction due to ice contamination

The radiance from the three illuminated surface conditions (dry, thin ice, and thick ice) is illustrated in Fig 7-2. The images show a clear reduction in brightness as the thickness of the ice contamination increases. The corresponding histograms of the images quantify this reduction. The dry pavement histogram (Fig. 7-2a) exhibit two peaks, one at the low intensity levels (near $I = 0$) and one at the highest intensity levels (near $I = 255$). The number of pixels with a high intensity is reduced by the thin ice layer (Fig. 7-2b). On the thick ice layer there are no pixels left with an intensity $I \geq 200$ (Fig. 7-2c).

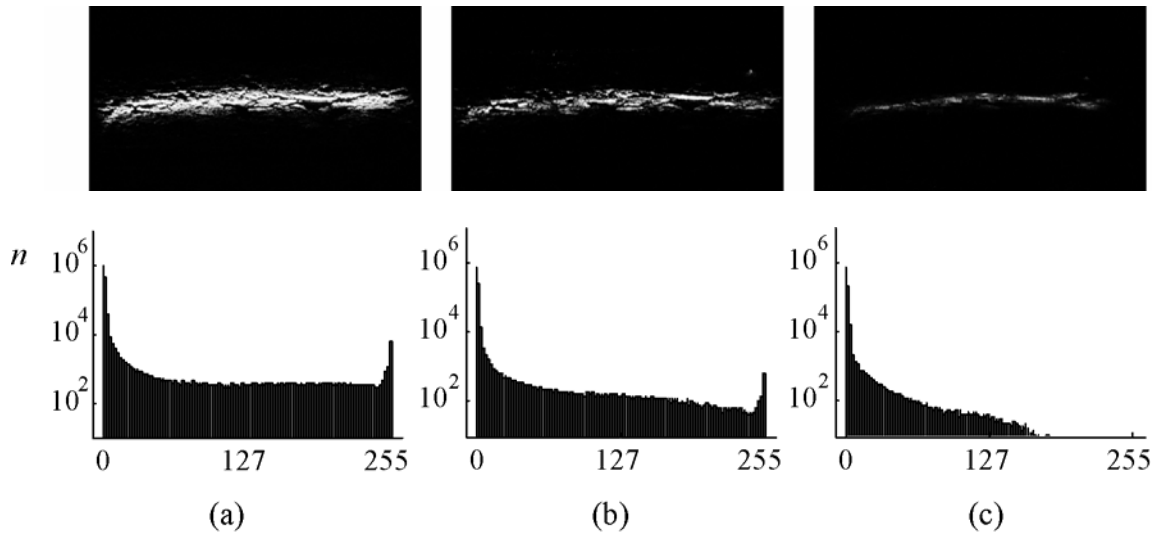

Figure 7-2. Images taken at $\theta_l = 87°$, $\theta_c = 75°$ and their corresponding histograms from (a) the dry pavement, (b) thin ice, and (c) thick ice. Sand was not applied.

The response of the high intensity levels in the histogram (the brightest pixels) was investigated at all laser and camera angles. A bright pixel was defined as a pixel with $I \geq 230$ (90 % of the maximum intensity) and the total number of bright pixels were counted

in all ROIs. This number, however, is dependent on the camera angle, due to differences in optical perspective. Hence, it is normalized with respect to the dry pavement recording of corresponding camera angle. The normalized number of bright pixels n_n is plotted against the surface condition for all laser angles in Fig. 7-3.

Fig. 7-3 shows that the number of bright pixels was significantly reduced when the dry pavement became contaminated with the thin ice layer at all laser angles. The reduction was largest at $\theta_l = 87°$ (Fig. 7-3a), where it reduced to 20 - 40 %, compared to the dry pavement. At this laser angle, the number of bright pixels continued to reduce as the pavement was covered by the thick ice. Here, less than 1 % bright pixels were recorded, irrespective of camera angle. This shows that a negligible amount of light scattered on the surface and most light was specularly reflected at the ice-air interface.

At lower angles of incidence (Fig. 7-3b-d) there was still an appreciable amount of light that scattered from the pavement covered by the thick ice layer. Here, the intensity of the scattered light strongly varied with camera angle, showing the non- Lambertian properties of iced surfaces.

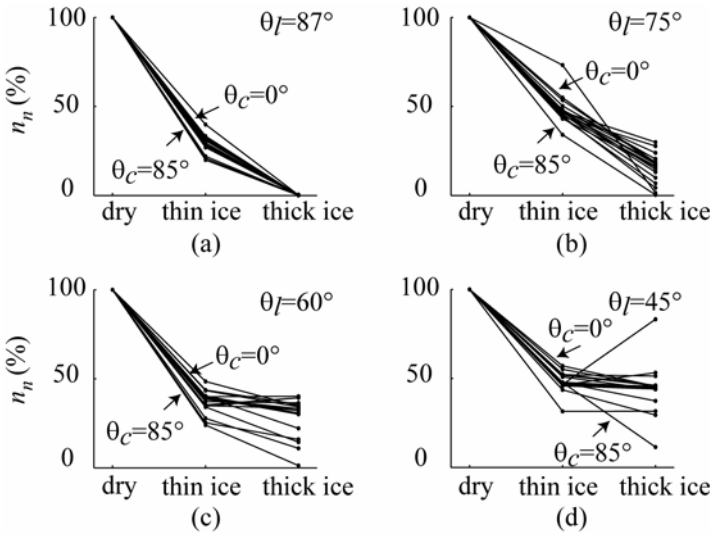

Figure 7-3. The normalized number of bright pixels for different surface conditions at four different laser angles: (a) $\theta_l = 87°$, (b) $\theta_l = 75°$, (c) $\theta_l = 60°$, and (d) $\theta_l = 45°$. Each graph shows the recordings at all camera angles ranging between 0° and 85°.

7.3.2 Radiance increase due to sand particles

The increase in radiance due to the applied sand is illustrated Fig. 7-4. The images show that the sand appears as very bright, distinct spots in the scene. The histograms show that this intensity increase is most pronounced at the high intensity end of the histogram. With sand present, a significant amount of pixels had the highest possible intensity value, $I = 255$, which implies that the sand was overexposed.

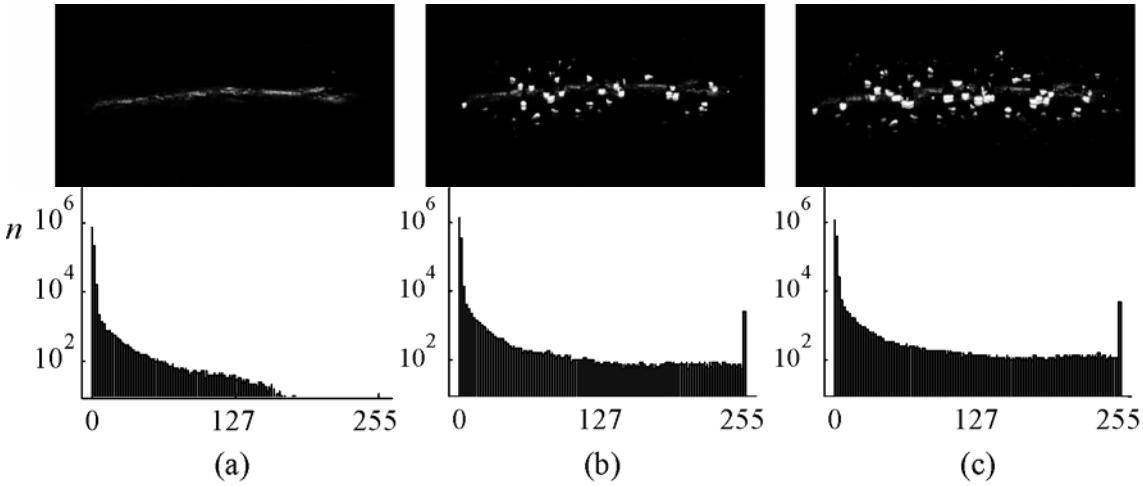

Figure 7-4. Images and corresponding histograms, taken from the thick ice with (a) 0 g/m^2, (b) 35 g/m^2, and (c) 70 g/m^2 sand.

The normalized number of bright pixels as a function of sand application rate is shown in Fig. 7-5. On the dry pavement and $\theta_l = 87°$ and $\theta_l = 45°$ (Fig. 7-5 a-1 and a-4), there exists a large variability between the different camera angles A trend cannot be distinguished. At $\theta_l = 75°$ and $\theta_l = 60°$ (Fig. 7-5 a-2 and a-3), the variability with camera angle is less but there is no clear correlation between number of bright pixels and sand application rate.

The number of bright pixels in the thin ice recordings (Fig. 7-5 b) show little variation with laser or camera angles. The number of bright pixels ranges around 50 % of the dry pavement and did not increase with increasing sand application rate.

On thick ice and $\theta_l = 87°$ (Fig. 7-5 c-1), the number of bright pixels increase with increasing application rate. Here, the slope depends on the camera angle. A similar correlation can be observed at $\theta_l = 75°$ (Fig. 7-5 c-2), but only when the images have few bright pixels at 0 g/m^2 sand. The correlation diminishes as the number of bright pixels at 0 g/m^2 sand increases. No correlation was found between the number of bright pixels and sand application rate at $\theta_l = 60°$ and $\theta_l = 45°$ (Fig. 7-5 c-3 and c-4).

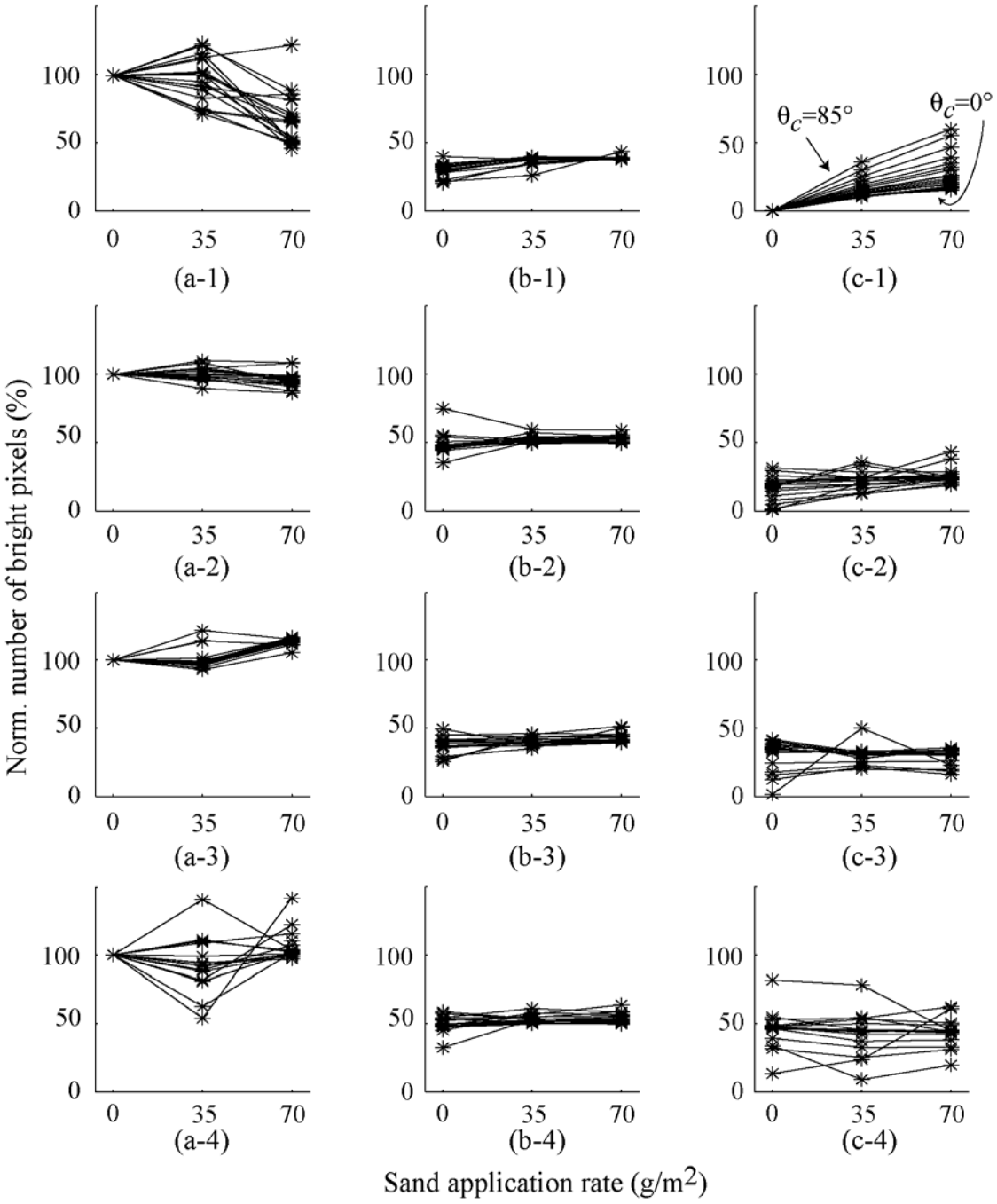

Figure 7-5. The normalized number of bright pixels as a function of sand application rate recorded for (a) dry pavement, (b) thin ice, and (c) thick ice, at a laser angle (1) $\theta_l = 87°$, (2) $\theta_l = 75°$, (3) $\theta_l = 60°$, and (4) $\theta_l = 45°$. Each graph shows camera angles ranging from 0° to 85°.

7.4 Discussion

The radiance of the illuminated area can be calculated from the intensity output of a pixel (Holst, 1998), given that all details of the optical and capturing systems are known. Without this knowledge, the radiance can only be represented by the dimensionless pixel intensity. The latter approach was used in this study because camera details such as sensor efficiency, sensor gain, and processing algorithms performed by the camera's embedded software were unknown.

The higher end of the intensity histogram was most responsive to both ice contamination and the presence of sand particles. In other words, the reduction in radiance due to the ice contamination was pronounced in the brightest areas of the scene. The sand particles also appeared mainly as very bright areas. The total radiance could therefore be expressed in a single index value, which was the number of bright pixels. Normalization of this number was required to make recordings at different camera angles (hence different perspectives) comparable.

Fig. 7-3 showed that the number of bright pixels was significantly reduced by the thin ice layer. This reduction was observed at all laser angles. However, the number of bright pixels could not be reduced to negligible values on the thin ice covered pavement. At least 20 % of bright pixels remained in the scene. These bright pavement regions could not be distinguished from the sand particles because both had a similar intensity level. Although, there may have been a measurable difference in radiance from the sand and the iced pavement, it could not be detected because the upper detection limit (I = 255) was locally reached. On thick ice, at $\theta_l = 87°$, the number of bright pixels indeed reduced to negligible values, irrespective of the camera angle. At lower laser angles, however, the radiance from the pavement with a thick ice layer remained significant.

Hence, only a combination of a very high laser angle ($\theta_l = 87°$) and a thick layer of ice on the pavement resulted in negligible backscatter from the pavement. This observation can be explained approximating scattering on rough surfaces by local specular reflections (the Kirchhoff approximation) and considering the refraction at the air-ice interface. On the dry pavement there is only one interface, the air-pavement interface. This interface is rough, meaning that the local surface normal varies throughout the surface. Waves that arrive at points with a different surface normal will be reflected in different directions.

When this interface becomes covered with a thin ice layer there are two interfaces to consider: the air-ice interface and the ice-pavement interface. A part of the light will reflect on the air-ice interface, while the rest refracts into the ice. Little light is absorbed in the ice due to its transparency in the visible range. Ones refracted, the light travels through the ice and scatters at the ice-pavement interface. How much light is refracted into the ice depends on the real angle of incidence. The thin ice cover is sufficiently thick to smoothen the surface on a small scale, but it is insufficient to smoothen the surface on a larger scale. The air-ice interface of the thin ice cover still follows the larger surface topography. The surface normal of the air-ice interface will therefore still vary significantly throughout the illuminated area. As a consequence, on pavements with a thin ice cover there are still regions where the real angle of incidence is significantly less than the laser angle, for example on the sloping sides of the aggregates. This implies that refraction into the ice cannot be fully avoided on the thin ice by adjusting the laser angle, resulting in bright regions in the scene.

On the thick ice, however, the air-ice interface is also smooth on a larger scale. It does not follow the larger scale pavement topography. Here, the local surface normal does not vary as much as on the thin ice cover. The real angle of incidence approaches the laser angle at all points in the illuminated area. At sufficiently high angles of incidence (for example θ_l = 87°) most light will be specularly reflected, leaving only negligible amount of light refracted into the ice. The result is a negligible amount of bright regions in the scene.

These considerations show that for detection on thin ice covers it will not be possible to prevent scattering at the ice-pavement interface by adjusting the laser angle. Hence, the sand detection on thin ice covered pavements has to take place with significant bright regions in the scene.

The number of bright pixels (index for the total radiance) did not correlate with sand application rate for most laser angles and pavement contaminations. A correlation was only observed on thick ice at θ_l = 87° and at θ_l = 75° when the there were initially (i.e. with 0 g/m^2 sand) few bright regions in the scene. The slope of this correlation depended on the camera angle. At θ_l = 87° on thick ice without any sand particles there were also few bright regions (less than 1 %). This suggests that the correlation is affected by radiation from the pavement.

An explanation for this observation was found by inspecting the images more closely. At non-normal illumination occurs a shadow behind the sand particles. Sand particles introduce new scatter sources which increase the number of bright pixels, but they are accompanied with the removal of bright pixels from the pavement due to the shadow. An illustration of this effect is given in Fig. 7-6. This only occurs when there is significant pavement radiance in the scene. In the absence of pavement radiance (such as at θ_l = 87° on thick ice), the pavement regions that become masked by the shadows were not bright enough to be considered as a bright pixel. Here, the introduction of a shadow does not remove bright pixels.

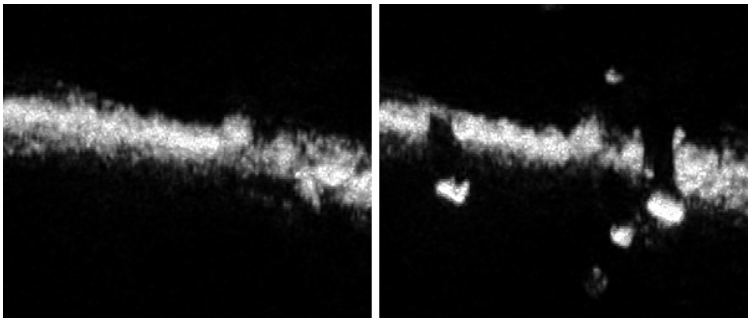

Figure 7-6. Example of shadows behind sand particles: (a) a part of the illuminated area without sand. (b) The same area with sand particles (θ_l = 75°, θ_c = 20°).

In absence of this shadow effect, the correlation between the number of bright pixels and sand application rate is expected to be approximately linear; as long as the added particles become similarly illuminated (i.e. no significant number of particles is located in the shadow of other particles). When the sand has approximately isotropic dimensions, the slope is expected to be positively correlated with the camera angle. The reason is that at the image plane, the projected area is recorded, rather than the real illumination area. The projected area of the sand (which is located on top of the surface) becomes almost

invariant with camera angle (a sphere has the same projected area at all lines of sight), while the projected area of the "flat" illuminated pavement decreases with camera angle with the factor cos θ_c. Therefore, the relative contribution of sand to the number of pixels increases with increasing camera angle, resulting in a higher slope. The data shown in Fig. 7-5 c-1 at $\theta_l = 87°$ on thick ice exhibit both the linear relationship and the expected correlation between slope and camera angle.

To be of practical value, a detection method should be able applicable on thin ice covers and preferably even on dry pavements. The transparency of ice in the visible range implies that the sand detection has to take place with significant pavement radiance in the scene. With pavement radiance present it will be necessary to either discriminate between pavement radiance and sand radiance, or to account for the reduction of pavement radiance by the shadows that are cast behind the sand particles. The collected data cannot prove the possibility for a distinction based on the pixel intensity level because information was lost by the overexposure of the sand. However, due to the similarities between the sand and pavement aggregates (both materials are made from crushed rock), such distinction may not be feasible, especially on dry pavements. Therefore, other approaches for the distinction may be explored.

7.5 Conclusion

This study explored possibilities to detect the amount and distribution of sand particles on dry and iced pavements by imaging the radiance from an illuminated pavement. With the used camera settings and illumination in the experiment, the higher end of the histogram was found most responsive to changes in the radiance, both to ice contamination and sand application. The radiance could therefore be expressed by the number of pixels above a defined intensity level.

A correlation between the radiance and the sand application rate was only found in cases where there was little radiance coming from the pavement itself. Here, the sand particles increased the total radiance linearly with sand application rate. The slope of the correlation depends on the angle at which the pavement is viewed. This correlation, however, diminishes with increasing radiance form the pavement. This can be explained by the shadows that occur behind sand particles. Bright pavement regions that become located in the shadow behind a particle become dark. In this way, the addition of bright pixels by the sand particles is accompanied with a reduction in bright pixels from the pavement.

On thin ice covered pavements, the radiance from the pavement could not be reduced to negligible values by adjusting camera and laser angle. This implies that sand detection on thin ice covered pavements has to take place with significant pavement radiance in the scene. Due to the similarities in optical properties of the sand and the aggregates in the pavement (both originate from crushed rock) and the transparency of ice in the visible range, it is unlikely that the distinction can be made on the basis of radiance intensity, with the used illumination wavelength of 635 nm.

8 APPLICATION OF IMAGE PROCESSING TECHNIQUES FOR THE DETECTION OF SAND PARTICLES ON PAVEMENTS

8.1 Introduction

The experiment in Chapter 7 investigated the radiance from sanded, iced pavements that was illuminated by a laser. It was found that the radiance originating from the pavement should, in some way, be distinguished from the radiance originating from the sand. Without such a distinction the principle appeared not feasible because total radiance (originating from the sand particles and from the pavement surface) did not correlate with the sand application rate when "pavement radiance" was present in the scene.

In the experiment, the radiance was imaged rather than directly measured. It preserved the information where inside the illuminated area the radiance originates from. This information may be used to obtain the desired distinction. The idea is to find a region in the image where the radiance originates only from the sand. The detection can then be performed within this region of interest (ROI), rather than using the whole image.

This chapter describes a principle to define the ROI. The principle is programmed in an algorithm that determines the ROI from the images taken in the experiment. As illustration, it was attempted to detect the number of sand particles that were located inside the ROI. Common image processing techniques were used in the algorithms (Jähne, 2004; Umbaugh, 2005).

The dataset collected in the experiment included an additional image, taken under normal lighting conditions, for each image that was taken with laser illumination. These two images were taken directly after each other, without changing the camera's position. Hence, the ROI determined from the image with laser illumination can directly be placed on the image with normal illumination. This allowed a manual identification of each sand particle inside the ROI and gave a possibility to assess the detection performance of the algorithm.

8.2 Principle of triangulation to determine the ROI

Consider a flat surface that is illuminated by a line-shaped laser with a divergence angle θ_d and a width w. A schematic drawing of this arrangement is given in Fig. 8-1. The shape of the laser light source was shown earlier in Fig. 7-1. The illuminated area on the surface is denoted as "pavement footprint". The surface forms the xy-plane of the Cartesian coordinate system, where z is the height above the surface. The laser is positioned such that the point p_1 where the lowest rays leave the laser is located at $z = z_1$ above the origin ($p_1 = [0, 0, z_1]$). The surface is illuminated at an angle of incidence θ_l. The x-direction is defined towards the centre of the illuminated area. Point p_2 is defined as the point where the lowest ray reaches the surface at $y = 0$. The distance between p_1 and p_2 equals the laser to target distance l_2. The height $h(x,y)$ is the distance in the z-direction between the lowest rays and the surface. The scattered radiance is recorded by a camera, positioned in the xz-plane of the laser, at an angle θ_c.

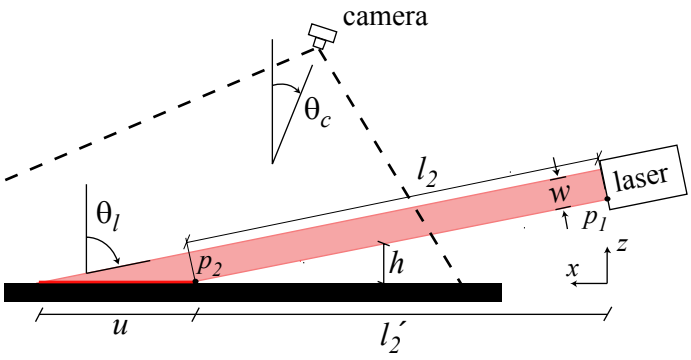

Figure 8-1. Side view of the laser-camera arrangement on a flat surface.

The surface, as viewed from the camera position at $\theta_c = 0°$, is shown in Fig. 8-2. The shape of the pavement footprint is a trapezium. The line l_3 is the collection of points where the lowest rays intersect the surface and the u is the width of the trapezium:

$$l_3 = 2\, l_2 \tan\theta_d \qquad u = \frac{w}{\cos\theta_l} \tag{8.1}$$

The area A in the xy-plane is the area where the lowest rays travel a distance $h > 0$ above the surface. A is enclosed by l_3 and two lines, k_1 and k_2 that originate from the origin with an angle $+\theta_k$ and $-\theta_k$ to the x-axis, respectively. Hence, the angle θ_k is the projected divergence angle of the laser beam θ_d. The distance from the origin to p_2 is the projected laser to target distance l_2' (also indicated in Fig 8-1) and is given by:

$$l_2' = l_2 \sin\theta_l \tag{8.2}$$

The angle θ_k is given by:

$$\theta_k = \tan^{-1}\left(\frac{\frac{1}{2}l_3}{l_2'}\right) = \tan^{-1}\left(\frac{\tan\theta_d}{\sin\theta_l}\right) \tag{8.3}$$

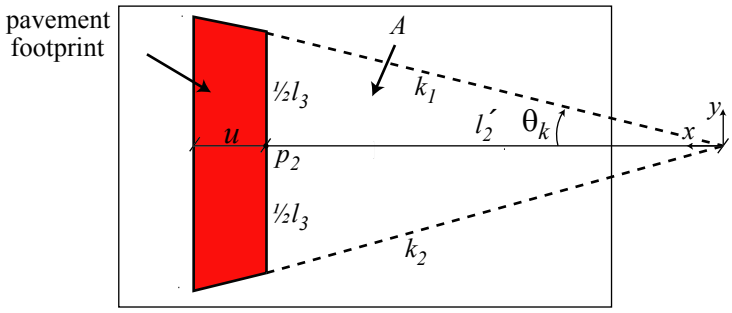

Figure 8-2. Camera view of the flat surface at $\theta_c = 0°$ (top view).

If sand particles are present on top of the surface, they will be slightly elevated. The minimum elevation height of the sand h_s is known from the minimum sieve fraction of the applied sand. The top of all sand particles will be illuminated when the lowest rays travel at a height $h < h_s$ above the surface. So within the area A there is a region where $h < h_s$. This region is the ROI because here the rays travel low enough to illuminate the tops of all sand particles while the surface is not illuminated. Therefore, the ROI is defined as:

$$\text{ROI}=\{x,y\} \quad \big| \quad 0 \le h(x,y) \le h_s\,, \tag{8.4}$$

And it is recognized that:

$$\text{ROI} \in A\,, \tag{8.5}$$

The ROI is enclosed by the four boundaries B_1, B_2, B_3, and B_4, which are defined as:

$$\begin{aligned} B_1 &= l_3 = \{x,y\} \quad \big| \quad h(x,y) = 0 \\ B_2 &= \{x,y\} \quad \big| \quad h(x,y) = h_s \\ B_3 &= k_1 \quad \big| \quad 0 \le h(x,y) \le h_s \\ B_4 &= k_2 \quad \big| \quad 0 \le h(x,y) \le h_s \end{aligned} \tag{8.6}$$

The ROI is indicated in Fig. 8-3.

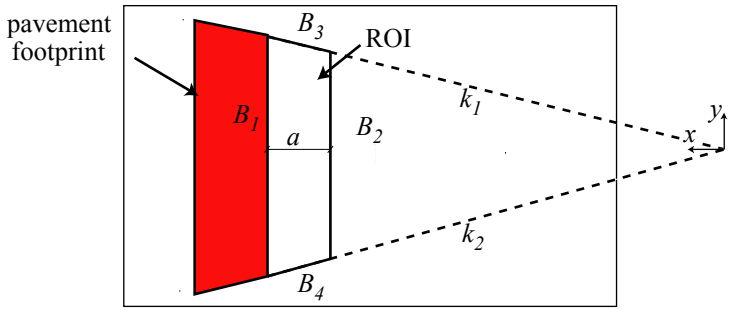

Figure 8-3. Definition of the ROI on a flat surface.

The boundary B_2 is displaced from B_1 by a distance a in the negative x-direction. This distance is denoted as "ROI width" and is given by:

$$a = h_s \tan\theta_l\,, \tag{8.7}$$

Hence, on a flat surface the ROI can be defined when θ_l, θ_d, l_2, and h_s are known.

In practice, however, the surface is not flat, especially for runway or road surfaces. Variations in the surface height $g(x,y)$ make it impossible to determine the height h in all locations of A when $g(x,y)$ is unknown. The only information available is the location where $h = 0$ because this is the inner edge of the pavement footprint. This line (similar to an altitude line on a topographical map) can have a very complex shape, as illustrated in Fig. 8-4. Note that the pavement footprint has become a group of discontinuous areas, caused by valleys and shadows behind surface peaks.

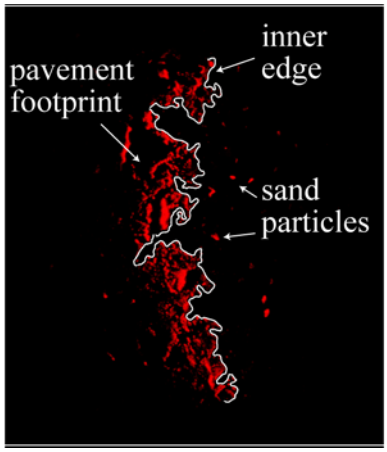

Figure 8-4. The pavement footprint on a rough surface: the inner edge where $h = 0$ has a very complicated shape due to the surface topography of the surface.

In theory, all the radiance that originates on the right hand side of the inner edge comes from the sand. However, use of this statement requires that the pavement footprint (and thus the inner edge) can be accurately determined. In an image it is difficult to distinguish between a small local peak that belongs to the pavement footprint from a sand particle that is located close to the inner edge. This uncertainty makes it more useful to define a boundary that, with a higher level of confidence, separates the pavement footprint from the ROI. Finding local maxima in the x-direction on the inner edge and interpolating them can provide such boundary. This is illustrated in Fig. 8-5 by the boundary B_1.

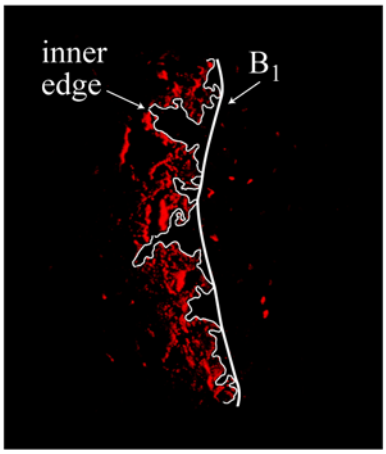

Figure 8-5. Description of the boundary B_1 by interpolating local maxima on the inner edge.

The line B_1 gives a more confident (but more conservative) distinction between the pavement footprint and the ROI than the inner edge. So, at the right hand side of B_1 it is *very likely* that $h > 0$. This makes B_1 the closest estimate to $h = 0$ with the adopted level of confidence. In the negative x-direction there is no information available about the topography, other than the knowledge that $h > 0$. This lack of information leaves no choice but to assume that the approximate location of $h = h_s$ is located the distance a in front of B_1. This assumption may be accepted under the condition that $a << B_1$. The boundaries B_3 and B_4 can be defined by k_1 and k_2, respectively because their position is not dependent on the surface topography. Hence, the ROI on a rough surface of unknown

surface topography can be defined when B1 is determined from the image and θ_l, θ_d, l_2, and h_s are known. The ROI is illustrated in Fig. 8-6.

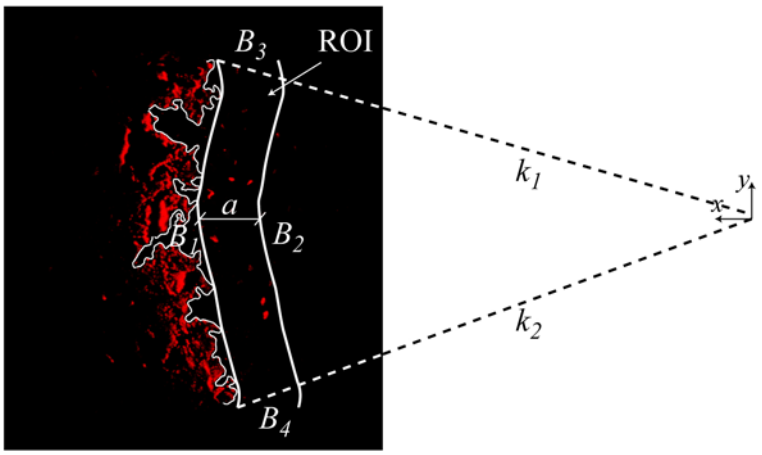

Figure 8-6. The definition of the ROI on a rough surface.

The physical interpretation of the ROI on a rough surface of unknown topography is the region with a minimum likelihood for pavement radiance and a maximum likelihood that a sand particle is illuminated.

8.3 Algorithm to determine the ROI

The main task for the algorithm is to identify the pavement footprint in the image. The input data is the 8-bits red channel of the images taken from the rough surface (Fig. 8-7a). The first step is to extract useful information and remove unwanted information. In this case, useful information is whether or not a pixel (representing the radiance from that area) belongs to the pavement footprint. All other information is, at this moment, unwanted. The removal of unwanted information is known as pre-processing and is in the algorithm performed by two processes, called quantization and segmentation. Quantization is the process where the amount of the pixel intensity information is reduced. The 8-bit red channel contains intensity information in 256 levels. This can be reduced to two levels (0 and 1) by thresholding at a certain intensity level I_{th}. This process results in a new image where the pixels with $I > I_{th}$ become white ($I = 1$) and the pixels with $I \leq I_{th}$ become black ($I = 0$), as shown in Fig. 8-7b. Underestimating the pavement footprint will cause pavement radiance in the ROI. So, the most conservative estimate of the pavement footprint (the largest footprint) is obtained when the threshold level is set equal to the noise level I_n of the signal: $I_{th} = I_n$.

The quantized image (Fig. 8-7b) contains three groups of pixels: (1) pixels belonging to illuminated sand particles, (2) pixels belonging to the pavement footprint, and (3) "loose" pixels that do not clearly belong to either the footprint or the sand. The last group of pixels form unwanted information and is removed during the image segmentation. Image segmentation is the transformation from pixel level information to object level information. The objects are meaningful areas of interconnected white pixels, surrounded by black pixels. In this case the objects belong either to pavement footprint (footprint objects) or the sand (sand objects). Segmentation is performed by convolution with an $m \times m$ matrix **C,** where m is the size of the matrix. Matrix **C** is called the convolution mask and is given in Eq. 8.8. A detailed description of the convolution operation can be found in Umbaugh (2005).

$$\mathbf{C} = \begin{bmatrix} 1 & 1 & \dots & 1 \\ 1 & 1 & \dots & 1 \\ . & . & \dots & . \\ 1 & 1 & \dots & 1 \end{bmatrix} \frac{1}{m^2}, \qquad m \in (1,3,5,7,\dots) \tag{8.8}$$

The convolution with **C** averages each pixel in the image with its neighbourhood (pixels that are in its vicinity). The result is rounded so the pixel becomes 0 when the average value of its neighbourhood is less than 0.5. The pixel value becomes 1 when the neighbourhood average is 0.5 or more. The convolution removes the smaller objects and smoothens the shape of the larger objects. A larger value for m defines a larger neighbourhood and lead to a more rigorous removal and smoothening. A suitable value for m is found by trial and error and forms one of the optimization parameters of the algorithm. The result of the segmentation is illustrated in Fig. 8-7c.

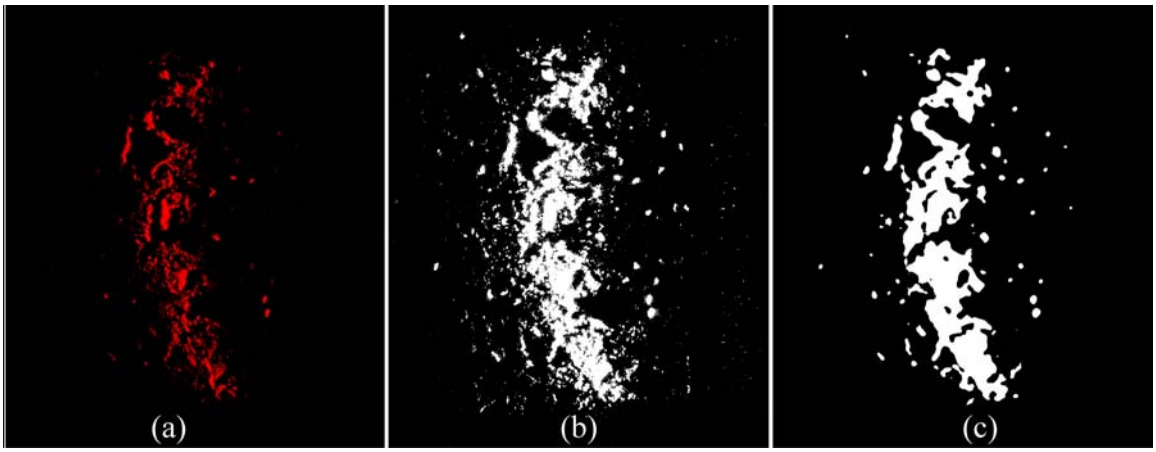

Figure 8-7. Illustration of the pre-processing steps: (a) the red channel of the original image, (b) quantized image by thresholding at $I_{th} = 3$, (c) segmented image by convolution with convolution mask **C** with $m = 11$ pixels.

After the pre-processing the image contains a finite number of objects. Each object has certain properties such as shape, area, position, and perimeter. The sand objects cannot exceed a certain perimeter, due to the maximum dimensions given by the sieve fraction. So, objects with a perimeter $P > P_{min1}$ are footprint objects. Removal of all objects with $P \leq P_{min1}$ leaves only footprint objects in the image (Fig. 8-8a).

The pavement footprint is now found and is represented by all footprint objects shown in Fig. 8-8a. Hence, the inner edge is also known and the ROI can be defined. Boundary B_1 is found by interpolating the local maxima on the inner edge. There are different approaches to find these maxima. In this case the image is divided into a number of equally sized horizontal segments n_{seg}. The outermost pixel of each segment is determined and compared with its neighbouring segments. Only when the x-position of the outermost pixel exceeds the value of both neighbour segments it is considered as a local maximum. The value for n_{seg} influences the number (and thus the length scale) of the found local maxima. With $n_{seg} = 1$ only a single maximum is found whereas n_{seg} equal to the number of rows in the image gives all local maxima with the image. The optimal value for n_{seg} is determined by trial and error. The identified local maxima are marked by red points in Fig. 8-8b. These points are interpolated with a cubic spline function to

describe B_1. B_2 is obtained by displacing B_1 the distance a, calculated in Eq. 8.7 towards the light source. B_3 and B_4 that are defined by Eq. 8.2 enclose the ROI. A mask is placed on top of the original image to exclude all pixels outside the ROI for further analysis (Fig. 8-8c).

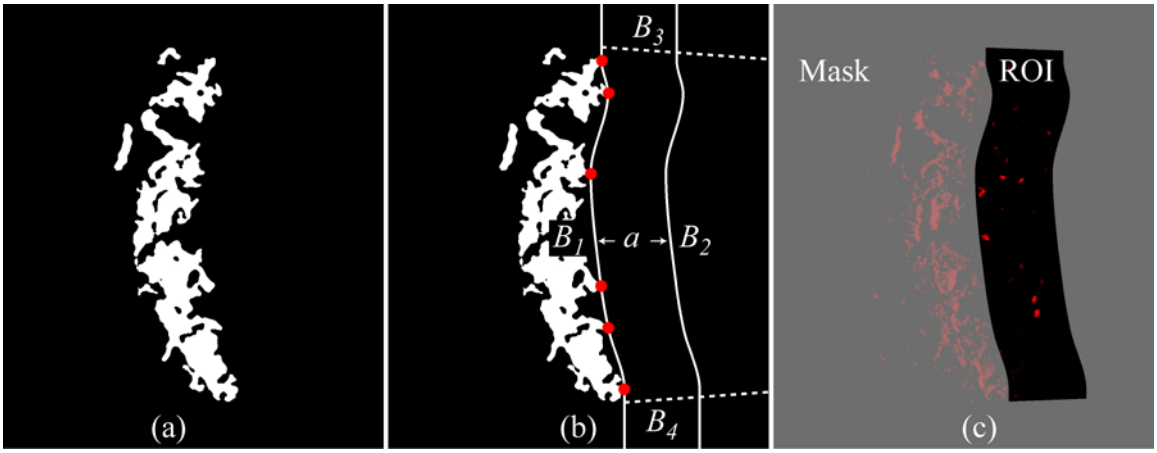

Figure 8-8. Illustration of the processing steps to determine the ROI. (a) Objects with $P <$ 150 pixels are removed, leaving only footprint objects. (b) Local maxima are determined (red points) and interpolated to obtain B_1. The other boundaries are defined by a, k_1 and k_2. (c) A mask is placed on the original red channel to exclude all pixels outside the ROI.

8.4 Algorithm to detect sand particles

As an illustration it was attempted to detect the sand particles inside the ROIs determined by the algorithm described in the previous section. The detection was based on identifying individual sand objects, so a similar strategy was adopted as the strategy used to identify the pavement footprint objects. In this case the masked original red channel (Fig. 8-8c) was taken as input data and the pre-processing was optimized to bring out the sand objects, rather than the footprint objects.

The sand particle size has little relation to the measurable sand object size because the particles are only partially illuminated. The sand object size is dependent on the location of the particle inside the ROI and on the topography of pavement. So each sand object is considered equally, irrespective of its size. Such criterion, however, makes the outcome of the detection very sensitive for very small objects. Hence the quantization and image segmentation needs to be more rigorous than during the footprint detection. The pre-processing removed most pixels that did not belong to the sand, but occasionally a few small objects remained that were not related to sand particles. Therefore, a minimum perimeter criterion p_{min2} was introduced. Objects with a perimeter lower than p_{min2} were removed from the segmented image. The remaining objects formed the identified particles and could be counted.

The sand objects were placed on top of the corresponding image taken under normal lighting conditions. This allowed distinction between the following categories: (1) correctly identified particles, (2) not detected particles, and (3) mistakes (objects that are a part of the pavement, but incorrectly identified as sand particles). An illustration of this distinction is given in Fig. 8-9.

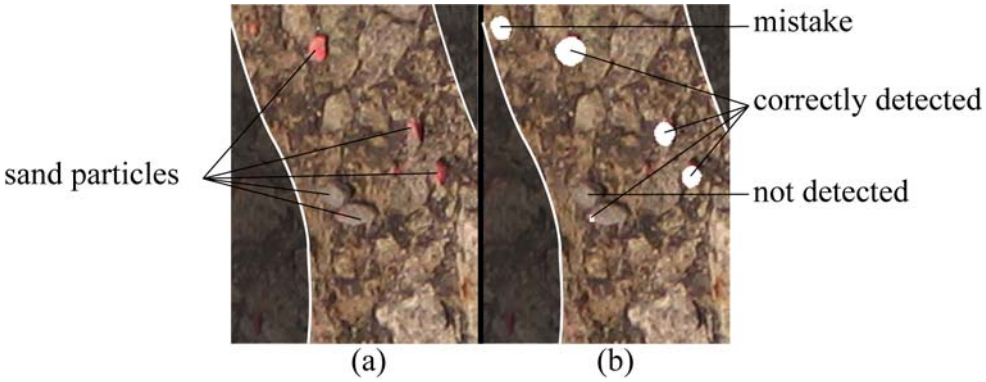

Figure 8-9. Illustration of the sand detection performance. (a) The image with normal lighting shows the particles that present inside the ROI. (b) The detected sand objects are placed on top of the same area.

The sand application rate was calculated from the number of particles inside the ROI to judge if the results are in a reasonable range. This required the number of sand particles per gram sand and the area of the ROI. The number of sand particles in 20 batches of 1 g sand was counted. For each image, ROI area was determined from the number of pixels forming the ROI and the resolution of the respective image. The resolution of the image was determined using the marked area on the pavement (0.2 m × 0.2 m), described in Chapter 7.

8.5 Testing and optimization

The algorithms were programmed in MATLAB^{tm} and various trials were performed to explore a suitable laser and camera angle and optimize the performance of the algorithms. Case specific optimization was not allowed so the same parameter values were used for all 9 images taken at a given laser and camera angle.

The used sand had a sieve fraction 2 – 4 mm, so h_s = 2 mm. Eq. 8.7 with $\theta_l = 87°$ results in a ROI width of 38 mm. At $\theta_l = 75°$, $\theta_l = 60°$, and $\theta_l = 45°$, the ROI width is 7.4, 3.5, and 2 mm, respectively. A large ROI is favourable because it is more representative for the whole area. Therefore, $\theta_l = 87°$ was selected for further analysis.

The angle at which the pavement is viewed is given by θ_c. Hence, the areas measured in the image represent the projected area, rather than the real area on the pavement. At $\theta_c = 0°$ the images taken from the dry pavement contained footprint objects with similar dimensions as the sand particles. This caused an incorrect determination of the pavement footprint boundary and numerous mistakes were made during the sand detection. Objects become increasingly "merged" with increasing θ_c, so the problem could be solved by increasing the camera angle. However, increasing θ_c also merges sand particles that are closely located behind each other in the x-direction. This led to occasions where two particles were identified as one. $\theta_c = 45°$ was found to be an acceptable compromise for these two conflicting effects.

Tests on the dataset for $\theta_l = 87°$ and $\theta_c = 45°$ revealed that the algorithm made several mistakes on the dry pavement and thin ice. These mistakes were mostly located in the vicinity of B_1. Therefore, a margin, a', was introduced between the interpolated footprint boundary and B_1. An overview of the optimized parameter values is given in Table 8-1.

Table 8-1. List of used parameter *values* for $\theta_l = 87°$ and $\theta_c = 45°$.

Parameter	Value
Determination ROI	
l_2 (mm)	1180
θ_d (°)	4.3
h_s (mm)	2
a (mm)	38
a' (mm)	5
I_{th}	3
m (pixels)	11
P_{min1} (mm)	16.4
n_{seg}	35
Sand detection inside the ROI	
I_{th}	10
m (pixels)	13
P_{min2} (pixels)	25
Particles per gram sand (g^{-1})	50 (± 2)

8.6 Results

Fig. 8-10 shows the 9 images taken at $\theta_l = 87°$ and $\theta_c = 45°$ with the ROIs that are determined by the algorithm. The ROIs are positioned far enough from the pavement footprint to exclude the pavement radiance in all the 9 images. In general, the ROIs are also positioned reasonably close to the pavement footprint. However, a locally larger separation between the pavement footprint and B_1 can be observed on thin and thick ice, with 35 and 70 g/m^2 sand (Fig. 8-10 b-2, b-3, c-2, and c-3). This caused rather sharp curvatures in the boundaries.

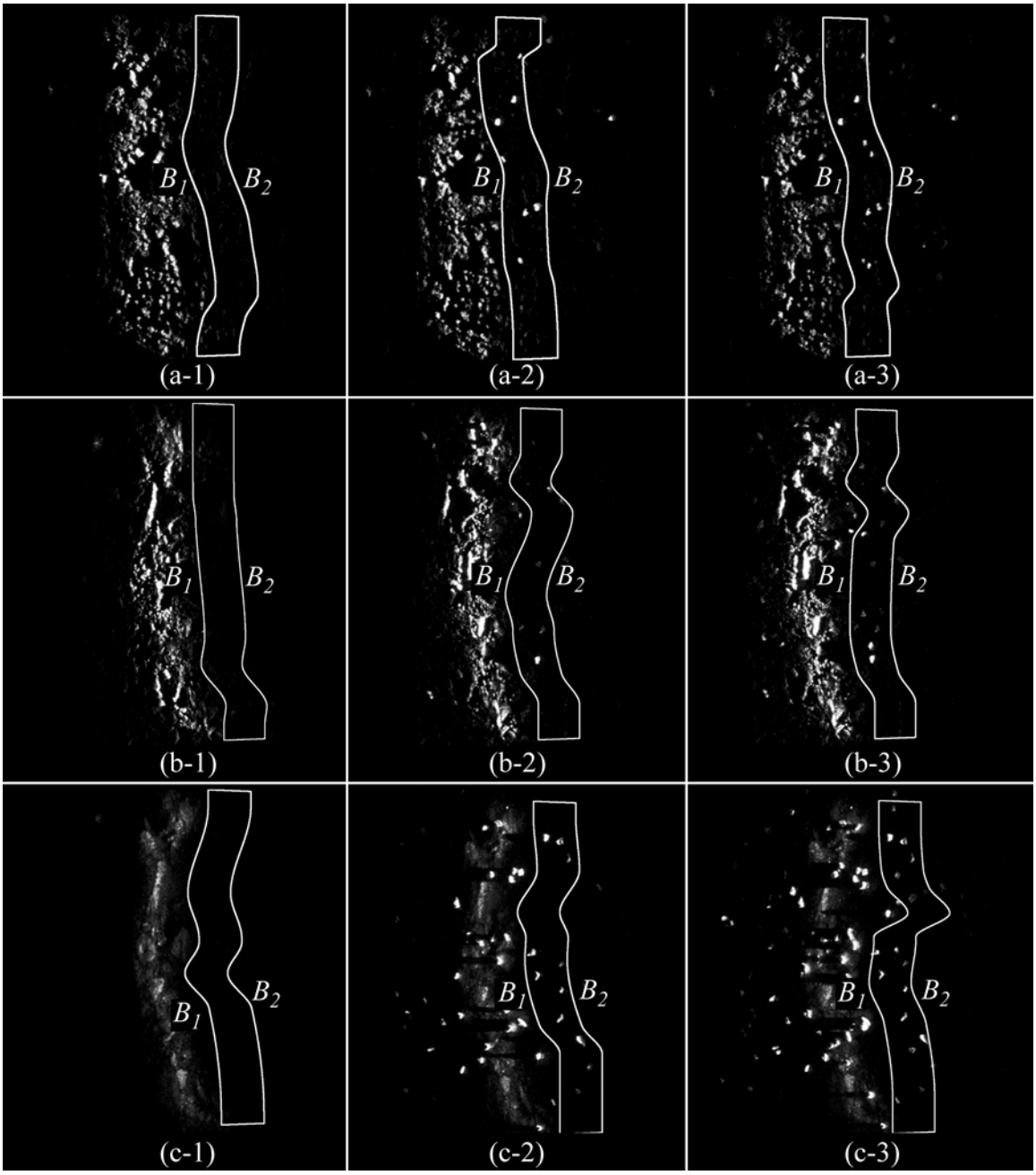

Figure 8-10. The determination of the ROIs from the images taken at $\theta_l = 87°$ and $\theta_c = 45°$. The images are taken from (a) the dry pavement, (b) thin ice layer, and (c) thick ice layer, with (1) 0 g/m^2, (2) 35 g/m^2, and (3) 70 g/m^2 applied sand.

The detection performance inside the ROIs is presented in Table 8-2. The actual number of particles n_a is the number of sand particles that were manually counted. Particles located on the boundaries were considered as inside when at least 50 % of their area was located inside the ROI. The total number of total errors n_e is the sum of the number of mistakes n_m and the number of not-detected particles n_{nd}. The success rate of the detection is calculated by:

$$\text{success rate} = \frac{n_{cd}}{n_a} \cdot 100\ \% \quad \Big| \quad n_a > 0\,, \tag{8.9}$$

where n_{cd} is the number of correctly detected particles.

Table 8-2. Detection performance of the algorithm for the images taken at $\theta_l = 87°$, $\theta_c = 45°$.

Pavement surface	Applied sand (g/m^2)	Number of sand particles				Success rate (%)	Total errors
		actual	correctly detected	mistakes	not-detected		
Dry	0	0	0	1	0		1
Dry	35	9	7	0	2	78	2
Dry	70	16	10	1	6	63	7
Thin ice	0	0	0	1	0		1
Thin ice	35	9	6	0	3	67	3
Thin ice	70	19	13	0	6	68	6
Thick ice	0	0	0	0	0		0
Thick ice	35	11	11	0	0	100	0
Thick ice	70	17	16	0	1	94	1

The position of the errors in the x-direction was measured, relative to the boundary B_1. Note that the distance from B_1 to B_2 equals a-a' = 33 mm. The position distribution of the errors made in all 9 images is shown in Fig. 8-11. Most errors were made within 10 mm from B_1.

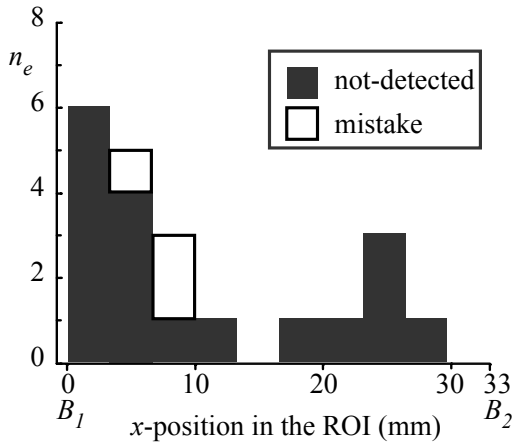

Figure 8-11. Position distribution of errors inside the ROI. The position is given in the x-direction, relative to the boundary B_1.

The application rate inside the ROI is calculated from the actual number of particles, the ROI area and the number of particles per gram sand. The detected application rate is determined similarly from the total number of detected particles ($n_{cd} + n_m$). The results are tabulated in Table 8-3 and plotted in Fig. 8-12.

Table 8-3. The calculated and detected application rate inside the ROIs at $\theta_l = 87°$, $\theta_c = 45°$.

Pavement surface	Applied sand (g/m^2)	ROI area ($\cdot 10^{-3}$ m^2)	Calculated application rate (g/m^2)	Detected application rate (g/m^2)
Dry	0	3.8423	0	5.2
Dry	35	3.6745	49.4	38.4
Dry	70	3.6799	87.7	60.3
Thin ice	0	3.9655	0	5.0
Thin ice	35	3.8553	47.0	31.3
Thin ice	70	3.8778	98.0	67.0
Thick ice	0	3.7256	0	0
Thick ice	35	3.7422	58.8	58.8
Thick ice	70	3.7666	90.3	85.0

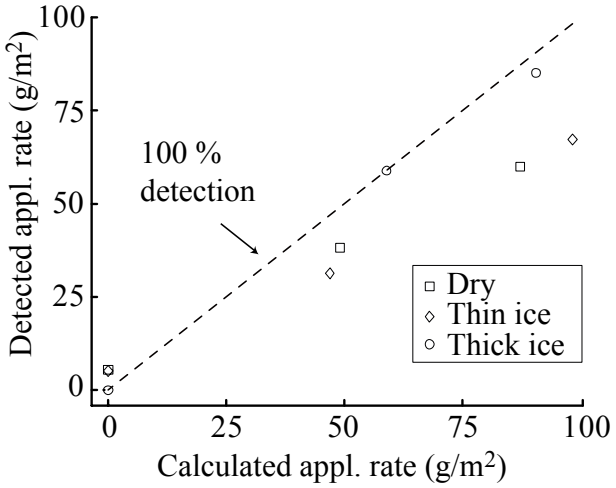

Figure 8-12. Comparison between detected and calculated sand application rate inside the ROI.

8.7 Discussion

The shape of the pavement footprint, shown in Fig. 8-4, differs significantly from the theoretical trapezium, shown in Fig. 8-3. Small variations in the pavement topography have a large impact on the footprint geometry, particularly at high laser angles. The footprint geometry will therefore change significantly when measurements are taken on different positions of a pavement, as in the case of mobile measurement applications. The area of the ROI was therefore determined from each image, using the image resolution. The ROI area also can be calculated theoretically by:

$$A_{ROI} = l_3 a - (a^2 \tan\theta_k) - (l_3 a' - (a'^2 \tan\theta_k)), \tag{8.10}$$

For $l_2 = 1.18$ m, $\theta_d = 4.3°$ and $\theta_l = 87°$, Eq. 8.1 and Eq 8.3 results $l_3 = 0.177$ m and $\theta_k = 4.306°$, respectively. Eq. 8.7 gives $a = 38$ mm. For the used margin $a' = 5$ mm, Eq. 8.10 results $A_{ROI} = 5.75 \cdot 10^{-3}$ m^2. The theoretical ROI area is about a factor 2 larger than the average ROI area measured in the 9 images ($3.79 \cdot 10^{-3}$ m^2). The difference in shape may have caused some difference, but it seems unlikely that shape difference alone can

explain the whole difference. A possible error source may be variations in the slit width that determines θ_d. The angle θ_d was determined at room temperature, while the images were taken at -5°C ± 1°C. This particular uncertainty is not present in the results presented in Fig. 8-12, because it uses the measured ROI area.

The positioning of the ROI is important for the quality of the distinction between pavement radiance and sand radiance. A ROI positioned too close to the pavement footprint incorporate unwanted pavement radiance, whereas a positioning too far away increases the chance that sand particles inside the ROI are not illuminated. It is shown in Fig. 8-10 that the algorithm positioned the boundary B_1 sufficiently far away from the pavement footprint to exclude pavement radiance in all the 9 images analyzed. Fig. 8-10 also shows that, in general, B_1 is reasonably close positioned to the pavement footprint. However, there occurred locally unnecessary large separation between B_1 and the pavement footprint. This increases the risk that small particles closely located to B_2 are not illuminated. So, it can be concluded that in general the ROI was reasonably positioned, but there remains room for improving the algorithm.

The occasions when B_1 became locally more separated from the pavement footprint were caused by sand particles that were identified as pavement footprint objects. Hence, their perimeter was larger than the perimeter criterion p_{min1}. Close inspection of the original images and each image processing step revealed two causes for this effect: (1) sand particles were located in clusters and became merged during the pre-processing, and (2) radiance from the particle reflected on the ice surface and created a virtual image of the particle that merged with the real particle during the pre-processing. The incorrect identification could be reduced by increasing the perimeter criterion p_{min1} but this led to the opposite effect of identifying footprint object as sand particles on the dry pavement. Without adopting a case specific algorithm (an algorithm where the parameters such as p_{min1} are optimized with information extracted from the image), the effect could not be avoided. Improvements of the algorithm may thus be achieved by improving the p_{min1} criterion or, for example, evaluating the curvature of the boundary.

The sand detection algorithm was able to detect between 63 and 100 % of the actual particles inside the ROI. The number of mistakes was limited, not exceeding 1 particle per ROI, so most errors were made by not-detecting actual particles. Two reasons can be identified why sand particles inside the ROI are not detected: (1) the boundary B_2 is extended too far from the pavement footprint and (2) particles are situated in the lower parts of the surface topography. In the former case the non-detected particles will mainly be located close to B_2. In the latter case the detection should perform better on smoother surfaces. Fig. 8-11 shows no evidence that B_2 was extended too far from the pavement boundary because few not-detected particles were located in the vicinity of this boundary. Table 8-2 and Fig. 8-12 show that the algorithm performs significantly better on the thick ice than on dry pavement or thin ice. The thick ice is considerably smoother because all pavement topography was filled with ice. So the fact that particles were not detected was mainly because the particles were situated in the valleys of the surface topography.

When a particle is located in a valley and its height does not exceed the height of the surrounding surface peaks it cannot be detected with the used method. So 100 % detection will not be achievable when the surface topography exceeds the smallest sieve fraction of the used sand. However, from a practical point of view it may be argued that these particles serve limited purpose anyway because it is questionable if they contribute

to improving the friction. So practically, these particles may be considered as lost, even though they are still located on the pavement. But the particle height do exceed the height of the surface, they can contribute to the friction because they become in contact with the tire. The sensitivity of the detection (ability to detect small elevations) increases as the pavement footprint is approached. Therefore, it is important that the boundary B_1 is located close to the pavement footprint.

The calculated application rate inside the ROI differs significantly (up to 40 %) from the application rate inside the marked area of 0.2×0.2 m^2. This can partly be attributed to the subjective way of distributing the particles in the experiment, but it can also indicate that the size of the ROI is not large enough to represent the marked area. The average ROI area of the 9 measurements ($3.79 \cdot 10^{-3}$ m^2) is only 9.5 % of the marked area. The size of the ROI can be changed in two ways: (1) adjusting the length of the B_1 boundary by either increasing l or θ_d, or (2) increasing the ROI width a by increasing θ_l or using larger sand size fraction. The latter option appears to be very limited: The sand size is bonded to practical restrictions and the used value for $\theta_l = 87°$ is probably already close to practical limitations. Thus B_1 needs to be increased and/or multiple measurements on different locations are required to represent a larger surface area.

An important question is the feasibility of the adopted principle and image analysis techniques for practical applications. Here two applications may be considered: stationary and mobile applications.

The method used here required a rather small camera angle. This implies that the camera needs to be positioned above the surface or close to the surface at a considerable height. For stationary applications at runways, this will certainly give practical difficulties due to the strong height restrictions of any structure or object in the vicinity of the runway. Hence, on runways both camera and laser angle are restricted to values close to 90°. It is unlikely that useful results can be obtained under these angles with the concept. The reason is the merging of sand particles and a very small projected area of the ROI at these camera angles. For roads however, these restrictions do not apply and a camera can be mounted above the pavement. For stationary applications it will be more difficult to obtain a representative ROI size than for mobile applications, because successive readings cannot be averaged without changing the laser position or angle of incidence. However, these practical difficulties may be overcome.

For mobile applications the practical limitations are for example the exposure time of the image and variations in θ_l and θ_c, due to the roll and pitch of the vehicle. But the benefit of mobile applications is that the pavement can be "scanned" and a representative ROI can be obtained by averaging successive readings, given that the image acquisition and processing times are limited.

The measurement concept will have increasing difficulties in detecting sand when the used sand size is finer in size. In that sense a rather sharply defined sand fraction of 2-4 mm is favourable for the concept. These sand fractions are not uncommon (most airports in Norway use this type of sand), suggesting the practical value of detecting this type of sand. To evaluate the practical value it is important how the obtained information is used. One may think of a situation where winter maintenance personnel want to have a certain amount of sand on the pavement and wishes to account for the remaining sand in a new sanding operation. Such usage demands a very high detection performance. On rather

smooth surfaces the attainable detection performance may indeed sufficient for such utilisations. However, on rough surfaces the success rate of the detection was considerably less (in the range of 60-80 %). Here the measurement gives not more than an indication and the obtained data should be interpreted accordingly. One may also think of a situation were the system gives a warning that the amount of sand is below a certain level. The fact that little mistakes were made in by the algorithm shows that it is rather conservative (most error comes from not detected particles). A conservative estimate is favourable for the intended purpose because it is more serious when no warning is given when needed, than that a warning is unnecessarily given. The information obtained with the concept may be of large practical value for such utilisations.

8.8 Conclusion

The principle of triangulation has been developed as a measurement principle for the detection of sand on pavements by illuminating the surface and imaging the scattered radiance. With this principle it is possible to define a region of interest in the image where the radiance solely originates from the sand. The principle is developed theoretically for flat surfaces and adapted for application on rough surfaces of unknown topography.

Digital image analysis techniques have been applied to use the principle on images taken from a piece of pavement that was formerly used at an airport, under both dry and iced conditions in a stationary arrangement. The algorithm positioned the region of interests reasonably in all analyzed images, giving a rather conservative result in the subsequent analysis of the region. The positioning may be further improved which will increase the sensitivity of the subsequent detection, specifically on surfaces with large topography.

The concept and analytical procedure was illustrated by attempting to detect the sand particles inside the region for a selected camera and laser angle. The success rate of the detection ranged between 63 and 100 %. The errors were mainly due to particles that were located in the lower parts of the surface topography. The algorithm made only few mistakes by incorrectly identifying particles, so the number of detected particles was a conservative estimate of the actual number of particles located in the region.

9 FREEZE BONDING SAND TO PAVEMENTS BY PRE-WETTING WITH HOT WATER

9.1 Introduction

It has been recognized for a long time that the effectiveness and the durability of sanding operations on ice covered pavements could be improved by adhering the sand particles to the ice. By recalling the sand displacement shown in Fig. 3-6 it is not difficult to see the large operational benefits of freeze bonded sand, compared to loose sand because it avoids that sand is blown off the runway by the engine thrust of aircraft. Additionally, when sand is well bonded to the surface it can survive the exposure to the runway sweepers. New sanding operations are therefore not necessarily required after mechanical removal of snow.

Different adhering techniques have been tested and practiced, such as using warm sand (Hayhoe, 1984) and heating the contaminated pavement prior to, or after sand application. The latter method is still practiced at some airports in Norway. Heating the ice surface partly melts the ice. The melt water refreezes and the sand particles become bonded to the pavement. This method can give good, long lasting results, but is may take several hours to treat a whole runway. The method is therefore time and fuel consuming.

In 1997, the Norwegian Public Road Administration started a project that was focused on practical, technical, and economic problems arising in providing good friction on winter roads (Dahlen and Vaa, 2001). Two concepts of freeze bonded sanding were evaluated within this project. The first concept was based on heated sand, while the second concept was based on pre-wetting the sand with hot water. The latter was found to have most potential. Different manufacturers were encouraged to develop the technology further. Through the years 1999 to 2005, the technology evolved and the dominant design became a rotating disk spreader where the water and sand is mixed in the feeding tube of the disk spreader. Currently, sand spreaders with warm pre-wetting functionality are commercially available and different Norwegian airports have adopted this sanding method. The traditional and the modern methods of freeze bonding sand to iced pavements are illustrated in Fig. 9-1.

(a) (b)

Figure 9-1. Traditional and modern methods of freeze bonded sanding. (a) The iced pavement is heated with open flames prior to the sanding operation. (b) A modern sand spreader that pre-wet the sand with hot water.

With the warm pre-wetted sanding technology in an implementation phase, there are many questions to be answered. On a practical level there different settings to be optimized, such as the application rate, the type of sand, the water temperature, the water/sand ratio, the application speed and the width of the spreading pattern. More generally, questions are raised about the application range of the method, the limitations, and possible negative effects, if any.

This chapter addresses three questions regarding freeze bonded sanding: (1) how friction is provided to aircraft by freeze bonded sand, (2) how do the surface conditions change by using warm pre-wetted sanding, and (3) why have airports, that use the new sanding method, received comments from the pilots that they experienced the runway more slippery than reported? It is hoped that addressing these questions broadens the view on freeze bonded sanding methods as tools for winter maintenance at airports.

The data for this study was collected during the field activities at three Norwegian airports during the winter seasons 2004-2005 and 2005-2006. A detailed description of these studies will be presented elsewhere (Klein-Paste and Sinha, in press). This chapter summarizes the study and is organized as follows: Section 9.2 gives a brief description of the warm pre-wetted sanding method. It is followed by observations from operational runways in Section 9.3. An aircraft braking experiment is described in Section 9.4 and comments from pilots regarding the surface conditions are investigated in Section 9.5. All the collected data is jointly discussed in Section 9.6.

9.2 Description of the warm pre-wetted sanding method

The sanding truck shown in Fig. 9-1b carries 9 m^3 sand and 2.7 m^3 l water. Prior to the application, the water in the tanks is pre-heated to 45°C. Immediately before the application, the water is heated further to about 95°C. The hot water is then mixed with the sand in the feeding tube of the rotating disk spreader. The water is heated by three diesel fuel driven heaters, each having a capacity of 88 kW.

The warm sand/water slurry deposits in lumps that form a bow shaped pattern on the pavement. Fig. 9-2 shows an image taken with an infrared camera during an application. It shows that the lumps are still above 0°C when they deposit. This implies that a part of the contamination layer melts before the added and melted water freezes and the lump solidifies. It was found that the creation of these lumps was a key factor in improving the durability of the sanding operation (Vaa and Dahl, 2002; Vaa, 2004; Vaa, 2005). It was also found that the sand needs to contain a certain amount of fine sand to obtain durable lumps.

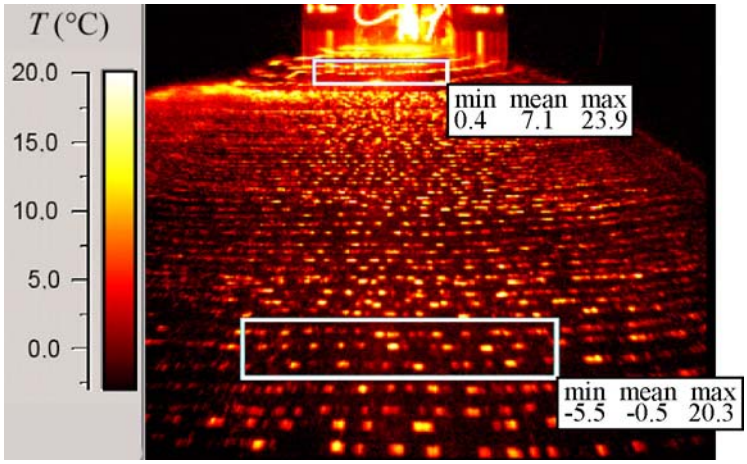

Figure 9-2. An image of warm pre-wetted sand application, taken with an infrared camera (Vaa, 2005), reprinted with permission.

A detailed view of the lumps applied on smooth ice is shown in Fig. 9-3a. Here, the sand (0-4 mm) was applied on a continuous ice surface (T_i = -6°C, T_a = -2.5°C) without loose snow contamination present. Spot checks revealed that almost all particles from the pre-wetted sand were bonded to the surface after the slurry froze. For comparison, the same sand, applied on the same ice without adding the water is shown in Fig. 9-3b.

(a) (b)

Figure 9-3. The difference between dry and warm pre-wetted sand: (a) 150 g/m^2 natural sand with 30 vol% hot water, (b) same amount and type of sand applied without water.

The larger particles in Fig. 9-3a are well-bonded to the surface by a mixture of fine sand and ice. When warm pre-wetted sand is applied on compacted snow, the spreading pattern becomes different. Here, the fine sand/water mixture penetrates into the snow while the larger particles remain located on the top (Fig. 9-4). The large particles could be removed with relative ease by rubbing them with a shoe sole.

(a) (b)

Figure 9-4. A top view (a) and side view (b) of warm pre-wetted sand that is applied on compacted snow.

9.3 Observations from an operational runway

Kirkenes Airport is located at 69° 43' 30'' N and 029° 53' 16'' E in the north east of Norway, close to the Russian border. The location of Kirkenes Airport has been shown earlier in Fig. 3-1. The airport adopted the warm pre-wetted sanding method in 2004. Observations could be made on the runway of Kirkenes Airport, which was iced and repeatedly treated with the warm pre-wetted sanding method in the weeks prior to the observations. At the time of the observation, the last sanding operation was performed four days earlier and the surface had been swept several times afterwards (the exact number could not be determined).

A detailed view of the iced surface is shown in Fig. 9-5. The ice layer contained particles that are fully embedded. It also contains particles that have reached the surface, but are still attached to the ice. These particles formed fixed asperities and gave the surface a rough, sand paper like appearance. Additionally, there were loose particles present on the ice.

Figure 9-5. Example of an iced runway that is regularly treated with freeze bonded sand, four days after the last application.

Observations could also be made after a new sanding operation The application was performed with 0-4 mm natural sand at an application rate of about 240 g/m^2, including about 30 vol% hot water. The application width and velocity were 3 m and 25 km/h, respectively. The air temperature during the application was -6°C and it had been colder

for a few days prior to the observations. This suggests that the runway surface temperature (not measured) was colder than -6°C at the time of the application. The surface contamination consisted of a thin ice layer. Practically no compacted snow was present on the runway. The spreading pattern was inspected after the application, which revealed that the sand was well bonded to the surface.

Fig. 9-6a shows the track of a BV-11 test tire on the sanded surface. The track is shows that most of the large particles broke loose. Careful inspection of the photograph shows, however, rows of particles inside the track that remained attached to the pavement. These rows coincide with the longitudinal grooves that are present on the test tire. Fig. 9-6b shows a track of a Beach King Air 200 main gear. The aircraft landed on a virgin sanded runway. The track is visible because a part of the larger particles broke loose under the action of the tire and displaced to the sides after the interaction. However, a part of the sand remained attached to the ice. This gave the ice inside the track a rough appearance (checked by rubbing the track with a shoe sole).

When particles break loose under the action of the tire, it is expected to find scratch marks on the ice. These scratches were indeed found. The figures Fig. 4-5b and Fig 4-6 shown in Chapter 4 were taken on the runway of Kirkenes Airport, after the warm pre-wetted sanding was implemented.

(a) (b)

Figure 9-6. Tracks on newly applied freeze bonded sand. (a) The track from a BV-11 test tire. (b) The track of a Beach King Air 200. Both tracks show that large particles broke loose under the action of the tire.

9.4 Aircraft braking experiments

Bardufoss Air Force Base, Norway was visited during the winter 2005-2006. This airport is one of the first airports in Norway that adopted the warm pre-wetted sanding method. The available facilities, a naturally formed, uniformly ice contaminated apron, and the cooperation of the staff provided all the required boundary conditions for aircraft braking experiments. The test area was not otherwise in use, which gave a time-window of several hours to conduct the experiment.

The objective was to compare the tire-sand-ice interaction in two cases: (1) ice treated with loose sand, and (2) ice treated with warm, pre-wetted sand. The available aircraft was a small propeller aircraft from air force training school that was based at the airport. Although the aircraft was not instrumented to measure or derive tire-pavement friction, it was a unique opportunity to observe the tire-sand-ice interaction in more detail. The

available time also allowed ice surface observations with the etching and replicating method, described in Chapter 5. Hence, the tire-sand-ice interaction could be studied both on a macroscopic and microscopic level. The aircraft was not equipped with an anti-skid braking system. This turned out to provide important information regarding the whole tire-sand-ice interaction.

9.4.1 Experimental details

The tests were performed on January 25, 2006. The whole day it was cloudy. There was little wind and it was relatively mild (T_a = -2.5°C). The apron was about 200 × 100 m and was covered with a thick, uniform layer of ice. A layer of loose, undisturbed snow covered the ice. To minimize mechanical damages of the underlying ice, it was tried to remove the snow using only the blower unit of a runway sweeper. Although most of the snow was still loose, some snow particles had sintered to the ice surface and could not be removed by blowing. Therefore, the snow had to be removed with the rotating steel brush, combined with the blower. The snow plough was not used for the cleaning.

The snow cleaning was finished at 12:31. The ice had a white, bluish colour and was very uniform over the whole area. Only few visible cracks were present. The thickness, colour and uniformity of the ice indicate that it was formed by snow that had undergone melt-refreeze metamorphism or that rain had precipitated on top of the undisturbed snow layer and subsequently froze. Maintenance personnel confirmed that it had been mild weather with rain a few days earlier.

Before snow removal, the snow layer and the ice surface temperature were -4°C and -6°C, respectively. At the time of the tests, the ice surface had warmed up to T_i = -5°C, while the air temperature remained stable at T_a = -2.5°C. It took about 1.5 hour from the start of the snow cleaning to the first test run. The untreated ice surface was investigated by making replicas of the surface.

Two sand test beds were prepared. The first test bed (about 150 m in length, 6 m wide) was made by 150 g/m^2 loose, natural sand, 0-4 mm sand size fraction. The second bed was made with the same type of sand, applied at 150 g/m^2 sand plus 30 vol% water (T_w = 95°C). Both sanding operations were performed at 25 km/h and 3 m application width. The test beds were finished at 13:31. An overview of the two test beds is shown in Fig. 9-7. A detailed view of the loose and freeze bonded sand has been presented earlier in Fig. 9-3.

(a) (b)

Figure 9-7. Overview of the test beds: (a) freeze bonded sand and (b) loose sand.

The available aircraft was a Saab Safari MFI 17. On each test bed, one braking test was performed. First, the aircraft was accelerated to about 50 km/h, then the engine was turned to idle, and finally the brakes were applied until the aircraft had come to a complete stop. The first run was performed at 13:54 on loose sand. At 14:30 the run on freeze bonded sand took place. A photograph of the aircraft during the first test run is shown in Fig. 9-8. The tracks were photographed after each brake test and the replicas were made from the main gear track at locations where the brakes were applied.

Figure 9-8. The SAAB Safari MFI 17 during the test on loose sand.

9.4.2 Results

Macroscopic observations

An overview of the track on the loose sand test bed is shown in Fig. 9-9a. The track is clearly visible because most of the sand particles were removed from the track. Both the (braked) main gears and the free-rolling nose gear displaced the sand particles. The aircraft experienced two non-simultaneous tire lock-ups, one on each main gear. The pilot informed that he had sensed the skidded tires and released the brake pressure twice to get the tires rolling again. He did not experience tire lockups on the freeze bonded sand. The tracks on the freeze bonded sand test bed are also visible (Fig. 9-9b) because some of the particles have been removed by the tire. However, there was still a significant amount of

sand left in the track. This remaining sand survived the stresses from the tire and remained bonded to the underlying ice. Scratch marks on the ice were observed inside the tracks, both in loose sand test bed and in the freeze bonded sand test bed (Fig 9-10).

(a) (b)

Figure 9-9. Overview of the tracks after the braking test on (a) loose sand, and (b) freeze bonded sand.

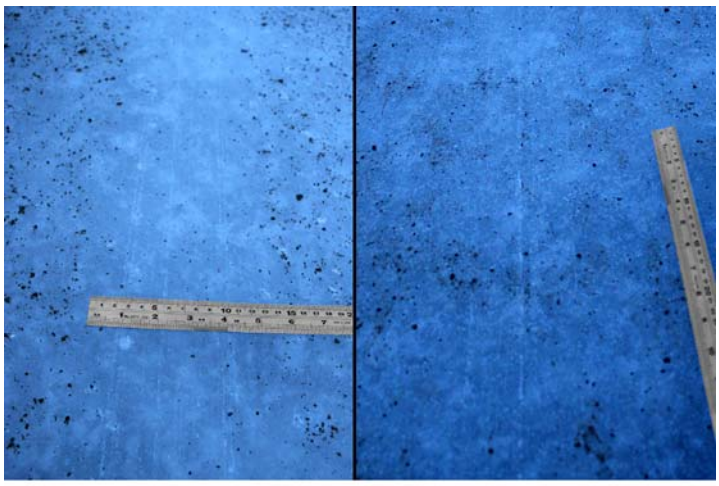

(a) (b)

Figure 9-10. The ice in the tracks exhibited scratch marks, both on (a) loose sand and on (b) freeze bonded sand.

The skidding tires caused sand particles to pileup. The pileup of the right main gear is shown in Fig. 9-11a. The detailed view (Fig 9-11b) shows that the pileup consists of loose sand particles and a patch of packed particles and ice debris. The loose particles were located in the front of the pileup. The patch of packed particles and ice debris was broken into two pieces. The largest piece (Piece 1) was still located in the track, while Piece 2 deposited a few centimetres above the track. Two "ridges" were present in the patch; one of them was fragmented when the two pieces broke loose from each other. The spacing between the two ridges was about 37 mm, which corresponded well with the measured spacing between the longitudinal grooves of the tire (40 mm).

The ridges and the known spacing distance were used to reconstruct the approximate dimensions of patch before it broke into pieces Fig. 9-11b. The dimensions of the patch correspond reasonably well with the apparent contact area of the tire. This suggests that sand particles were not only pushed in front of the skidding tire, but particles and ice debris also collected under the tire. It created a patch of sand and ice debris that slid together with the skidding tire on the ice.

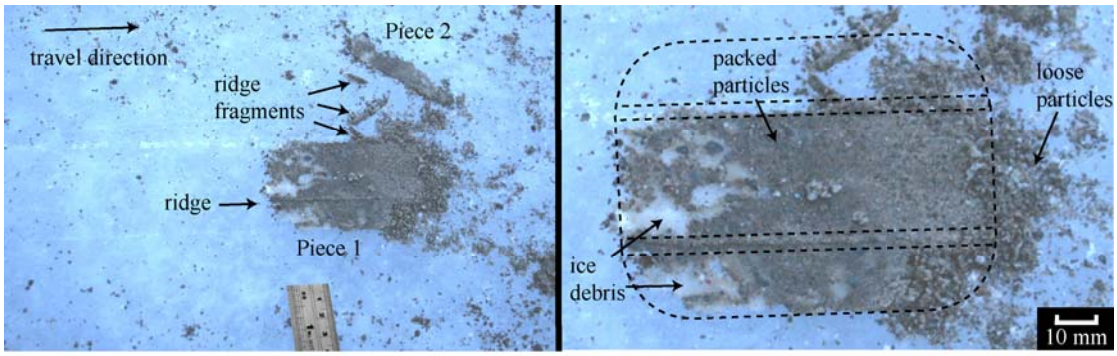

Figure 9-11. (a) The pile-up of sand and ice debris, caused by the skidding right main gear tire. (b) The dashed lines show the approximate dimensions of the patch.

The pilot noticed a clear difference in the response of the aircraft during the braking on the two test beds. He estimated the braking action as “poor” for ice treated with loose sand and “medium” for the ice treated with freeze bonded sand. This difference, however, was not reflected in the friction measurements performed with a Saab Friction Tester. It measured consistently a friction coefficient of 0.17 on the loose sand and 0.19 on the freeze bonded sand. This means that the friction measurements described both surfaces as “poor”.

Microscopic observations

The dual technique of etching and replicating was applied, using a 2.5 % formvar solution. Replicas were prepared from the ice surface after the snow was removed, but before the sanding in order to document the microstructure of the ice. The replicas revealed that the surface was, on a micro scale, severely damaged by the snow cleaning operation. An illustration of the replicated ice surface is shown in Fig. 9-12. The original grain boundaries can be identified, but the area is dominated by countless scratch marks, caused by the sweeper. Most of the surface was re-crystallized inside these scratches. It is also possible that the observed cells are the result of breaking the bond between the sintered snow and the ice surface. Nevertheless, it is clear that the sweeping caused significant microscopic damage to the ice surface.

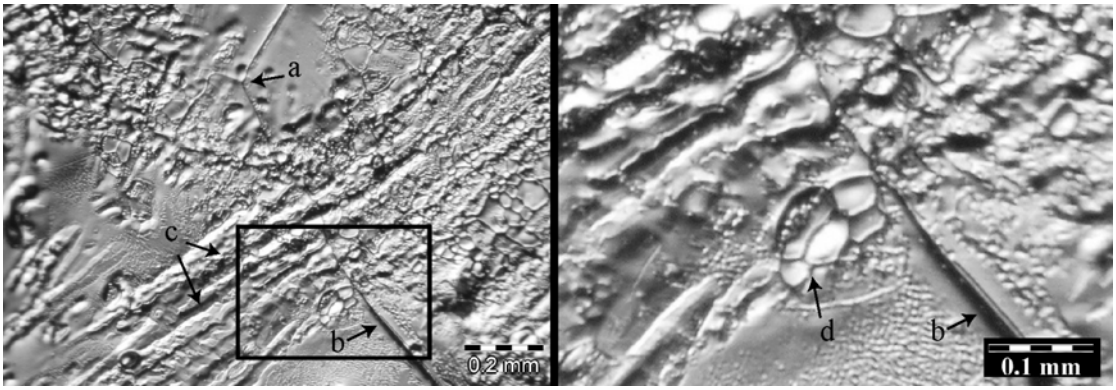

Figure 9-12. Replica of the ice surface before sand application. The micrograph shows (a) a triple-point and (b) the original grain boundaries. It also shows numerous trans-granular scratch marks (c), containing small cells (d) due to highly localized deformation.

After each braking test, replicas were prepared from the ice surface inside the tire tracks. Snow started to drift closely above the surface during the drying process of the replicas on the loose sand test bed. The replicas were covered by a plastic box, but snow contamination could not fully be fully avoided. This created dark, fluffy artefacts on the replica. Nevertheless, large scratch marks could be distinguished. Fig. 9-13a shows a part of the replica where two scratches run horizontally through the micrograph. It shows a region with small cells that were already present before the interaction (Fig. 9-13b). Inside the two scratches there are also small cells present (Fig. 9-13c-d) but it is not possible to determine if these cells are caused by the highly localized deformation induced by the ploughing sand particles.

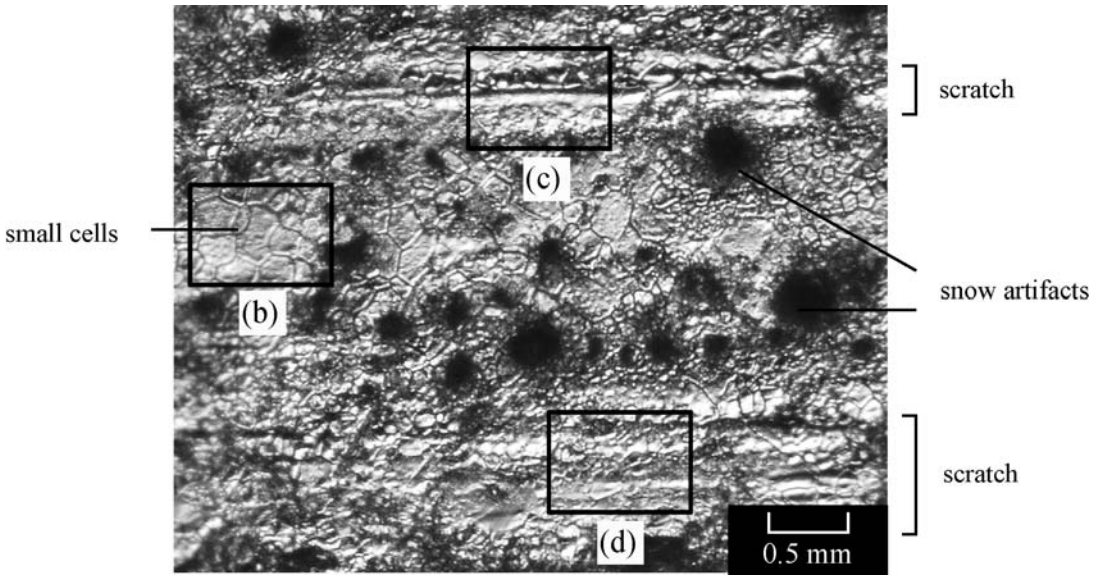

Figure 9-13a. Replica of the ice surface inside the tire track on the loose sand test bed. The replica shows two scratches and the small cells that were already present before the brake test. The black fluffy artefacts are snow crystals that deposited on replica during the drying process.

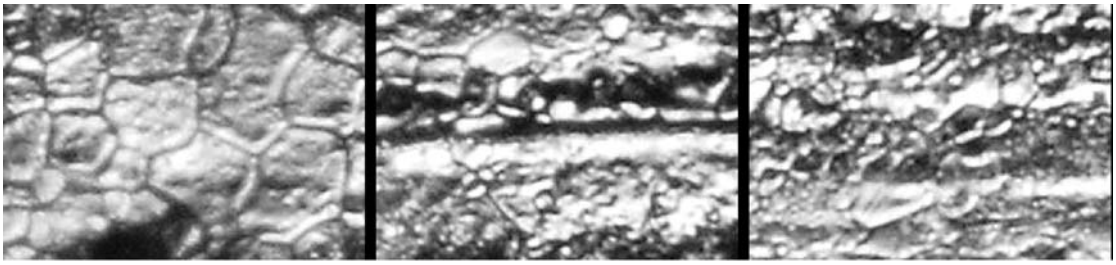

Figure 9-13b-d. Detailed view of three selected regions that are indicated in Fig. 9-13a.

The snow drift stopped before replicas were taken on the freeze bonded sand. Recovering replicas from freeze bonded sand surfaces difficult because the Formvar (the plastic film) strongly adheres to sand, which on its turn is bonded to the surface. Nevertheless, a few replicas from the ice between the sand lumps could be recovered. The replicas also showed the highly damaged surface, but an area was found where the original ice structure was reasonably intact (Fig. 9-14). This area contains several small scratches that were aligned along the travel direction and one scratch that was aligned at an angle θ of 23°. The latter scratch was presumably caused by a steel wire of the rotating brush. The angle coincides reasonably well with the attack angle of the brush, relative to the travel direction of the sweeper (about 30°). The small scratches that are aligned along the travel direction correspond well with the earlier observed small scale deformation found in the laboratory and in the track from a friction measurement device (Chapter 5). It also shows cell formation within the original grain structure. The ice temperature (T_i = -5°C) was too high to reveal dislocations.

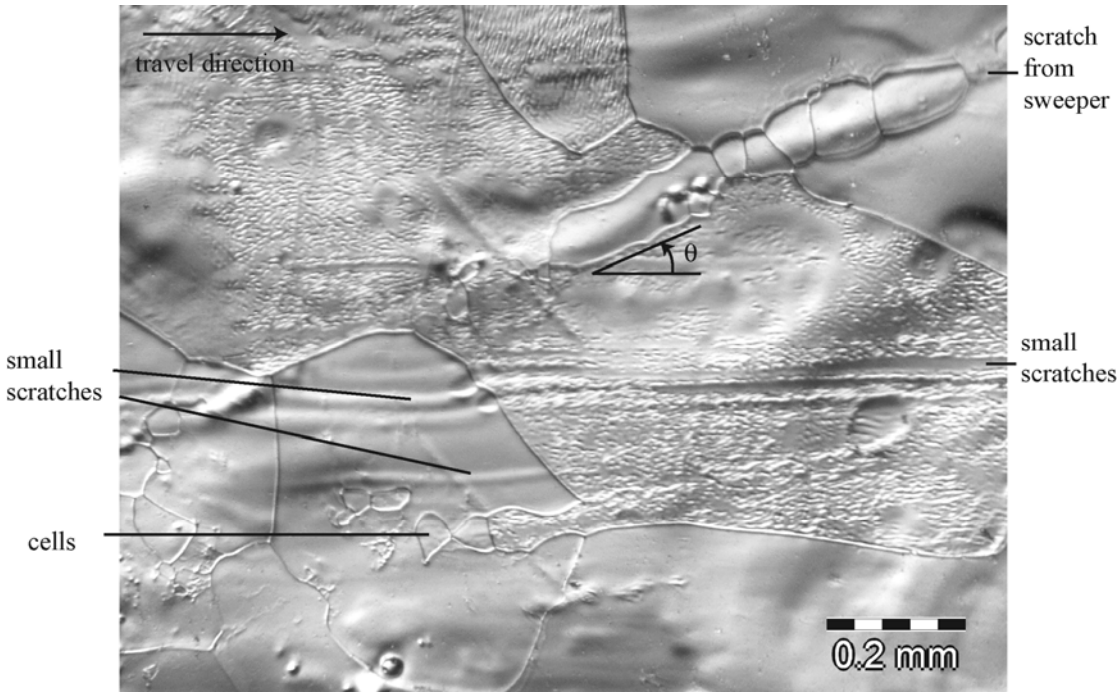

Figure 9-14. Replica of the tire track on freeze bonded sand test bed. The replica shows scratches aligned along the travel direction and a scratch that is aligned at an angle θ of 23° to the travel direction, presumably from the sweeping.

9.5 Feedback from pilots

Runway maintenance personnel that use the warm pre-wetted sanding method are generally positive towards the method. They indicate that the result lasts longer and that a higher friction level is obtained (Klein-Paste and Sinha, in press). Also pilots have frequently confirmed to Air Traffic Control (ATC) that they experienced the sanded surfaces indeed as "good". However, besides these positive indications, airports also have received comments that the surface was more slippery than reported. These comments show that the discrepancy between the reported and experienced surface conditions (Chapter 2) also occurs on surfaces treated with warm pre-wetted sand.

This discrepancy is first of all a safety issue for aircraft ground operations. But besides this important safety aspect, there is a simple business issue related to these comments. Airline companies are the primary customers of an airport. The pilots are the daily representatives of that customer. When a pilot comments that the surface is more slippery than reported, it is in fact a customer expressing his or her dissatisfaction of the offered service. Therefore, airports are to take these comments seriously, not only for safety purposes, but also because a customer expressed his or her dissatisfaction.

These pilot comments are subjective because aircraft that are currently in operational use are not instrumented to measure the attainable friction force. This leaves room for discussion how good or poor the actual conditions were. But regardless this discussion, airport operators want to avoid such comments. So the main question is why pilots commented the conditions in that particular situation.

During the winter 2005-2006, Kirkenes Airport, Norway and Svalbard Airport, Norway received in total 12 negative comments regarding the surface conditions. These comments were investigated in a case study. For each comment it was attempted to reconstruct the situation at, and prior to the comment by combining meteorological data, traffic data, performed winter maintenance and reported surface conditions. Although the investigation has similar characteristics as an aircraft accident investigation, there are some important differences: All data was made available by the airports on a voluntarily basis. The comments were treated anonymously, so no pilot or airline specific data was collected. The aircraft were not technically inspected and the pilots were not interviewed. The investigation should therefore be viewed as an "unsatisfied customer" investigation, performed for an airport operator. The aim is to provide the airport operator an explanation why these comments occurred, and thereby contributing to the question how these comments can be avoided in the future.

9.5.1 Available data

The data was compiled from the internal documentation that was made available by the airports. This included ATC logbooks, runway status reports, confirmed departure/arrival times, meteorological data, and reports of undesirable events. Between November 1, 2005 and March 31, 2006, 12 comments were received, 6 at Kirkenes Airport, and 6 at Longyearbyen Airport. Three comments occurred at the same airport, within 1.5 hours. These three comments are considered as one case (Case No. 6). In this case, the data of first comment is presented, unless otherwise mentioned. Additionally, one comment was received after the ATC requested the pilot to comments about the surface conditions. The reply: "probably a bit slippery" gave insufficient support to treat this comment on an equally basis with the other comments and was excluded from the data set. The remaining 9 cases were investigated further.

A summary of the runway status reports that were provided to the pilots is given in Table 9-1. The age of the report is the time between the time stamp of the friction measurement and the time of the comment. The interpretation of these measurements, based on the ICAO specification (given earlier in Table 2-2), is included in the table. Table 9-2 shows the phrases that the pilots used to inform ATC. The last runway maintenance operations that were performed within 24 hour prior to the comment are shown in Table 9-3. This table also includes the number of aircraft that used the runway between the last status report and the comment. A summary of the meteorological data is given in Table 9-4. Complimentary information that indicates insufficient retardation or directional control is listed in Table 9-5. The skid marks, which were observed in Case No. 9, are shown in Fig. 9-15. Control measurements or other observations that were obtained after the comments are listed in Table 9-6.

Table 9-1. Runway status reports that were provided to the pilots.

Case No.	Age (H:MM)	Measured braking action	ICAO specification	Description
1	0:00	47 / 46 / 46	Good / Good / Good	<3 mm dry snow, ice, sand
2	0:32	37 / 39 / 39	Med-good / Med-good / Med-good	Ice, sanded
3	0:18	46 / 45 / 45	Good / Good / Good	Rime, ice, sanded
4	2:01	59 / 56 / 51	Good / Good / Good	Ice and sand
5	1:15	61 / 55 / 60	Good / Good / Good	ice with sand on top
6	0:38	39 / 40 / 39	Med-good / Good / Med-good	Sanded ice
7	0:51	38 / 41 / 44[9]	Med-good / Good / Good	Sanded ice
8	0:27	32 / 33 / 39	Medium / Medium / Med-good	Sanded ice
9	0:33	50 / 47 / 48	Good / Good / Good	Sanded ice

Table 9-2. Phrases used by the pilots to comment on the runway surface conditions.

Case No.	Pilot comment
1	The braking action was much lower than reported
2	It is very slippery on the runway
3	It was slippery
4	It was slippery
5	It was slippery
6	It is very slippery; Braking Action below 30 on RWY and poor on apron
7	Estimated Braking Action around 20 (Poor)
8	It feels slippery
9	It was horribly slippery on the runway

Table 9-3. Runway maintenance operations in the last 24 hours and the number aircraft movements on the runway between the last status report and the comment.

Case	Last maintenance action within 24 hours			Previous movements	
No.		Start	Finish	Landing	Take-off
1	Sweeping	Unknown	unknown	0	0
2	Sweeping and Sanding	Unknown	Unknown	2	0
3	Sweeping	Unknown	>12 h	1	1
4	Sweeping and Sanding	10:30	8:30	2	0
5	No maintenance, sand from earlier application			2	1
6	Warm pre-wetted sanding	2 h	0:40	0	0
7	No maintenance, sand from earlier application			0	0
8	Continuous sweeping and loose sanding	3:35	0:00	0	0
9	Warm pre-wetted sanding	1 h	0:00	0	0

[9] The reported braking action (38 / 41 / 44) was measured 5 hours earlier, but the validity of this information was verified 51 min before the comment was received. The braking action measured during this last measurement was 46 / 42 / 38.

Table 9-4. Summary of the meteorological data.

Case No.	T_a (°C)	T_d (°C)	v_w (m/s)	Q (°)	Precipitation	Temperature trend last 12 hours	
						Trend	Magnitude
1	0.0	-2.3	4.2	335	-	Increase	↑ 8°C
2	-8.3	-9.1	3.2	130	Snow	Decrease	↓ 6°C
3	-15.4	-16.8	2.5	130	-	decrease	↓ 8°C
4	3.0	0.6	5.7	240	-	Increase	↑ 6°C
5	-16.8	-20.5	15.4	165	-	Increase	↑ 8°C
6	2.8	0.0	2.8	235	Rain/snow	Increase	↑ 2°C
7	1.9	-3.9	5.8	185	-	Fluctuating	± 1°C
8	5.8	-0.4	4.6	164	Rain before event	Increase	↑ 4°C
9	-7.8	-13.2	6.3	210	-	Fluctuating	± 2°C

Table 9-5. Documented indications of insufficient retardation or directional control.

Case No.	Indication
1	
2	Aircraft used long time to turn around on the runway and taxi back (after landing)
3	
4	
5	Difficulties to turn on runway
6	Skidded between taxiway and apron[10] / Pilot reports to skid on locked wheels on runway[11]
7	Difficulties to turn on the runway. Skidding on runway while turning to taxiway
8	Difficulties to turn on runway
9	Locked wheel skid marks were observed at the end of the track, just before the 180° turn

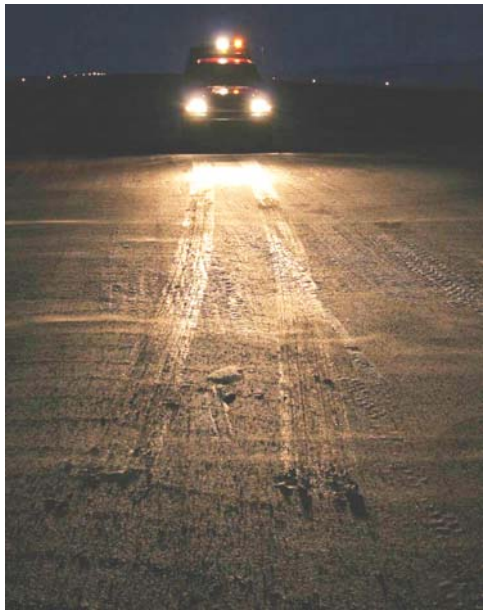

Figure 9-15. Skid marks of the right main gear that were observed on the runway, just before the aircraft turned 180° to taxi to the terminal building (Case No. 9).

[10] First of the three aircraft
[11] Second of the three aircraft

Table 9-6. Control measurements and other observations after the comment.

Case No.	Documented control measurements	Undocumented measurements and other reported indications
1		Control measurements confirmed reported values[12]
2		"It was slippery"; judgment officer in charge
3	46 / 46 / 52	
4	51 / 48 / 50	
5	54 / 50 / 56	
6		Around 34-35[13]
7	39 /36 /38[14] 49 /41 49[15]	
8		"From driving the ground vehicle it was noticed that the conditions were not good. The measured values were numbers were perceived as surprisingly good"[16]
9		

9.5.2 Indications for difficult situations

During a winter season, there are situations where it is relatively easy to warrant sufficient retardation and directional control. There are, however, also situations that are more difficult to handle. In general, difficult situations are those situations where maintenance measures are less effective or when the surface conditions change rapidly. Among maintenance personnel it is generally known that snow or ice contaminations, in combination with liquid water create such situations. But also other situations are known to be difficult, for example when the air above the pavement becomes supersaturated, relative to the surface temperature (see Section 3.4.5).

It was attempted to determine if the situation that led to the comment was indeed more difficult to handle than an average winter day. A list of difficult situations was generated for this purpose, mainly based on numerous informal conversations with airport winter maintenance personnel. The majority of these conversations took place during the field activities in the winter seasons between 2003 and 2006. Situations were added where the attainable friction level changes very rapidly, such as observed in Chapter 3. It is not possible to define clear criteria for something vaguely described as "a situation that is more difficult to handle than an average winter day". The list is therefore not intended to be complete or mutually exclusive. Neither is it intended to describe some kind or ranking in situations. But the list, shown in Table 9-7, gives a workable set of situations that winter maintenance personnel have been pointed out to be difficult, or that are otherwise known to be difficult. The situations are coded by roman letters for convenience.

An important missing parameter was the runway surface or sub-surface temperature. Therefore, the runway surface temperature was estimated by considering the 14 days air temperature history. If the air temperature in the days prior to the comment was lower, the runway will have been colder than the air temperature, at the time of the comment. Hence, a colder air temperature history indicates a colder runway.

[12] The measurements were performed, but not documented
[13] The measurements were performed, but not documented
[14] Measured in the track
[15] Measured outside the track
[16] Documented statement from the officer in charge

The indications that could be derived from the available data are summarized in Table 9-8. The indications that were found in the cases are presented in Table 9-9.

Table 9-7. Situations where it is difficult to warrant sufficient retardation and directional control.

Situation code	Description of the situation
A	Wet precipitation on a colder runway
B	Super-cooled rain
C	Ice deposition
D	Melting ice or melting compacted snow
E	Freezing of a wet runway
F	Heavy snow fall
G	Loose sand displacement
H	Many delayed flights + maintenance required
I	Insufficient maintenance crew available + maintenance required
J	Many flights in a short time + maintenance required

Table 9-8. Available indications to suggest a difficult situation.

Situation Code	Available indications
A	Reported wet precipitation + colder air temperature history, below 0°C
B	
C	Rapidly increasing dew point + colder air temperature history
D	Reported snow or ice on runway + air temperature prolonged above 0°C
E	Reported wet runway + decreasing air temperature below 0°C
F	Reported heavy snow precipitation
G	Reported loose sand on ice + air traffic between status report and comment
H	Difference between scheduled and confirmed departure or arrival
I	
J	Many confirmed departure or arrivals within a short time window

Table 9-9. Found indications that suggest a difficult situation.

Case No.	Indication	Situation
1	T_a = 0°C, T_d increase of 8°C within 12 hours, colder air temperature history	C
2		
3		
4	T_a = 3°C, T_d increase of 6°C within 12 hours, colder air temperature history	C or D
5	T_a = -16.8°C, T_d increase of 8°C within 12 hours, colder air temperature history	C
6	$0.9 < T_a < 2.8$°C, reported rain/wet snow	A and D
7	$T_a > 0$°C for 60 hours + reported ice	D
8	Melting ice, T_a = 5.8°C, Rain	A and D
9		

9.6 Discussion

The first question addressed in this study was how friction is provided by freeze bonded sand. In Norway, the warm, pre-wetted sanding method is called “fastsandmetoden” (“the fixed sand method”). But the observed removal of particles on newly applied sand (Fig. 9-6), the observed scratch marks on the ice of an operational runway (earlier shown in Fig. 4-5b and Fig 4-6), the macroscopic scratches observed in the aircraft braking experiment (Fig. 9-10) and the microscopic scratches shown by in the replicas (Fig. 9-13 and 9-14) show that loose sand particle interaction still plays a role in providing the friction. Particles can break loose under the exposed stresses of a tire, or they loosen because the surrounding ice sublimates or melts. These loose particles provide friction by scratching the ice surface. Scratching the surface involves ice deformation, which appears to be a main energy dissipation mechanism for loose particle interaction. However, the observations also revealed particles that stay attached to the ice, after the tire has past. Specifically the fine sand becomes firmly bonded and survives the action of a braking tire or the runway sweepers. It gives the surface “sand paper like” appearance. Fixed particles act in a similar way as road asperities. So, adding fixed sand asperities to an iced pavement provide friction by increasing interfacial adhesion and rubber deformation (hysteresis and rubber wear). According to the theory of rubber sliding on rough surfaces (Section 4.5.2) the energy dissipation appears mainly to be located within the rubber tire tread. These observations show that different interaction mechanisms are simultaneously operative when aircraft operate on ice with freeze bonded sand. The relative contribution of loose particle versus fixed particle interaction will be discussed later. First it is required to consider how the surface conditions change by the using warm pre-wetted sanding.

The fact that bonded sand particles can survive a sweeping operation not only prolongs the effectiveness of the sanding operation, it also has another effect on the surface conditions. As shown earlier, runway contaminations can build up in various ways. One common way is due to snow precipitation, compaction by aircraft and maintenance vehicles, and subsequent sintering of snow crystals. When sand is applied during this process, particles become embedded in the contamination layer, either because they are pressed into the layer, or the particles become covered by new snow that is subsequently compressed. These embedded sand particles may be viewed as a “stockpile” of sand that is located inside the contamination layer. This process also occurs during loose sand application (see for example Fig. 3-11a) but it is more pronounced when the sand is freeze bonded to the surface. The reason is simple - more sand remains situated on the pavement after mechanical snow removal or aircraft operations.

When the deposition of snow or ice on the pavement stops, and the air above the pavement is not saturated with water vapour, the snow and the ice gradually sublimates. Sand particles that were initially located inside the contamination layer gradually reach the surface again. An illustration of such a surface was given in Fig. 9-5. Eventually, the sand particles will loosen, not only by wear from the traffic or the maintenance activities, but also because of the sublimation of the surrounding ice. The presence of these loose particles can easily be noticed while driving on these surfaces by the sound of the particles hitting the wheel housing.

The amount of loose particles that are present on the pavement varies with time. Sublimation increases the number of loose particles, while sweeping removes loose

particles. Also aircraft operations can affect the amount of loose particles, specifically in the main region where tires travel (about 3-7 m from the centre line) by sand displacement. Directly after sweeping, there will be little or no loose particles present. The particles that survived the sweeping are well bonded to the surface. So at this stage, probably few particles will break loose under the exposed stresses of the tire. Friction forces seem therefore mainly provided by fixed sand interaction. When the runway is not swept for a longer period of time, and the relative humidity of the air above the pavement has been low, sublimation will have loosened a part of the particles. When an aircraft operate on such surface, loose particle interaction may very well provide a significant part of the friction forces.

A high attainable friction force is often the only considered quality factor of a pavement. Most maintenance personnel and pilots have the perception that the measured friction coefficient should be high, preferably as high as possible. But a surface will be exposed to different processes that change the conditions. A surface should therefore not only provide a high attainable friction, it should also hold this ability when the conditions change. How well the surface can maintain its ability to provide high friction can be described as the robustness of the surface. The concept of robustness will be illustrated by the following example:

A clean and dry pavement provides a high attainable friction. But this surface could be vulnerable to atmospheric ice deposition. This is because the mechanisms which provide the friction (interfacial adhesion and rubber deformation, such as hysteresis and wear) are lost when the pavement becomes covered with a thin layer of ice (rime). Maintenance personnel usually apply chemicals to increase the pavement's robustness against ice deposition. The chemicals do not improve the attainable friction, but avoid any dramatic drop in the attainable friction level when the air above the pavement becomes over-saturated, with respect to the pavement temperature. An analogy can be made to an iced pavement that is repeatedly treated with freeze bonded sand and swept. The surface mainly contains particles that are strongly bonded to the surface after the sweeping. These particles can provide a high attainable friction and are generally judged as good. The quality of this surface is in many situations indeed good to support traffic. However, it is vulnerable (not robust) against the atmospheric ice deposition. When loose particles (initially loose or broken loose by the tire) are also present, the robustness against ice deposition increases because the loose particles provide a friction mechanism (scratching this deposited ice layer) that is still operative. The surface will also loose its ability to provide friction, but will not be as severely as a surface with only fixed particles. An evident dramatic drop attainable friction occurred in the case "ice deposition", described in Section 3.4.5, which may have been directly related to the lack of loose particles to create friction.

Before discussing the last question addressed in this study, two side steps will be made by discussing the aircraft braking experiment in more detail. The first aspect is the effect of sweeping the ice surface and the second aspect is the observed tire lock-up on loose sand.

One of the objectives of the experiment was to study the interaction on a microscopic level. However, the replicas of the ice surface predominantly showed the effect of the sweeping. This complicated the investigation of microscopic scratch marks caused by the tire interaction, but it demonstrated the severe microscopic damage that sweepers cause to the surface. The surface structure of ice was full of small cells, grain and sub-grain

boundaries (note that the surface damage shown in Fig. 9-12 under-represents the actual damage in order to show also the original grain boundaries). This microscopic damage will not only increase the roughness on the microscopic level; the mechanical properties of this surface layer will also change significantly. A large amount of grain boundaries or other planar imperfections in the ice will increase the delayed elasticity of the material (Sinha, 1979) and make the ice to flow more readily because grain boundaries can act both as sources and sinks for dislocations (Sinha, 1987). It is important to realize that the process of friction creation (the whole interaction) takes place on different length scales (macro-, micro-, and nano-scale). Changes in the microstructure of the ice surface can result in significant changes of the attainable friction level. Since the sublimation takes place in time, this pre-disturbed layer is gradually removed, exposing less disturbed ice to the surface. This can change attainable friction level significantly in time, even though conditions appear stable to the naked eye.

The aircraft experiment illustrated what happens when an aircraft experiences a tire lock-up on loose sanded ice. The observations suggested that the skidding tire not only pushed sand particles in front of the tire, but it also collected particles and ice debris inside the contact area. Such patch of packed sand particles and ice is likely to reduce the attainable friction force for the following reasons: (1) the normal load is distributed over a large number of particles, which prevents high local contact pressures that are required to penetrate into the ice and scratch the ice surface, and (2) the presence of ice debris in the contact area replaces sand-ice interaction with ice-ice interaction. Additionally, locked tires do not give directional control to the aircraft. Modern aircraft are usually equipped with anti-skid braking systems to avoid tire lock-ups. These systems, however, are typically disabled below a certain ground speed. For a Boeing 737-600/700/800/900 this speed is 25 knots (46 km/h) (Boeing, 2002) and for a Dash-8 100/300 series it is 17 knots (31 km/h) (Widerøe, 2000). Below these limits, tire lockups can occur with loss of directional control as a result. In this speed range, the aircraft has become a “ground vehicle” which can obtain directional control solely by tire-pavement friction. Pilots can therefore experience iced surfaces that are treated with loose sand particularly slippery at very low ground speeds.

The last question addressed in this study is why airports that use the warm pre-wetted sanding method received comments from pilots that the runway was more slippery than reported. The first similarity within the cases is that the reported friction measurements were high. Only in one case (Case No. 8), the conditions were reported as “medium”. In all other cases the surface conditions were described as “good” or “medium to good”. The control friction measurements after the comment consistently described the conditions as “medium to good” or “good”. All pilots commented that the surface was slippery. This shows that in principle it reflects the known correlation issue (Chapter 2). The comments are primarily an expression of the discrepancy between that the pilots expected and what they experienced. When the runway surface conditions are described as “medium to good” or “good”, the pilots expect to obtain reasonable retardation and directional control.

Besides the subjective comments that the surface was slippery, there were more “objective” indications found for reduced or lost directional control available in 66 % of the cases (Table 9-5). All of these indications occurred all at very low ground speeds and involved either difficulties turning on the runway or skidding on locked wheels. This supports the idea that fixed slip friction measurements cannot correctly predict aircraft

performance on sanded surfaces at ground speeds where the anti-skid system is disabled. Difficulties with retardation (indicated when aircraft use exceptionally long landing distances to come to a complete stop) were not observed. Except from Case No. 5, the wind speeds at the time of the comment were not distinctively high ($v_w \leq 6.3$ m/s), indicating that there was no extraordinary need for tire-pavement friction to give the aircraft directional control. Given the reported runway surface conditions, these "objective" indications of reduced or lost directional control were also unexpected.

There is also another human factor that has to be considered. When friction measurements describe the surface conditions as "good", it easily inhibits a critical evaluation of other factors. Other available information sources can suggest that the conditions are not that good, but these may be neglected because it contradicts with the description given by the friction measurements. This can be a major cause why slippery conditions appear suddenly and unexpectedly. The core function of the surface conditions reporting system is to avoid such unexpected events. Focus should therefore be directed to ensuring that these other information sources are considered, irrespective of measured friction coefficient values. Such developments require a shift in mind set from "measuring the friction" to "creating the appropriate situation awareness".

The questions that are to be addressed are: (1)"how can the available information be used to create the appropriate situation awareness?", (2) "what key-information is currently missing to create the appropriate situation awareness?", and (3) "how (and by who) is this information interpreted?" Specifically the interpretation of the data is a difficult task and the methodology is still to be developed. A small first step in developing an alternative methodology was made in this chapter. The experiences from winter maintenance personnel were used as a starting point. The basic assumption behind this methodology is that slippery conditions can be expected when the situation at the airport is "generally known" (among pilots and winter maintenance personnel) to be difficult. The objective is to identify such situations with data that is available at the airport. The cases were used as an exercise for such identification.

In three cases (Case No. 6, 7, and 8) the runway was reported as iced, while wet precipitation was reported, and the air temperature was clearly above 0°C. So, it can be derived that the runway was covered with wet, melting ice. Obviously, it was attempted to improve the conditions by applying sand. But even though the attainable friction of wet, melting ice can be improved by sanding, and even though the wet, melting ice may have contained partially embedded particles, it is far from easy to create a large amount of tire-pavement friction in this situation. The reason is that two main mechanisms to create friction are lost: interfacial adhesion is lost because a macroscopic lubricating water film is present. Hysteresis is also lost (or at least significantly reduced) because melting readily destroys the (microscopic) surface roughness of the ice, if any. The generation of friction by fixed particle interaction require that the supporting ice withstands the stresses of the braking tire. With the ice at its melting point it is very difficult to warrant that this mechanism can occur. Summarizing, the situations that prevailed in Case no 6, 7, and 8 were clearly difficult.

In three cases (Case No. 1, 4 and 5), the dew points temperature had increased significantly (6 or 8°C) in the 12 hours prior to the comment. In addition, the runway was colder than the air temperature. This makes it highly probable that the air above the pavement was supersaturated, relative to the pavement temperature. Water vapour

deposits as ice on the runway in such conditions (situation C). As discussed earlier, pavement asperities or fixed sand particles can rapidly loose their ability to provide friction in these situations. The reason is that interfacial adhesion, hysteresis and rubber wear are lost or strongly reduced by presence of the thin ice cover. Only loose particle interaction can provide some friction by scratching this newly deposited ice layer. Hence, the situations that prevailed in Case No. 1, 4 and 5 were very likely to be difficult.

Summarizing, in 66 % of the cases there were clear indications available that basic friction mechanisms were likely to be lost or at least significantly reduced. When these indications are taken into consideration, it is not really unexpected that the runway surface was experienced as slippery. All used data was available at the airport, prior to the comments. This shows that in principle, this information could have been used to inform the pilots and maintenance personnel, given that it was interpreted in a real-time manner.

In the remaining three cases (Case No. 2, 3 and 9) there were no clear indications found that could suggest a difficult situation. The difference between air temperature and dew points temperature was less than 1°C in Case No. 2 and 3. This means that the air was humid. However, the warmer air temperature history suggests that the runway was warmer than the air temperature. Therefore there is no clear indication that ice deposition could have occurred. In Case No. 9 there was a difference of 5°C in the air temperature and dew points temperature.

It should be noted, however, that the available data was not tailored for this exercise. Specifically the identification of ice deposition conditions is uncertain due to lacking pavement temperature data. Moreover, there are some doubts on how representative the available humidity measurements are, specifically when snow drifting conditions prevail. Snow drift is a common type of snow transport in the arctic regions and takes place for prolonged periods of time. It involves the motion of snow particles just above the surface. The air temperature and humidity measurements were performed at 2 m height. During snow drift, the humidity in the lowest layer of air can significantly differ from the humidity at 2 m height. In fact, drifting snow can be observed in Fig. 9-15.

9.7 Conclusion

Two distinct interaction modes that provide tire-pavement friction have been observed when aircraft operate on iced pavements that are treated with warm, pre-wetted sand. These interaction modes are referred to as fixed and loose particle interaction and take place in the contact area between the tire and the iced pavement.

Loose particle interaction occurs when loose particles (initially loose, or broken loose by the exposed stresses of the passing tire) slide together with the rubber tread on the ice surface. Here, friction is generated by forcing the ice to deform (ploughing). Fixed particle interaction occurs when the sand particles remain attached to the contamination layer. In this case, friction is generated by forcing the rubber tread to deform (hysteresis and possibly rubber wear) and possibly by interfacial adhesion.

Microstructural investigation of the ice surfaces after aircraft braking tests on sanded ice revealed that the ice deformation during loose particle interaction can result in the creation of cells within the original crystal structure, generally known as re-

crystallisation. These observations are consistent with the observations shown in chapter 5. Cells were also produced during mechanical snow removal with a rotating steel brush.

Nine cases were investigated where the pilots commented that the runway was more slippery than reported. These cases occurred at airports that have implemented the warm, pre-wetted sanding method. The comments appear primarily to be the result of the known correlation issue. The pilots experienced unexpected slippery conditions, while the friction measurements described the surface as “medium to good” or “good”. Indications for malfunctioning measurement equipment were not found. In 66% of the cases there were clear signs of reduced directional control, all occurring at very low ground speeds. These signs were also unexpected, given the readings of the friction measurements.

In 66% of the cases there were indications available that the situation at the time of the comments was, from a maintenance perspective, clearly more difficult to handle than an average winter day. It either involved wet, melting ice contaminations or likely conditions for ice deposition onto the runway surface. Even though sanding can improve the surface conditions, basic friction mechanisms like interfacial adhesion and rubber deformation were significantly reduced or even lost. If these indications would have given consideration, slippery runway surfaces could have been expected.

The data that was used to derive these indications was available at the airports, prior to the comments. Hence, in principle it could have been used to inform the pilots, given that it could be interpreted in a real time manner.

10 SUMMARY, CONCLUSIONS, AND RECOMMENDATIONS FOR FURTHER WORK

The motivations for this thesis were two practical problems related to runway operability under cold weather conditions: (1) maintaining or improving the pavement surface conditions in an acceptable state and (2) accurately reporting the actual surface conditions. A central element in both problems is the surface's ability to provide tire-pavement friction to the operating aircraft. The objective of the thesis was to broaden the general knowledge base of these problems in general, and on the tire-pavement interaction on contaminated pavements in particular.

The practical part of the thesis investigated how runway surface conditions change and its consequences for runway operability. It also focused on a new sanding method, based on pre-wetting sand with hot water. The fundamental part addressed the question how friction is created between rubber and ice, in presence and absence of sand particles. The applied part explored an optical, non-contacting detection principle to determine the amount and distribution of sand particles on pavement surfaces.

10.1 Summary and conclusions

Runway operability
The development of runway surface conditions in time and the consequences are for the operability of the airport was investigated. Different situations were documented where the runway surface conditions changed due to snow fall, sand displacement by aircraft, ice deposition, snow compaction, and melting of the contamination layer. The main conclusions of the study are:

- Practical constrains, such as the time required for friction measurements and necessary clearance procedures to enter the runway, restrict the inspection frequency of the runway surface conditions. It therefore largely depends on the alertness and monitoring skills of maintenance personnel how quickly significant changes are detected, reported, or counteracted.

- There are currently limited possibilities to monitor runway surface conditions while the runway is open for air traffic. This hampers the objective to accurately report the actual surface conditions because significant changes can not always be immediately detected.

Warm, pre-wetted sanding
Wetting sand with hot water before its application on the pavement provides new possibilities to improve pavement surface conditions. Lumps of sand freeze onto the pavement, creating a sand paper-like surface. This method is particularly interested for airside applications because it provides a solution for the problem that loose sand is blown off the runway by the engine thrust of operating aircraft. The field studies identified the following operational aspects:

- Proper cleaning the pavement prior to the application has been pointed out as an important requirement to avoid Foreign Object Damage. The application on thick,

weakly bonded snow may cause the lumps to break loose in one piece, rather than disintegrating into individual sand particles.

- The high friction values that are typically measured on surfaces treated with warm pre-wetted sand can create a too optimistic picture of the prevailing conditions for aircrafts. Cases are documented where pilots faced worse conditions than they expected from the provided friction numbers. In 66 % of the cases there were clear indications available that the situation was not as good as suggested by the friction measurements.

- The sand particles become bonded to the pavement as the added water freezes. However, observations showed that particles can break loose under the action of aircraft tires. Particles do also loosen as a result of ice sublimation.

Tire-pavement friction on ice contaminated pavements

The level of friction that can be created between tire and pavement is determined by the whole interaction between the tire, the pavement, the contamination layer, and the atmosphere in which the interaction takes place. The presence of sand particles changes this interaction; it changes the way friction is generated. The total interaction takes place at different length scales.

Macroscopic observations of the tire-pavement interactions showed that:

- Loose sand particles that enter the contact area can slide together with the rubber tread and plough into the ice layer.

- Loose sand particles can pile-up in front of, and under, locked tires (full skid).

- Tire lockups can occur in operational situations at low ground speed because aircraft anti-skid braking systems become disabled below a certain threshold speed (typically ranging between 30 and 45 km/h, depending on the aircraft type).

- On freeze bonded sand, friction is provided by both loose particle interaction and fixed particle interaction.

Microscopic observations by etching and replicating ice surfaces after the interaction revealed that:

- Both rubber-ice and sand-ice sliding friction involved ice deformation as a mechanism of friction.

- During rubber-ice sliding friction, the original crystal structure of the ice remained intact during the interaction. However, small scale ice deformation was evident by the formation of dislocations, aligned in rows along the sliding direction.

- The ploughing of sand particles into the ice layer was accompanied with the formation of cells within the original crystal structure. This re-crystallization was observed both in the laboratory and in the field.

The friction mechanisms occurring during rubber-ice and sand-ice sliding friction was investigated with a British Pendulum Tester in a cold laboratory. The experiments showed that:

- The observed variability in friction measurements was significantly larger than the uncertainties introduced by the instrument itself. The variability may be caused by poorly controllable/reproducible, microscopic or nanoscopic surface properties of the ice and rubber.

- All friction measurements of rubber-ice friction at ice temperatures below -5°C were above $\mu = 0.2$. However, the presence of less than 1 mm snow on the ice surface reduced the friction level dramatically; down to $\mu=0.05$, even at temperatures below -20°C. These low friction levels were in the range of the measurements on ice at 0°C that was wetted by its own melt. It demonstrates that friction provided by rubber-ice interaction is very vulnerable to snow contamination.

- The sand-ice friction measurements did not show the dramatic drop in friction level by the presence of the same amount of snow (less than 1 mm). It demonstrates that friction provided by relatively large particles ploughing into the ice is more robust, compared to rubber-ice friction mechanisms.

Non-contacting detection of sand particles on iced pavements

The amount and distribution of sand particles are important quality factors of a sanded, contaminated pavement. Means of determining these parameters can therefore be of practical value. An optical, non-contacting measurement principle was investigated in a static laboratory arrangement. The pavement was illuminated by a visible laser with a wavelength of 635 nm. The radiance from the illuminated area was recorded with a digital camera at a target-to-detector range of 1.1 m. The main conclusions of experiment are:

- A correlation between the total radiance and sand application rate was only found when there was negligible radiance from the pavement in the scene.

- With the used experimental set-up, the sand detection requires a distinction between radiance originating from the sand and the radiance originating from the pavement.

- Due to the similarities in optical properties of the sand and the aggregates in the pavement (both originate from crushed rock) and the transparency of ice in the visible range, it seems unlikely that the distinction can be made on the basis of radiance intensity, with the used illumination wavelength of 635 nm.

An alternative method of discriminating between the radiance from the sand and pavement was investigated, based on triangulation. Image analysis techniques were used to define a region of interest where the radiance only originates from the sand. Within this region, individual sand particles are identified and counted.

- The principle is developed theoretically for flat surfaces and adapted for application on rough surfaces of unknown topography.

- The algorithm to define the region of interest placed the regions reasonably well in all analyzed images, resulting in a rather conservative input in the subsequent analyses.

- The detection algorithm had a success rate between 63 and 100 %, depending on the surface contamination. The errors were mainly caused by not detecting particles that were located in the lower parts of the surface topography.

- The algorithm made only few mistakes by incorrectly identifying particles. Hence, the number of detected particles was a conservative estimate of the actual number of particles located in the region.

Concluding remark on winter maintenance at airports
Within winter maintenance at airports there is a large focus on the pavement's ability to provide friction to aircraft (shortly, the friction level of the surface conditions). This focus is also reflected in regulations, procedures, and in the public literature on tire-pavement friction or winter maintenance. Hence the common view is that "good" surface conditions are surface conditions with a high friction level. Clearly, aircraft need tire-pavement friction for retardation and directional control. Hence, *for pilots*, a high friction level is indeed desirable.

But what kind of surface conditions do maintenance personnel need? Is a high friction level also desirable for them? Or are there also other quality factors that determine how good the surface conditions are for them? Any activity on a runway, whether it is a quick inspection, snow removal, or the application of sand or chemicals, takes time. During this time runway is temporary closed for air traffic. As soon as the runway re-opens, (and pilots are updated with the latest information on the runway status), a period starts were there are currently little options but to trust that the surface holds it ability to provide friction. How long the surface conditions can be trusted upon depends on the local weather and traffic situation at the airport. But it depends also on the surface conditions itself. The surface conditions can have a high friction level, but may be very vulnerable to loose the ability to provide friction. A rapid deterioration of the surface conditions is difficult due to the outlined practical constrains. Hence, *for maintenance personnel*, robust surface conditions are desirable.

10.2 Recommendations for further work

Runway operability
To improve runway operability under cold weather conditions in general, and the surface conditions reporting system in particular, it is recommended to:

- Further develop the understanding of the dynamical behaviour of runway surface conditions. The central question to be addressed is *how* surface conditions change. The case study contributed to this question but more work is needed to gain insight in all physical processes that affect runway surface conditions.

- Explore possibilities for remote sensing techniques that can assist runway maintenance personnel in monitoring the surface conditions of movement areas.

- Develop a prediction of the runway surface conditions for the time after the status is assessed by a runway inspection. Such prediction can give guidance when a new runway inspection is required, and can create a general awareness on the likelihood that surface conditions have deteriorated since the last inspection.

Tire-pavement interaction

General understanding of tire-pavement interaction is central to the problem of runway operability under winter conditions, in particular for the interpretation of readings from friction measurement devices. This thesis concentrated on one particular interaction process, which is the ploughing of sand particles into the ice layer. Further research may:

- Conduct laboratory experiments where the resistance during the ploughing process can be measured and parameters like normal load, sliding speed, ice temperature and sand geometry can be varied. The humidity and temperature of the air in which the interaction takes place should be controlled. Detailed ice surface observations after the interaction should be included to interpret the response.

- Focus on other interaction processes, for example lubrication phenomena when liquid water is present on snow, or ice contaminated pavements.

Non-contacting detection of sand particles on iced pavements

More research and development is needed before the feasibility of the optical non-contacting detection principle can be assessed for operational situations. To continue its development it recommended to:

- Conduct tests on snow covered pavements in a static arrangement and develop corresponding image processing algorithms for snow covered pavements.

- Improve algorithms such that are able to perform the detection in a range of pavement surface conditions.

- Develop an experimental arrangement that can be used for either stationary or mobile applications during operational (daylight) conditions.

11 REFERENCES

Ahagon, A., Kobayashi T., and Misawa M. (1988): Friction on ice. Rubber Chemistry and Technology, vol. 61[1], pp. 14-35.

Akkok, M., Ettles C. M. M., and Calabrese S. J. (1987): Parameters affecting the kinetic friction of ice. Transactions of the ASME, vol. 109, pp. 552-561.

Ambach, W. and Mayr B. (1981): Ski gliding and water film. Cold Regions Science and Technology, vol. 5[1], pp. 59-65.

Amontons, G. (1699): De la Résistance causée dans les Machines. Mémoires de l'Académie Royale A, pp. 247-260.

Andrássy, L. (1999): Overview of the Joint Winter Runway Friction Measurement Program. Report no. TP 13361E , Transportation Development Centre, Transport Canada.

Andresen, A. and Wambold J. C. (1999): Friction Fundamentals, Concepts and Methodology. Report no. TP 13837E , Transportation Development Centre, Transport Canada.

Avinor. (2005): Annual Report Avinor 2005.

Azarkhin, A. and Devenpeck M. L. (1997): Enhanced model of a plowing asperity. Wear, vol. 206[1-2], pp. 147-155.

Barer, S.S., Churaev N. V., Derjaguin B. V., Kiseleva O. A., and Sobolev V. D. (1980): Viscosity of nonfreezing thin interlayers between the surfaces of ice and quartz. Journal of colloid and interface science, vol. 74[1], pp. 173-180.

Barnes, P., Tabor D., and Walker J. C. F. (1971): The friction and creep of polycrystalline ice. Proceedings of the Royal Society of London, Series A, vol. 324, pp. 127-155.

Barrette, P.D. and Sinha N. K. (1994): Lattice misfit as revealed by dislocation etch pits in a deformed ice crystal. Journal of Materials Science Letters, vol. 13, pp. 1478-1481.

Bartenev, G.M. and El'kin A. I. (1965): Friction properties of high elastic materials. Wear, vol. 8[1], pp. 8-21.

Bernal, J.D. and Fowler R. H. (1933): A Theory of Water and Ionic Solution, with Particular Reference to Hydrogen and Hydroxyl Ions. Journal of Chemical Physics, vol. 1[8], pp. 515-548.

Bhushan, B. (1999): Principles and Applications of Tribology. New York, John Wiley & Sons, inc.

Bhushan, B. and Nosonovsky M. (2004): Comprehensive model for scale effects in friction due to adhesion and two- and three-body deformation (plowing). Acta Materialia, vol. 52[8], pp. 2461-2474.

Biggs, D.C. and Hamilton G. B. (2002): Runway friction accountability risk assessment, results of a survey of Canadian airline pilots. Report no. TP 13941E , Transportation Development Centre, Transport Canada.

Bluhm, H., Inoue T., and Salmeron M. (2000): The friction of ice measured using lateral force microscopy. Physical Review B, vol. 61[11], pp. 7760-7765.

Boccanfuso, A. (2004): History of the Joint Winter Runway Friction Measurement Program. in: Proceedings of the 3rd international meeting on aircraft performance on contaminated runways IMAPCR 2004, Report no. TP 13579, Transportation Development Centre, Transport Canada.

Boeing. (2002): Aircraft Maintenance Manual 737-600/700/800/900 Antiskid / Autobrake system _ Locked wheel Protection. pp. 31.

Bowden, F.P. and Hughes T. P. (1939): The mechanism of sliding on ice and snow. Proceedings of the Royal Society of London, Series A, vol. 172[949], pp. 280-298.

Bowden, F.P. and Tabor D. (1954): The Friction and Lubrication of Solids. 2nd edition, Oxford, Oxford University press.

Bowden, F.P. and Tabor D. (1964): The Friction and Lubrication of Solids, Part II. Oxford, UK, Clarendon Press.

Briscoe, B.J. (1998): Isolated contact stress deformations of polymers: the basis for interpreting polymer tribology. Tribology International, vol. 31[1-3], pp. 121-126.

Burwell, J. (1957): Survey of possible wear mechanisms. Wear, vol. 1[2], pp. 119-141.

CAA. (2004a): Forskrift om plasstjeneste. Report no. BSL E 4-2 FOR 2004-04-27 nr: 670 Oslo, Norway, Luftfartstilsynet.

CAA. (2004b): Vinteroperasjoner og rapportering av baneforhold. Report no. AIC-N32 , Norwegian Civil Aviation Authorities.

Castellano, B. (2005): Winter Operations (Friction Measurement Issues). Report no. CertAlert 05-01 , Federal Aviation Administration.

Churaev, N.V., Bardasov S. A., and Sobolev V. D. (1993): On the non-freezing water interlayers between ice and a silica surface. Colloids and Surfaces A: Physicochemical and Engineering Aspects, vol. 79[1], pp. 11-24.

Ciamberlini, C., Innocenti G., and Longobardi G. (1995): An optoelectronic prototype for the detection of road surface conditions. Review of Scientific Instruments, vol. 66[3], pp. 2684-2689.

Clark, S.K. (1971): The mechanics of pneumatic tires. Washington D.C., National Highway Traffic Safety Administration.

Colbeck, S.C. (1994): A review of the friction of snow skies. Journal of Sport Sciences, vol. 12, pp. 285-295.

Comfort, G. and Gong Y. (1999): Evaluation of the sand properties affecting sand selection for airside applications. Report no. TP 13447E , Transportation Development Centre, Transport Canada.

Conant, F.S., Dum J. L., and Cox C. M. (1949): Frictional Properties of Tread-type Compounds on Ice. Industrial and Engineering Chemistry, vol. 41[1], pp. 120-126.

Croll, J.B. (2004): Prediction of Aircraft Landing Distance on Winter Contaminated Runways Using the Canadian Runway Friction Index. in: Proceedings of the 3rd international meeting on aircraft performance on contaminated runways IMAPCR 2004, Report no. TP 13579, Transportation Development Centre, Transport Canada.

Croll, J.B., Bastian M., Martin J. C. T., and Carson P. (2002): Evaluation of Aircraft Braking Performance on Winter Contaminated Runways and Prediction of Aircraft Landing Distance using the Canadian Runway Friction Index. Report no. TP 13943E , Transportation Development Centre, Transport Canada.

Czichos, H. (1978): Tribology, a system approach to the science and technology of friction, lubrication, and wear. Amsterdam, Elsevier.

Dahlen, J. and Vaa T. (2001): Winter Friction Project in Norway. Transportation Research Record, [n 1741], pp. 34-41.

Dainty, J.C. (1975): Laser speckle and related phenomena. Berlin, Springer-Verlag. Topics in applied physics.

Dash, J.G. (2003): Theory of a tribometer experiment on ice friction. Scripta Materialia, vol. 49[10], pp. 1003-1006.

Dash, J.G., HaiyingFu, and Wettlaufer J. S. (1995): The premelting of ice and its environmental consequences. Reports on Progress in Physics, vol. 58[1], pp. 115-167.

Deffieux, J.Cl. (1999): IRFI Reference Device. in: Proceedings of the 2nd international meeting on aircraft performance on contaminated runways, Report no. TP 13579, Transportation Development Centre, Transport Canada. pp. 355-364

Derjaguin, B.V. (1986): Mecanical Properties of the Boundary Lubrication Layer. Soviet Journal of Friction and Wear, vol. 7[5], pp. 773-779.

Dutch Transport Safety Board. (2001): Final report of the investigation into the probable cause of the accident with the El Al Boeing 747, 4X-AXK, at Amsterdam Airport Schiphol on 8 February 1999. Report no. 1999011 Den Haag, Dutch Transport Safety Board.

Elbaum, M., Lipson S. G., and Dash J. G. (1993): Optical study of surface melting on ice. Journal of Crystal Growth, vol. 129[3-4], pp. 491-505.

Evans, D.C.B., Nye J. F., and Cheeseman K. J. (1976): The kinetic friction of ice. Proceedings of the Royal Society of London, Series A, vol. 347, pp. 493-512.

FAA. (1991): Aircraft winter safety and operation. Report no. AC 150/5200-30A , Federal Aviation Administration.

Faraday, M. (1859): On regulation, and on the conservation of forces. Philosophical Magazine, vol. 17, pp. 162-169.

Finkele, R. (1997): Detection of ice layers on road surfaces using polarimetric millimetre wave sensor at 76 GHz. Electronics Letters, vol. 33[13], pp. 1153-1154.

Fowler, A.J. and Bejan A. (1993): Contact melting during sliding on ice. International Journal of Heat and Mass Transfer, vol. 36[5], pp. 1171-1179.

Gauthier, C. and Schirrer R. (2000): Time and temperature dependence of the scratch properties of poly(methylmethacrylate) surfaces. Journal of Materials Science, vol. V35[9], pp. 2121-2130.

Gehman, S.D. (1971): Material Characteristics. in: Clark, S.K. Mechanics of pneumatic tires. Ch. 1. Washington D.C., National Highway Traffic Safety Administration.

Giles, C.G., Sabey B. E., and Cardew K. H. F. (1964): Development and Performance of the Portable Skid-Resistance Tester. Report no. 66 London, Road Research Laboratory.

Gilpin, R.R. (1980): Wire regelation at low temperatures. Journal of colloid and interface science, vol. 77[2], pp. 435-448.

Gnörich, W. and Grosch K. A. (1974): The friction of polymers on ice. Rubber Chemistry and Technology, vol. 48[4], pp. 527-537.

Grosch, K.A. (1963): The relation between the friction and visco-elastic properties of rubber. Proceedings of the Royal Society of London, Series A, vol. 274[1356], pp. 21-39.

Hayhoe, G.F. (1984): Application of Hot Sand for Winter Ice Control. Report no. fhwa_ak_rd_85_01 , State of Alaska, Department of Transportation and Public Facilities.

Higashi, A. (1988): Lattice defects in ice crystals. Sapporo, Japan, Hokkaïdo University Press.

Hobbs, P.V. (1974): Ice Physics. Oxford, Oxford University press.

Hokkirigawa, K. and Kato K. (1988): An experimental and theoretical investigation of ploughing, cutting and wedge formation during abrasive wear. Tribology International, vol. 21[1], pp. 51-57.

Holst, G.C. (1998): CCD arrays Cameras and Displays. Second Edition, Bellingham, Washington, USA, SPIE Optical Engineering Press.

Holzwarth, F. and Eichhorn U. (1993): Non-contact sensors for road conditions. Sensors and Actuators A: Physical, vol. 37-38, pp. 121-127.

Horrigan, J.T. (2004): Contaminated runways operations. in: Proceedings of the 3rd international meeting on aircraft performance on contaminated runways IMAPCR 2004, Report no. TP 13579, Transportation Development Centre, Transport Canada.

HSL. (2000a): Luftfartshendelse, avkjøring av glatt bane i forbindelse med oppstilling for start MD-80 Bardufoss 20-mar-2000. Report no. 30/2000 , Haverikommisjon for Sivil Luftfart.

HSL. (2000b): rapport om alvorlig luftfartshendelse på rullebane 19, Tromsø Lufthavn Langnes, 11 mai 2000 med Scandinavian Airlines System MD-87, LN-RMX. Report no. 77/2000 Kjeller, Norway, Haverikommisjonen for sivil luftfart.

HSL. (2001a): Rapport om luftfartshendelse, utforkjøring på siden av banen under landing Molde, 14 mars 2000. Report no. 05/2001 Kjeller, Norway, Haverikommisjonen for sivil luftfart.

HSL. (2001b): Rapport om luftfartsulykke på Oslo Lufthavn Gardermoen, Bane 19L, 6. Desember 1999 med premiair DC-10-10, OY-CNY. Report no. 05/2001 Kjeller, Norway, Haverikommisjonen for sivil luftfart.

ICAO. (2003): International standards and recommended practice, Annex 15 Aeronautical Information Services Chapter 5 NOTAM. Eleventh edition, International Civil Aviation Organization.

Inman, I.A., Datta P. K., Du H. L., Burnell-Gray J. S., Pierzgalski S., and Luo Q. (2005): Studies of high temperature sliding wear of metallic dissimilar interfaces. Tribology International, vol. 38[9], pp. 812-823.

Jähne, B. (2004): Practical Handbook on Image Processing for Scientific and Technical Applications. Boca Raton, Florida, CRC Press.

Jellinek, H.H.G. (1967): Liquid-like (transition) layer on ice. Journal of colloid and interface science, vol. 25, pp. 192-205.

Johnson, K.L. (1985): Contact mechanics. London, Cambridge University press.

Johnson, P.S. (2001): Rubber processing: an introduction. Munich Germany, Hanser Publishers .

Keyser, J.H. (1981): Chemicals and abrasives for snow and ice control. in: Gray, D.M. and Male, D.H. Handbook of snow. Toronto, Canada, Pergamon Press.

Klein-Paste, A. and Sinha N. K. (2006): Airport operations under cold weather conditions - observations on operative runways in Norway. Report no. TP 14648E , Transportation Development Centre, Transport Canada.

Klein-Paste, A. and Sinha N. K. (in press): Experiences with warm, pre-wetted sanding at airports in Norway. Transportation Development Centre, Transport Canada.

Kuroiwa, D. (1977): The kinetic friction on snow and ice. Journal of Glaciology, vol. 19[81], pp. 141-152.

Liang, H., Martin J. M., and Mogne T. L. (2003): Experimental investigation of friction on low-temperature ice. Acta Materialia, vol. 51[9], pp. 2639-2646.

Liu, X.B. and Wang H. M. (2007): Microstructure and tribological properties of laser clad [gamma]/Cr7C3/TiC composite coatings on [gamma]-TiAl intermetallic alloy. Wear, vol. 262[5-6], pp. 514-521.

Liu, Z., Sun J., and Shen W. (2002): Study of plowing and friction at the surfaces of plastic deformed metals. Tribology International, vol. 35[8], pp. 511-522.

Makkonen, L. (1994): Application of a new friction theory on ice and snow. Annals of Glaciology, vol. 19, pp. 155-157.

Makkonen, L. (2003): A theoretical approach to rubber friction on ice. in: Vainikka, J. and Pirjola, H. ARTTU Final Report. Ch. 3. Helsinki, Helsinky University of Technology.

Makkonen, L. (2004): Friction as a Result of Surface Tension. in: Proceedings of the 27th Annual Meeting of the Adhesion Society, Inc. Wilmington, NC, USA 15 - 18 Feb. 2004, Blacksburg, VA, USA. pp. 399-401

Martin, B.R. (1971): Statistics for Physicists. London, Academic Press.

Meyer-Arendt, J.R. (1995): Introduction to classical and modern optics. Englewood Cliffs, New Jersey, Prentice Hall.

Michel, B. and Ramseier R. O. (1969): Classification of River and Lake Ice Based on its Genesis, Structure and Texture. Report no. S-15 , Département de Génie Civil, Université Laval, Quebec.

Moore, D.F. (1965): A review of squeeze films. Wear, vol. 8[4], pp. 245-263.

Moore, D.F. (1972): The Friction and Lubrication of Elastomers. Oxford, Pergamon press.

Moore, D.F. (1975): The friction of pneumatic tyres. Amsterdam, Elsevier Scientific publishing Company.

Moshansky, P.J. (1992): Commission of inquiry into the Air Ontario crash at Dryden, Ontario. Ottawa (Ontario).

Munro Stanley London. (2006): Certificate of conformity for TRRL rubber.

Niven, C.D. (1955): On the friction of rubber covered wheels on ice. Canadian Journal of Technology, vol. 33, pp. 204-210.

Niven, C.D. (1958): On the friction of inflated rubber tires on ice. Canadian Journal of Physics, vol. 36, pp. 599-610.

Niven, C.D. (1959): A proposed mechanism for ice friction. Canadian Journal of Physics, vol. 37[3], pp. 247-255.

Niven, C.D. (1963): The magic surface: A discussion on the remarkable sliding quality of ice. Pageant Press Inc. New York.

Norheim, A. (2004): Braking on snow and ice, past, present, and future. in: Proceedings of the 3rd international meeting on aircraft performance on contaminated runways IMAPCR 2004, Report no. TP 13579, Transport Development Centre, Transport Canada.

Norheim, A., Sinha N. K., and Yager T. J. (2001): Effects of the structure and properties of ice and snow on the friction of aircraft tyres on movement area surfaces. Tribology International, vol. 34, pp. 617-623.

Ogura, T., Kageyama I., Nasukawa K., Miyashita Y., Kitagawa H., and Imada Y. (2002): Study on a road surface sensing system for snow and ice road. JSAE Review, vol. 23[3], pp. 333-339.

Oksanen, P. (1983): Friction and Adhesion of Ice. Ph.D. thesis, Helsinki University of Technology

Oksanen, P. and Keinonen J. (1982): The mechanism of friction of ice. Wear, vol. 78[3], pp. 315-324.

Pacejka, H.B. (2002): Tyre and vehicle dynamics. Oxford, Butterworth&Heinemann.

Pauling, L. (1935): The Structure and Entropy of Ice and of Other Crystals with Some Randomness of Atomic Arrangement. Journal of the American Chemical Society, vol. 57[12], pp. 2680-2684.

Persson, B.N.J. (2000): Sliding friction. Berlin, Springer.

Persson, B.N.J. (2001): Theory of rubber friction and contact mechanics. Journal of Chemical Physics, vol. 115[8], pp. 3840-3861.

Pfalzner, P.M. (1950): On the Friction of Various Synthetic and Natural Rubbers on ice. Canadian Journal of Technology, vol. 28 sec F, pp. 468-489.

Rabinowicz, E. (1995): Friction and wear of materials. Second edition, pp. 191-238. New York, John Wiley & Sons, Inc.

Reynolds, O. (1901): On the slipperiness of ice. Papers on Mechanical and Physical Subjects. Cambridge, Cambridge University press.

Roberts, A.D. (1981): Rubber-Ice Adhesion and Friction. Journal of Adhesion, vol. 13, pp. 77-86.

Roberts, A.D. and Lane J. D. (1983): Friction of rubber on ice in the presence of salt. Journal of Physics D: Applied physics, vol. 16, pp. 275-285.

Roberts, A.D. and Richardson J. C. (1981): Interface study of rubber-ice friction. Wear, vol. 67[1], pp. 55-69.

Sarabandi, K., Li E. S., and Nashashibi A. (1997): Modelling and Measurements of Scattering from Road Surfaces at Millimeter-wave frequencies. IEEE Transactions on Antennas and Propagation, vol. 45[11], pp. 1679-1688.

SAS. (1972): Winter Operations - in AFM bulletin DC-9. Report no. bulletin nr 63 , Scandinavian Airlines Service.

Schallamach, A. (1963): A theory of dynamic rubber friction. Wear, vol. 6[5], pp. 375-382.

Schallamach, A. (1971): How does rubber slide? Wear, vol. 17[4], pp. 301-312.

Sinha, N.K. (1977a): Dislocations in ice as revealed by etching. Philosophical Magazine, vol. 36[6], pp. 1385-1404.

Sinha, N.K. (1977b): Technique for Studying Structure of Sea Ice. Journal of Glaciology, vol. 18, pp. 315-323.

Sinha, N.K. (1978a): Observation of basal dislocations in ice by etching and replicating. Journal of Glaciology, vol. 21[85], pp. 385-395.

Sinha, N.K. (1978b): Rheology of Columnar-grained ice. Experimental Mechanics, vol. 18[12], pp. 464-470.

Sinha, N.K. (1978c): Short-term rheology of polycrystalline ice. Journal of Glaciology, vol. 21[85], pp. 457-473.

Sinha, N.K. (1979): Grain boundary sliding in polycrystalline materials. Philosophical Magazine A, vol. 40[6], pp. 825-842.

Sinha, N.K. (1981): Rate sensitivity of compressive strength of columnar-grained ice. Experimental Mechanics, vol. 21[6], pp. 209-218.

Sinha, N.K. (1984): Intercrystalline cracking, grain-boundary sliding, and delayed elasticity at high temperatures. Journal of Materials Science, vol. 19, pp. 359-376.

Sinha, N.K. (1987): Dislocation climb in ice observed by etching and replicating. Journal of Materials Science Letters, vol. 6, pp. 1406-1408.

Sinha, N.K. (1999): What do we really know about snow and ice that make hazardous runways? in: Proceedings of the 2nd international meeting on aircraft performance on contaminated runways, Report no. TP 13579, Transportation Development Centre, Transport Canada. pp. 273-284

Sinha, N.K. (2004): Uniform snow- or ice-contaminated runway surface - variability in readings from friction measurement devices. in: Proceedings of the 3rd international meeting on aircraft performance on contaminated runways IMAPCR 2004, Report no. TP 13579, Transportation Development Centre, Transport Canada.

Sinha, N.K. and Norheim A. (2000): A new retrospect of snow and ice, tribology and aircraft performance. in: Hjorth-Hansen, E., Holand, I., Løset, S., and Norem, H. Snow Engineering, Recent Advances & Developments, Rotterdam, Balkema. pp. 427-435

Southern, E. and Walker R. W. (1972): Friction of rubber on ice. Nature (Physical Science), vol. 237[78], pp. 142-144.

Southern, E. and Walker R. W. (1974): A Laboratory Study of the Friction of Rubber on Ice. in: Lee, L.-H. Advances in polymer friction and wear, New York, Plenum. pp. 223-236

Strausky, H., Krenn J. R., Leitner A., and Aussenegg F. R. (1998): Sliding plastics on ice: fluorescence spectroscopic studies on interfacial water layers in the micrometer thickness regime. Applied Physics B: Lasers and Optics, vol. 66[5], pp. 599-602.

Suh, N.P. and Sin H.-C. (1981): The genesis of friction. Wear, vol. 69[1], pp. 91-114.

Telford, J.W. and Turner J. S. (1963): The Motion of a Wire through Ice. Philosophical Magazine, vol. 8, pp. 527-531.

Tusima, K. (1977): Friction of a steel ball on a single crystal of ice. Journal of Glaciology, vol. 19[81], pp. 225-235.

Umbaugh, S.E. (2005): Computer Imaging - Digital Image Analysis and Processing. Boca Raton, Florida, CRC Press.

Vaa, T. (2004): Implementation of the new sanding method in Norway. in: Proceedings of the Sixth International Symposium on Snow Removal and Ice Control Technology, Spokane, Transportation Research Board.

Vaa, T. (2005): Resultater tester fastsandspredere i uke 3/2005. Report no. 2413 , Norwegian Public Road Administration.

Vaa, T. and Dahl T. (2002): Development of a new sanding method based on a mix of sand and hot water, and implementation and consequences for the organization of gritting operations. in: XIth International Winter Road Congress, Sapporo, World Road Association AIPCR.

Weeks, W.F. and Ackley S. F. (1986): The growth, Structure, and Properties of Sea Ice. in: Untersteiner, N. New York, Plenum Press. NATO Advanced Science Institutes Series.

Widerøe. (2000): Pilot Training Manual DHC-8. Ch. 10.6, pp. 10-17.

Wilkinson, C.S. (1953): Study of the Factors Affecting the Friction of Tread Compounds on Ice. India Rubber World, vol. 128[4], pp. 475-481.

Williams, M.L., Landel R. F., and Ferry J. D. (1955): The Temperature Dependence of Relaxation Mechanisms in Amorphous Polymers and Other Glass-forming Liquids. Journal of the American Chemical Society, vol. 77[14], pp. 3701-3707.

Wismar, M.J. and Elinder H. (2003): Incident involving aircraft G-FLTA at Arvidsjaur airport, BD County, Sweden, on the 22nd of February 2002. Report no. RL 2003:08e Stockholm, Board of Accident Investigation.

Zhang, J., Moslehy F. A., and Rice S. L. (1991): A model for friction in quasi-steady-state sliding part I. Derivation. Wear, vol. 149[1-2], pp. 1-12.

Zhang, S.W. (2004): Tribology of elastomers. Amsterdam, Elsevier.

APPENDICES

A MICROSTRUCTURAL ANALYSIS OF SNOW COMPRESSED BY AN AIRCRAFT TIRE

Based on: Klein-Paste, A., Sinha N. K., Loset S., and Norheim A. (2007): Microstructural analytical techniques for snow compacted by an aircraft tire. Tribology International, vol. 40[2], pp. 412-417.

A.1 Introduction

The majority of the thesis work was related to ice contaminated pavements. But attention was also given to snow contaminated pavements. When aircraft travel on snow covered pavements, the snow becomes compressed. After the compression it is difficult to remove the snow mechanically, which often results in persistent runway contaminations. Over time and with multiple compressions the snow transforms into ice. Because snow contaminations on movement areas are very common, and its presence has consequences for aircraft performance, it is of interest to study the structural characteristics of snow, as it is located on the pavement. Such study requires an analytical technique and a procedure to sample the snow.

Snow is, in the environment present on the ground (temperature, vapor pressure), thermodynamically unstable. It is therefore subjected to continuous structural changes before, during, and after the interaction with the tire. To investigate such material it is important to slow down the natural snow metamorphism and minimize mechanical and thermal stresses during sample handling, transport, and analysis. Borel and Brzoska (2000) presented an method for sectioning snow/pavement samples. This method preserves the snow-pavement interface during sampling and sectioning. Unfortunately, the required pavement sampling complicates its applicability on operational airports. Therefore it was decided to sample only the snow, leaving the pavement intact. This, however, implies that the original snow-pavement interface has to be destroyed. Satyawali et al. (2003) presented an analytical technique for snow studies, which is an adaptation of the double-microtoming technique for ice (Sinha, 1977). The objective of this study was to test the applicability of the double microtoming technique for snow on tracks that were formed by aircraft taxiing on undisturbed, freshly fallen snow. To illustrate some of the possibilities, digital image analysis of the thin-sections were applied to quantify general characteristics like density, surface topography and grain/cluster size distribution.

A.2 Experimental details

Snow samples (temperature T = 0°C, density $\rho \approx 400$ kg/m3) were taken from a track made by a free-rolling main gear tire of an aircraft (Dash-8 100 series), taxing at a speed of about 15 km/h. The freshly fallen snow (20 to 30 mm in thickness, density $\rho \approx 150$ kg/m^3) deposited from 30 min to 5 min before compression, roughly in two showers. The snow was moist but no liquid water could be squeezed out, indicating that the liquid water content did not exceed ~8 % (Colbeck et al., 1990). Samples were taken shortly (between 30 and 60 s) after compression, using a stainless steel auger (diameter 50 mm) that was inserted vertically in the middle of the snow track. After removal of surrounding snow, a steel plate was inserted horizontally under the auger to release the sample from the pavement. During and after the release procedure the sample was inspected visually on damages in the form of cracks. Whenever the sample showed cracks or broke in fragments, it was discarded. Most of the successfully recovered snow samples were taken on iced

pavements. The smoothness of the ice surface and is poor adherence to snow (shortly after the compression) assisted the snow sampling.

The released samples were transferred to a paper cup containing super-cooled dimethyl-phthalate to fill the pore space (Perla, 1982). The phthalate was allowed to penetrate into the pore space before the cup was stored below -20°C to solidify the sample. Filling the pore space and lowering the temperature slows down the snow metamorphism and supports the snow crystals during further handling. After transportation to a field laboratory, thin-sections were made by using the double-microtoming technique for snow. The method prescribes the use of water to mount the sample on the glass plates. After the first microtoming sequence it was found difficult to release the sample from the glass plate without damaging it. The mounting was therefore performed with a few drops of phthalate in stead of water. Frozen phthalate is softer and adheres less to the glass plate and this reduces the stresses on the sample while releasing it. The mounting step for the second microtoming sequence was performed, as prescribed, with water to ensure a good sample support during microtoming to the final thickness.

The thin-sections were studied with an optical microscope under crossed-polarized light. Ice is, in contrast to dimethyl-phthalate, optically active and will appear coloured under cross-polarized light, whereas phthalate appears grey. The colour is caused by the birefringence of the light and depends on the thickness and the crystallographic orientation of the ice grains. Hence, the ice needs to have a certain thickness to have a good colour contrast. Freshly fallen snow usually contains small crystals, requiring that the sections are thin (less than ~0.3 mm) to provide a 2D view of the crystals. Such thicknesses result in little or no colour contrast. A retardation plate (mica) was used under the sample to increase the contrast and bring out the colours. Pictures were taken using a digital camera mounted on the microscope. A series of pictures were stitched together, using photo stitch software, in order to cover a large area with sufficient resolution.

A.3 Results

Fig. A-1 shows a part of a vertical thin-section of the track (full thin-section measures 33 mm × 9 mm). The original image has a resolution of 140 pixels/mm. The light areas are phthalate (pore space) and the ice grains have different grey levels, depending on their crystallographic orientation. The tire has rolled at the top of the image from right to left and the pavement is located at the bottom. Note that the snow-pavement interface could not be recovered by the used sample release technique. The topography of the tire-snow interface is enhanced by digitally masking the phthalate above the uppermost grains.

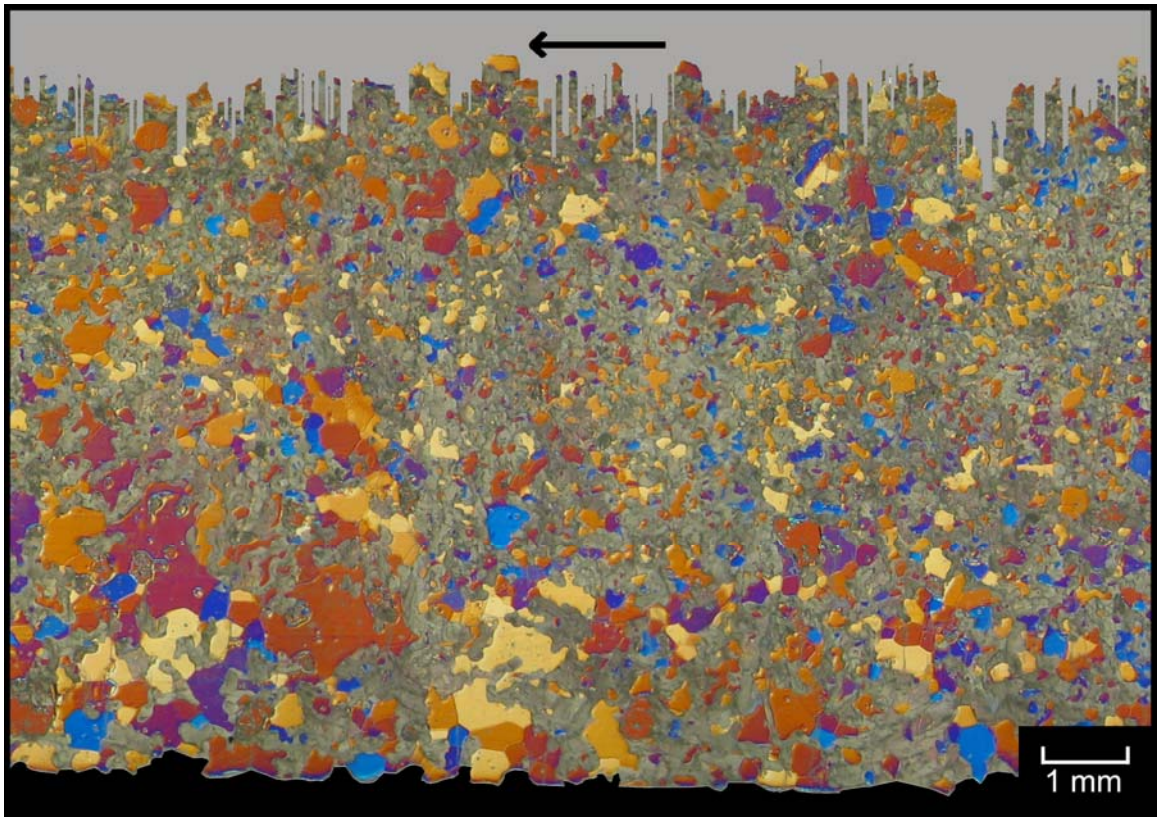

Figure A-1. A vertical thin-section of a snow track. The arrow indicates the rolling direction of the tire and the pavement is located at the bottom of the image.

The thin-section in Fig. A-1 shows individual grains and grain clusters with a large variety of size. The largest clusters are dominantly located at the bottom. The crystals have a smooth texture; no sharp angular faces of the crystals were observed.

Fig. A-2 shows a horizontal thin-section of the same sample, about 2 mm below to the tire-snow interface. The tire has rolled in the plane of the paper from right to left. The horizontal thin-section shows mainly single crystals. The crystals also exhibit a smooth texture in this plane.

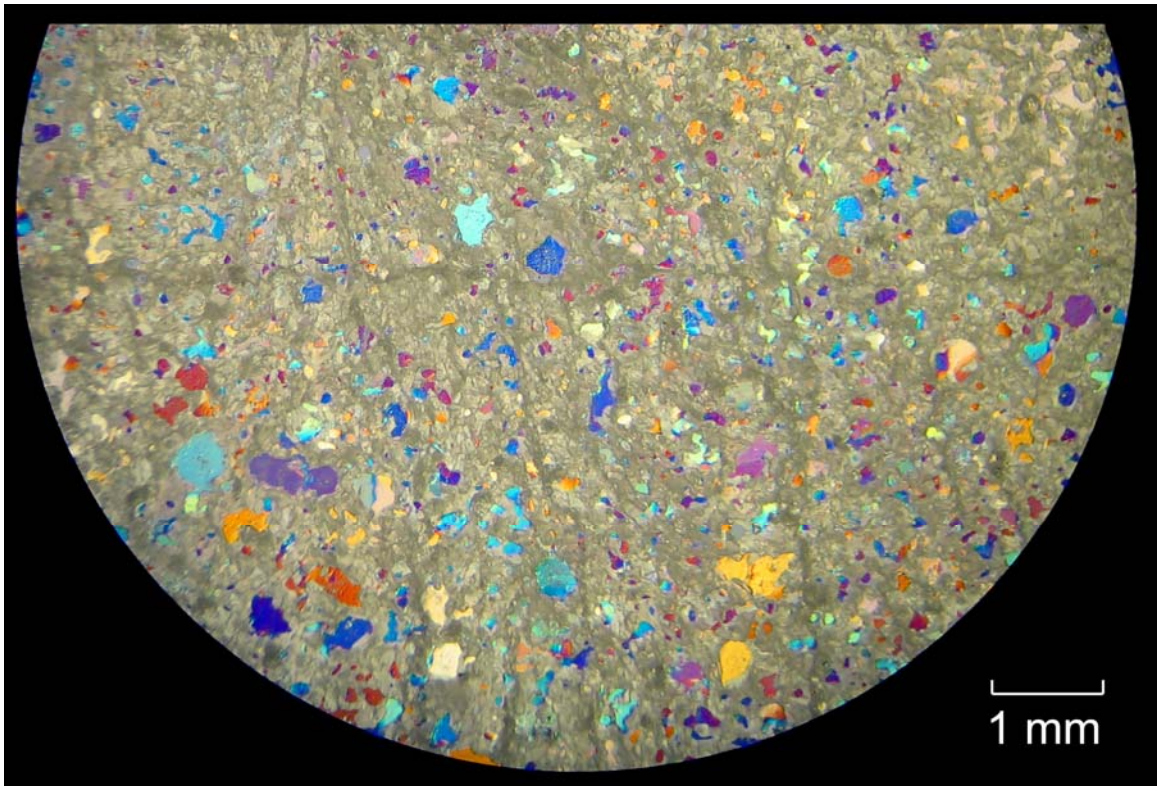

Figure A-2. Horizontal thin-section of the same sample about 2 mm below the tire-snow interface.

A.4 Image analysis

The success of digital image analysis largely depends on the resolution of the image and on the colour contrast between the different objects of interest. The first task in analysing snow thin-sections is to discriminate between ice (snow crystals) and phthalate. This was performed by transforming the colour images first to a greyscale image and further to a binary image where white and black pixels represent ice and phthalate, respectively. The original and binary images were placed on top of each other to visually inspect the quality of the conversion procedure. The vertical thin-section could be converted without introducing significant errors. The horizontal thin-section, however, had insufficient colour contrast to obtain a representative conversion into the binary image. The image analysis was therefore continued with the vertical thin-section only.

A.4.1 Image enhancement

A dust filter was applied that removed all objects with a radius of 1 pixel (~7.1 μm). Some portions of the grain boundaries appeared very dark in the original image and were incorrectly interpreted as pore space (phthalate). A second filter was applied on the ice phase only that removed all black objects located within the ice phase with a radius below 3 pixels (~21 μm). The result of this image enhancement was judged visually. The image was cropped to a size of 27 x 8 mm (3894 x 1175 pixels) to remove the grains close to the side edges and bottom of the sample. A part of the binary image is shown in Figure 3.

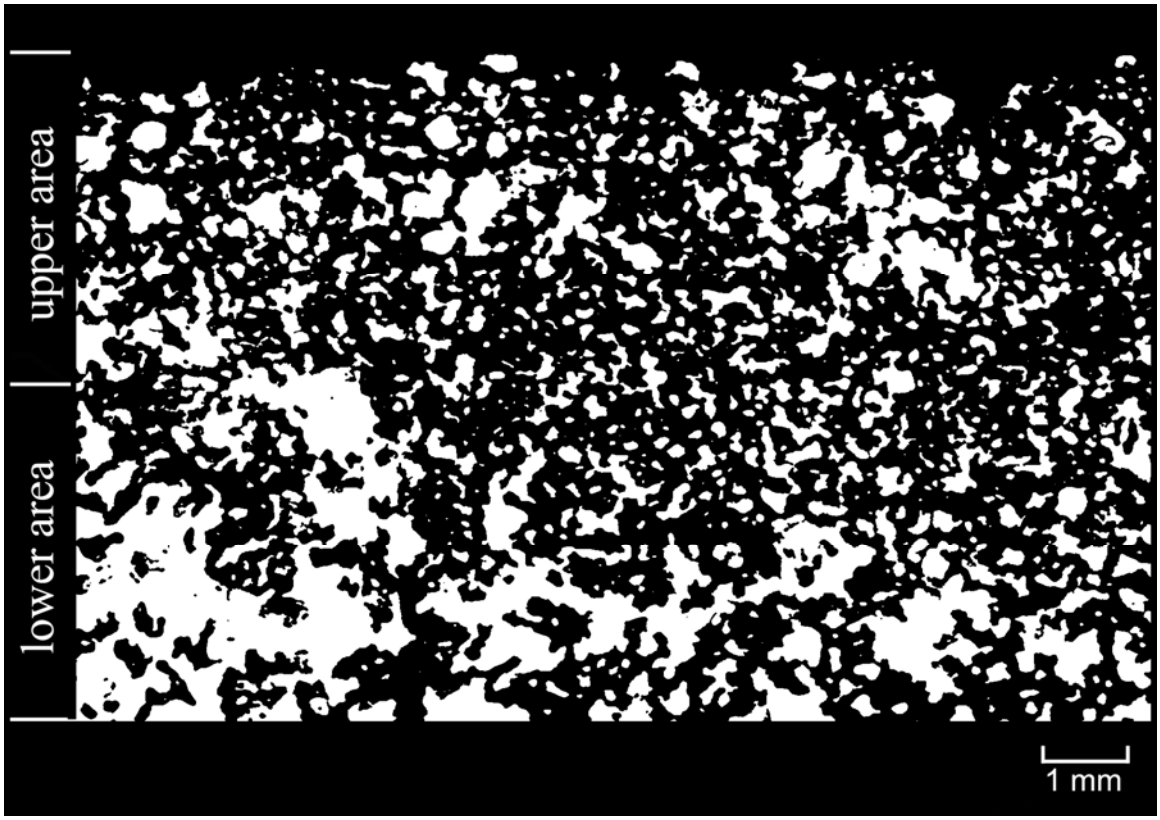

Figure A-3. Binary image of the area shown in Fig. A-1. The white areas are ice, the black areas the pore space.

A.4.2 Snow density

The average density of the snow in the thin-section ρ_s was calculated from the cropped image (excluding the surface topography) using eq. A.1:

$$\rho_s = \frac{\sum \text{ice pixels}}{\sum \text{all pixels}} \rho_i \qquad \text{(A.1)}$$

where ρ_i is the density of ice (918 kg/m^3). The calculated average density of the whole image was 374 kg/m^3, which agrees well with the density measured after sampling (~ 400 kg/m^3). The density calculation depends on the used algorithm to convert the colour image to the binary image. The uncertainty involved with this conversion was investigated. A filter was applied that expanded all white (ice) objects in the image with one and two pixels. A similar filter was applied that contracted all white objects with one and two pixels. The average density was recalculated after each filtering. The results are given in Table A-1.

Table A-1. Calculated average density for different ice coverage in the binary image.

ice areas	average density (kg/m^3)	absolute deviation (kg/m^3)	relative deviation (%)
contracted 2 pixels	273	102	-27
contracted 1 pixel	331	44	-12
original image	374	0	
expanded 1 pixel	436	62	17
expanded 2 pixel	481	106	28

The coverage of the expanded/contracted images was visually compared with the original colour image of the thin-section. The images where the ice area was expanded by two pixels clearly overestimated the ice fraction in the original thin-section. Similarly, contracting the area by two pixels clearly underestimated the ice fraction. The one-pixel expansion/contraction did not show a clear over-/under- estimation. Based on these observations the uncertainty involved with the image conversion was estimated to be in the order of 10-20%.

A depth profile of the density was calculated by dividing the binary image into horizontal layers and calculating the density of each layer using Eq. A.1. It was found that a layer thickness of 5 pixels (35 μm) gave an optimum result between reducing high frequency noise and preserving the general trend. The density profile along the depth is shown in Fig. A-4. The origin of the depth axis was placed on the highest ice pixel of the sample.

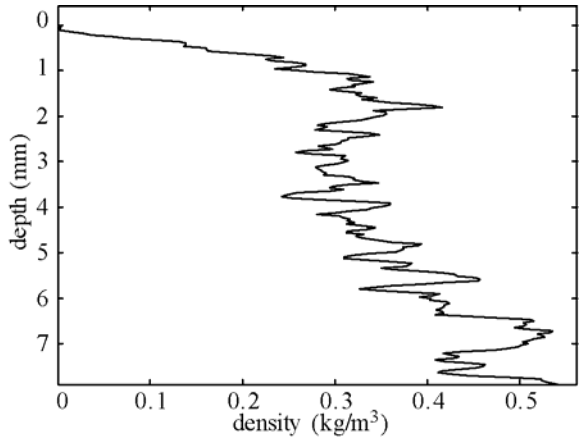

Figure A-4. Vertical density profile of the thin-section.

Fig. A-4 shows that the density starts from zero and increases rapidly within the first millimetre. After about one millimetre the snow layer shows a gradual increase of density with depth. The density pattern within the first millimetre can be attributed to the surface topography of the snow. The rapid variations of density with depth are within the inaccuracy of the image conversion

A.4.3 Surface topography

A measure for the surface topography of the sample was found by detecting the position of the uppermost ice pixel in every column of the image. The position of these pixels gives a

signal that represents the 2D surface topography profile of the snow. A part of the profile is given in Fig. A-5.

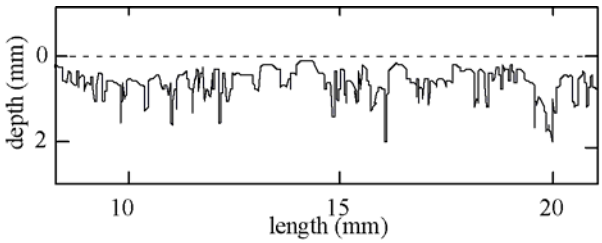

Figure A-5. The surface topography profile of area shown in Fig. A-1.

The distance between the highest peak and lowest valley of the profile was 2.01 mm. When comparing this result with the density profile in Fig. A-4 it can be seen that only the first mm shows a clearly different density compared to the rest of the sample. The frequency distribution of the uppermost ice pixel positions was calculated to investigate how frequently these deep pixels occur. The frequency distribution is shown in Fig. A-6.

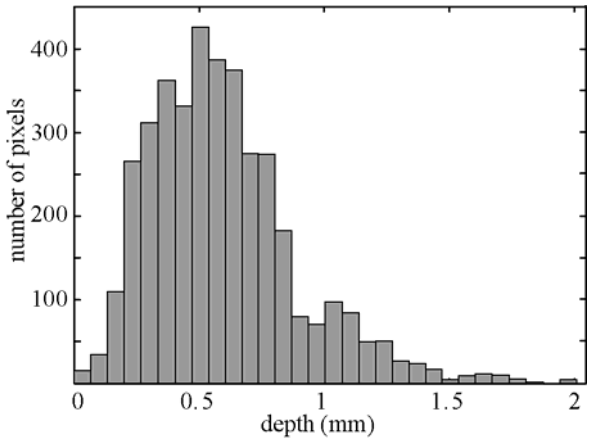

Figure A-6. Frequency distribution of the uppermost ice pixel position in each column of the image.

Fig. A-6 shows that the majority of the surface topography (~90 %) is located within the first mm and that the distribution is skewed. This can be interpreted by the fact that snow is a porous material. At some locations, the uppermost ice pixel lies deep in the pore space. The curve that represents the surface topography shows therefore at some locations deep spikes between two grains. These spikes can also be observed in Figure 4.

A.4.4 Grain and cluster size

A general microstructural characteristic of the snow is the size distribution of the individual grains and grain clusters. As the snow layer sinters, the grains grow together to complex structures resulting in large clusters and fewer individual grains. All individual ice areas (grains and clusters of grains) that are surrounded by pore space were identified in the binary image. The cropped binary image consisted of 2347 of such ice grains or clusters and the area of each individual grain/cluster was calculated. The image was than divided in two equally sized areas, the upper and lower part, indicated in Fig. A-3, and the calculations were performed on each of these areas. The largest single grain in the sample was found to

have a size of 0.94 mm^2. Hence, an object larger than 0.94 mm^2 is certainly a cluster of at least two grains. The cumulative grain/cluster size distribution of the three areas is presented in Fig. A-7.

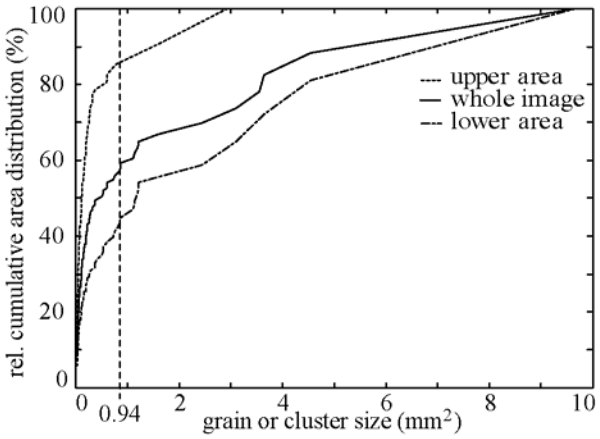

Figure A-7. Relative cumulative area distribution of grains and clusters.

Fig. A-7 shows a large difference in size distribution between the upper and lower area of the sample. The lower area contains much larger grains and clusters. In fact, in the lower area, 56 % of the clusters are larger than the largest single grain (0.94 mm2), whereas the upper area contains only 15 % of such clusters. It should be noted that when liquid water is present in the sample the amount of consolidation may be overestimated. Liquid water freezes when the sample is cooled down and this can bind grains that were initially not connected by an ice-ice bond. The level of consolidation as seen in this thin-section can therefore be higher than the actual level before sampling.

A.5 Discussion

The study illustrates that it is possible to perform detailed microstructural analysis on snow that is compressed by aircraft under operational conditions. With the used sampling procedure it was possible to recover snow samples from the pavement without visual damage and thin-sections could be made using the double-microtoming technique for snow. The presence of an ice layer on the pavement assisted the recovery of the snow samples because it provided a smooth and weakly bonded interface between the snow and pavement.

A modification in the first mounting step of the thin-sectioning procedure made it easier to release the sample from the glass plate. The use of a retardation plate was necessary to bring out the colours due to the required thickness of the thin-section. Although the contrast was sufficient for visual observations and colour photography, some crystals in the horizontal thin-section were lost in the conversion to the greyscale image. Hence, conversion of this image to a binary image was not possible. The colour contrast may be further improved by optimizing the optical properties of the retardation plate.

The colours observed in the thin-section are the result of a phase shift that occurs when linearly polarized white light falls on a plane parallel bi-refracting crystal. As the light enters the crystal, it splits into two components which travel at different velocities through the crystal. When leaving the crystal, this difference has caused a phase shift between the

two components. A particular wavelength becomes attenuated when the phase shift of that wavelength is 180°. When this wavelength is a part of the visual spectrum, the crystal appears coloured. The phase shift e is determined by the wavelength λ, the crystal thickness U and the effective refractive indices c_1 and c_2 of the bi-refracting crystal (Weber, 1999):

$$G = U(c_1 - c_2) \tag{A.2}$$

$$e = 2\pi \frac{G}{\lambda} \tag{A.3}$$

where G is the path-length difference. The thin-sections of freshly fallen snow are too thin to create sufficient path-length difference. The function of the retardation plate, which is also a bi-refracting material, is therefore to increase the path-length difference with a constant value throughout the sample. At a path-length difference of 551 nm the colour is very sensitive for small path-length variations (Weber, 1999). A retardation plate that produces such a path length difference is therefore optimal for investigating thin thin-sections of weak bi-refracting materials like ice. These types of retardation plates also known as “sensitive-tint plates” or “first order red plates”.

The tribology of a tire braking on a snow covered pavement is characterized by a process of compression, combined with loading the snow in shear. The compression of snow by vehicles has mainly been investigated in terms of the amount of rolling resistance that is experienced (Abele and Gow, 1976; Harrison, 1981b; Harrison, 1975; Harrison, 1981a; Richmond, 1995; van Es, 1999; Haehnel and Shoop, in press; Richmond et al., 1995; Shoop, 2001; Blaisdell, 1981; Abele and Gow, 1975). However, modern winter pavement maintenance, as it is practiced at Norwegian airports includes intensive removal of snow. Snow is frequently removed by runway sweepers that have combination of ploughing, brushing, and blowing units. Freshly fallen snow is usually not allowed to accumulate more than about 20-30 mm. The resistance due to compression is expected to be limited as a consequence of this intensive snow removal. Hence, during braking on snow covered runways, the snow compression may not be a major part of the total resistance force. This suggests that the loading of the snow in shear and the ability to transfer the force through the interfaces and through the (solid) interfacial medium towards the underlying pavement is of more importance.
In practice, more friction is expected on a snow contaminated runway, compared to an ice contaminated runway under otherwise similar environmental conditions. This expectation is also reflected in regulations: The proposed amendment on certification specifications for large aeroplanes specifies default values for the effective braking coefficient of an anti-skid controlled braked wheel/tire that are a factor 3.4 to 4 higher for snow than for ice contaminated runways (EASA, 2004) . But why would a snow covered pavement provide more friction than an ice covered pavement? The density of the snow track in the present study was about 400 kg/m^3. This implies an average pore volume of about 56 %. As can be seen in A-4, the first millimetre in depth exhibited an even lower density, so the relative pore volume close to the tire/snow interface was higher. These observations show that freshly fallen snow can have a very open structure after its initial compression. The elastic modulus of rubbers used for tire treads is generally low (Gehman, 1971) the rubber can thereby relatively easily drape around surface asperities (Moore, 1975; Moore, 1972). An open snow structure at the rubber-snow interface might therefore be a important factor to increase friction on snow covered pavement above the level that is achieved on ice covered pavements, at otherwise similar conditions.

A.6 Conclusion

The double-microtoming technique for snow can be applied for analysis of thin snow tracks made by aircraft tires. It provides a tool for tribological investigations of the tire-snow interaction. The use of a retardation plate is required for snow containing small crystals. Digital image analysis of the obtained thin-sections was found applicable to quantify general microstructural characteristics of the snow.

A.7 References

Abele, G. and Gow A. J. (1975): Compressibility characteristics of undisturbed snow. Research report no. 336, Cold Regions Research and Engineering Laboratory, Hanover, New Hampshire.

Abele, G. and Gow A. J. (1976): Compressibility characteristics of compacted snow. Report no. 76-21 Cold Regions Research and Engineering Laboratory, Hanover, New Hampshire.

Blaisdell, G.L. (1981): Predicting wheeled vehicle motion resistance in shallow snow. Special Report no. 81-30 Cold Regions Research and Engineering Laboratory, Hanover, New Hampshire.

Borel, S. and Brzoska J. B. (2000): A method for sectioning natural snow / pavement samples. Cold Regions Science and Technology, vol. 31, pp. 83-93.

Colbeck, S.C., Akitaya E., Armstrong R., Gulber H., Lafeuille J., Lied K., McClung D., and Morris E. (1990): The International Classification for Seasonal Snow on the Ground. International Commission on Snow and Ice (IAHAS), World Data Center A for Glaciology, U. of Colorado, Boulder, CO.

EASA. (2004): Notice of proposed amendment (NPA) No 14/2004 on certification specifications for large aeroplanes (CS-25) Operation on contaminated runways. Report no. NPA 14/2004

Gehman, S.D. (1971): Material Characteristics. in: Clark, S.K. Mechanics of pneumatic tires. Ch. 1. Washington D.C., National Highway Traffic Safety Administration.

Haehnel, R.B. and Shoop S. A. (2004): A macroscale model for low density snow subjected to rapid loading. Cold Regions Science and Technology vol. 40[3], pp. 193-211.

Harrison, W.L. (1975): Vehicle Motion Resistance Due to Snow. Technical Report No. 268 Hanover, Cold Regions Research and Engineering Laboratory, Hanover, New Hampshire.

Harrison, W.L. (1981a): Proceedings of the international society for terrain-vehicle systems workshop on snow traction mechanisms. Special Report no. 81-16, Cold Regions Research and Engineering Laboratory, Hanover, New Hampshire.

Harrison, W.L. (1981b): Shallow snow model for predicting vehicle performance. Report no. 81-20, Cold Regions Research and Engineering Laboratory, Hanover, New Hampshire.

Moore, D.F. (1972): The Friction and Lubrication of Elastomers. Oxford, Pergamon press.

Moore, D.F. (1975): The friction of pneumatic tyres. Amsterdam, Elsevier Scientific publishing Company.

Perla, R. (1982): Preparation of section planes in snow specimens. Journal of Glaciology, vol. 28[98], pp. 199-204.

Richmond, P.W. (1995): Motion Resistance of Wheeled Vehicles in Snow. Report 95-7, Cold Regions Research and Engineering Laboratory, Hanover, New Hampshire.

Richmond, P.W., Shoop S. A., and Blaisdell G. L. (1995): Cold Regions Mobility Models. Report no. 95-1, Cold Regions Research and Engineering Laboratory, Hanover, New Hampshire.

Satyawali, P.K., Sinha N. K., and Sethi D. N. (2003): Double-microtoming technique for snow studies. Canadian Journal of Physics, vol. 81, pp. 529-537.

Shoop, S.A. (2001): Finite Element Modeling of Tire-Terrain Interaction. Technical Report no. 01-16, Cold Regions Research and Engineering Laboratory, Hanover, New Hampshire.

Sinha, N.K. (1977): Technique for Studying Structure of Sea Ice. Journal of Glaciology, vol. 18, pp. 315-323.

van Es, G.W.H. (1999): Method for predicting the rolling resistance of aircraft tires in dry snow. Journal of Aircraft, vol. 36[5], pp. 762-768.

Weber, K. (1999): Polarization and bi-refringence of light. in: Bergmann, L. and Scheafer, C. Optics of waves and particles. Ch. 4, pp. 439-586. Berlin, Walter de Gruyter.

B DERIVATION

This appendix is a derivation, related to Chapter 6, to show that a relative error in the sliding length adjustment δl/l directly propagates as the relative error in the friction coefficient δμ/μ.

Recall Eq. 6.3:

$$\mu_{BP} = \frac{W(h_0 - h_1)}{lF_n}, \tag{6.3}$$

and the partial derivation of Eq. 6.3 with respect to *l*:

$$\delta\mu_2 = \left|\frac{\partial\mu_{BP}(l)}{\partial l}\right|\delta l \tag{A.1}$$

Eq. 6.3 can be re-written as:

$$\mu_{BP}(l) = \frac{W(h_0 - h_1)}{lF_n} = cl^{-1}, \tag{A.2}$$

where:

$$c = \frac{W(h_0 - h_1)}{F_n} \tag{A.3}$$

Derivation of Eq. A.2 results:

$$\frac{\partial\mu_{BP}(l)}{\partial l} = -\frac{c}{l^2} \tag{A.4}$$

c can be substituted according:

$$c = \frac{W(h_0 - h_1)}{F_n} = \mu_{BP}l \tag{A.5}$$

Substitution of Eq. A.4 and Eq. A.5 in Eq A.1 and the notion that both the friction coefficient and the length are positive real numbers it follows that:

$$\delta\mu_2 = \left|-\frac{\mu_{BP}l}{l^2}\right|\delta l = \mu_{BP}\frac{\delta l}{l} \tag{A.6}$$

Which can be rewritten as:

$$\frac{\delta\mu_2}{u_{BP}} = \frac{\delta l}{l} \tag{A.7}$$

Eq. A.7 shows that the relative error in the length adjustments δl/l results in an equal relative error in the friction coefficient $\delta\mu_2/\mu_{BP}$.